

**Functional characterisation of FEVR-related  
*LGR4* missense mutations. Implications in  
Norrin- $\beta$ -Catenin signalling pathway and  
angiogenesis**

By  
Carla Sanjurjo Soriano

Submitted in accordance with the requirements for the degree of  
Doctor of Philosophy

The University of Leeds  
School of Medicine

February 2017

The candidate confirms that the work submitted is his/her own, except where work has formed part of jointly-authored publications has been included. The contribution of the candidate and the other authors to this work has been explicitly indicated overleaf. The candidate confirms that appropriate credit has been given within the thesis where reference has been made to the work of others.

This copy has been supplied on the understanding that it is copyright material and that no quotation from the thesis may be published without proper acknowledgement.

The right of Carla Sanjurjo Soriano to be identified as Author of this work has been asserted by her in accordance with the Copyright, Designs and Patents Act 1988.

© 2017 The University of Leeds  
and  
Carla Sanjurjo Soriano

## Acknowledgements

Firstly, I wish to express my sincere gratitude to my lead supervisor during my PhD, Dr. Carmel Toomes, for her support, patience and enthusiasm. For always having her office door open and ready for discussion. My sincere thanks also goes to my other two supervisors, Prof. Chris Inglehearn and Dr. Jaqueline Bond, for their constant supervision and insight throughout the years of my PhD. I would like to thank all my supervisors for giving me the opportunity of conducting my PhD with a great deal of freedom in developing my work, which has definitely helped to develop myself as a scientist.

I am also very grateful to the EyeTN network, which founded my project and gave me the opportunity to collaborate with the Marie Curie European network. I wish to thank Dr. Rob Collin, member of the EyeTN, for his supervision and guidance during my stay in Radboud Medical Centre (Nijmegen). Thank you to all the EyeTN fellows, whom have become friends as well as colleagues throughout the journey of my PhD.

I would like to thank all of the members of Level 8, who made my time in Leeds happier, easier and most of all, memorable. But a special thanks has to go to James and Evi, without whom, this project and my time spent in Level 8 would simply not have been the same. Thank you for all of the scientific (and not so scientific) conversations we have shared. Thank you for your understanding, for your patience and for always knowing how to deal with me. I will always remember the awesome trio!

Last but not least I want to deeply thank all my friends and family back in Barcelona, who have always supported me from the distance. In particular, I would like to thank Monica, for all your help as a fellow scientist, but also for being such a dear friend throughout all this time. But most of all and always, I want to thank my Mum and Dad - Pepa and Daniel - for your constant support, your guidance, your love, and for teaching me that with hard work, dedication and determination, anything is possible. This thesis also belongs to you!

## Abstract

Familial exudative vitreoretinopathy (FEVR) is a genetically heterogeneous blinding disorder characterised by the abnormal development of the retinal vasculature. Genetic studies have led to the identification of eight different genes mutated in FEVR and an additional autosomal dominant locus (EVR3) has been mapped. Recently the EVR3 locus was sequenced using next generation technology leading to the identification of an *LGR4* missense variant in the EVR3 family. Subsequent sequencing of *LGR4* in a cohort of FEVR patients identified further missense variants. The work in this thesis describes the functional characterisation of *LGR4* and its FEVR-related variants to confirm it as a new FEVR disease gene.

Zebrafish *lgr4* morpholino knockdown followed by mRNA rescue showed that the FEVR-related *LGR4* variants were unable to rescue the retinal vasculature defects induced in the fish. Furthermore, the majority of mutations underlying FEVR encode components of the Norrin- $\beta$ -Catenin signalling pathway. The TOPflash  $\beta$ -Catenin reporter assay was used to show that *LGR4* potentiates Norrin signalling but the variants located in the binding domain of *LGR4* reduce this. Norrin and *LGR4* binding assays show that the EVR3 mutation increases the binding affinity between these two proteins hinting at a potential disease mechanism. Finally, an *in vitro* angiogenesis assay demonstrated that *LGR4* plays a role in the development of vascular structures.

The identification of *LGR4* as a new FEVR gene, and confirmation that *LGR4* is a component of the Norrin- $\beta$ -Catenin pathway, helps to decipher the molecular mechanisms underlying the normal development of the retinal vasculature and the FEVR disease mechanism. Knowing the gene underlying a disease translates into immediate benefit for patients and families through access to a precise genetic diagnosis and more accurate genetic counselling. Furthermore, this new understanding should contribute to the development of new treatments or therapy, ultimately providing a better quality of life for the patients.

## Abbreviations

A	Adenine
AMD	Age-macular degeneration
AON	Antisense oligonucleotide
AP	Alkaline phosphatase
APC	Adenomatous polyposis coli
ATOH7	Atonal homolog 7
BLAST	Basic local alignment tool
BBB	Blood brain barrier
BMD	Bone mineral density
bp	base pair
BRB	Blood retinal barrier
C	Cytosine
cAMP	cyclic adenosine monophosphate
cDNA	complementary DNA
CK1 $\alpha$	casein kinase 1 alpha
CNS	Central nervous system
CRD	Cysteine rich domain
DCV	Dorsal ciliary vein
DEPC	Diethylpyrocarbonate
dH <sub>2</sub> O	De-ionised water
DMEM	Dulbecco's Modified Eagle's Medium
DMSO	Dimethyl sulphoxide
DNA	Deoxyribonucleic acid
DVL	Deshevelled
EC	Endothelial cells
EDTA	Etylenediaminetetraacetic acid
EGFR	Epidermal growth factor receptor
EGM	Endothelial growth medium
ExoSAP-IT	Exonuclease I shrimp alkaline phosphatase
FA	Fluorescein angiography
FCS	Fetal calf serum

FEVR	Familial exudative vitreoretinopathy
FGFs	Fibroblast growth factors
FSH	Follicle-stimulating hormone
FZD	Frizzled receptor
FZD4	Frizzled-4
G	Guanine
GFAP	Glial fibrillary acidic protein
GHR	Glycoprotein hormone receptors
GPCR	G-protein coupled receptor
GSK3 $\beta$	Glycogen synthase kinase 3 beta
HB-EGF	Heparin binding EGF
HDF	Human dermal fibroblasts
HMG	High-motility group
HPLC	High performance liquid chromatography
HUVEC	Human umbilical vein endothelial cells
IF	Immunofluorescence
iPSC	Induced pluripotent stem cells
INL	Inner nuclear layer
IOC	Inner optic circle
IPL	Inner plexiform layer
IVF	<i>In vitro</i> fertilisation
JMJD	Jumonji domain-containing histone demethylase
kb	Kilobase
LB	Luria-Bertani
LEF	Lymphoid enhancing factor
LGR4	Leucine-rich repeat containing G-protein-coupled receptor 4
LH	Leutinizing hormone
LRP5	Low-density lipoprotein receptor-related protein 5
LRR	Leucine-rich repeats
M	Molar
Mb	Megabase
ml	Millilitre
mM	Millimolar
MO	Morpholino

mRNA	Messenger RNA
NCA	Nasal ciliary artery
ND	Norrie disease
NDP	Norrie disease protein
ng	Nanogram
NGS	Next generation sequencing
NMD	Nonsense-mediated mRNA decay
OIR	Oxygen-induced proliferative retinopathy
ONL	Outer nuclear layer
OPL	Outer plexiform layer
OPPG	Osteoporosis–pseudoglioma syndrome
OV	Optic vein
PAGE	Polyacrylamide gel electrophoresis
PBS	Phosphate-buffered saline
PCR	Polymerase chain reaction
PDGFA	Platelet derived growth factor A
PDGFR $\alpha$	Platelet derived growth factor receptor alpha
PHPV	Persistent hyperplastic primary vitreous
PIGD	Pre-implantation genetic diagnosis
PLAP	Placental alkaline phosphatase
pmol	Picomoles
qRT-PCR	Quantitative real-time PCR
REC	Retinal endothelial cells
RGC	Retinal ganglion cell
RT-PCR	Reverse transcription PCR
RNA	Ribonucleic acid
RNF43	Ring finger protein 43
ROP	Retinopathy of prematurity
RPE	Retinal pigment epithelium
SDM	Site directed mutagenesis
SDS	Sodium dodecyl sulphate
SNP	Single nucleotide polymorphism
SOC	Super optimal broth with catabolite repression
SOX17	SRY-box17

SOX18	SRY-box18
T	Thymine
Taq	<i>Thermus aquaticus</i> derived DNA polymerase
TALEN	Transcription activator-like effector nuclease
TBE	Tris HCl-borate EDTA buffer
TBS	Tris-buffered saline
TCF	T-cell factor
TE	Tris EDTA
TGF- $\beta$	Transforming growth factor- $\beta$
TM	Transmembrane domain
TNF	Tumor necrosis factor
TSPAN12	Tetraspanin-12
TSH	Thyroid-stimulating hormone
TSR	Thrombospondin repeat
Tris	Tris (hydroxymethyl) aminomethane
UCSC	University of California Santa Cruz
UTR	Untranslated region
V	Volt
VEGF	Vascular endothelial grow factor
VEGFR2	Vascular endothelial grow factor receptor 2
WB	Western blotting
WG	Weeks gestation
$\mu$ l	Microliter
$\mu$ M	Micromolar
ZIRC	Zebrafish International Resource Centre
ZFIN	Zebrafish information network
ZFN	Zinc finger nuclease
ZNF408	Zinc finger protein 408
ZNRF3	Zinc and ring finger 3

## Contents

Acknowledgements.....	iii
Abstract.....	iv
Abbreviations .....	v
Contents .....	ix
List of Figures .....	ix
List of Tables.....	xii
1 Introduction.....	1
1.1 General Overview .....	1
1.2 Structure and development of the eye .....	2
1.2.1 Structure of the human eye .....	2
1.2.1.1 The structure of the retina.....	3
1.2.2 General features of eye development .....	6
1.2.3 The vasculature in the developing eye .....	8
1.3 Retinal Vascularisation .....	8
1.3.1 The hyaloid vasculature .....	9
1.3.2 Vasculogenesis .....	10
1.3.2.1 General features of vasculogenesis.....	10
1.3.2.2 Vasculogenesis in the retina .....	11
1.3.3 Retinal astrocytes form a template for angiogenesis.....	11
1.3.4 Angiogenesis.....	13
1.3.4.1 General features of angiogenesis .....	13
1.3.4.2 Sprouting angiogenesis of the retinal vasculature .....	15
1.4 Familial exudative vitreoretinopathy (FEVR).....	16
1.4.1 Clinical features of FEVR .....	16
1.4.2 Genetics of FEVR.....	18
1.4.3 Mouse models of FEVR .....	21
1.5 Norrin- $\beta$ -Catenin signalling .....	23
1.5.1 Activation of the Norrin- $\beta$ -Catenin pathway .....	25
1.5.2 The role and regulation of $\beta$ -Catenin.....	27
1.5.3 Degradation of $\beta$ -Catenin in the absence of Norrin binding.....	28
1.5.4 The role of the Norrin- $\beta$ -Catenin pathway .....	29
1.5.5 Other proteins involved in Norrin signalling .....	31

1.6	The Wnt signalling pathway .....	32
1.6.1	Wnt signalling pathway classification .....	33
1.6.2	The Wnt- $\beta$ -Catenin heterodimeric receptor complex and pathway activation.....	34
1.6.3	R-spondins (RSPOs) activate the Wnt- $\beta$ -Catenin pathway .....	35
1.6.3.1	E3 ubiquitin ligases regulate Wnt- $\beta$ -Catenin signalling through an LGR4/5/6 and R-spondin pair.....	37
1.6.4	Wnt signalling in vascularisation.....	39
1.7	Leucine-rich repeat containing G protein-coupled receptor 4 (LGR4)	43
1.7.1	LGR4 is a member of the GPCR family.....	43
1.7.2	LGR4 mice models.....	44
1.7.3	LGR4 signalling pathways.....	48
1.8	Identification of missense variants in <i>LGR4</i> .....	51
1.8.1	Exome sequencing of the <i>EVR3</i> locus and <i>LGR4</i> screening in the Leeds FEVR cohort .....	51
1.9	Aims.....	53
2	Materials and Methods .....	54
2.1	General buffers .....	54
2.2	Polymerase chain reaction (PCR).....	55
2.2.1	Primer design.....	55
2.2.1.1	Site Directed Mutagenesis primer deign.....	56
2.2.2	Hot-Shot PCR (Clent Life Science).....	56
2.2.3	Platinum Pfx PCR .....	57
2.2.4	Reverse transcription PCR (RT-PCR).....	57
2.3	Agarose gels.....	58
2.3.1	Size fragmentation .....	58
2.3.2	DNA extraction from agarose gels .....	58
2.4	Sanger sequencing.....	58
2.4.1	PCR template clean-up for sequencing .....	58
2.4.2	Sequencing reaction .....	59
2.4.3	Precipitation of sequencing reaction products .....	59
2.5	Bioinformatics .....	59
2.5.1	Literature Searches.....	59

2.5.2 UCSC Genome Bioinformatics Browser .....	60
2.5.3 Protein alignment sequence using BLAST.....	60
2.6 Molecular cloning.....	60
2.6.1 TA cloning of PCR products.....	60
2.6.2 Restriction enzyme digestion .....	61
2.6.3 Site Directed Mutagenesis (SDM).....	61
2.6.4 Creation of expression constructs using Gateway technology .....	61
2.6.5 Bacterial transformation and culture .....	62
2.6.6 Plasmid DNA isolation and purification .....	63
2.7 mRNA synthesis and purification .....	63
2.8 Morpholino, zebrafish manipulation and rescue experiments .....	64
2.8.1 Zebrafish Information Network (ZFIN).....	65
2.8.2 Gene Tools MO design.....	65
2.8.3 Zebrafish whole-mount immunofluorescence .....	65
2.9 RNA extraction.....	66
2.10 Cell culture.....	66
2.10.1 Cell lines .....	66
2.10.2 Cell culture.....	67
2.10.3 Cell counting .....	68
2.10.4 Cell storage and recovery .....	69
2.10.5 Conditioned medium.....	69
2.10.6 Transfections .....	69
2.10.6.1 Transient DNA transfections.....	69
2.10.6.2 Transient siRNA transfections.....	70
2.10.7 Cell lysis.....	71
2.10.8 Protein assay .....	72
2.10.9 Luciferase assays .....	72
2.10.9.1 Luciferase Assay using recombinant Norrin .....	72
2.10.9.2 Dual Luciferase TOPFlash assay .....	72
2.10.9.3 HEK293 and STF co-culture TOPFlash assay .....	74
2.10.10 <i>In vitro</i> tube formation angiogenesis assay.....	74
2.10.11 Quantitative real-time PCR (qRT-PCR) .....	75
2.10.12 Binding assays.....	76
2.10.12.1 Cell surface binding assay .....	76

2.10.12.2 Cell based binding assay .....	77
2.10.13 Live cell imaging using Nikon BioStation IM microscope .....	77
2.11 Immuno-techniques .....	78
2.11.1 Antibodies .....	78
2.11.2 Western Blotting (WB) .....	80
2.11.3 Immunofluorescence (IF) .....	81
2.12 Microscopy.....	81
2.12.1 Light Microscopy .....	81
2.12.2 Confocal microscopy.....	81
2.12.3 EVOS™ Cell Imaging System.....	82
3 Functional characterization of FEVR-related <i>LGR4</i> missense variants using a zebrafish model .....	83
3.1 Background.....	83
3.2 Morpholino antisense oligonucleotide (MOs) design .....	86
3.2.1 MO injection to assess the zebrafish phenotype.....	89
3.2.1.1 Optimising the <i>lgr4</i> morpholino dose-response .....	90
3.2.1.2 Classification of the eye phenotype in <i>lgr4</i> MO knockdown zebrafish.....	93
3.3 Creating <i>LGR4</i> expression constructs for MO rescue experiments in zebrafish.....	96
3.3.1 Identification of <i>LGR4</i> splice variants.....	96
3.3.2 Creating a mutation series of expression constructs for <i>LGR4</i> by site directed mutagenesis .....	100
3.3.3 Linearization of the plasmid, mRNA synthesis and RNA recovery .....	105
3.4 Rescue of the aberrant eye phenotype using human WT <i>LGR4</i> mRNA.....	105
3.4.1 Scoring method validation.....	108
3.5 Zebrafish phenotype rescue using <i>LGR4</i> mRNA variants.....	110
3.5.1 Statistical analysis.....	113
3.6 Discussion .....	117
4 Investigating the effects of <i>LGR4</i> missense variants on the Norrin- $\beta$ -Catenin signalling pathway .....	125
4.1 Background.....	125

4.2	Identification of a suitable cell line in which to perform the TOPflash assay.....	127
4.3	Topflash assay using recombinant human Norrin (rhNorrin).....	130
4.4	TOPflash assay transfecting Norrin- $\beta$ -Catenin pathway components into STF cells.....	131
4.4.1	Creating expression constructs for the TOPflash assay.....	131
4.4.2	Validation of the expression constructs.....	134
4.4.3	Elucidating if LGR4 plays a role in Norrin- $\beta$ -Catenin signalling	139
4.4.3.1	Investigating the effects of the <i>LGR4</i> missense variants on the Norrin- $\beta$ -Catenin signalling pathway .....	141
4.4.3.2	Genetic update on <i>LGR4</i> Variants.....	143
4.4.4	Investigating the effects of the <i>LGR4</i> missense variants on R-spondin signalling .....	144
4.5	Discussion .....	147
4.5.1	Investigation of LGR4 variants on RSPO1 signalling .....	152
5	Investigating the role of LGR4 in angiogenesis and the interaction of Norrin and LGR4.....	157
5.1	Background.....	157
5.2	<i>In vitro</i> organotypic co-culture angiogenesis assay .....	158
5.2.1	Validation of <i>FZD4</i> and <i>LGR4</i> knockdown in siRNA treated HUVECs .....	158
5.2.2	Validation of <i>FZD4</i> and <i>LGR4</i> knockdown using RT- qPCR.....	160
5.2.3	HDF-HUVEC co-culture angiogenesis assay.....	161
5.3	Investigating Norrin binding to WT and variant LGR4.....	164
5.3.1	Investigating Norrin binding to WT and variant LGR4 in co-culture assays.....	164
5.3.2	Investigating Norrin binding to WT and variant LGR4 using an AP cell surface binding assay.....	167
5.3.3	Replicating the study by Deng et al 2013.....	173
5.4	Investigating any effects on LGR4 localisation caused by the FEVR-related <i>LGR4</i> variants .....	174
5.5	LGR4 and Norrin co-localisation assay.....	178
5.6	Discussion .....	184
6	General discussion.....	195

6.1	Key findings of this thesis .....	195
6.2	LGR4's role in the Norrin- $\beta$ -Catenin signalling pathway .....	198
6.3	Verifying pathogenic missense variants.....	203
6.4	The impact of this study .....	205
6.5	The treatment of FEVR.....	207
7	References .....	210
8	Appendices.....	249
8.1.	Human LGR4 and zebrafish lgr4 protein alignment .....	249
8.2.	MO sequences.....	250
8.3.	Primers used in RT-PCR .....	250
8.4.	SDM primers.....	251
8.5.	attB primers for Gateway technology constructs.....	252
8.6.	Sequencing primers of expression constructs .....	253
8.7.	pCR2.1-TOPO vector.....	254
8.8.	Expression vectors .....	255

## List of Figures

Figure 1-1: Anatomy of the human eye.....	2
Figure 1-2: Organisation of neurons and retinal layers in the human retina...	4
Figure 1-3: Embryonic development of the human eye.....	7
Figure 1-4: Regression of the hyaloid vasculature in the human eye.....	9
Figure 1-5: Vascular sprouts are guided by tip/stalk cell specification. ....	14
Figure 1-6: Clinical appearance of FEVR.....	17
Figure 1-7: The Norrin- $\beta$ -Catenin signalling pathway.....	26
Figure 1-8: The $\beta$ -Catenin destruction complex in the absence of Norrin. ...	29
Figure 1-9: Canonical and Non-canonical Wnt signalling pathways.....	33
Figure 1-10: regulation of Wnt receptor degradation by the LGR4-6/RSPO/ RNF43/ZNRF3 module. ....	38
Figure 1-11: Diagram of <i>LGR4</i> gene and LGR4 protein structures, showing the locations of the variants identified in FEVR patients. ....	52
Figure 3-1: Protein sequence alignment of human LGR4 with its orthologues. .....	85
Figure 3-2: <i>lgr4</i> prediction in zebrafish.....	86
Figure 3-3: Translational MO design BLAT and BLAST search.....	88
Figure 3-4: Splice MO design BLAT and BLAST search.....	89
Figure 3-5: Schematic representation of the experimental procedure carried out in the zebrafish. ....	90
Figure 3-6: <i>lgr4</i> morpholino dose-response results.....	92
Figure 3-7: Classification of the eye phenotypes found in <i>lgr4</i> MO zebrafish. .....	95
Figure 3-8: MO <i>lgr4</i> morphologies and vascular abnormalities in the trunk.	96
Figure 3-9: LGR4 transcripts on UCSC Genome Browser (hg.19).....	97
Figure 3-10: cDNA amplification of <i>LGR4</i> in different human tissues. ....	98
Figure 3-11: EcoRI digestion of <i>LGR4</i> kidney TA-cloning colonies.....	99
Figure 3-12: Schematic representation of the <i>LGR4</i> transcripts. ....	100
Figure 3-13: Sequence electropherogram results of all the point changes introduced in pCMV6_ <i>LGR4</i> . ....	102

Figure 3-14: Schematic representation of the Gateway Technology system. .....	103
Figure 3-15: PCR products amplified from pCMV6_ <i>LGR4</i> WT or variant clones. ....	104
Figure 3-16: Phenotypic classification of zebrafish larvae when 6 ng of MO <i>lgr4</i> was co-injected with 50 pg, 100 pg or 150 pg of WT <i>LGR4</i> mRNA. .....	106
Figure 3-17: Phenotypic classification of MO-knockdown rescue assays using WT <i>LGR4</i> mRNA.....	107
Figure 3-18: Different eye phenotype classification by scoring fish or by scoring eyes.....	109
Figure 3-19: Results of the MO knockdown rescue assays using variant <i>LGR4</i> mRNAs. ....	111
Figure 4-1: Measuring activation of the Norrin- $\beta$ -Catenin signalling pathway using the TOPflash reporter construct. ....	126
Figure 4-2: Expression of <i>LGR4</i> and Norrin signalling pathway components in a panel of cell lines. ....	128
Figure 4-3: cDNA expression of <i>LGR4</i> and the Norrin signalling pathway components in STF cells.....	129
Figure 4-4: TOPflash assay in STF cells activated using 50, 100, 150 and 250ng/ml of human recombinant Norrin.....	131
Figure 4-5: Western blots to confirm the expression of the pDEST40 fusion proteins.....	135
Figure 4-6: Western blot to confirm the expression of the <i>LGR4</i> fusion proteins.....	137
Figure 4-7: Western blot to confirm the expression of the AP-Norrin fusion protein.....	138
Figure 4-8: TOPflash assay in STF cells transfected with different Norrin pathway components.....	140
Figure 4-9: TOPflash assay to assess the effect of <i>LGR4</i> variants on Norrin- $\beta$ -Catenin signalling. ....	142
Figure 4-10: TOPflash assay to determine the optimum RSPO1 concentration required to activate $\beta$ -Catenin signalling. ....	145

Figure 4-11: TOPflash assay to determine if the <i>LGR4</i> variants alter RSPO1- β-Catenin signalling. ....	146
Figure 4-12: Norrin stimulation of LGR4-mediated Wnt signalling is augmented by LRP5 and LRP6. ....	150
Figure 5-1: Confirmation of <i>FZD4</i> and <i>LGR4</i> mRNA expression in WT HUVECs. ....	159
Figure 5-2: Western blot of HUVEC protein extract incubated with anti-FZD4 or anti-LGR4 antibodies. ....	159
Figure 5-3: Relative mRNA expression levels of <i>FZD4</i> and <i>LGR4</i> in siRNA treated HUVECs. ....	160
Figure 5-4: HDF and HUVEC co-culture tubule formation assay. Quantification of tubule length, number of tubules, number of tubule junctions and area of undifferentiated HUVEC clusters. ....	163
Figure 5-5: Schematic representation of the co-culture experiment. ....	165
Figure 5-6: TOPflash luciferase assay in HEK293-STF co-culture. ....	166
Figure 5-7: Cell surface binding assay of WT and variant LGR4 with AP- Norrin. ....	169
Figure 5-8: Cell surface binding assay comparing the binding of AP-Norrin to LGR4, LRP5 and TSPAN12. ....	170
Figure 5-9: Quantification of AP-Norrin binding assay. ....	172
Figure 5-10: AP-Norrin binding assay performed at room temperature. ....	173
Figure 5-11: Confocal images of HEK293 cells transfected with pDEST504_ <i>LGR4</i> expression constructs showing LGR4 localisation. ....	176
Figure 5-12: Live-cell imaging of HEK293 cells transfected with WT pDEST504_ <i>LGR4</i> . ....	178
Figure 5-13: Co-localisation of FZD4 and Norrin in HEK293 cells by immunofluorescence microscopy. ....	180
Figure 5-14: Confocal images of the two controls used for the co-localisation of LGR4 and Norrin experiment. ....	181
Figure 5-15: Co-localisation of LGR4-YFP and AP-3myc-Norrin in HEK293 cells analysed by confocal microscopy. ....	183
Figure 6-1: Schematic diagram of the suggested role of LGR4 in Norrin signalling. ....	199

Figure 6-2: Schematic diagram suggesting different possible pathogenic mechanism of action for the LGR4 variants.....202

## List of Tables

Table 1-1: FEVR loci for the FEVR genes implicated in Norrin- $\beta$ -Catenin signalling pathway. ....	18
Table 1-2: Expression of Norrin pathway components in tissue and retina..	25
Table 2-1: Cell lines used. Name, origin and source of cell lines. ....	67
Table 2-2: siRNAs utilised. Target gene, organism, sequence and commercial source of siRNA pools. Non targeting siRNA pool 1 refers to scrambled siRNA. ....	71
Table 2-3: TaqMan® gene expression assay details for FZD4, LGR4 and GAPDH. ....	75
Table 2-4 A and B: Table 2-4 A (upper table) showing primary antibodies. Table 2-4 B showing secondary antibodies. Names of primary and secondary antibodies. Conjugates of the secondary antibodies are also listed. ....	79
Table 3-1: Summary of bioinformatics analyses undertaken to predict the pathogenic nature of the six <i>LGR4</i> missense variants identified in FEVR patients. ....	84
Table 3-2: Number of embryos analysed, percentage of the fish present with each phenotype and survival numbers of the fish. ....	92
Table 3-3: Number of embryos analysed, percentage of fish present with each phenotype and fish survival rates. ....	106
Table 3-4: Number of embryos analysed, percentage of fish present with each phenotype and fish survival rates in the replicate rescue experiment. ....	107
Table 3-5: Experimental data for the MO knockdown rescue assays using variant <i>LGR4</i> mRNAs. ....	112
Table 3-6: Number of normal or aberrant eyes present in fish injected with MO <i>Igr4</i> or co-injected with the MO <i>Igr4</i> and <i>LGR4</i> mRNA and Fisher's test P value. ....	115

Table 3-7: Number of normal, moderate, mild or severe eyes present in fish injected with MO <i>lgr4</i> or co-injected with the MO <i>lgr4</i> and <i>LGR4</i> mRNA and Fisher's test P value.....	116
Table 4-1: Variants present in the cDNA clones purchased from Transomic technologies.....	132
Table 4-2: Population frequencies from ExAC Browser Beta database for the <i>LGR4</i> variant c.2248G>A p.(A750T).....	143

# 1 Introduction

## 1.1 General Overview

Angiogenesis has been and remains a major target for research due to the wide range of pathologies and diseases associated with abnormal vascular development. Vascular disorders can be caused either by excessive vascular growth or insufficient angiogenesis (Carmeliet, 2003). Deficient vascular growth can lead to heart and brain ischemia. Similarly, avascularity in the retina can lead to blinding disorders such as inherited familial exudative vitreoretinopathies (FEVR). Conversely, excessive vascular growth is a component of ocular disorders such as age-related macular degeneration (ARMD) and diabetic retinopathy, and also promotes tumour growth. Studying the mechanism and regulation of blood vessel growth is therefore an important area of developmental research. Understanding the molecular, genetic and cellular mechanisms of vessel growth could offer therapeutic opportunities and drug targets for a wide range of human disorders, including blinding disorders, but also many other disorders affecting vascular development (Folkman, 2007).

The eye, and more specifically the retina, as part of the central nervous system (CNS), provides a powerful model for studying neuronal vascular diseases because the retinal vasculature can be accessed and observed relatively easily. The study of the genetic basis of retinal avascularisation in FEVR patients has led to the identification of genes encoding proteins involved in a molecular pathway controlling vascularisation of the retina, known as the Norrin- $\beta$ -Catenin signalling pathway (Junge et al., 2009; Xu et al., 2004; Ye et al., 2009). Interestingly, this pathway shares many similarities with the well-defined Wnt- $\beta$ -Catenin signalling pathway, which is involved in many aspects of development, including vascularisation (Clevers and Nusse, 2012).

## 1.2 Structure and development of the eye

### 1.2.1 Structure of the human eye

The adult human eye (Figure 1-1) consists of three major layers. The external layer is formed by the sclera and the cornea (Tottora and Derrickson, 2005). These tissues provide strength and maintain the eye shape covering the whole eyeball (McLananahan, 2008). The intermediate layer lies beneath the external layer and consists of the choroid, ciliary body, iris and pupil (Tottora and Derrickson, 2005). The choroid, a highly vascularised tissue, supplies nourishment to the outer layers of the retina and removes waste products. The iris and the ciliary body control the amount of light entering the eyeball by adjusting the size of the pupil, and the ciliary body also produces the clear liquid aqueous humour which fills the anterior chamber of the eye. The internal layer, which is the sensory part of the eye, is made up of the neural and pigmented retina (discussed in detail in section 1.2.1.1). The retina detects the light and translates it into an electrical impulse sent to the visual cortex.

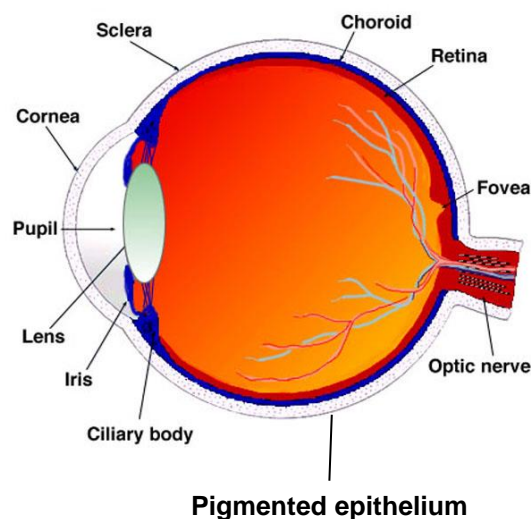


**Figure 1-1: Anatomy of the human eye.**

Sagittal and horizontal section of the human eye showing the gross structures. Adapted from webvision ([www.webvision.med.utah.edu](http://www.webvision.med.utah.edu)). Image used with a non-exclusive rights under a Attribution, Noncommercial, No Derivative Works Creative Commons license.

### **1.2.1.1 The structure of the retina**

The retina is an embryological extension of the prosencephalon, making it an excellent model system from which to infer the likely mechanisms of vascular development of the CNS as a whole (Hughes et al., 2000). It is a thin layer of neural tissue that covers the back of the eye (Figure 1-1) and it is responsible for the detection and processing of visual information. It is highly active metabolically, with the highest oxygen consumption rate per gram of any tissue in the body (Warburg, O. 1928), the vast majority which is being used by the photoreceptor layer.

The retina has a highly structured architecture consisting of a pigmented layer and a neural layer. The pigmented layer, the retinal pigment epithelium (RPE), lies between the choroid and the neural layer and is required to absorb light, preventing internal reflection. Its high melanin content also helps protect the choroid against light-induced cell toxicity (Peters et al., 2006). The neural retina is responsible for light detection and transmission of the light impulse to the visual cortex. The retina (pigmented layer and neural layer) is composed of seven major neuronal types and is organised into 10 major layers (Figure 1-2).

In addition to the neuronal cell types present in the retina, Müller glial cells are also present, providing metabolic and homeostatic support and protection of retinal neurons (Dyer & Cepko, 2001; Hoon et al., 2014).

The first retinal layer, the RPE, is the outermost layer, between the photoreceptor layer and the choroid. The RPE consists of pigmented epithelial cells and the functions of the RPE include phagocytosing outer segment discs shed by the photoreceptors, nourishing the photoreceptor cell layer, optimising ion concentration in the surrounding tissues and regeneration of visual pigments (Cai et al., 2000; Gu et al., 2012).

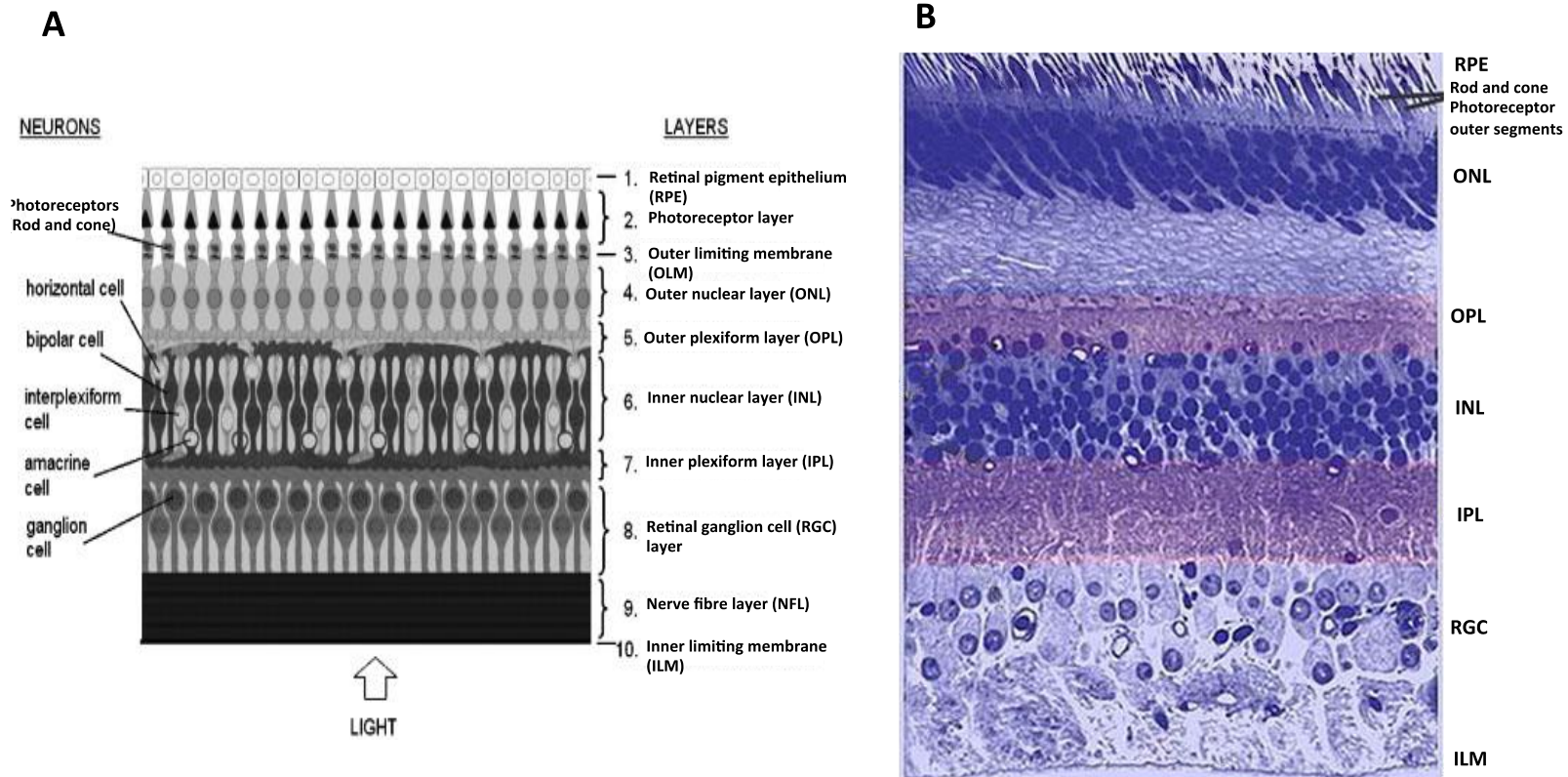


**Figure 1-2: Organisation of neurons and retinal layers in the human retina.**

**A:** Diagram representation of a cross section of the retina. All neuronal cell types and retinal layers are detailed. Image adapted with permission from (Martinez J. et al., 2008). **B:** Light micrograph of a vertical section through central human retina. Image adapted from webvision ([www.webvision.med.utah.edu](http://www.webvision.med.utah.edu)). Image used with a non-exclusive rights under Attribution, Noncommercial, No Derivative Works Creative Commons license.

The next layer is the photoreceptor outer segment layer, containing the cone and rod outer segments. Photoreceptors are photopigment-expressing cells, which mediate light-dependent functions. The photopigments, G-protein coupled receptors (GPCRs) known as opsins, are synthesised in the rod and cone inner segments then transported to the light-sensitive outer segments. The opsins translate captured photons into electrical signals by binding to their ligand, a retinal-derived chromophore, together forming a light-sensitive photopigment (Nathans, 1999; Nickle and Robinson, 2007). Rods are responsible for vision in low light via rhodopsin, detecting wavelengths of light of around 500nm. Cones are responsible for colour vision and for high-acuity foveal vision, and are classified into three subtypes, each one containing a different opsin absorbing at a different wavelength of light. Short-wavelength (blue) opsin absorbs light between 358 and 425 nm. The other two opsin types detect medium-wavelength (green) and long-wavelength (red) light of approximately 530 and 560 nm respectively (Nathans, 1999; Nickle and Robinson, 2007).

The outer nuclear layer (ONL) contains the nuclei of rods and cones. Immediately after this is the outer plexiform layer (OPL), consisting of a synaptic region connecting the photoreceptors with the bipolar cells to allow transmission of nerve impulses. The inner nuclear layer (INL) is composed of the bipolar cells which transmit the signal from the photoreceptors to the retinal ganglion cells via the second synaptic region known as the inner plexiform layer (IPL). In the INL lateral connections are made through horizontal and amacrine cells, which modulate the signalling pathway from photoreceptors to ganglion cells (Dyer and Cepko, 2001). The nerve impulse arriving at the ganglion cells is then transmitted from the eye to the brain via the axons of the retinal ganglion cells, which form the nerve fibre layer then progress to become the optic nerve. The innermost layer is the inner limiting membrane, providing a physical barrier between the transparent vitreous humour filling the eye cavity and the neural retina. The integrity of the inner limiting membrane is important for ganglion cell layer survival (Halfter et al., 2005).

## **1.2.2 General features of eye development**

The formation of the human eye takes place between the third and the tenth week of embryonic development (Larsan's 2015). The eye develops from several embryonic tissue layers. First, the neuroepithelium gives rise to the optic vesicle and optic cup, which eventually form the RPE, the neural retina, the non-neural ciliary body and the iris structures including the smooth muscles. Second the surface ectoderm develops into the lens, the corneal epithelium, conjunctiva and the eyelid skin. Third, the mesenchyme forms the extraocular muscles and the orbital and ocular vascular endothelium (Larsan's 2015). See Figure 1-1 for the anatomy and structure of the eye and Figure 1-3 for eye development.

The formation of the optic sulcus in the prosencephalic neural groove is the first morphologic evidence of the eye. This occurs 22 days after fertilisation. The optic sulcus appears in the neural folds on both sides of the developing forebrain. The evagination of the neural tube, together with the formation of out-pocketings of the optic sulcus and enlargement of these, give rise to the optic vesicles that extend toward the surface ectoderm approximately at day 28 of gestation (Larsan's, 2015; Tottora and Derrickson, 2005). The next event is the formation of the optic cup. The optic vesicle and lens placode interact, leading to invagination of the neuroectoderm, which forms the optic cups. These consisting of two layers, the neural retina and the RPE (Graw, 2003). Shortly after, at around 5 weeks of gestation, the lens placode separates from the surface ectoderm which eventually detaches to form the lens (Figure 1-3).

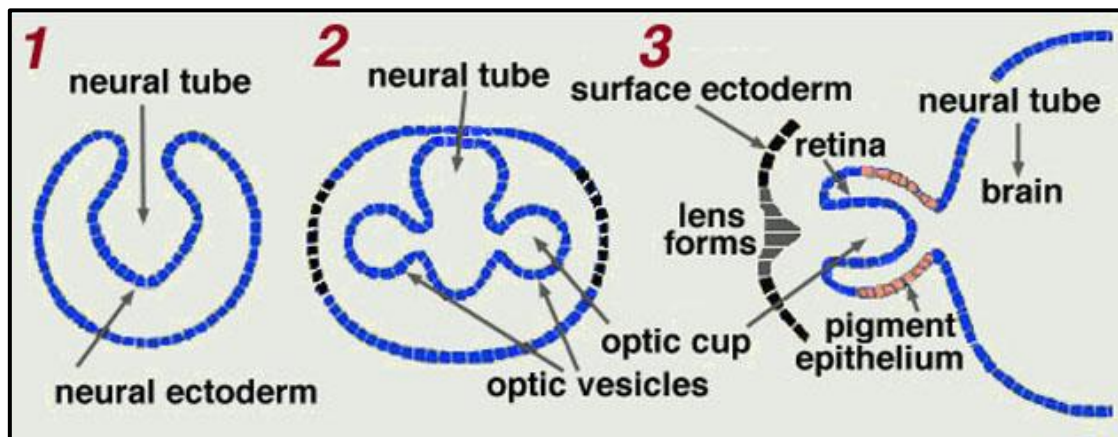


**Figure 1-3: Embryonic development of the human eye.**

During development of the embryo, the eye develops from the optic vesicles which form at both sides of the developing neural tube (1-2). The optic cups develop from the primordial optic vesicles, with the inside of the cup forming the retina and the outside forming a single monolayer of epithelium known as retinal pigment epithelium. The lens vesicles detach to form the lens from the surface ectoderm (3). Image from [webvision \(www.webvision.med.utah.edu\)](http://www.webvision.med.utah.edu). Image used with non-exclusive rights under an Attribution, Noncommercial, No Derivative Works Creative Commons license.

The mesenchyme layer surrounding the developing eye differentiates to form the choroid from the inner layer and the sclera and cornea from the outer layer (Tottora and Derrickson, 2005). The cornea forms just after the detachment of the lens placode to make a transparent multi-layered structure (Graw, 2003). The inner wall of the optic cup forming the neural retina starts to undergo retinal differentiation at around day 47 after gestation, and full development continues until the ninth month of gestation, with the fovea becoming fully functional only after birth (Graw, 2003). The definitive retinal structure and the cell layers of the mature retina are produced in an evolutionarily conserved order: ganglion cells, cone photoreceptors and horizontal cells are produced first; amacrine cells and rod photoreceptors are next; and Müller glia and bipolar cells are the last to differentiate (Larsen's 2015) (See Figure 1-2 for retinal structure).

At around 48 days of gestation, axons begin to form from the retinal ganglion cells (RGCs) and grow along the inner wall of the optic stalks to the brain, forming the optic nerves. The optic nerves join to form an X-shaped structure called the optic chiasm before entering the brain (Larsen's, 2015).

### **1.2.3 The vasculature in the developing eye**

There are two main sources of vascularisation in the developing eye: the choroid layer surrounding the eye and the transient hyaloid vasculature (Larsen's, 2015). The choroidal vasculature resides immediately beyond the RPE and supports the ONL, RPE and photoreceptors. The inner part of the eye is initially metabolically supported by the hyaloid vasculature. In later stages of development the vascularisation of the retina starts as the hyaloid vasculature regresses. The retinal vasculature emerges from the optic nerve and goes on to form the stereotyped architecture of the three parallel retinal layers at three different depths in the retina (Section 1.3). The switch from hyaloid vasculature into retinal vasculature occurs during the final trimester of gestation in humans and at around birth in mice (Fruttiger, 2007; Larsen's, 2015).

### **1.3 Retinal Vascularisation**

The retinal vasculature in the fully developed human eye is a uniform vascular plexus composed of three parallel layers of vessels that are joined by fine capillaries (Fruttiger, 2007; Ye et al., 2010). However the process by which the individual vascular plexus layers are laid down, and whether this is achieved by vasculogenesis or angiogenesis, is still under investigation. Vasculogenesis is *de novo* formation of vessels from vascular endothelial precursor cells, whereas angiogenesis is the sprouting of vessels from vasculature that is already present (Hughes et al., 2000). The most widely accepted hypothesis at this time suggests that the primary plexus on the vitreal surface of the retina is developed by vasculogenesis while the deeper vascular layers develop later by angiogenic sprouting of the primary plexus. Therefore the retinal vasculature is mainly formed by angiogenesis but vasculogenesis is also thought to play a lesser role (Scott McLeod et al., 2006).

### 1.3.1 The hyaloid vasculature

Early in development, the retina is avascular and the inner part of the eye is nourished by the choroidal and hyaloid vasculature. In humans, the hyaloid vasculature develops during the sixth or seventh weeks of gestation (Hasegawa et al., 2008) and it is maximally developed after 10 weeks of gestation (Zhu et al., 2000). The hyaloid vasculature is a temporary arterial network in the vitreous between the lens and the retina. Blood is supplied by the central hyaloid artery, which begins in the optic nerve and runs into the vitreous. The blood then exits the hyaloid vascular system via an annular collection vessel found at the anterior of the eye called the choroidal vein (Fruttiger, 2007). As the retina develops and gets thicker, the hyaloid vasculature regresses and the retinal vascular plexuses start to develop (Figure 1-4).

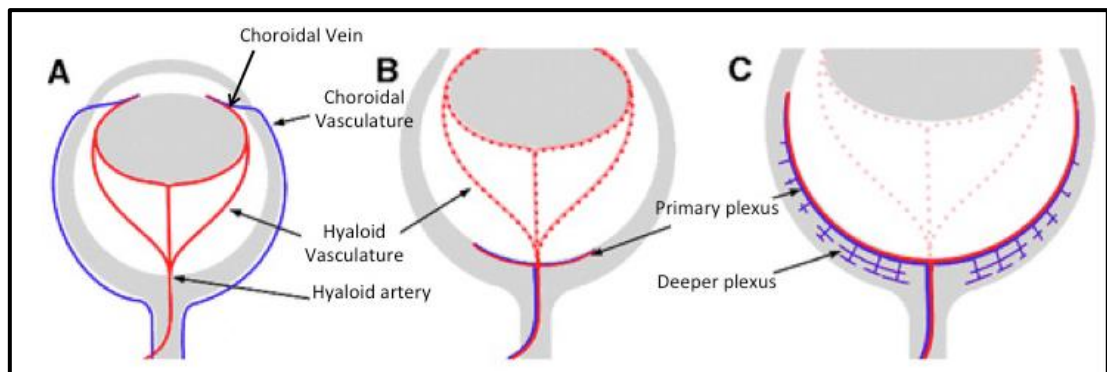


**Figure 1-4: Regression of the hyaloid vasculature in the human eye.**

**A:** The hyaloid artery found in the optic nerve supplies the blood for the hyaloid vascular net. The hyaloid vasculature runs through the vitreous cavity and surrounding anterior segment structures before draining into the choroidal veins. Choroidal vasculature is shown in blue **B:** The hyaloid vasculature regresses as the primary retinal plexus develops. **C:** The deeper retinal vascular plexus develops from the existing primary plexus. Image adapted with permission from (Fruttiger, 2007).

The regression of the hyaloid vasculature is partly controlled by macrophages secreting factors to trigger cell death in the endothelium, such as Wnt7b mediated signalling through the Frizzled-4 (FZD4) receptor expressed in the hyaloid capillaries (Lang and Bishop, 1993; Lobov et al.,

2006). More recently, retinal neurons and vascular endothelial growth factor (VEGF) signalling through vascular endothelial growth factor receptor 2 (VEGFR2) have also been shown to participate in this process. Neonatal neurons sequestering VEGF and binding to VEGFR2 causes endothelial apoptosis, which mediates the switch from the foetal to the postnatal vasculature system (Yoshikawa et al., 2016).

Failure of hyaloid vessel regression causes persistent hyperplastic primary vitreous (PHPV), which impairs visual function (Silbert and Gunwood, 2000). Failure of hyaloid vascular regression is also found in mice with mutations in *Fzd4*, Norrie disease protein (*Ndp*), Low-density lipoprotein receptor-related protein 5 (*Lrp5*) and Tetraspanin-12 (*Tspan12*) (Xu et al., 2004; Richter et al., 1998; Kato et al., 2002; Junge et al., 2009), as described later in more detail in section 1.4.2.

### **1.3.2 Vasculogenesis**

#### **1.3.2.1 General features of vasculogenesis**

Vasculogenesis is the process of *de novo* formation of blood vessels from endothelial precursor cells which proliferate, migrate and come together to form primitive tube-like vessels. The tube-like vessels then differentiate into endothelial cells, forming a vascular lumen and depositing a basal lamina (Patel-hett and Amore, 2011). Formation of blood vessels by vasculogenesis normally occurs in developing organs of endodermal origin such as lung, pancreas and heart (Beck and D'amore, 1997) and to a lesser degree in the retina, forming the primary plexus at the inner surface of the retina (Chan-ling et al., 2004; Hughes et al., 2000; Scott McLeod et al., 2006).

Less is understood about the molecular mechanisms controlling vasculogenesis than those controlling angiogenesis, but it has been reported that fibroblast growth factors (FGFs), hedgehog morphogens, VEGF, neuropilins and Transforming Growth Factor- $\beta$  (TGF- $\beta$ ) are all required for the correct formation of blood vessels by vasculogenesis (Patel-hett and Amore, 2011).

### **1.3.2.2 Vasculogenesis in the retina**

The retina is an extension of the brain, and therefore vascularisation of the retina was expected to occur mainly by angiogenesis as is the case in the brain (Risau W 1997). Evidence suggesting vasculogenesis in the foetal human retina came from the observation of mesenchymal precursors in the developing retina before the in-growing vasculature developed (Ashton, 1970). The presence of spindle-shaped vascular precursor cells, angioblasts, in the developing retina was later confirmed, first in dogs (McLeod et al., 1987) and most recently in humans. This was achieved using Nissl-stained whole-mount preparations (Hughes et al., 2000) and with the identification of ADPase/CD39 and CXCR4 markers in retinal vasculature precursor cells (Chan-ling et al., 2004; Scott McLeod et al., 2006; Hasegawa et al., 2008).

In the centre of the retina the vascular precursor cells aggregate to form putative vascular cords, a critical step for early vasculogenesis (Hughes et al., 2000). However detection of VEGFR2, which is a marker for developing endothelial cells ( Yamashita et al., 2000; Yamaguchi et al., 1993) has not been reported yet in the human retina. The lack of retina specific endothelial precursor cell markers makes it difficult to confirm the presence of endothelial precursor cells in the developing blood vessels of the inner retina, and as a result there is controversy around this matter (Gariano, 2003; Urbich and Dimmeler, 2004). In contrast, in the mouse retina no vascular precursors cells have been found, suggesting that vascularisation of the mouse retina is achieved exclusively by angiogenesis and is driven by “endothelial tip cell” expression in the growing vascular network (Fruttiger, 2001; Gariano, 2003; Gerhardt et al., 2003).

### **1.3.3 Retinal astrocytes form a template for angiogenesis**

Prior to the development of the retinal vasculature by angiogenesis, astrocytes emerge from the optic nerve head and disperse to the inner surface of the retina, developing an astrocyte network that will be used as a

template to form the retinal vasculature (Chan-ling et al., 2004; Fruttiger et al., 1996; Stone and Dreher, 1987). There is a direct correlation between the presence of astrocytes in the retina and the development of the retinal vasculature. It is known that the retinal astrocyte network and retinal vascularisation are highly associated because absence of retinal astrocytes correlates with avascular retinas (Stone and Dreher, 1987). Similarly, highly vascularised retinal areas correlate with high levels of astrocytes, while in avascular areas such as the fovea, astrocytes have not been detected (Schnitzer, 1987).

An astrocyte precursor population found in the optic nerve and expressing the transcription factor *Pax2* is the astrocyte precursor lineage that will form the retinal astrocyte network (Chu et al., 2001). These astrocyte precursors give rise to two astrocyte lineages, the optic nerve and retinal astrocytes. Retinal astrocytes express platelet derived growth factor receptor alpha (PDGFR $\alpha$ ), which is the earliest marker distinguishing between retinal and optic nerve astrocytes (Mudhar et al., 1993). These start to proliferate upon stimulation by the platelet derived growth factor A (PDGFA) ligand, which is secreted by retinal ganglion cells (Fruttiger et al., 2000). Retinal astrocytes continue to proliferate in response to PDGFA ligand stimulation and they reach the retinal periphery, establishing a mesh-like network that will be used as a template for the development of the retinal vasculature. At this stage the mesh-like astrocytes express glial fibrillary acidic protein (GFAP), which is used as a retinal astrocyte marker, whereas *Pax2* staining is used as an astrocyte precursor marker (Scott McLeod et al., 2006).

Astrocytes experience hypoxia before the formation of blood vessels. This induces expression of VEGF driven by hypoxia, which promotes angiogenesis (Stone and Dreher, 1987). The formation of the blood vessels providing oxygen to the astrocyte environment in turn reduces hypoxia, negatively regulating VEGF expression and consequently astrocyte proliferation, suggesting a negative feedback loop between astrocytes and vascular development in the retina (West et al., 2005).

### 1.3.4 Angiogenesis

#### 1.3.4.1 General features of angiogenesis

Angiogenesis, the process by which vessels sprout from a pre-existing vasculature, is the most common mode of blood vessel formation during late embryogenesis and in adults and is highly controlled by VEGF and Dll4/Notch signalling pathway (Tammela et al., 2011; Hellström et al., 2007). Blood vessels are lined by endothelial cells, which differentiate into specialized cell types with distinct phenotypes during angiogenesis; tip and stalk cells exhibiting different gene expression profiles (Smet et al., 2009). VEGF and Notch pathway are critical for the specification of endothelial cells into tip and stalk cells during sprouting angiogenesis. First a “tip cell” expressing VEGFR2 develops, emerging from its parent blood vessel and becoming the leading cell of the sprouting vessel. This process is controlled by a chemotactic VEGF gradient, which stimulates tip cells to produce protrusions (Fantin et al., 2010). The tip cells produce long filopodia that extend towards areas with high levels of VEGF (Gerhardt et al., 2003; Jakobsson et al., 2010). Not all the endothelial cells stimulated with VEGF become tip cells, and this is depended on the activity of Dll4/Notch signalling. Under VEGF stimulation, Dll4 expression is up-regulated in the tip cells. In turn, Dll4 ligand activates Notch signalling in the stalk cells, which consequently supresses the tip cell phenotype in adjacent cells by reducing VEGFR2 expression and increasing VEGFR1 expression. Using *in silico* and mouse models, Jakobsson et al., showed that cells with high levels of *Vgfr2* and low levels of *Vgfr1* are more likely to become a tip cell, whereas cells containing low levels of *Vgfr2* and high levels of *Vgfr1* are likely to become stalk cells (Jakobsson et al., 2010). The stalk cells rapidly proliferate, extending vessel length and creating the lumen through which blood will flow (Fantin et al., 2010) (Figure 1-5). Therefore, Notch signalling determines the ability of individual cells to become tip or stalk cells within the sprout.

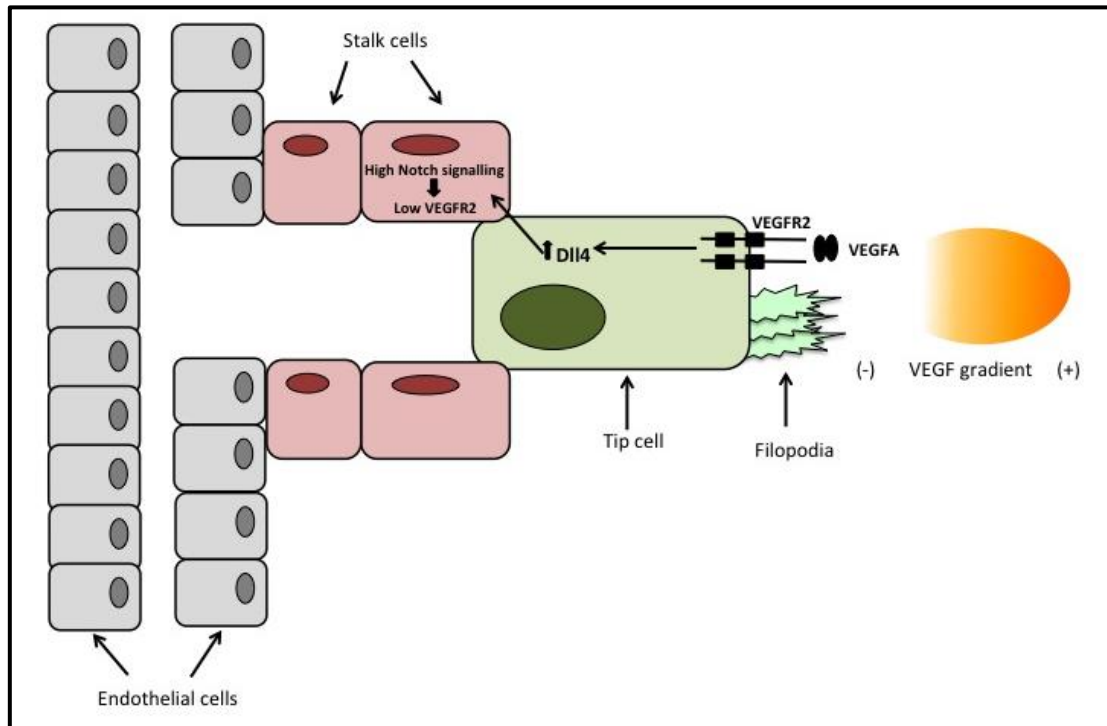


**Figure 1-5: Vascular sprouts are guided by tip/stalk cell specification.**

Schematic representation of a tip cell (green) extending filopodia towards an angiogenic stimulus (orange VEGF gradient), followed by stalk cells (red) proliferating and extending the blood vessel. VEGFA interacts with VEGFR2 expressed at the cell surface of the tip cell. This interaction up-regulates Dll4 expression in tip cells, up-regulating Notch signalling in stalk cells and suppressing the tip cell phenotype.

Direct evidence for the implications of VEGF and Notch signalling in sprouting angiogenesis comes from the study of knockout mice models. Homozygous deletion of VEGFA or any of the VEGFR occurs in embryonic lethality as a consequence of abnormal vascular development (Dumont et al., 1998; Fong et al., 1995; Shalaby et al., 1995). Similarly, Notch signalling deficient mice also occurs in embryonic lethality (Krebs et al., 2000). Interestingly, embryonic lethality has also been observed with heterozygous deletion of VEGFA and Dll4 (Carmeliet et al., 1996; Gale et al., 2004), suggesting the essential and unique role of both proteins during sprouting angiogenesis.

The final step of angiogenesis is the joining of vessels to create new circuits in the established vascular network, known as anastomosis. This occurs

when macrophages express Tie2 and Neuropilin-1, which attract filopodia from two sprouting vessels in order to join them together (Fantin et al., 2010).

#### **1.3.4.2 Sprouting angiogenesis of the retinal vasculature**

The two intraretinal capillary beds, the inner and outer deeper retinal plexuses, develop by angiogenesis from the pre-existing primary vascular plexus in a process mediated by VEGF. Studies have shown the expression of VEGF and its receptors VEGFR1 and VEGFR2 by Müller cells in the INL, suggesting that angiogenic sprouting of the deeper retinal plexus is driven by VEGF produced by Müller cells (Saint-geniez et al., 2008). The deeper plexus of the retinal vasculature starts developing in the centre of the retina and it expands towards the periphery by developing vertical angiogenic sprouts from the primary plexus (Gariano et al., 1994; Provis, 2001). Angiogenic sprouts penetrate the retina perpendicularly to the primary plexus in process independent of retinal astrocytes, in contrast to the formation of the primary vascular plexus, giving rise to the deeper retinal vascular plexus.

The cellular and molecular mechanisms controlling sprouting of the primary plexus to form the deeper retinal plexus are still under investigation. Mouse models in which the deeper retinal vascular plexus is affected have been studied in order to better understand the formation of the intraretinal capillary beds. Mice lacking Angiopoietin-2 (*Ang2*), a vascular growth factor, presented with complete absence of the deeper retinal vascular plexus, while maintained the primary vascular plexus with just a slight delay in the development of the primary vascular plexus. Additionally, *Ang2*<sup>-/-</sup> mice presented absence of ischemia-induced neovascularisation and persistence of the hyaloid vasculature (Hackett et al., 2002). Similarly, knockout mice with loss of function mutations in *Fzd4*, *Ndp*, *Lrp5* and *Tspan12* lack the two intraretinal capillary beds flanking the INL (Xu et al., 2004; Richter et al., 1998; Kato et al., 2002; Junge et al., 2009). This suggests that the Norrin- $\beta$ -Catenin signalling pathway, components of which these genes encode, plays an important role in the development of the deeper retinal plexus, as described in section 1.5.4 (Junge et al., 2009; Wang et al., 2012; Xu et al.,

2004). Interestingly, these mice also presented with disruption of hyaloid vessel regression (section 1.4.2), suggesting that formation of the deeper retinal vascular plexus and regression of the hyaloid vasculature are functionally linked and modulated by the same signalling pathways.

## **1.4 Familial exudative vitreoretinopathy (FEVR)**

FEVR (MIM #133780) is a rare inherited retinal disorder characterised by hypovascularisation of the peripheral retina, causing sight-threatening manifestations. FEVR was first described by Criswick and Schepens in 1969. They described FEVR as an inherited retinal disease with many clinical features in common with retinopathy of prematurity (ROP) (Criswick VG et al., 1969).

### **1.4.1 Clinical features of FEVR**

FEVR is a heterogeneous disorder presenting with a variety of clinical phenotypes. The primary clinical feature is avascularity of the peripheral retina, which alone usually causes no clinical symptoms (Toomes and Downey, 1993 [updated 2008], Benson 1995). Peripheral retinal avascularity in FEVR is the minimum defining clinical feature of a highly variable ocular phenotype. The premature arrest of the retinal vasculature in the peripheral retina leads to retinal ischemia, which can cause secondary complications. These secondary phenotypes include neovascularisation, development of hyperpermeable blood vessels, dragging of the macula, vitreoretinal traction, exudates, retinal folds and retinal detachments (Benson, 1995; Ranchod et al., 2011). Some of these clinical features are represented in Figure 1-6.

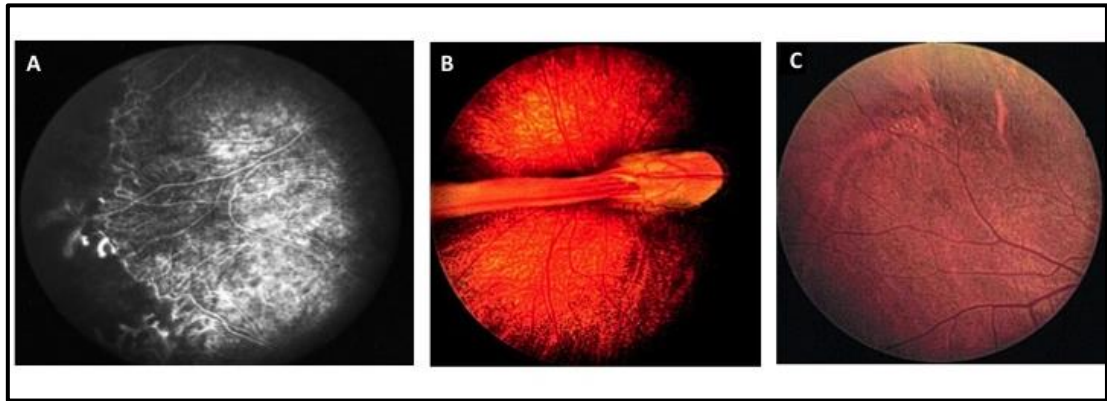


**Figure 1-6: Clinical appearance of FEVR.**

**A:** Avascularisation of the peripheral retina is observed in a fluorescein angiogram of an FEVR patient. **B:** Optic nerve and macula in an FEVR patient, viewed through a dilated pupil. The retinal vessels are dragged together into a retinal fold. **C:** Presence of exudates (yellow dots) in the peripheral retina of an FEVR patient. Macula and optic nerve (not seen in this image) appeared normal in this patient. Pictures were provided by Dr. Carmel Toomes.

The most severely affected patients are often diagnosed blind during infancy. Some mildly affected patients have no visual problems throughout life, presenting only a small area of avascularity in the peripheral retina (Toomes and Downey, 1993 [updated 2008]). The variability in both phenotype and disease severity observed among FEVR patients has led clinicians to use the term “FEVR phenotype spectrum” when studying the clinical features associated to the disease.

FEVR phenotype also varies widely among patients from the same family. Individuals with the same mutation present with a wide range of severities, ranging from asymptomatic cases to patients with retinal detachments (Robitaille et al., 2009). Furthermore, FEVR features can occur with a degree of symmetry between both eyes or the condition can be completely unilateral (Gal et al., 2014; Gilmour, 2015). Intravenous fluorescein angiography (IVF) is normally used in order to detect the minimal FEVR phenotype in asymptomatic carriers (Canny and Oliver, 1976). In addition to the variability in the FEVR clinical spectrum, the disease is also genetically heterogeneous. It can be inherited in three different modes of inheritance, as described in section 1.4.2. Studying the genetics of FEVR has helped further our

understanding of the processes driving retinal vascular development, as explained in section 1.5.

### 1.4.2 Genetics of FEVR

FEVR is a rare inherited retinal disorder that is genetically heterogeneous (Toomes et al., 2005; Qin et al., 2005). It can occur with autosomal-dominant (adFEVR, MIM# 133780), autosomal-recessive (arFEVR, MIM# 601813), or X-linked (MIM# 305390) inheritance, with autosomal dominant FEVR being the most common form. The identification of genes mutated in FEVR patients led to the identification and characterisation of a highly conserved Wnt signalling pathway known as the Norrin- $\beta$ -Catenin signalling pathway, described in more detail in section 1.5.

The FEVR loci (EVR loci) mapping to genes involved in Norrin signalling pathway are detailed in Table 1-1.

FEVR locus	Region	Gene	Reference
<b>EVR1</b>	11q13-23	<i>FZD4</i>	(Li et al., 1992; Robitaille et al., 2002)
<b>EVR2</b>	Xp11.22	<i>NDP</i>	(Berger et al., 1992; Chen et al., 1993)
<b>EVR3</b>	11p12-13	See section 1.8	(Downey et al., 2001)
<b>EVR4</b>	11q13	<i>LRP5</i>	(Toomes et al., 2004a, 2004c)
<b>EVR5</b>	7q31-31	<i>TSPAN12</i>	(Junge et al., 2009; Nikopoulos et al., 2010a; Poulter et al., 2010)

**Table 1-1: FEVR loci for the FEVR genes implicated in Norrin- $\beta$ -Catenin signalling pathway.**

The EVR loci is indicated for every corresponding gene along with their regions mapping into the chromosomes.

Three genes encoding components of Norrin- $\beta$ -Catenin signalling pathway have been found to harbour mutations causing autosomal dominant FEVR, namely the *FZD4*, *LRP5* and *TSPAN12* genes (Gong et al., 2001; Nikopoulos et al., 2010; Poulter et al., 2010; Robitaille et al., 2002; Toomes et al., 2004). These genes are also mutated in patients with the recessive form of FEVR

(Gal et al., 2014; Jiao et al., 2004; Poulter et al., 2012; Downey et al., 2006; Khan et al., 2016). Patients with recessively inherited FEVR tend to have a severe early onset form of the condition, or are diagnosed with retinal dysplasia, suggesting that FEVR severity can be influenced by gene dosage (Poulter et al., 2012). In addition, mutations in *NDP* have been identified in an X-linked form of FEVR (Chen et al., 1993).

The identification of mutations in these four genes in FEVR patients, together with the phenotype consistently observed in mice in which any one of these genes have been knocked out (section 1.4.3), suggests that vascularisation of the peripheral retina is controlled by a highly conserved and specific molecular pathway (the Norrin- $\beta$ -Catenin signalling pathway), which is involved in retinal vascular development (Junge et al., 2009; Xu et al., 2004; Ye et al., 2009). This signalling pathway is similar to, and shares many components with, the Wnt- $\beta$ -Catenin signalling pathway. These signalling pathways are described in section 1.5 and section 1.6.

Interestingly, mutations in the *NDP* gene can also cause X-linked Norrie disease (ND, MIM #310600). ND patients, like those with FEVR, present with retinal hypovascularisation, retinal retraction and persistence of the hyaloid vasculature (Berger and Ropers, 2001). However, ND patients also have mental retardation and hearing loss. Another condition sharing many phenotypic features with FEVR is Retinopathy of Prematurity (ROP), a leading cause of blindness in children exposed to high oxygen exposure after being born prematurely with immature lungs. Disruption of the hypoxia driving retinal vascular development in these children causes retinal hypovascularisation and VEGF overproduction, which in turn induces neovascularisation. Although ROP is normally thought to be none-genetic, missense mutations in the *NDP* gene have been associated with ROP (Shastry et al., 1997).

Similarly, As well as being a cause of FEVR in some cases, mutations in *LRP5* can also cause osteoporosis–pseudoglioma syndrome (OPPG; MIM #259770). This is a rare autosomal recessive disorder characterised by bone

weakness and reduced bone mass, together with ocular features such as retinal hypovascularisation resembling those observed in ND patients (Gong et al., 2001; Ai et al., 2005).

Other genes found to be mutated in FEVR patients have also been described, but whether and how they contribute to the Norrin signalling pathway remains to be determined.

Mutations causing recessive FEVR have been identified in the transcription factor atonal homolog 7 (*ATOH7*). *ATOH7* is required for the formation of the retinal ganglion cell layer (Brown et al., 2001). Knocking out *lak* (the zebrafish *ATOH7* homolog) results in the absence of a retinal ganglion cell layer in zebrafish (Kay et al., 2001). The primary ocular defects observed in human patients with mutations in *ATOH7* are most likely to be due to the absence of retinal neuronal cells (Khan et al., 2012). However, persistence of the hyaloid vasculature, which is one of the common clinical features of FEVR, and retinal dysplasia, were also phenotypes observed in these patients (Khan et al., 2012).

Mutations in *KIF11* have also been reported as causing autosomal dominant FEVR (Robitaille et al., 2014). These authors suggested that mutations in *KIF11* cause a spectrum of phenotypes ranging from classical FEVR to microcephaly, chorioretinal dysplasia and mental retardation. *KIF11* is a kinesin family member and is a motor protein required for spindle development and mitotic progression (Kenneth et al., 1992). Recently, a study published by Costa and colleagues reported that asymmetric positioning of the mitotic spindle during endothelial tip cell division generates randomized tip or stalk daughter cells (Costa et al., 2016). This investigation suggests that the vascular abnormalities observed in FEVR patients with *KIF11* mutations could be the result of disorganisation in the formation of endothelial cells due to abnormal positioning of the mitotic spindle before division.

Missense mutations in the *ZNF408* gene, encoding a zinc finger transcription factor, have been associated with autosomal dominant FEVR. A missense variant was identified in *ZNF408*, and Morpholino (MO) studies in zebrafish showed a link between *znf408* and the development of the vasculature in zebrafish. Furthermore, this variant p.(His455Tyr) acted with a dominant-negative effect, retaining the wild-type (WT) ZNF408 protein in the cytoplasm (Collin et al., 2013).

More recently, heterozygous frameshift mutations in *RCBTB1* have also been reported as a cause of FEVR. Knockdown of *rcbtb1* in zebrafish using MO resulted in vascular abnormalities in the developing fish. Furthermore, the authors showed a possible role for RCBTB1 in Norrin signaling by regulating the nuclear accumulation of  $\beta$ -Catenin (Wu et al., 2016b).

Interestingly, recessive mutations in *ZNF408* and *RCBTB1* have also been found in patients with the progressive photoreceptor degeneration Retinitis pigmentosa (RP) (Avila-fernandez et al., 2015; Coppieters et al., 2016).

Screening of the genes implicated in FEVR to date, described above, solves only around 50% of FEVR cases. This may be due to mutations in known genes being missed due to limitations in the screening methods used, but may also suggest that other genes mutated in FEVR remain to be discovered (Nikopoulos et al., 2010).

### **1.4.3 Mouse models of FEVR**

Knockout (KO) mice lacking *Ndp*, *Fzd4*, *Lrp5* and *Tspan12* all share a phenotype characterised by absence of the deeper retinal plexuses, together with intraocular haemorrhage and delay of hyaloid vasculature regression (Xu et al., 2004; Richter et al., 1998; Kato et al., 2002; Junge et al., 2009; Berger et al., 1996). This resembles the clinical features observed in FEVR patients (section 1.4.1).

Norrin mutant mice model (*Ndph*) was first produced by removing the coding sequence of exon 2 (Berger et al., 1996). The investigation of female hemizygous (-/ ) mice revealed fibrous masses in the vitreous and disorganisation of the retinal ganglion cells. The retinal vasculature was also found to be abnormal, with irregular distribution of vessels in the central and peripheral retina (Richter et al., 1998). Additionally, a significant decrease in the number of blood vessels in the deeper retinal plexus and the persistence of hyaloid vessels was also observed (Luhmann et al., 2005).

*Fzd4*<sup>-/-</sup> was first created by Wang and colleagues (Wang et al., 2001). These mice showed defects in the cerebellum, cochlea and oesophagus. After the identification of *FZD4* as an FEVR gene, the *Fzd4*<sup>-/-</sup> mice were again examined for a retinal phenotype (Xu et al., 2004). Homozygous mutant mice displayed large abnormal vessels on the surface of the retina and a lack of vasculature in the two intraretinal beds. Vessels were also seen in the vitreous suggesting a failure in hyaloid vasculature regression. Abnormal vasculature was also observed in the cochlea of the ear and a reduction in blood vessel density in the cerebellum. These mice shared very similar phenotype to *Ndph* KO mice. Condition knockout of *Fzd4* showed that it was the lack of Fzd4 protein specifically in the retinal endothelial cells that caused the retinal defects observed in *Fzd4*<sup>-/-</sup> mice (Ye et al., 2009). The phenotype of the mice included a complete lack of intraretinal capillaries and some vessels penetrating into the retina and terminating in ball-like clusters and intraocular haemorrhaging. Interestingly, the retinal phenotype was not observed when conditional knockout of *Fzd4* was performed in vascular smooth muscle cells and pericytes or retinal neurons and glia. These findings suggested that the defects observed in *Fzd4*<sup>-/-</sup> mice are consequence of deficient Norrin signalling in endothelial cells. Interestingly, Mice producing ectopic Norrin were also created by Ye and colleagues. These mice presented growth retardation and had severely disorganized embryo and yolk sac vasculature. The defects caused by Norrin overproduction are fully suppressed in *Fzd4*<sup>-/-</sup> mice and partially suppress in *Fzd4*<sup>+/-</sup> mice suggesting that in embryonic vasculature biology Fzd4 is the major receptor for Norrin. In addition, REC from *Fzd4*<sup>-/-</sup> mice cultured in matrigel were unable to create

capillary-like networks. Interestingly, when WT and *Fz4*<sup>-/-</sup> RECs were plated together on Matrigel, many of the *Fz4*<sup>-/-</sup> RECs adopted a more differentiated morphology and were incorporated into the WT capillary-like network (Ye et al., 2009). This cooperative behavior is similar of the in vivo integration of some *Fz4*<sup>AP/-</sup> RECs into normal appearing capillaries when mutant and WT RECs are in close proximity.

Kato and colleagues generated *Lrp5*<sup>-/-</sup> mouse and they described a defect in osteoblast proliferation and regression of the hyaloid vasculature (Kato et al., 2002). The retinal vasculature of *Lrp5*<sup>-/-</sup> mice was leaky in homozygous, but not heterozygous, mutant mice. Furthermore, the retinal vasculature in the deeper intraretinal beds was missing, especially in the outer plexiform layer (Chen et al., 2011; Xia et al., 2010). Interestingly, *Lrp5* KO mice manifest a milder retinal phenotype when compared to *Fzd4* or *Ndp* KO mice. In some cases *Lrp5* KO mice have small capillary networks surrounding the INL, which suggests there may be partial compensation for lack of *Lrp5* through the action of its closely related coreceptor *Lrp6* (Ye et al., 2009).

Junge and colleagues created *Tspan12*<sup>-/-</sup> mice, which showed delayed centrifugal outgrowth of the vasculature of the nerve fibre layer and a lack of vasculature in the two intraretinal beds (Junge et al., 2009). The homozygous mice also presented microaneurisms extending from the nerve fibre layer to the inner nuclear layer, highly fenestrated retinal vessels and delayed of hyaloid vasculature regression.

## 1.5 Norrin-β-Catenin signalling

The identification of mutations in *FZD4*, *LRP5*, *TSPAN12* and *NDP* in FEVR patients led to the characterisation of a new signalling pathway known as the Norrin-β-Catenin signalling pathway, also referred to as the Norrin/Frizzled-4 pathway (Xu et al., 2004; Junge et al., 2009; Ye et al., 2010). This pathway has many similarities to the Wnt-β-Catenin pathway, including the involvement of a Frizzled receptor acting together with an LRP5/6 coreceptor

in order to transduce the signal after ligand binding (Clevers and Nusse, 2012) (section 1.6.2).

However there are also a number of specific differences between the Norrin and Wnt pathways. Norrin, instead of Wnt, acts as a ligand for the pathway, and it binds only to the FZD4 receptor and no other Frizzled receptors (Smallwood et al., 2007). The other difference found in the Norrin pathway is the enhancement of the pathway by an auxiliary protein TSPAN12, which most likely induces receptor clustering (Junge et al., 2009). To date, while TSPAN12 has been associated in Norrin signalling, none Tetraspanins have been associated with Wnt signalling. The expression of the Norrin pathway components in tissues and within the retina is detailed in Table 1-2.

Due to the wide expression of *Fzd4* in the retina, which is expressed in ECs, Mural cells, photoreceptors and a subset of inner retinal neurons, Ye and colleagues performed cell type specific deletion of *Fzd4* in mice (Ye et al., 2009). Deletion of *Fzd4* in Mural cells and in most or all retinal neurons and glia showed no changes in retinal vasculature morphology. By contrast, deletion of *Fzd4* in endothelial retinal cells occurred in complete absence of intraretinal capillaries. In addition, vessels penetrating from the vitreal surface terminating in ball-like clusters and intraocular hemorrhages were commonly found in these mice. These retinal phenotypes closely resemble those seen in *Fzd4*<sup>-/-</sup>, *Lrp5*<sup>-/-</sup> and *Ndp*<sup>-/-</sup> mice, indicating that the defective *Fzd4* signalling in retinal endothelial cells is responsible of the vasculature defects observed in these mice.

	Tissue	Retina
<b>Norrin</b>	Eye, ear, brain (Berger et al., 1996)	INL and GCL (Berger et al., 1996) It is produced by Müller cells (Ye et al., 2009)
<b>FZD4</b>	Ubiquitously expressed in humans (The Human Protein atlas, <a href="http://www.proteinatlas.org">http://www.proteinatlas.org</a> )	Photoreceptors (Wang et al., 2001) RECs, Mural cells and subset of inner retinal neurons (Ye et al., 2009)
<b>LRP5</b>	Ubiquitously expressed in humans (The Human Protein atlas, <a href="http://www.proteinatlas.org">http://www.proteinatlas.org</a> ) Osteoblasts, liver, pancreas, skin brain and ocular macrophages (Kato et al., 2002)	INL (specifically in Müller cells) and in vessels near GCL (Xia et al., 2010) Newly formed retinal blood vessels (Chen et al., 2011)
<b>TSPAN12</b>	Ubiquitously expressed in humans (The Human Protein atlas, <a href="http://www.proteinatlas.org">http://www.proteinatlas.org</a> ) Meningeal vasculature and smooth muscle cells in neonatal intestine (Junge et al., 2009)	Neonatal retinal vasculature (Junge et al., 2009)

**Table 1-2: Expression of Norrin pathway components in tissue and retina.**

The expression of the Norrin pathway components has been studied in mouse models. The human expression pattern can be accessed through The Human Protein atlas, (<http://www.proteinatlas.org>). INL: inner nuclear layer, GCL: ganglion cell layer, RECs: retinal endothelial cells.

### 1.5.1 Activation of the Norrin- $\beta$ -Catenin pathway

The binding of the Norrin ligand to the receptor complex FZD4/LRP5/TSPAN12 at the cell membrane transduces a molecular signal inside the cell that prevents the destruction of  $\beta$ -Catenin in the cytoplasm (see section 1.5.3). The cytoplasmic C-terminus of LRP5 binds Axin with the aid of glycogen synthase kinase 3 beta (GSK3 $\beta$ ) (Mao et al., 2001). Consequently, the destruction complex is captured and bound to the cell membrane along with Dishevelled (DVL), which binds the cytoplasmic tail of FZD4. Therefore  $\beta$ -Catenin is no longer phosphorylated and targeted for

degradation. Instead it accumulates in the cytoplasm and translocates into the nucleus of the cell, where it interacts with the T-cell factor (TCF)/Lymphoid enhancing factor (LEF) family of transcription factors to turn on the expression of Norrin target genes (Figure 1-7).

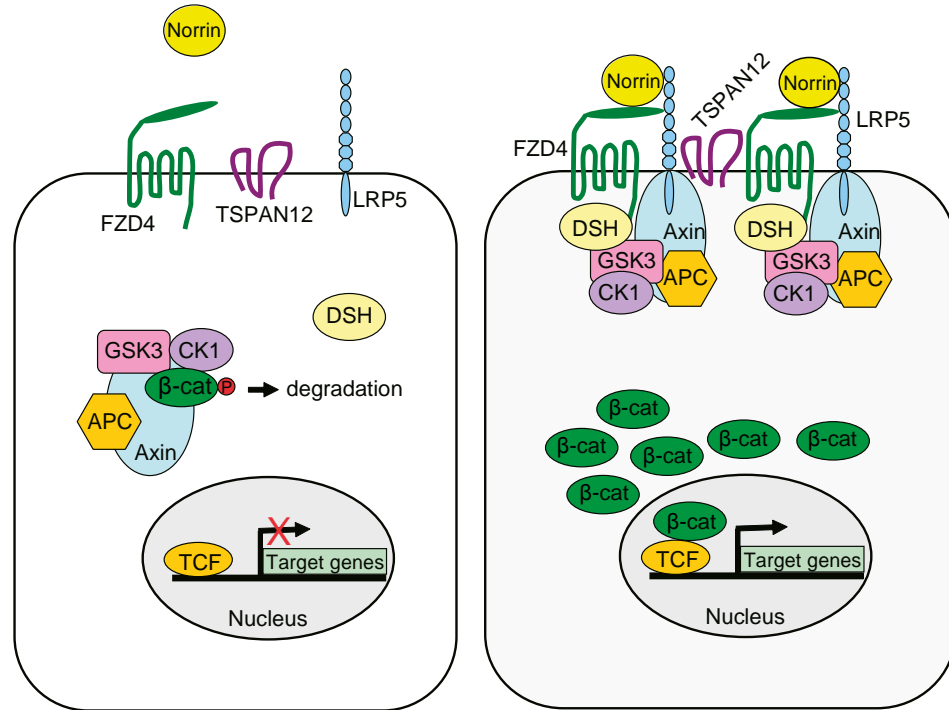


**Figure 1-7: The Norrin-β-Catenin signalling pathway.**

On the left, when Norrin is not bound to the FZD4/LRP5/TSPAN12 receptor complex, β-catenin is targeted by the destruction complex, phosphorylated and degraded in the cytoplasm and the target genes are not transcribed. On the right, when Norrin binds to the FZD4 receptor complex, β-catenin accumulates in the cytoplasm and translocates into the nucleus where it binds to the TCF transcription factor, leading to transcription of target genes. Figure provided by Dr. Carmel Toomes.

Norrin is a secreted protein that belongs to the cysteine knot growth factor superfamily. It has homology to transforming growth factor-β (TGF-β) (Meitinger et al., 1993). Crystal structure analysis of Norrin revealed its novel dimeric structure, which is required for activation of the FZD4 receptor and for the assembling of the Norrin complex consisting of FZD4, LRP5/6 and TSPAN12 in order to undergo signal transduction (Chang et al., 2015; Ke et al., 2013).

Norrin binds to FZD4 through the extracellular amino-terminal cysteine-rich domain (CRD) of FZD4, which is also the site of Wnt binding (Chang et al., 2015; Smallwood et al., 2007). The presence of LRP5/6 is also required in the ligand-receptor complex to initiate signalling. Interestingly, Norrin does not seem to have a preference for LRP5 over the homologous LRP6 in enhancing the pathway (Xu et al., 2004). Even though Norrin binding to LRP5/6 has not been reported yet, a possible Norrin binding site for LRP5/6 has been described and this differs from Norrin-FZD4 binding site (Ke et al., 2013; Chang et al., 2015).

### **1.5.2 The role and regulation of $\beta$ -Catenin**

The Norrin pathway, like the Wnt- $\beta$ -Catenin dependent pathway, regulates the amount of  $\beta$ -Catenin translocating into the nucleus and interacting with TCF/LEF family of transcription factors in order to activate expression of the target genes. The dysregulation of  $\beta$ -Catenin levels in retinal endothelial cells is believed to lead to the FEVR disease phenotype (Junge et al., 2009; Ye et al., 2009).

$\beta$ -Catenin is not just a component of the Norrin/Wnt signalling pathways. It was independently discovered in 1980s by two groups, each describing different functions within the cell to it. The first function described for  $\beta$ -Catenin, as described above, was as a transcription factor in the nucleus (Wieschaus and Riggelman, 1987). However, two years later it was also found to function in cell adhesion and structure in epithelial cells, by binding to E-cadherin (Ozawa et al., 1989). This “double” function of  $\beta$ -Catenin suggests that the complex mechanism by which  $\beta$ -Catenin is regulated within the cell may involve different signalling pathways. In this thesis  $\beta$ -Catenin is studied with regard to its role as the nuclear effector triggering activation of Norrin/Wnt target genes.

Phosphorylation is the main process regulating  $\beta$ -Catenin levels in the cytoplasm and the resultant signal transduction.  $\beta$ -Catenin can get phosphorylated by different kinases at different sites in the protein. The

position where it gets phosphorylated will determine if  $\beta$ -Catenin is triggered for degradation, or if it enhances signalling of the Norrin/Wnt pathways by weakening the interaction between E-cadherin and  $\beta$ -Catenin and therefore releasing more  $\beta$ -Catenin in the cytoplasm to transduce the signal (Valenta et al., 2012). Thus phosphorylation of  $\beta$ -Catenin is a crucial step in regulating Norrin/Wnt signalling.

### **1.5.3 Degradation of $\beta$ -Catenin in the absence of Norrin binding**

In the absence of the Norrin (or Wnt) ligand, signalling is not activated in the cell. As a result,  $\beta$ -Catenin is phosphorylated and targeted for degradation through the  $\beta$ -Catenin destruction complex, which keeps the levels of  $\beta$ -Catenin low (Kimelman and Xu, 2006). In this situation the Norrin pathway target genes remain repressed (Figure 1-7).

Axin is the main component of the destruction complex, providing a scaffold for the other components, adenomatous polyposis coli (APC), casein kinase 1 alpha (CK1 $\alpha$ ) and GSK3 $\beta$ . Axin and APC become phosphorylated when GSK3 $\beta$  binds to Axin, allowing enhanced binding of circulating  $\beta$ -Catenin (Lee et al., 2003).  $\beta$ -Catenin binds to the destruction complex and is phosphorylated at four specific sites containing serine/threonine by GSK3 $\beta$ . The phosphorylated  $\beta$ -Catenin is subsequently joined by the destruction complex and is detected by  $\beta$ -TRCP ( $\beta$ -transducin repeat-containing protein), which is part of the SCF complex containing Cul1, Skp1 and F-box, bound to an E2 ubiquitin-conjugating enzyme. This binding facilitates the ubiquitination and degradation of  $\beta$ -Catenin (Figure 1-8) (Kimelman and Xu, 2006). Thus in the absence of Norrin (or Wnt),  $\beta$ -Catenin intercellular levels and pathway activation levels remain low.

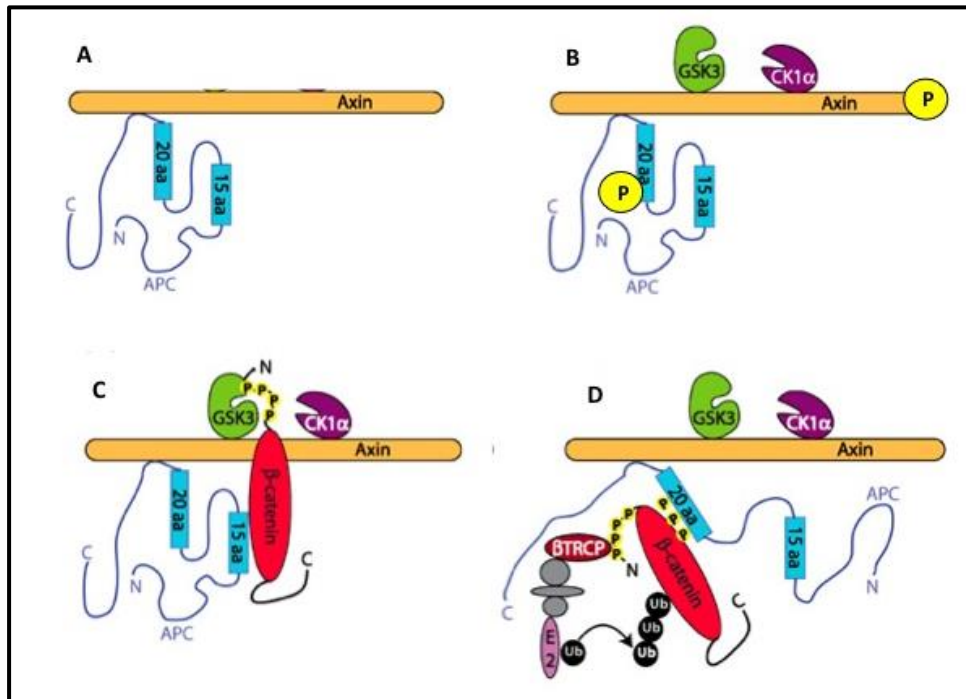


**Figure 1-8: The  $\beta$ -Catenin destruction complex in the absence of Norrin.**

**A:** Initially Axin and APC bind together. **B:** Axin and APC become phosphorylated after GSK3 and CK1 $\alpha$  join the destruction complex. **C:**  $\beta$ -Catenin binds to the destruction complex and gets phosphorylated at four specific sites by GSK3. **D:** Phosphorylated  $\beta$ -Catenin is targeted for degradation after ubiquitination by an E2 ligase. Image adapted with permission from (Kimelman and Xu, 2006).

#### 1.5.4 The role of the Norrin- $\beta$ -Catenin pathway

The Norrin/Frizzled-4 pathway has been shown to regulate the development of the retinal vasculature (Junge et al., 2009; Kato et al., 2002; Luhmann et al., 2005; Rehm et al., 2002; Xu et al., 2004; Ye et al., 2009). *Fzd4* is expressed in neuronal and vascular cells in the retina. Despite its widespread expression, Norrin/Frizzled-4 signalling has been shown to be particularly important in endothelial cells (ECs), since conditional EC-*Fzd4* knockout mice present with the same retinal phenotype as *Fzd4* and *Ndp* KO mice. In addition, *Fzd4* mutant retinal ECs (RECs) are unable to form capillary-like structures when cultured in Matrigel (Ye et al., 2009). Norrin signalling in the retina modulates multiple aspects of retinal vascular development such as proliferation, migration and invasion of endothelial cells. Furthermore, it mediates the maintenance of the integrity of the blood brain barrier (BBB) and blood retinal barrier (BRB), and it has been shown to be involved in the

regulation of neural-endothelial cell communication in the cerebellum (Wang et al., 2012).

As well as the role of the Norrin signalling pathway in retinal vascular development, Norrin and its receptor complex have also been shown to modulate angiogenesis in the colorectal cancer tumour microenvironment by promoting endothelial cell motility and contributing to the formation of branching points in endothelial cells (Planutis et al., 2014). This suggests that the Norrin pathway in endothelial cells may play multiple roles, modulating angiogenesis in other environments beyond the retina.

More recently, loss of Norrin/Frizzled-4 signalling in a *Ptch*<sup>+/-</sup> cerebellar medulloblastoma (MB)-like tumour mouse model was found to accelerate MB formation by creating a tumour-permissive stroma with progression to tumour malignancy. This suggests a novel tumour inhibitory role for Norrin/Frizzled-4 signalling (Bassett et al., 2016). The authors of the study also suggested that the Norrin/Frizzled-4 pathway mediates neural-endothelial crosstalk within the MB and tumour microenvironment. Furthermore, *Ndp*<sup>-/-</sup> *Ptch*<sup>+/-</sup> tumours, when compared to *Ptch*<sup>+/-</sup> tumours, exhibited up-regulation of Pecam1, the angiogenic regulator Ang2 and other components of endothelial cells, suggesting increased vascularity in the *Ndp*<sup>-/-</sup>; *Ptch*<sup>+/-</sup> tumours.

A question that still remains under investigation is the spatial distribution of the Norrin ligand. The well-studied Wnt family member Wingless in *Drosophila* requires a gradient of concentration for its role in tissue patterning (Han et al., 2005). Similarly, a short-range Wnt gradient in intestinal stem cells has been visualised *in vivo* and shown to be crucial for the maintenance of intestinal organoids (Farin et al., 2016). This confirms the short-range gradient mechanism of action of Wnt proteins previously proposed by other researchers (Alexandre et al, 2014; Goldstein et al., 2006; Thorpe et al., 1997). In contrast, Norrin is produced by Müller glia in the developing retina and no spatial gradient was observed with an alkaline phosphatase (AP) reporter gene knocked-in at the *Ndp* locus (Ye et al., 2009). Furthermore, the presence of exogenous Norrin in the lens is sufficient to restore the vascular

defects observed in *Ndp* KO mice (Ohlmann et al., 2005) suggesting that Norrin, unlike other Wnt ligands, does not form a spatial concentration gradient.

### **1.5.5 Other proteins involved in Norrin signalling**

Insights into other proteins involved in Norrin signalling came from a study of gene expression changes in *Lrp5*<sup>-/-</sup> retinas when compared to WT retinas. The genes with most altered expression in *Lrp5*<sup>-/-</sup> retinas were cell adhesion proteins, and genes involved in vessel growth and morphogenesis (Chen et al., 2012). Chen and colleagues found that the tight junction protein Claudin5 (Cldn5) is downregulated in *Lrp5*<sup>-/-</sup> retinas. Interestingly Cldn5 has been shown to be an endothelial specific protein playing a critical role in maintaining BRB (Campbell et al., 2009). Furthermore, a previous experiment from the same group showed that intraocular injections of Cldn5 antibody into wild-type mice resulted in significantly delayed retinal vascular growth in the superficial layer of the retina (Chen et al., 2011), suggesting that the tight junction protein Cldn5 is required for correct vascularisation of the mouse retina. Similarly Slc38a5, a sodium coupled neutral amino acid transporter expressed mainly in Müller cells, ganglion cells and endothelial cells, is also down-regulated in *Lrp5*<sup>-/-</sup> mice retinas (Chen et al., 2012). These findings confirmed the earlier report of a 22 fold decrease in Slc38a5 expression in Müller cells in the *Lrp5* mutant retinas (Xia et al., 2010). This reduction in levels of Slc38a5 is also seen in *Ndp*<sup>-/-</sup> retinas (Schafer et al., 2008), suggesting a role for this molecule in Norrin/Frizzled-4 signalling.

Ye and colleagues performed a targeted micro-array comparison of RNA from yolk sacs of E8.5 WT mice and E8.5 mice over-expressing Norrin (Ye et al., 2009). The results showed that ubiquitous expression of Norrin causes vascular disorganisation in the embryo. Furthermore, this study found that the high-motility group (HMG) box transcription factor Sox17 was over-expressed in the over-expressing Norrin mice. Further confirmation was obtained by studying *Fzd4*<sup>-/-</sup> mouse RECs, which showed a decrease in Sox17 expression compared to WT RECs. Interestingly, the addition of

Sox17 to *Fzd4*<sup>-/-</sup> RECs in an *in vitro* angiogenesis assay restored the number of capillary-like structures formed to wild-type levels (Ye et al., 2009). Furthermore *Lrp5*<sup>-/-</sup> mouse retinas had reduced Sox17 mRNA expression (Chen et al., 2011). These findings suggest that Sox17 is a major mediator of the angiogenic program controlled by Norrin/Frizzled-4 signalling. The mouse *SoxF* genes-*Sox7*, *Sox17* and *Sox18* have overlapping and redundant roles in controlling vascular growth, differentiation and remodelling. These genes have been shown to be regulated by Norrin signalling but not by VEGF signalling. This is shown by the stable expression of *SoxF* family members in EC-specific deletion of VEGF coreceptor Neuropilin-1 (*Nrp1*) mice. In contrast, *Ndp* KO retinas had reduced *SoxF* gene expression in EC (Zhou et al., 2015). Similarly, *Sox18* is down-regulated in *Lrp5*<sup>-/-</sup> retinas (Chen et al., 2012), further supporting the requirement of *SoxF* family members for normal EC function in the adult peripheral vasculature and implicating Norrin/Frizzled-4 signalling as a *SoxF* regulatory pathway (Zhou et al., 2015).

## 1.6 The Wnt signalling pathway

Wnt signalling is an ancient and evolutionarily conserved signalling pathway that is required for the correct development of all metazoans. Cellular proliferation, cell polarity, morphogenesis and the maintenance of stem cells are all processes regulated by Wnt signalling (Clevers and Nusse, 2012). This molecular pathway has been a major topic for scientific research for over 30 years. The complexity of Wnt signalling is due to the multitude of Wnt and Frizzled combinations possible, which regulate different aspects of development. Additionally, the recent identification of regulatory components and pathway crosstalk further show the complexity of this pathway. This section gives a general overview of the pathway, with a particular focus on the Wnt- $\beta$ -Catenin pathway and the implications of this signalling in vascularisation.

### 1.6.1 Wnt signalling pathway classification

Wnt signalling is divided into two major subtypes referred to as the Canonical and Non-Canonical Wnt signalling pathways. Both pathways are activated by the binding of a Wnt ligand to a Frizzled receptor to trigger transduction of the signal. The canonical subtype is the  $\beta$ -Catenin dependent pathway (Wodarz and Nusse, 1998), whereas non-Canonical Wnt signalling is independent of  $\beta$ -Catenin. There are two  $\beta$ -Catenin independent pathways; the Wnt/ $\text{Ca}^{2+}$  pathway and the planar cell polarity (PCP) pathway (Figure 1-9).

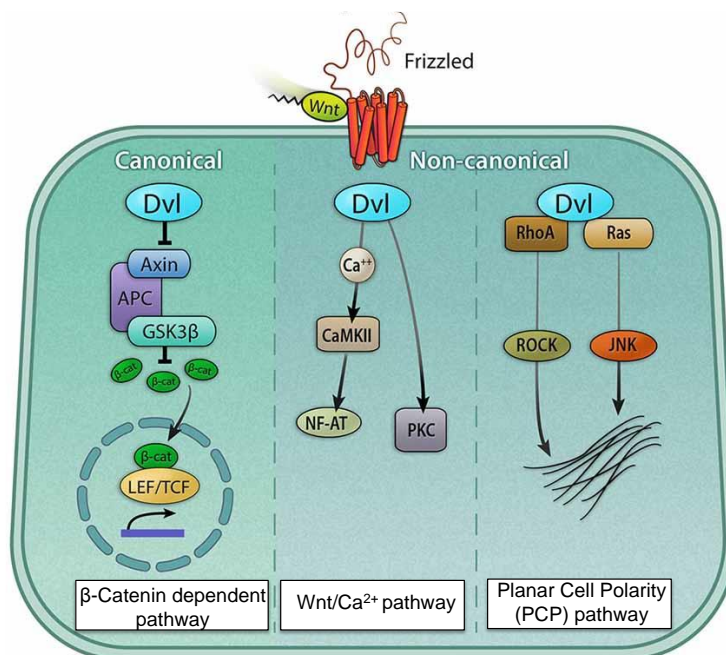


**Figure 1-9: Canonical and Non-canonical Wnt signalling pathways.**

Wnt signalling has been subdivided into canonical and non-canonical pathways. The activation of both pathways is dependent on the Wnt ligand binding to a Frizzled receptor. On the left the Canonical  $\beta$ -Catenin dependent pathway is represented. Binding of Wnt to a Frizzled receptor leads to the translocation of  $\beta$ -Catenin into the nucleus where it binds to the TCF/LEF transcription factor, resulting in upregulation of Wnt target genes. The middle pathway shows Wnt/ $\text{Ca}^{2+}$  signalling through intracellular calcium, which modulates migration and cell fate. The PCP pathway shown on the right is mediated by the GTPases RhoA and Ras with effects on the cytoskeleton assembly. Image adapted from (Jansson et al., 2015) and used under the terms of the Creative Commons Attribution License (CC BY).

The first one induces  $\text{Ca}^{2+}$  release and activation of calmodulin-dependent protein kinase (CaMKII) or protein kinase C (PKC) to ultimately activate

genes involved in migration and cell fate (Kuhl et al., 2001). The planar PCP pathway, also classified as Non-Canonical, activates signals through the GTPases RhoA and Ras, which activates downstream effectors Rho-associated kinase (ROCK) and N-terminal kinase (JNK) to promote tissue polarity, cell morphology changes and cytoskeleton rearrangements (McEwen and Peifer, 2000) (Figure 1-9).

Most recently the old Canonical and Non-Canonical nomenclature is increasingly being discontinued by researchers, who instead refer to these as variants of a single molecular pathway which gets activated by Wnt ligands binding to Frizzled receptors. It is important to note that these Wnt pathway “branches” are not exclusive one from the other, but rather they are coupled together with simultaneous cross-talk occurring between them (Florian et al., 2013).

The main pathway of relevance to FEVR and to this thesis is the Norrin- $\beta$ -Catenin signalling pathway, which is a variation of the Wnt- $\beta$ -Catenin dependent pathway described in Section 1.5. The main features of the Wnt- $\beta$ -Catenin dependent pathway and the implications for vascularisation are therefore described in this section.

### **1.6.2 The Wnt- $\beta$ -Catenin heterodimeric receptor complex and pathway activation**

The first indication of the existence of this pathway was discovered in 1980 with the identification of the *Wingless (wg)* gene in *Drosophila*, which controls polarity and tissue patterning (Nüsslein-Volhard and Wieschaus, 1980). Later, the *wg* gene was found to be a homolog of *Wnt1* in mice (Rijsewijk et al., 1987). Some years later still, the identification of TCF/LEF transcription factors as Wnt nuclear effectors (Molenaar et al., 1996), Frizzleds as Wnt receptors (Bhanot et al., 1996) and LRP5/6 as coreceptors (Wehrli et al., 2000) led to the characterisation of a molecular signalling pathway controlling many aspects of development (Clevers and Nusse, 2012).

In mammalian genomes there are 19 Wnt genes. Wnt proteins serve as ligands for one or more of the 10 Frizzled receptors present in the human genome, in a promiscuous interaction, since a single Wnt can bind multiple Frizzled receptors and vice versa (Bhanot et al., 1996).

When Wnt ligand binds to the CRD domain of the Frizzled receptor (Dann et al., 2001; Janda et al., 2012), Frizzled receptors cooperate with a single transmembrane protein LRP5/6 to transduce the signal (Pinson et al., 2000; Tamai et al., 2000). Different binding sites for Wnt in LRP6 have been described using monoclonal antibodies against LRP6. Surprisingly, these antibodies antagonised or enhanced the pathway depending on the Wnt ligand used, suggesting different interaction sites of Wnt with LRP6 (Gong et al., 2010). In order to transduce the signal, Wnt ligand binds to both LRP6 and FZD, inducing a conformational change followed by phosphorylation of LRP5/6 by CK1 $\alpha$  and GSK3 $\beta$  and the formation of a signalosome containing the receptor complex, Axin, DVL, CK1 $\alpha$  and GSK3 $\beta$  (Bilic et al., 2007). The binding of Axin at the cytoplasmic tail of LRP5/6 regulates the Axin destruction complex and  $\beta$ -Catenin phosphorylation and degradation (detailed in section 1.5.3) (Tamai et al., 2004). The interaction between Axin and LRP5/6 is facilitated by DVL interacting at the cytoplasmic part of the Frizzled receptor, which is thought to promote the formation of the Frizzled-LRP5/6 receptor complex to transduce the signal (Chen et al., 2003).

Wnt binding to Frizzled and LRP5/6 receptor complex triggers disassembly of the  $\beta$ -Catenin destruction complex. As a result,  $\beta$ -Catenin accumulates in the cytoplasm and translocates into the nucleus where it interacts with the TCF/LEF family of transcription factors to turn on expression of target genes, as described for the Norrin activating Norrin/Frizzled-4 signalling pathway.

### **1.6.3 R-spondins (RSPOs) activate the Wnt- $\beta$ -Catenin pathway**

RSPOs are members of a large family of secreted proteins characterised by the presence of thrombospondin repeats (TSRs) in combination with two N-terminal Furin repeats (Lau et al., 2012). RSPO proteins are evolutionarily

conserved and are present in all deuterostomes. The four secreted RSPO proteins (RSPO1-4) act as agonists of Wnt ligands, inducing upregulation of the Wnt- $\beta$ -Catenin signalling pathway.

The first hint of RSPOs enhancing the Wnt- $\beta$ -Catenin pathway came from an expression screen in early frog embryos that found *Rspo2* as an activator of the pathway acting upstream of Wnt proteins, at the level of receptor-ligand binding. The authors also reported that blocking of Wnt-LRP5/6 interaction by DKK1 abolished RSPO-induced activation of Wnt signalling (Kazanskaya et al., 2004). Kim and colleagues generated transgenic mice in which *Rspo1* was constitutively secreted by circulating lymphocytes. These mice had increased expansion of their intestinal crypts. In the same study *Rspo1* was shown to enhance Wnt signal strength by stabilising  $\beta$ -Catenin and phosphorylation of the Wnt coreceptor Lrp6 (Kim et al., 2005).

*Rspo* deficient phenotypes are consistent with disrupted Wnt signalling, which gave insights into the implications of these secreted proteins in Wnt signalling. Mutations in *RSPO1* cause a rare human syndrome with X female-to male sex reversal (Parma et al., 2006). A similar phenotype was observed in *Rspo1* knockout mice (Tomizuka et al., 2008) and in *Wnt4*<sup>-/-</sup> mice (Yao et al., 2004). Vascular defects in the placenta in *Rspo3* knockout mice (Aoki et al., 2007; Kazanskaya et al., 2008) resemble the vascular phenotypes in *Wnt2*<sup>-/-</sup> mice (Monkley et al., 1996a) and *Fzd5* knockout mice (Ishikawa et al., 2001). Absence of fingernails and toenails in humans is known as onychia and it is a genetic disorder caused by mutations in *RSPO4* (Blaydon et al., 2006). Similarly, mutations in either *FZD6* or *Wnt10A* mutations are associated with nail defects (Adaimy et al., 2007; Frojmark et al., 2011).

Together, the RSPO functional studies and the genetic studies supported the role of these secreted proteins in Wnt- $\beta$ -Catenin signalling. However the receptor for RSPO through which this action was mediated remained unknown for many years. Frizzled-8 (FZD8) and LRP6 were first described as the receptor complex pair triggering *Rspo3* mediated Wnt- $\beta$ -Catenin

signalling (Nam et al., 2006). Similarly, RSPO1 was suggested to induce phosphorylation of LRP6 and to be a high affinity ligand for LRP6 to transduce signal (Wei et al., 2007).

It was not until 2011 when the RSPO receptors were finally characterised and proven to be a subclass of Leucine-rich repeat containing G-protein-coupled receptors denoted LGR4, LGR5 and LGR6 (LGR4-6), which are members of the GPCR family (section 1.7.1). Physical binding of RSPOs to LGR4 and LGR5 when expressed on the surface of cells, together with further biochemical experiments revealed high-affinity interactions of LGR4-5 and RSPOs (Carmon et al., 2011). In an independent study, Lau and colleagues found LGR4 and its homolog LGR5 to be receptors for RSPO1 using mass spectrometry (Lau et al., 2011), confirming the results obtained by Carmon and colleagues. All four RSPOs were found to bind LGR4-6 with high affinity and to increase phosphorylation of LRP5/6. A third study identified LGR4-6 as RSPO receptors using a genome-wide siRNA screen. They suggested that receptor internalisation occurred by Clathrin mediated endocytosis, implying that receptor internalisation plays a role in RSPO and LGR signalling (Glinka et al., 2011). A further study confirmed the LGR4-5 and RSPOs as a ligand-receptor pair, enhancing the Wnt- $\beta$ -Catenin signalling pathway (Ruffner et al., 2012).

#### **1.6.3.1 E3 ubiquitin ligases regulate Wnt- $\beta$ -Catenin signalling through an LGR4/5/6 and R-spondin pair**

The regulation of Wnt- $\beta$ -Catenin signalling became still more complicated with the identification of two highly homologous Wnt target genes belonging to the E3 ubiquitin ligases: ring finger protein 43 (RNF43) and Zinc and ring finger 3 (ZNRF3). In the absence of RSPO, RNF43/ZNRF3 mediate ubiquitination of Frizzled receptors, triggering rapid endocytosis of Wnt Frizzled receptors and LRP5/6 coreceptors and their destruction in lysosomes (Hao et al., 2012; Koo et al., 2012). These E3 ubiquitin ligases are considered to function as negative feedback regulators of Wnt- $\beta$ -Catenin signalling, as RNF43 and ZNRF3 are encoded by Wnt target genes.

Interestingly, an ortholog of RNF43 and ZNRF3 in *C. elegans*, PLR-1, regulates Wnt receptor turnover, suggesting that this regulatory pathway is evolutionarily conserved, as is the entire Wnt signalling pathway (Moffat et al., 2014).

The membrane clearance of Frizzled receptors mediated by RNF43 and ZNRF3 is reversed upon addition of RSPO. RSPO binds simultaneously to the extracellular domain of RNF43/ZNRF3 and to LGR4/5/6, resulting in ubiquitination and membrane clearance of RNF43/ZNRF3 and the LGRs (Hao et al., 2012). The presence of RSPO binding to LGR4/5/6 neutralises RNF43/ZNRF3 clearance of Frizzled receptors, allowing the persistence of Frizzled receptors at the cell membrane and boosting Wnt- $\beta$ -Catenin signalling strength (Figure 1-10).

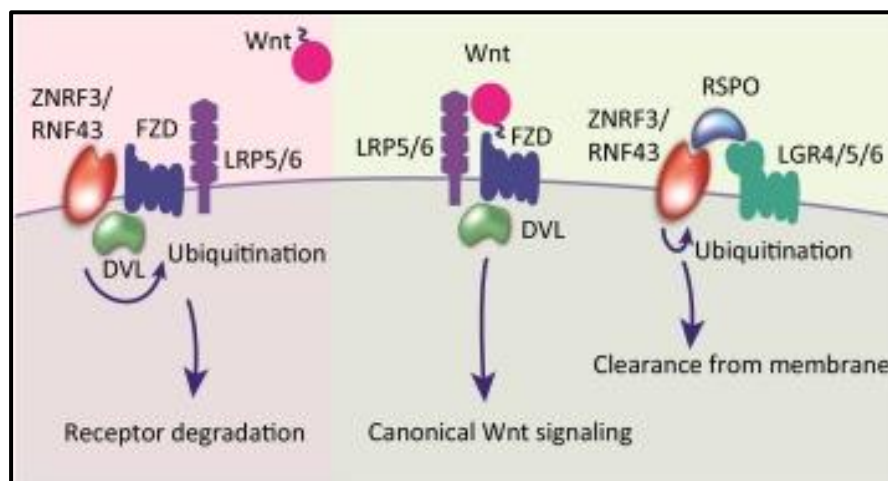


**Figure 1-10: regulation of Wnt receptor degradation by the LGR4-6/RSPO/RNF43/ZNRF3 module.**

On the left (pink shading): In the absence of RSPO, RNF43/ZNRF3 inhibits Wnt signalling by promoting the ubiquitination and consequent degradation of the FZD and LRP5/6 receptor complex. On the right (green shading): The binding of RSPO to LGR4-6 and to RNF43/ZNRF3 promotes the ubiquitination of LGR4-6 and RNF43/ZNRF3, resulting in membrane clearance of this receptor complex. Consequently, Wnt ligand binds to FZD and LRP5/6 receptor complex and Wnt signalling gets activated. Image taken with permission from (Jiang and Cong, 2016).

The mechanism by which ZNRF3/RNF43 recognises Frizzled receptors remains unclear and is still under investigation. Jiang and colleagues

suggested DVL as the link targeting ZNRF3/RNF43 to Frizzled receptors to negatively regulate Wnt signalling (Jiang et al., 2015). DVL is known as a positive regulator of Wnt signalling, triggering formation of the Wnt receptor complex (Kikuchi et al., 2011). DVL KO cells stimulated with RSPO1 had no increase of Frizzled or LRP6 levels at cell surface, whereas WT cells stimulated with RSPO1 had increased cell surface levels of Wnt receptors. Similarly, overexpression of RNF43 resulted in a decrease in the level of Frizzled receptor in the membrane in WT cells, but this effect was abolished in DVL KO cells. These results suggest that DVL is required for the activity of ZNRF3/RNF43 in regulating cell surface levels of Frizzled receptors (Jiang et al., 2015).

#### **1.6.4 Wnt signalling in vascularisation**

As mentioned before, Wnt signalling is implicated in a variety of cellular processes including cell proliferation and polarity, stem cell pluripotency, differentiation and specification. All these processes require the development of vascular structures, which is largely dependent on VEGF. Although the implication of Wnt signalling in the vasculature is quite novel by comparison with the VEGF signalling pathway, an increasing number of studies showing the vasculature implications of this signalling pathway have been reported in recent years (Reis & Liebner, 2013). As described in Section 1.5, Wnt signalling activated by the Wnt agonist Norrin controls the development of the retinal vasculature, which was studied by assessing the vascular phenotype of mice lacking Norrin pathway components. Similarly, most of the evidence for the role of Wnt signalling in the vasculature comes from mouse models with target disruption of Wnt/Frizzled genes.

Mouse models with double *Wnt7a/b* mutations displayed severe abnormalities such as haemorrhaging phenotypes and disorganisation of the endothelium of the CNS. Interestingly, when a single active *Wnt7a* or *Wnt7b* was present no phenotype was observed, suggesting some redundancy of function with respect to *Wnt7a* and *Wnt7b* (Stenman et al., 2008). In *Wnt7a/b* KO embryos the endothelial sprouts invading the CNS failed to elaborate

capillaries and they remained as disorganised EC clusters (Zhou et al., 2009). These EC clusters are similar to the intraretinal vascular sprouts observed in *Ndp*, *Fz4*, *Lrp5* and *Tspan12* KO retinas. Furthermore, *Wnt7b* has also been linked to regression of the hyaloid vasculature by triggering apoptosis and cell death in endothelial cells (Lang and Bishop, 1993; Lobov et al., 2006).

A member of the adhesion GPR family, GPR124, has been shown to activate Wnt signalling via FZD4 and LRP5 in a reporter cell line using Wnt7a or Wnt7b as a ligand (Zhou & Nathans, 2014). This receptor complex controls the development and maturation of EC, promoting angiogenesis in the CNS. In addition, a recent study showed that GPR124/Wnt7a/b dependent Wnt- $\beta$ -Catenin signalling operates at the level of the tip cells during EC invasion in the zebrafish brain. It was demonstrated that this signalling is required for angiogenic sprouting of the zebrafish brain (Vanhollebeke et al., 2015) demonstrating the role of Wnt- $\beta$ -Catenin signalling in regulating endothelial tip cell function.

Targeted deletion of *Wnt2* in mice resulted in reduced foetal capillaries in the placental vasculature, which is consistent with the expression of *Wnt2* in foetal vessels of the placenta (Monkley et al., 1996). Knocking out Frizzled-5 in mice is embryonically lethal (Ishikawa et al., 2001). Heterozygous mice are viable and present with no abnormal phenotype, whereas *Fzd5*<sup>-/-</sup> lethality is due to improper yolk sac and placental angiogenesis, characterised by disorganisation of the capillary plexus. *Wnt4* has also been shown to be involved in the formation of the vasculature in the mammalian gonads, which occurs in a sex-specific manner. In the male a large coelomic vessel grows from endothelial cells, migrating into the gonad, but this vessel is absent in the ovary. *Wnt4*<sup>-/-</sup> homozygous XX embryos were found to have a large ectopic coelomic blood vessel in the ovary, suggested that *Wnt4* represses the mesonephric endothelium in the XX gonad, preventing the formation of male-specific coelomic blood vessels (Jeays-ward et al., 2003).

As well as the retinal vascularisation defects observed in *Fzd4* null mice, they also presented other vascular phenotypes. In these mice the vascularisation of the cochleae in the inner ear progressively degenerated. Similarly the vascularisation of the cerebellum gradually lost its normal morphology leading to progressive neuronal degeneration (Xu et al., 2004; Wang et al., 2001). These phenotypes are not observed in the *Ndp* KO mice, suggesting that other Wnt ligands expressed in the brain can activate *Fzd4* signalling to promote correct vascularisation.

A recent study done by Chen and colleagues demonstrates the role of Wnt signalling in the formation of pathological neovascularisation in retinopathy (Chen et al., 2011). The authors showed that Wnt activity and the expression of Fzd4 receptor and Wnt ligands (Wnt3a, Wnt7a and Wnt10a) are upregulated in pathological neovessels in the retina in a mouse model of oxygen-induced proliferative retinopathy (OIR). Furthermore OIR in mice lacking *Lrp5* or *Dvl2* results in decreased levels of pathological neovascularisation in retinopathy, suggesting that pathological neovascularisation is driven by Wnt- $\beta$ -Catenin signalling. In addition, loss of *Lrp5* results in abnormal retinal vascularisation (Kato et al., 2002). Furthermore, transcription factors *Sox17* and *Sox18* are downregulated in *Lrp5*<sup>-/-</sup> vessels, which equates to the downregulation of *Sox17* in *Fzd4*<sup>-/-</sup> endothelial cells (Ye et al., 2009). This study demonstrated that modulation of Wnt signalling has implications not only in inherited retinal diseases with mutations in Wnt signalling components, but also other retinal vascularisation diseases characterised by pathological vascular growth such as diabetic retinopathy or ROP.

Wnt and Frizzled expression in endothelial cells has also been studied over the past years. Endothelial cells and vascular smooth muscle cells cultured *in vitro* were shown to express Wnt7a, Wnt10b, Wnt5a, FZD1 and FZD3 (Wright et al., 1999). Another study demonstrated FZD4, 5 and 6 and TCF/LEF are expressed in primary endothelial cells. Furthermore, Wnt1 was shown to activate the Wnt- $\beta$ -Catenin signalling pathway and to promote endothelial cell survival and proliferation (Shawber et al., 2005). In addition a

Frizzled related protein, known as sFrp-1, acts as inhibitor of Wnt signalling by binding to FZD4 and FZD7 of cultured endothelial cells and reducing the proliferation of the cultured cells (Duplaa et al., 1999). Taken together these observations implicate Wnt- $\beta$ -Catenin signalling as mediator of endothelial cell growth and survival.

Another group of Wnt components implicated in vascular formation are the R-spondins, the Wnt agonists activating Wnt- $\beta$ -Catenin signalling through LGR4-6 receptors. Through its action on Wnt- $\beta$ -Catenin signalling, Rspo3 was shown to play a critical role in promoting angioblast differentiation and angiogenesis in *Xenopus* and in mice, mediated by its immediate downstream target gene *Vegf*, (Kazanskaya et al., 2008). Similarly, a mutation in *rspo1* in zebrafish (*dtty<sup>135</sup>* strain) results in an abnormal trunk vascular network and presents multiple angiogenic defects. The authors confirmed that *rspo1* promotes angiogenesis during early embryogenesis through Wnt- $\beta$ -Catenin signalling and VEGFC, as expression of *vegfc* is strongly reduced in *rspo1* mutant zebrafish. Furthermore, stimulation of endothelial cells with Wnt3a in culture activates *Vegfc* expression (Gore et al., 2011). More recently, RSPO1 has been shown to be important during testicular morphogenesis and to participate in the formation of the testicular coelomic blood vessel. However it is not clear if this process is mediated by the  $\beta$ -Catenin dependent pathway as  $\beta$ -Catenin staining in the nucleus of testicular cells was never observed (Caruso et al., 2015).

Taking all these findings and observations together, this suggests that the Wnt- $\beta$ -Catenin signalling pathway is implicated in vascularisation in different cell types and at different stages of the development. It is important to note that endothelial cells derived from different cell types may express distinct types of receptors and respond differently to Wnts, explaining the multiple vascular defects observed in mice that are null for various Wnt pathway components. Furthermore VEGF is upregulated by Wnt signalling, and is a potent stimulator of endothelial proliferation, migration and survival (Zhang et al., 2001) linking to some extent these two molecular pathways for vascular remodelling and for the correct development of the vasculature.

## **1.7 Leucine-rich repeat containing G protein-coupled receptor 4 (LGR4)**

LGR4, also known as GPR48, together with LGR5 and LGR6, were orphan receptors until the RSPO secreted proteins were found to act as the ligands of these receptors and to promote Wnt- $\beta$ -Catenin signalling activation through the E3 ubiquitinase ligases, as described in section 1.6.3.1. In this section, an overview of our understanding of the LGR4 receptor and its functions, both prior to and after the identification of RSPOs as the LGR4 ligands, are described.

### **1.7.1 LGR4 is a member of the GPCR family**

GPCRs are a superfamily of receptors that include mammalian neurotransmitter receptors, glycoprotein hormone receptors and cyclic adenosine monophosphate (cAMP) receptors. They are structurally similar in that they all contain 7 transmembrane domains (7TM) (Strader et al., 1994). These are cell surface proteins responding to a variety of stimuli and triggering intracellular response, generally by activating heterotrimeric G-proteins.

The glycoprotein hormone receptors for thyroid-stimulating hormone (TSH), follicle-stimulating hormone (FSH), and leutinizing hormone (LH) are a subgroup of GPCRs with an N-terminal extracellular domain containing leucine-rich repeats (LRR). These repeats are crucial for binding of the glycoprotein hormones. Two new LRR-GPCR receptors were identified and cloned based on the conserved sequences of putative glycoprotein hormone receptors and they were named as LGR4 and LGR5. These two new receptors have 17 LRR, in contrast to the glycoprotein hormone receptors which have only 9 LRR in their ectodomain (Hsu et al., 1998). A few years later, the same group identified a third member of this subfamily with homology and structural similarity to LGR4 and LGR5. It contained 13 LRR and was named LGR6 (Hsu et al., 2000).

Since that time, these 3 receptors LGR4/5/6 have been classified as a subfamily of GPCR receptors containing a large LRR extracellular domain. Protein structure prediction modelling suggested that the LRR domain occurs in a horseshoe-like structure necessary for ligand binding (Kajava, 1998; Xu et al., 2013). These 3 receptors appeared very early in evolution and homologous proteins are found in invertebrates, including the nematode *C. elegans*, the sea anemone and *Drosophila* (Hauser et al., 1997; Notchacker et al., 1993; Kudo et al., 2000) confirming the ancient evolutionary origin of this GPCR subfamily of receptors.

After the identification of further LGR proteins, the LGR receptors were phylogenetically classified in 3 subgroups: the FSH, LH and TSH receptors, known as the glycoprotein hormone receptors (GHR) (Vassart et al., 2004); the relaxin receptor subgroup including LGR7 and LGR8 (Hsu et al., 2002); and the LGR receptor group including LGR4, LGR5 and LGR6. After these subfamilies of receptors were identified, the function and expression of the LGR4 receptor were studied using reverse genetics approaches in mice models in order to elucidate its physiological roles.

### **1.7.2 LGR4 mice models**

Several mutant alleles of mouse *Lgr4* have been generated and studied, and the *Lgr4* expression pattern has been well characterised using these mice models.

Mazerborough and colleagues used the secretory-trap approach for the generation of transgenic *Lgr4* mice (Mazerbourg et al., 2004). The trap vector was integrated into an *Lgr4* intron, causing  $\beta$ -galactosidase fusion protein to be produced, which allowed the expression of *Lgr4* to be studied.  $\beta$ -galactosidase insertions also mutated the trap gene, which created null alleles, allowing the study of *Lgr4* null mice. *Lgr4* expression was determined using *Lgr4*<sup>+/-</sup> fetuses stained with X-gal, which revealed *Lgr4* expression in various tissues including brain, spinal cord, heart, intestine, kidney, adrenal gland, bone and stomach. The expression of *Lgr4* in fetuses was similar to

the *Lgr4* expression pattern that the authors found in adult heterozygous mice. *Lgr4*<sup>-/-</sup> genotype resulted in 60% foetal death and 8 out of 14 surviving null *Lgr4* mice died 1 day after birth, which confirmed the near complete lethality of the *Lgr4* knockout genotype. The most observable morphological abnormality was the reduction in body weight and the intrauterine growth retardation of the *Lgr4* null mice compared to WT mice. *Lgr4* homozygous null mice also presented reduction in absolute organ weight, especially in kidney and liver with a 30% and 40% reduction respectively. These results demonstrated for the first time the importance of *Lgr4* for the survival and development of mice.

A parallel study also used the gene trapping approach for the generation of *Lgr4* heterozygous mice (Schoore et al., 2005). The expression of *Lgr4* was evaluated in *Lgr4*<sup>+/-</sup> mice expressing LacZ and placental alkaline phosphatase (PLAP) after the secretory trap vector was inserted into the first intron of *Lgr4*. The expression pattern found in this study resembles very much the one found by Mazerborough and colleagues. *Lgr4* was found to be expressed in the peripheral and central nervous system, heart, kidney, gonads, bones, hair follicles and cartilages, confirming the findings of the Mazerborough study.

A follow up study using one more time the gene trapping approach applied to *Lgr4* in a different mouse genetic background (CD1 outbred strain) resulted in *Lgr4*<sup>-/-</sup> mice that survived through to adulthood and presented abnormal postnatal development of the reproductive tract (Mendive et al., 2006). The homozygous null mice occurred with expected Mendelian frequencies and no utero or perinatal death was observed, even though a reduction in body weight was measured. Further characterisation of null *Lgr4* adult mice showed a malformation of the reproductive tract and sterility. A similar study to that of Mendive and colleagues was performed, again using the gene trap allele approach (Hoshii et al., 2007). In this study 60% of homozygous mutant mice survived to adulthood. These mice were infertile and had abnormalities in the testis and epididymides, similar to those found by Mendive and colleagues.

Yet another gene trap *Lgr4* mouse allele was generated and the effects on erythropoiesis (Song et al., 2008) and eye development (Weng et al., 2008) were analysed in another study. Foetal livers of the *Lgr4* null mice weighed 41% less than WT mice and these mice also presented with an impairment of definitive erythropoiesis at midgestation, which was correlated with downregulation in the expression levels of c-Myc, cyclin D1 and Activating Transcription Factor 4 (ATF4). These studies showed that *Lgr4* acts through cAMP-PKA-CREB signalling (see section 1.7.3). These mice also presented transient anemia during midgestation, probably due to the erythropoiesis impairment (Song et al., 2008).

The effects of *Lgr4* knockout on the anterior segment structures of the eye were also studied in the *Lgr4* null mice from the Song et al., (2008) study. Mice lacking *Lgr4* had a spectrum of anterior segment dysgenesis (ASD) phenotypes including microphthalmia, iris hypoplasia, cornea dysgenesis and cataracts (Weng et al., 2008). Homozygous *Lgr4* mutant mice presented with downregulation of the transcription factor *Pitx2*, which is a key gene controlling myogenesis and extracellular matrix synthesis in the developing extraocular muscles (Diehl et al., 2006). In addition *Pitx2*<sup>+/-</sup> and *Lgr4*<sup>-/-</sup> mice share similar phenotypes (Weng et al., 2008).

The same *Lgr4* transgenic mice from the Song et al., (2008) and Weng et al., (2008) studies were used to assess the spatial and temporal expression of *Lgr4* in the developing eye (Siwko et al., 2013). At E12.5, *Lgr4* is expressed in a layer of mesenchymal cells but is poorly expressed in the lens and in the outer layer of the optic cup. The *Lgr4* expression pattern in adult *Lgr4*<sup>+/-</sup> mice changes, being expressed in the lens epithelium, ganglion cells of the retina and in the inner nuclear layer.

In addition to the phenotypes described above in this particular *Lgr4* null mouse strain, *Lgr4*<sup>-/-</sup> mice had delayed embryonic bone formation. *Lgr4* was shown to regulate osteoblast differentiation and osteoclast number and activity through the cAMP-PKA-CREB signalling pathway (Luo et al., 2009).

More recently LGR4 has been shown to negatively regulate osteoclast differentiation and bone resorption by acting as a second receptor for Tumour necrosis factor (TNF) superfamily member 11 (TNFSF11), also known as RANKL (Luo et al., 2016). This promiscuous binding of LGR4 to RANKL revealed LGR4 as a novel RANKL receptor, which competes with RANK receptor and acts in a negative feedback loop regulating osteoclast differentiation. RANKL acting through LGR4 induces intracellular calcium release, suggesting that LGR4 activates  $G\alpha q$ - $Ca^{2+}$  signalling in response to RANKL.

All the mouse models described until now were obtained using a gene trap approach, with the introduction of a gene trap vector in the first intron of *Lgr4*. Kato and colleagues generated a conditional knockout mouse by targeted deletion of part of exon 18, which encodes the 7TM domain of Lgr4 implicated in signal transduction (Kato et al., 2006). *Lgr4* null mice had high levels of embryonic lethality and the surviving newborn *Lgr4*<sup>-/-</sup> mice died within 2 days of birth. Homozygous *Lgr4* null mice had reduced body weight compared to heterozygous or WT mice. Furthermore, these mice showed a decrease in kidney volume and weight and several kidney malformations including renal hypoplasia. The authors also observed that the eyes of *Lgr4* null mice were open at birth, suggesting that Lgr4 plays a critical role in the formation of the eyelid by contributing to the keratinocyte motility (Kato et al., 2007).

As noted during analysis of the *Lgr4* mouse models, Lgr4 appears to be expressed in a wide range of tissues and organs of ectodermal, mesodermal and endodermal origin. The *Lgr4* null mouse phenotypes suggest a regulatory role for Lgr4 in the correct development of multiple organs. However, at that time little was known about the Lgr4 signalling pathways controlling the correct development of the mice.

Interestingly, a heterozygous nonsense mutation in human *LGR4* in the Icelandic population (c.376C>T) causes low bone mineral density (BMD) in individuals carrying the mutation. These individuals also presented with other

abnormal phenotypes that resembled the *Lgr4* mouse phenotypes such as reduced birth size, lower weight, electrolyte disturbances, reduced testosterone levels and late onset menarche (Styrkarsdottir et al., 2013), confirming the requirement for LGR4 in a wide range of different organs.

### 1.7.3 LGR4 signalling pathways

The LGR4 receptor has been shown to bind to RSPO1-4 and trigger enhancement of the Wnt signalling pathway, as described in section 1.6.3 (Carmon et al., 2011; Glinka et al., 2011; Lau et al., 2011; Ruffner et al., 2012). The LGR4-RSPO pair function upstream of  $\beta$ -Catenin signalling in order to enhance Wnt- $\beta$ -Catenin signalling mediated by the E3 ubiquitin ligases ZNRF3/RNF43 (Hao et al., 2012). However, LGR4 acting through RSPOs does not involve GPCR activation (Ruffner et al., 2012). LGR4 has been shown to act through other molecular signalling pathways, including GPCR activation, which are briefly described in this section.

Song and colleagues showed that the defective erythropoiesis of *Lgr4* null mice was the result of a decrease in cell proliferation in foetal liver, as shown by c-Myc and Cyclin D1 cell proliferation reduction markers, whereas no effect was found in apoptosis (Song et al., 2008). Furthermore, these mice had a significant decrease in ATF4 (also known as CREB 2) expression in foetal livers during midgestation. ATF4 is a member of the CREB family of transcription factors, acting downstream of the cAMP-PKA pathway. At the time of the study *Lgr4* was an orphan receptor. Therefore, generation of *Lgr4* mutants was performed as a ligand-independent method to test the function of *Lgr4* examining the intracellular levels of cAMP. The p.(T755I) variant in *Lgr4* was associated with an increase in intracellular cAMP levels, suggesting that *Lgr4* is coupled to G-protein *Gas* and the cAMP-CREB pathway (Song et al., 2008).

The “eyes open at birth” phenotype observed in *Lgr4*<sup>-/-</sup> mice by Kato and colleagues (Kato et al., 2007), was further investigated to determine the contributions of *Lgr4* to eyelid development. *Lgr4* was found to be essential

in epithelial cell proliferation and migration during eye lid development through phosphorylation and further activation of epidermal growth factor receptor (EGFR), as shown by the dramatic decrease of phosphorylated EGFR in *Lgr4*<sup>-/-</sup> cultured keratinocytes and developing eye lids (Jin et al., 2008). Further investigation found that heparin binding EGF (HB-EGF) is the primary ligand responsible for LGR4-mediated EGFR signalling, as shown by the rescue of *Lgr4*<sup>-/-</sup> keratinocyte proliferation after addition of HB-EGF. Similarly, blockade of HB-EGF inhibited the LGR4-induced activation of EGFR (Wang et al., 2010).

LGR4 and the closely related receptor LGR5 were shown to be critical for R-spondin mediated Wnt PCP signalling in *Xenopus* embryos (Glinka et al., 2011). Knockdown of *lgr4* and *lgr5* using MO was performed in *Xenopus*, and ATF2-luciferase reporter expression was used to measure Wnt/PCP signalling activation (Ohkawara et al., 2011). Knockdown of *lgr4* and *lgr5* abolished ATF2-luciferase activity, suggesting that *lgr4* and *lgr5* are required for RSPO signalling by the Wnt/PCP pathway in *Xenopus* embryos. These results provide evidence that LGR4/5 mediate RSPO signalling by the Wnt- $\beta$ -Catenin signalling but also by Wnt/PCP signalling (Glinka et al., 2011).

Interestingly, Deng and colleagues suggested that LGR4 could act as a receptor for the Norrin ligand, linking the Norrin- $\beta$ -Catenin signalling pathway with LGR4 (Deng et al., 2013). The authors suggested Norrin as a ligand for LGR4 based on sequence homology between Norrin and its invertebrate ortholog burs/pburbs. The authors showed LGR4 mediated enhancement of Norrin pathway when LGR4 and LRP5 were overexpressed in HEK293 cells. They also showed that this pathway activation was more potent with LGR4 than with the known Norrin receptor FZD4. Norrin binding to LGR4 was also shown, as well as Norrin binding to LGR5 and LGR6, suggesting that Norrin acts at the junction of two important signalling pathways, binding and activating both mediated by two different receptors.

The effects of LGR4 on migration, invasion, proliferation and apoptosis in prostate cancer cell lines was investigated. LGR4 was shown to promote cell

invasion and proliferation and to inhibit apoptosis in prostate cancer cultured cell lines. Overexpression of LGR4 significantly increased the tumour growth, while LGR4 knock down inhibited tumour growth (Liang et al., 2015). Furthermore, Liang and colleagues showed that LGR4 regulates the expression of PI3K/Akt signalling genes, as *Akt*, *mTOR* and *GSK3 $\beta$*  were upregulated after LGR4 overexpression. These results suggest that LGR4 acts via PI3K/Akt signalling, which is a central regulator of cell proliferation and tumorigenesis (Jr and Janku, 2014), and could be regulating tumorigenesis in prostate cancer. Interestingly, regulation of prostate tumorigenesis has recently been reported to be driven by LGR4 through *Jmjd2a*/AR signalling (Zhang et al., 2016). *Jmjd2a* is a member of the histone demethylase JMJD family (Jumonji domain-containing histone demethylase), implicated in epigenetic regulation and gene expression regulation by forming complexes with transcription factors. Overexpression of LGR4 in prostate cancer cell lines resulted in reduced cell apoptosis and increased of the cell number in the S phase. These results correlated with the increase of *Jmjd2a* mRNA expression and elevated androgen receptor (AR) levels interacting with *Jmjd2a*.

As described above, LGR4 acts through multiple molecular pathways in order to regulate different aspects of the development, which might explain the broad range of abnormal phenotypes observed in the various mouse models described in section 1.7.2. LGR4 is known to act through R-spondin and activates Wnt- $\beta$ -Catenin signalling, but other molecular pathways controlling other aspects of the development are also involved in or influenced by LGR4 signalling. The ubiquitous *Lgr4* expression observed in mice and humans is also consistent with LGR4 having functions in a range of cellular signalling pathways (Van Schoore et al., 2005; Yi et al., 2013).

## 1.8 Identification of missense variants in *LGR4*

### 1.8.1 Exome sequencing of the *EVR3* locus and *LGR4* screening in the Leeds FEVR cohort

The dominant FEVR locus *EVR3* (Table 1-1) was originally identified in 2001 by undertaking a whole genome linkage screen in a large Scottish FEVR family and it was mapped on chromosome 11p12-13 (Downey et al., 2001). The same family had previously been excluded from the only known dominant locus at the time, *EVR1* (Bamashmus et al., 2000). Downey et al. mapped the locus for this family consisting of a 14-cM region lying between the microsatellites GATA34E08 (tel.) and D11S4102 (cen.).

Next generation sequencing (NGS) was used to screen the genes within this locus in members of the *EVR3* family using a targeted capture approach. This led to the identification of a heterozygous missense mutation, c.188C>T, p.(R40W) in *LGR4*, as the only coding variant which segregated with the phenotype in the whole *EVR3* family (work done by Dr. James Poulter).

Further screening of the FEVR cohort identified 5 additional heterozygous missense mutations: c.933G>C, p.(Q311H); c.1289C>T, p.(T430M); c.1924G>A, p.(E642K); c.2164G>A, p.(A722T); c.2248aG>A, p.(A750T) (work carried out by Dr James Poulter and Evangelia Panagiotou). Three of the *LGR4* variants identified are found in the extracellular domain of *LGR4* and the other three variants are found in the transmembrane domain of *LGR4*. The locations, both in the gene and protein, of the 6 *LGR4* missense variants found in FEVR patients, together with a graphic illustrating *LGR4* structure, are shown in Figure 1-11.

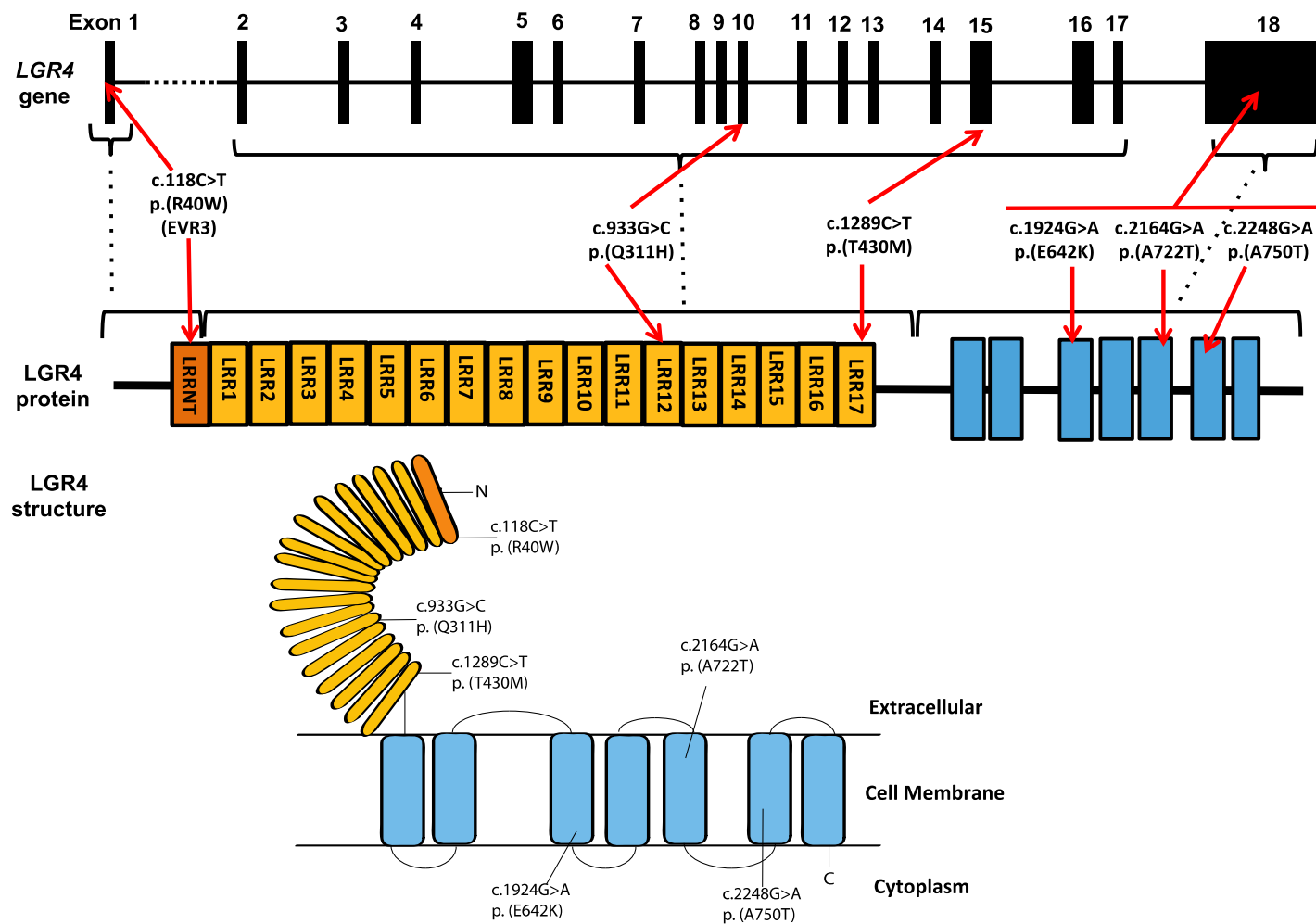


**Figure 1-11: Diagram of *LGR4* gene and LGR4 protein structures, showing the locations of the variants identified in FEVR patients.**

The *LGR4* (NM\_018490.3) structure was taken from human genome browser (GRCh38/hg38). The extracellular domain structure of the protein was inferred using the crystal structure (K. Xu et al., 2013). The locations of the 6 *LGR4* variants are shown in the genomic and protein representation of LGR4.

As shown in Figure 1-11, 3 of the variants identified are present in the extracellular domain of LGR4, which is the ligand-binding domain for LGR4. The remaining 3 variants are present in the transmembrane domain of LGR4, which transduces the molecular signal (Xu et al., 2013).

## 1.9 Aims

The main aim of the work described in this thesis was to find further evidence in support of the hypothesis that *LGR4* is the *EVR3* gene underlying autosomal dominant FEVR. For this purpose, functional characterisation of WT and mutated LGR4 was performed. In addition, the involvement of LGR4 in angiogenesis was explored. In order to address these aims a series of functional experiments were performed:

Pathogenesis of the *LGR4* missense variants was investigated using a zebrafish model. MO *lgr4* knockdown in the fish and mRNA rescue experiments were performed with both WT and mutant human LGR4, and the effect on vasculature of the developing fish eyes was assessed.

The role of LGR4 in Norrin- $\beta$ -Catenin signalling was explored and the implications of the *LGR4* variants in the Norrin pathway investigated. The effects of the *LGR4* variants in RSPO-LGR4 signalling were also studied.

The interaction between Norrin and LGR4 was characterised using a variety of cell-based techniques to determine if these two proteins are a receptor-ligand pair.

A possible role for *LGR4* in angiogenesis was assessed using an *in vitro* angiogenesis assay to gain insights into the function of LGR4 and blood vessel development.

## 2 Materials and Methods

Room temperature (RT) is typically in the range of 18-24°C.

Overnight incubations are approximately 16-20 hours.

All materials used were purchased from Sigma-Aldrich or Thermo Scientific unless indicated otherwise in the text.

### 2.1 General buffers

#### 1. Phosphate-buffered saline (PBS) (1x)

#### 2. Tris- Ethylenediaminetetraacetic acid (EDTA) (TE) buffer

10 mM Tris-HCl pH7.5

1 mM EDTA

#### 3. Tris/Borate/EDTA (TBE) (10x) pH8.0

890 mM Tris

890 mM Boric acid

20 mM EDTA

#### 4. 10x Gel loading buffer

3x TBE

20% Ficoll 400

0.1% Bromophenol Blue

0.2% Xylene Cyanol

#### 5. NP40 cell lysis buffer

1% NP40

50 mM Tris-HCl pH8.0

150 mM NaCl

1x Protease/phosphatase Inhibitors

0.3M PMSF

## **6. Luria-Bertani (LB) Broth**

1% Tryptone

0.5% Yeast extract

1% Sodium Chloride

For plates, 1.5% agar was added

## **7. Super optimal broth with catabolite repression (SOC)**

2% bacto-tryptone

0.5% bacto-yeast extract

10 mM NaCl

2.5 mM KCl

10 mM MgCl<sub>2</sub>

20 mM glucose

## **8. Denaturation buffer**

7 M guanidine hydrochloride

2 mM EDTA

50 mM Dithiothreitol (DTT)

50 mM Tris-HCl pH8.3

## **9. Tris-buffered saline (TBS)**

10 mM Tris-HCl

150 mM NaCl, pH7.4

## **2.2 Polymerase chain reaction (PCR)**

### **2.2.1 Primer design**

Initially, oligonucleotide primers were designed by eye aiming for an annealing temperature of 60°C. Approximate annealing temperatures ( $T_A$ ) were calculated using the following equation, where (A+T) is the total number of Adenine and Thymine residues in the primer and (G+C) is the total number of Guanine and Cytosine residues:

$$T_A = 2(A+T) + 4(G+C)$$

Alternatively, primer design software tools were used. Primer 3 software tool v0.4.4 (<http://bioinfo.ut.ee/primer3-0.4.0/>) was used to design primers. A primer length of 20bp was requested (range 18-27), with a primer melting temperature of 60°C (range 57-65°C) and a GC% between 20% and 80%.

Gateway technology primers for cloning were designed as described in the manufacturer's instructions. Briefly, the forward primer was designed using four guanine (G) residues at the 5' end, followed by the 25 bp attB1 site then a Kozak consensus and then 18-25 bp of template of the specific gene. The reverse primer was designed to allow expression of a C-terminal fusion protein. The gene-specific nucleotides had to be in frame with the 25bp attB2 sequence and the stop codon of the gene was removed.

#### **2.2.1.1 Site Directed Mutagenesis primer design**

The primers designed to introduce point mutations into specific plasmids were designed using the QuickChange Primer Design Programme, which supports mutagenic primer design for your QUickChange mutagenesis experiment (<http://www.genomics.agilent.com/primerDesignProgram.jsp>). Primers were designed selecting the position and the base pair change to be introduced and introducing the DNA sequence to be mutated in the software.

#### **2.2.2 Hot-Shot PCR (Clont Life Science)**

Reactions were carried out in a 10 µl final volume. 1 µl of the cDNA generated from section 2.2.4, 1 ng of human retinal cDNA (Clontech Catalog No. 637216) or 25 ng of genomic DNA, 10 pmols of each primer, 5 µl of the Master mix and 3.5 µl of Milli-Q water (MQ) were used in every reaction as indicated in the manufacturer's protocol (Clont Life Science). An initial denaturation step at 95°C for 5 minutes was followed by 35 cycles of denaturation at 95°C for 1 minute, annealing (60°C to 65°C depending on

primers) for 1 minute and extension at 72°C for 1 minute. A final extension was performed at 72°C for 10 minutes.

### **2.2.3 Platinum Pfx PCR**

Reactions were carried out in a final volume of 50 µl using 5 µl of amplification buffer, 1.5 µl of 10 mM dNTPs, 1 µl of 50 mM MgSO<sub>4</sub>, 1.5 µl of 10 µM primer mix composed of forward and reverse primer, 10 ng of DNA and 0.4 µl of Platinum *Pfx* DNA polymerase (Invitrogen). 30 cycles of PCR amplification were performed, starting with an initial denaturation step at 94°C for 5 minutes followed by 30 cycles of denaturation at 94°C for 15 seconds, annealing at 60°C for 30 seconds and an extension step at 68°C for 5 minutes. A final extension was performed at 68°C for 10 minutes.

### **2.2.4 Reverse transcription PCR (RT-PCR)**

Complementary DNA (cDNA) was synthesized from 1 µg of human total RNA from the Master Panel II (Clontech Catalog No. 636643) set of human tissue RNAs or 1 µg of total RNA extracted from different cell lines (section 2.10.1). RNA was reverse transcribed using Moloney Murine Leukemia Virus Reverse Transcriptase (M-MLV RT) (Invitrogen). The RNA was first incubated for 10 minutes at 70°C with 100ng random primer hexamers, then samples were chilled on ice before the addition of M-MLV RT buffer, 1 mM dNTPs, 10 mM DTT and 0.5U RNAsin (Promega). All the samples were then equilibrated at 37°C for 2 minutes and incubated with 200U of M-MLV RT (Invitrogen) for 1 hour at 37°C. A final incubation of 2 minutes at 95°C was undertaken to denature the enzyme and 1 µl of the resulting cDNA was used in subsequent PCR reactions.

## **2.3 Agarose gels**

### **2.3.1 Size fragmentation**

Size fractionation of DNA using agarose gel electrophoresis was carried out in 0.8% to 2% agarose gels (Fisher Scientific) in 0.5X TAE buffer. To visualize the DNA, ethidium bromide (10mg/ml, Sigma Aldrich) was added at a final concentration of 0.5 µg/ml. Gels were run for 30 minutes at 120 volts using Sub-Cell® GT Agarose Gel Electrophoresis Systems and DNA was visualized in a Bio-Rad gel documentation system with an ultraviolet transilluminator and displayed using Image Lab 1-D analysis software.

### **2.3.2 DNA extraction from agarose gels**

DNA was extracted from agarose gel using the QIAquick gel extraction kit (Qiagen) according to the manufacturer's instructions. Briefly, DNA was run on a 1% agarose/TAE/ethidium bromide gel alongside a DNA EasyLadder I (Bioline) size marker. DNA bands were visualized under UV in a dark room and cut from the gel using sterile scalpel blades. The gel was dissolved in solubilisation buffer at 50°C for 10 minutes then the resultant sample was mixed with an equal volume of isopropanol to precipitate DNA. DNA was adsorbed onto a silica membrane by passing the sample through a DNA binding column by centrifugation at 10000 x g. RNA, protein, metabolites and agarose were removed and discarded. The DNA was then washed with ethanol wash buffer and eluted from the binding column in dH<sub>2</sub>O.

## **2.4 Sanger sequencing**

### **2.4.1 PCR template clean-up for sequencing**

PCR template DNA to be sequenced underwent a clean-up step using ExoSAP-IT (Affymetrix USB, Santa Clara, USA) in a 5:2 ratio followed by incubations of 15 minutes at 37°C and 15 minutes at 85°C. This was only performed on DNA amplified by PCR, and was used to remove

unincorporated primers and dNTP's, which could interfere with subsequent sequencing reactions.

### **2.4.2 Sequencing reaction**

PCR products (first treated with ExoSAP-IT) or plasmid DNA template were sequenced in a reaction mixture with 1.5 µl BigDye<sup>®</sup> Terminator v3.1 Sequencing Buffer (5X) (Applied Biosystems), 1 µl BigDye<sup>®</sup> Terminator v3.1 (Applied Biosystems), 1 µl sequencing primer (1.6 µM). Distilled water (dH<sub>2</sub>O) was added to a final volume of 10 µl. The sequencing reactions were processed with an initial denaturation step at 96°C for 1 minute, followed by 25 cycles of 96°C for 10 seconds, 50°C for 5 seconds and 60°C for 4 minutes. Temperatures were ramped at 1°C/second.

### **2.4.3 Precipitation of sequencing reaction products**

Sequencing products were precipitated from the sequencing reaction mixture using 5 µl 125 mM EDTA and 60 µl 100% ethanol per sequencing reaction and centrifuging the samples at 3061 x g for 30 minutes. The resulting pellets were washed in 60 µl freshly prepared 70% ethanol and centrifuged at 805 x g for 15 minutes at 4°C. Samples were inverted onto tissue and spin inverted at 155 x g for 1 minute to remove the excess of ethanol. The pellet was left to air dry out of the light before the precipitates were redissolved in Hi-Di deionized formamide (Applied Biosystems) and resolved on an ABI3130xl Genetic Analyser (Applied Biosystems). The results were analyzed using Seqscape software (V2.5, Applied Biosystems).

## **2.5 Bioinformatics**

### **2.5.1 Literature Searches**

Literature searches play a key role in scientific research, finding out information about a particular topic. Nowadays the majority of journals are available online and scientific literature searching platforms have been developed. PubMed (<https://www.ncbi.nlm.nih.gov/pubmed/>) an online

database of journal articles, was used to find relevant previously published information. Further information about disease phenotypes, loci and known genes was found using Online Mendelian inheritance in Man (OMIM-<https://www.ncbi.nlm.nih.gov/omim>).

### **2.5.2 UCSC Genome Bioinformatics Browser**

The UCSC genome bioinformatics browser was launched for the human genome in 2002 (Kent et al., 2002) to bring together the human genome data into a single database. The browser allows free access to the genome sequence alongside a multitude of tools to analyse and combine the output from an increasing number of tracks. Bioinformatic searches of genomic regions and initial information about specific genes were obtained using the UCSC Genome Bioinformatics browser (<https://genome.ucsc.edu>). This includes intron-exon structures, genomic sequences and protein sequences.

### **2.5.3 Protein alignment sequence using BLAST**

BLAST is an online tool provided by NCBI that aligns two sequences of two proteins of interest. Using the default settings, two proteins can be aligned and the identities and similarities between protein sequences are given ([https://blast.ncbi.nlm.nih.gov/Blast.cgi?PROGRAM=blastp&PAGE\\_TYPE=BlastSearch&BLAST\\_SPEC=blast2seq&LINK\\_LOC=blasttab](https://blast.ncbi.nlm.nih.gov/Blast.cgi?PROGRAM=blastp&PAGE_TYPE=BlastSearch&BLAST_SPEC=blast2seq&LINK_LOC=blasttab)).

## **2.6 Molecular cloning**

### **2.6.1 TA cloning of PCR products**

PCR products were excised from agarose gels (section 2.3.2) and cloned into a pCR-2.1-TOPO plasmid vector (Invitrogen, Appendix 8.7) using 2 µl of the PCR product, 1 µl of salt solution (1.2 M NaCl, 0.06 M MgCl<sub>2</sub>), 2 µl of water and 1 µl of linearized pCR2.1-TOPO vector. The reaction mixture was gently mixed and incubated for 5 minutes at RT. After, the reaction was placed on ice and transformation of competent cells was performed as described in section 2.6.5.

## **2.6.2 Restriction enzyme digestion**

Restriction enzymes were obtained from New England Biolabs (NEB), Fermentas or Life Technologies. Manufacturers' instructions were followed for all enzyme digests. Usually this involved digesting 500 ng to 1 µg of DNA with 20 units (U) of the chosen endonuclease. The reactions were typically carried out in 10 µl volumes with a 2 hour incubation at 37°C unless a different optimal temperature was specified by the manufacturer. Overnight digestions were carried out when 5 µg of plasmid was used. All the reactions were accompanied by the appropriate buffer, had the optimal pH, and salt conditions and bovine serum albumin (BSA) was added where recommended by the manufacturers.

## **2.6.3 Site Directed Mutagenesis (SDM)**

Point mutations were introduced individually using the QuikChange II XL SDM kit (Agilent Technologies) according to the manufacturer's instructions. The primers were designed using the online Agilent QuikChange Primer design program (<http://www.genomics.agilent.com/primerDesignProgram.jsp>). Primers were manufactured by Sigma and purified by high performance liquid chromatography (HPLC) or polyacrylamide gel electrophoresis (PAGE). Mutagenesis was performed by amplifying purified plasmid DNA (section 2.6.3) with the SDM primers using *Pfu* Ultra high fidelity polymerase (Agilent Technologies). Following amplification, the reaction was digested with *DpnI* restriction endonuclease, eliminating the parental DNA template and leaving only the mutated plasmid, which was transformed into XL10-Gold ultracompetent cells.

## **2.6.4 Creation of expression constructs using Gateway technology**

Primers introducing attB1 and attB2 sites were designed manually for every gene (Appendix 8.5). Clones containing the entire open reading frame (ORF)

of the genes of interest were purchased from Transomic Technologies or Origene and they were used as a template. The entire ORF was amplified using *Pfx* Polymerase (section 2.2.3). After PCR amplification, PCR products were run on a 1% agarose gel and the DNA was extracted from the gel (section 2.3.2). The DNA was cloned into the pDONR201 plasmid using BP clonase (Invitrogen) to generate the entry clone according to the manufacturer's protocol. The entire ORF cassette was then transferred to the destination vectors pDEST40, pCS2+ or pDEST504 using LR clonase (Invitrogen) following the Invitrogen protocol to create the expression constructs. All constructs were fully validated by Sanger sequencing (section 2.4).

### **2.6.5 Bacterial transformation and culture**

DNA was transformed into super-competent  $\alpha$ -select Gold Efficiency E. Coli (Bioline) using a heat shock method. Bacteria were defrosted on ice for 3 minutes and incubated with DNA on ice for 30 minutes. Cells were then heat shocked for 30 seconds at 42°C using a water bath and placed on ice immediately for 2 minutes. Cells were then mixed with 250µl of Super Optimal Broth with Catabolite repression (SOC) medium (2% w/v bacto-tryptone, 0.5% w/v bacto-yeast extract, 10 mM NaCl, 2.5 mM KCl, 10 mM MgCl<sub>2</sub>, 20 mM glucose) and incubated at 37°C with 200 rpm shaking for 1 hour. Cells were then spread on LB (10 g/l tryptone, 5 g/l yeast extract, 5 g NaCl) agar (15 g/l agar) plates containing appropriate antibiotic and incubated at 37°C overnight.

Single colonies were picked from agar plates using sterile loops and used to inoculate 5 ml LB broth containing the appropriate antibiotic. 5 ml cultures were grown at 37°C with 200 rpm shaking overnight. For large scale plasmid purification, 1 ml of the 5 ml culture was used to inoculate a large conical flask containing 100 ml LB broth with the appropriate antibiotics at 37°C, 200 rpm overnight. The antibiotics used were Ampicillin at a final concentration of 50 µg/ml and Kanamycin at a final concentration of 25 µg/ml.

### **2.6.6 Plasmid DNA isolation and purification**

Small-scale plasmid DNA isolation and purification was performed using the QIAprep Miniprep kit (Qiagen) according to the manufacturer's recommendations. Cells from the 5 ml bacterial culture were pelleted by centrifugation at 3000 x g and resuspended in neutral buffer P1 containing RNase A (Qiagen). Cells were then mixed with an equal volume of alkaline lysis buffer and neutralization solution. After removal of cell debris, lysates were adsorbed onto a silica membrane by passing through a spin column at 100 x g, and the flow-through containing RNA, protein and metabolites was discarded. The DNA was then washed with ethanol buffer (Qiagen) and eluted in 50 µl dH<sub>2</sub>O. These mini-prepped plasmids were used for sequencing confirmation, SDM experiments and restriction enzyme digests.

Large-scale plasmid preparation was performed using the EndoFree Plasmid Maxi Kit (Qiagen). Cells from a 100 ml LB overnight culture were pelleted by centrifugation at 3000 x g for 30 minutes at 4°C. Cells were then resuspended and lysed as per the manufacturer's instructions. Cell debris were removed using a Qiafilter, and the resulting cleared solution applied to a Qiagen column to allow DNA to bind to the membrane. The membrane was washed and the DNA eluted. Plasmid DNA was precipitated by adding 0.7 volumes of room-temperature isopropanol and centrifuged at 15000 x g for 30 minutes at 4°C. Carefully the supernatant was discarded and the pellet was washed with 70% ethanol with a centrifugation of 15000 x g for 15 minutes. The supernatant was discarded and pellets allowed to air dry. Pellets were dissolved in 200 µl of filter-sterilized TE. These maxi-prepped plasmids were used for cell transfection, after they were fully sequence verified.

### **2.7 mRNA synthesis and purification**

5 µg of plasmid DNA were linearized overnight using restriction endonuclease enzyme digestion at a site downstream of the insert to be transcribed. *NotI* restriction enzyme was used. The linearized plasmid was

purified and cleaned up using a Nucleo spin gel and PCR clean-up Kit (Macherey Nagel) according to the manufacturer's protocol. Approximately 1 µg of the linearized plasmid was used for the mRNA synthesis using the mMMESSAGE mMACHINE kit (Life Technologies), which is designed for *in vitro* synthesis of large amounts of capped RNA. Briefly, the linearized DNA template containing the SP6 RNA polymerase promoter site was mixed with 2X NTP/CAP, reaction buffer and enzyme. Nuclease-free water was added to a final volume of 20 µl. The reaction was carried out for 1 hour at 37°C. The recovery and purification of the mRNA was performed using MEGAclean Kit spin columns (Life Technologies) and the recovered RNA was dissolved in Diethylpyrocarbonate (DEPC)- treated water.

## **2.8 Morpholino, zebrafish manipulation and rescue experiments**

Flk:GFP<sup>inx</sup> zebrafish were treated and bred under standard conditions, in accordance with Dutch Institutional guidelines. The Zebrafish knockdown for *lgr4* was created using morpholino oligonucleotides (MO) splice MO and ATG MO, designed and obtained from Gene Tools LLC (MO sequences in Appendix 8.2). The Vivo-Morpholino standard control oligo (Gene Tools LLC), which targets a human β-globin intron mutation that causes β-thalassemia, was used as a negative control against morpholino toxicity. Morpholinos were dissolved in sterile water and injected using a Pneumatic PicoPump pv280 (World Precision Instruments) in the yolk sac of 1 or 2 cell stage zebrafish embryos. 6ng of splice MO *LGR4* were injected in a volume of one nl containing 0.025% phenol red as an optical marker. Embryos were kept at 28.5°C for 4 days in E3 medium (5 mM NaCl, 0.17 mM KCl, 0.33 mM CaCl<sub>2</sub>, 0.33 mM MgCl<sub>2</sub>) which was refreshed daily.

For *in vivo* rescue experiments, human wild type and mutant *LGR4* mRNAs (100 pg/nl) were co-injected together with 6ng of MO *LGR4*. At 4 days post-fertilization, the fish were fixed overnight at 4°C with 4% paraformaldehyde (PFA). The fish eyes were individually scored by manual inspection using a Zeiss Axio Imager Z1 fluorescence microscope and Alexa fluor 488 GFP

filter. Images were taken with the aforementioned microscope after washing the embryos twice in 1X PBS.

### **2.8.1 Zebrafish Information Network (ZFIN)**

The ZFIN is an online zebrafish model organism database, which supports integrated zebrafish genetic, genomic and developmental information. This resource was consulted in order to obtain information about zebrafish gene sequences (<http://zfin.org>).

### **2.8.2 Gene Tools MO design**

Translational and splice MO were designed using the Gene Tools MO design website (<https://oligodesign.gene-tools.com/request/>). Using the default settings, the sequence of the gene of interest was introduced and splice and translational MO were automatically designed to match the input sequence.

### **2.8.3 Zebrafish whole-mount immunofluorescence**

After fixation in 4% PFA, larvae were washed twice in PBS Tween-20 (Sigma Aldrich) (PBST), followed by incubation at 37°C for 30 minutes in 10 µg/ml proteinase K (Roche) in order to increase antibody permeation. Larvae were post-fixed in 4% PFA for 20 minutes. After washing 3 times with PBST, samples were incubated in blocking buffer (PBST with 1% DMSO, 1% BSA, 5% normal donkey serum (Sigma Aldrich), and 0.8% Triton X-100 (Sigma Aldrich) for 1 hour. After this, larvae were incubated overnight at 4°C with primary antibody (rabbit anti-GFP, 1:1000, Thermo Fisher Scientific) diluted in blocking buffer. The anti-GFP was used to enhance the EGFP signal and to optimize confocal imaging. After rinsing the larvae with 1% BSA in PBST, larvae were incubated with secondary antibody (goat anti rabbit-alexafleur 488, 1:300 Life Technologies) in blocking buffer at room temperature for 3 hours. Next, larvae were washed in PBST and stored in PBS at 4°C.

## 2.9 RNA extraction

Total RNA from cell lines was extracted using the RNeasy Mini kit (Qiagen) according to the manufacturer's protocol. Briefly, cells growing in a monolayer were washed twice with PBS and trypsinized (section 2.10.2). After the cells detached from the flask, the trypsin was neutralized using twice the volume of complete medium, the flask contents were transferred to a 50 ml falcon tube and spun at 300 x g for 5 minutes. The supernatant was removed and the cell pellet lysed in a highly denaturing guanidine-thiocyanate-containing buffer, which inactivates RNases, and passed through a QIAshredder spin column to homogenize the sample. 1 volume of 70% ethanol was then added to the homogenized lysate to provide appropriate binding conditions. The sample was passed through a QIAamp spin column and the sample subjected to serial washes to wash away any possible contaminants. RNA was then eluted in 50µl DEPC treated water.

## 2.10 Cell culture

### 2.10.1 Cell lines

Cell line	Origin	Source
HEK293	Human embryonic kidney	ATCC
STF	SUPER 7x TOPflash Stable transfected HEK293	Kind gift from J. Nathans (Xu et al., 2004)
COS7	African green monkey kidney	ATCC
HUVEC	Human umbilical vein endothelial cells	GIBCO
HDF	Human dermal fibroblasts	TCS cellworks
U2OS	Human osteosarcoma cell line	European Collection of cell Cultures (ECACC)

MCF7	Human breast adenocarcinoma cell line	ATCC
RPE1	Retinal pigment epithelium	ATCC
HB2	Human breast epithelial	ATCC
HRT18	Human colorectal carcinoma	ATCC
HCT116	Human intestinal adenocarcinoma	ATCC
HT29	Human colon adenocarcinoma	ATCC
SW480	Human colon adenocarcinoma	ATCC
SH-SY5Y	Human neuroblastoma	ATCC
MCF10A	Epithelial cell line derived from human fibrocystic mammary tissue	ATCC

**Table 2-1: Cell lines used. Name, origin and source of cell lines.**

### **2.10.2 Cell culture**

All cells were propagated in Corning 25 cm<sup>2</sup> or 75 cm<sup>2</sup> flasks (T25 or T75) (Sigma Aldrich) at 37°C with 5% CO<sub>2</sub> in Sanyo MCO 20AIC cell culture incubators. Cell culture work was performed in NuAire Labgard 437 ES Class II Biosafety Cabinets under sterile conditions.

HK293 cells, U2OS cells, COS7 cells and HDF were grown in Dulbecco's Modified Eagle's Medium (DMEM) (Sigma Aldrich) and supplemented with 10% fetal calf serum (FCS) (Sigma Aldrich) and 100 U/ml penicillin and 100 mg/ml streptomycin (Sigma Aldrich).

STF cells were grown in Dulbecco's Modified Eagle's Medium (DMEM) and Ham's F12 medium (Gibco) with 10% FCS (Sigma Aldrich) and 100 U/ml penicillin and 100 mg/ml streptomycin (Sigma Aldrich). STF cells were incubated in the presence of 100µg/ml of Geneticin® (G418, [50 mg/ml]) (Gibco) prior to performing the assays.

HUVEC cells were grown in Endothelial Growth Medium (EGM-2) (Lonza) and supplemented with EGM-2 BulletKit (Lonza) containing 0.5 ml human Epidermal Growth Factor (hEGF), 0.5 ml Vascular Endothelial Growth Factor (VEGF), 0.5 ml R3- Insulin-like Growth Factor-1 (R3-IGF-1), 0.5 ml Ascorbic Acid, 0.5 ml Hydrocortisone, 0.2 ml human Fibroblast Growth Factor-Beta (hFGF-β), 0.5 ml heparin, 10 ml Fetal Bovine Serum (FBS) and 0.5 ml Gentamicin/Amphotericin-B (GA).

Cells were grown to 80-90% confluency. Cells were passaged by removing the culture medium and washing with Dulbecco's phosphate buffered saline (DPBS) (Sigma Aldrich), followed by the addition of trypsin/EDTA (Sigma Aldrich). Cells were then incubated at 37°C for approximately 5 minutes until the cells dissociated from the surface of the culture flask and from each other. The trypsin was neutralized by adding an equal volume of complete cell culture media (containing FCS) and the suspension collected in a falcon and centrifuged at 200 x g (HUVEC cells were centrifuged at 125 x g) for 5 minutes. Cell pellets were resuspended in culture medium and split into fresh culture flasks.

### **2.10.3 Cell counting**

To count cells prior to seeding, 10 µl of resuspended cells were mixed 1:1 with trypan blue stain 0.4% (Life Technologies) and counted using the Countess™ Automated Cell Counter (Life Technologies) according to the manufacturer's instructions. The required volume of viable cells was then calculated to allow accurate and consistent seeding of cells in each plate well.

#### **2.10.4 Cell storage and recovery**

Long-term storage of cells was performed in their normal cell culture medium supplemented with 10% DMSO (Sigma Aldrich), in 1.5 ml cryovials (Nunc) in liquid nitrogen. Freezing medium for HDF was complete medium supplemented with 5% DMSO. Cells were gradually frozen in Mr. Frosty™ freezing containers (Nalgene) in a -80°C freezer overnight and transferred to liquid nitrogen the following morning.

For all cell types other than HUVECs, frozen cells were recovered by rapidly defrosting the cryovial in a 37°C water bath, adding cells drop-wise to 10 ml complete medium, collecting by centrifugation at 200 x g, resuspending in complete cell culture media and transferring to a T25 or T75. Frozen HUVEC cells were recovered without the centrifugation step. HUVEC cells were diluted in 30 ml complete EGM-2 medium (LONZA) and two T75 flasks were each seeded with 15 ml of the EGM-2/cells suspension. The next morning complete medium was changed to remove the DMSO.

#### **2.10.5 Conditioned medium**

Norrin alkaline phosphatase (AP-3myc-Norrin) conditioned medium was prepared as described in (Smallwood et al., 2007). Conditioned medium was prepared from HEK293 cells transfected with the AP-3myc-Norrin construct (Section 2.10.6). Cells were seeded in a T150 flask and grown to 80% confluency prior to transfection. 48 hours post-transfection, medium containing WT Norrin fused with alkaline phosphatase and myc tags was collected and passed through a 0.2 µm filter and stored at -20°C until use.

#### **2.10.6 Transfections**

##### **2.10.6.1 Transient DNA transfections**

Single plasmid transfections were carried out using Lipofectamine 2000 (Invitrogen) according to the manufacturer's instructions.

For COS7, U2OS and HEK293 cells,  $3 \times 10^5$  cells/well were plated 24 hours prior to transfection and grown to 80% confluency in 6-well plates. After 24 hours 1.5  $\mu\text{g}$  of DNA was dissolved in 250  $\mu\text{l}$  Gibco OptiMEM medium (Life Technologies) and incubated for 5 minutes at room temperature. 5  $\mu\text{l}$  of Lipofectamine was suspended in 250  $\mu\text{l}$  OPTI-MEM and incubated for 5 minutes at room temperature. The DNA mixture was then added to the lipofectamine mixture and incubated for 20 minutes at room temperature. The medium of the cells to be transfected was changed to complete medium and the lipofectamine/DNA mixture was added drop-wise to the cells.

Multiple plasmid transfections were carried out using the Fugene 6 transfection reagent (Roche) according to the manufacturer's instructions.

$1.0 \times 10^5$  STF cells/well were plated 24 hours prior to transfection in a 24-well plate. After 24 hours, 1.5  $\mu\text{l}$  of Fugene was added to 50  $\mu\text{l}$  OPTI-MEM followed by addition of 400 ng of DNA. The Fugene/DNA mixture was then incubated at room temperature for 20 minutes and added drop-wise to the cells to be transfected.

#### **2.10.6.2 Transient siRNA transfections**

Transfection of siRNA was performed using Lipofectamine RNAiMAX transfection reagent (Invitrogen) according to the manufacturer's instructions. For each gene a pool of four siRNAs was utilised.  $1.5 \times 10^5$  HUVEC cells were plated per well in a 6-well plate 24 hours prior to transfection. A total of 100  $\mu\text{M}$  of the siRNA pool (Table 2-2) was diluted in 150  $\mu\text{l}$  of reduced serum media OPTI-MEM and incubated for 5 minutes at room temperature. 5  $\mu\text{l}$  lipofectamine RNAiMAX was diluted in 150  $\mu\text{l}$  OPTI-MEM and incubated for 5 minutes. The siRNA solution was added to the RNAiMAX mixture and incubated at room temperature for 20 minutes. The medium of the cells was changed to OPTI-MEM and the transfection complexes were added drop-wise. After 3-4 hours the OPTI-MEM media was changed for complete medium.

Target	Organism	Sequence	Source
<i>FZD4</i>	Human	GAAAUGCACAGCUCUUAUU	Dharmacon
		GACAAAGACAGACAAGUUA	ON-TARGETplus
		GAUCGAUUCUUCUAGGUUU	SMARTpool,
		AGUCAAUCAUGUCGAGUCA	M-005503-02-0005
<i>LGR4</i>	Human	UAAGAGACCUUCCAAGUUU	Dharmacon
		GUAGAAACCUGAUACAUGA	ON-TARGETplus
		GCAUGUCGCUUGGCUAAUC	SMARTpool,
		UAAGCAGCAUACCUAUUAA	M-003673-03-0005
<i>Non-Targeting siRNA pool 1</i>	N/A	UAGCGACUAAACACAUCAA	Dharmacon
		UAAGGCUAUGAAGAGAUAC	ON-TARGETplus
		AUGUAUUGGCCUGUAUUAG	SMARTpool,
		AUGAACGUGAAUUGCUCAA	D-001206-13-05

**Table 2-2: siRNAs utilised. Target gene, organism, sequence and commercial source of siRNA pools. Non targeting siRNA pool 1 refers to scrambled siRNA.**

Transfection protocols were scaled up or down accordingly for transfection in larger or smaller cell culture vessels.

### 2.10.7 Cell lysis

Cells were washed twice with cold PBS before cells were collected using a cell scraper into Eppendorf microcentrifuge tubes and lysed using ice-cold NP40 lysis buffer, consisting of 20 mM Tris HCl pH8 (Sigma), 150 mM NaCl, 10% v/v glycerol (Sigma), 1% v/v NP40 (Sigma), 2 mM EDTA (Sigma), 1x complete protease inhibitor cocktail (Roche) and 0.3 M Phenylmethylsulfonyl fluoride (PMSF). Cells were incubated at 4°C with agitation for 30 minutes and the resulting cell debris was pelleted by centrifugation at 15000 x g. The pellet was discarded and the lysate supernatant was stored at -80°C.

### **2.10.8 Protein assay**

Concentration of protein in whole cell lysates was determined using the Pierce BCA Protein Assay Kit (Pierce, Thermo Scientific), which uses a detergent-compatible formulation based on bicinchoninic acid (BCA) for colorimetric detection. The assay was performed according to the manufacturer's instructions. A series of standards were prepared using BSA of known concentration in the same buffer as the protein samples. Samples and standards were mixed with the working reagent (WR) from the kit, which allows the colorimetric detection of  $\text{Cu}^{1+}$  using BCA. Samples and WR were incubated for 30 minutes at 37°C. After incubation time the plate was cooled to room temperature and the absorbance determined at 550 nm on a Jenway 6305 spectrophotometer.

### **2.10.9 Luciferase assays**

#### **2.10.9.1 Luciferase Assay using recombinant Norrin**

$3 \times 10^5$  STF cells/well ("Super TOPFLASH" HEK 293 cells stably transfected with a luciferase reporter under the control of 7 LEF/TCF binding sites) were plated into 6-well plates. 24 hours later, with a cell density of about 75-80% confluency, the media was removed and replaced with new media containing different concentrations of recombinant human Norrin (R&D systems). After 16-18 hours of incubation with recombinant Norrin, TOPFlash activities were measured using the Luciferase Assay System (Promega) according to the manufacturer's instructions.

#### **2.10.9.2 Dual Luciferase TOPFlash assay**

The Dual Luciferase TOPFlash assay was performed according to the protocol originally described by Xu and colleagues (Xu et al., 2004).

$1 \times 10^5$  STF cells/well were plated into 24-well plates and transfected (section 2.10.6) 24 hours later using Fugene-6 (Promega) with a total of 400 ng of DNA comprising 60 ng of Norrin plasmid, 60 ng of FZD4 plasmid, 60 ng of

TSPAN12 plasmid, 100 ng of LRP5 plasmid, 100 ng of WT or mutant LGR4 plasmid and 1 ng of the transfection control Renilla luciferase plasmid, pRL-TK (Promega). For experiments in which one or more components were omitted, the DNA was adjusted to 400 ng per well with empty pDEST40 vector. 48 hours after transfection, cells were washed with PBS and lysed using passive lysis buffer from the Promega Dual-Luciferase Reporter Assay System kit (Promega). Renilla and Firefly luciferase levels were determined using the Dual Luciferase reporter assay (Promega). The Firefly signal was normalized to the Renilla signal for every well and pathway activation levels were expressed as relative luciferase units (RLU) using the Firefly/Renilla ratio. The expression of Renilla in the cells provided an internal control value allowing the expression levels of the Firefly luciferase reporter gene to be normalized. The pRL-TK contains the herpes simplex virus thymidine kinase (HSV-TK) promoter to provide low to moderate levels of Renilla luciferase expression in co-transfected mammalian cells.

TOPFlash assays using R-spondin 1 (RSPO1) (Life Technologies) as the ligand in place of Norrin were performed similarly.  $1 \times 10^5$  STF cells/well were plated in a 24 well-plate and transfected 24 hours later with 100 ng of WT or mutant LGR4 plasmid and 100 ng of LRP5 plasmid. 24 hours after transfection, media was removed and replaced with complete media containing 50 ng/ml of recombinant RSPO1. Luciferase activities were measured 24 hours later.

The Dual-Luciferase assay was carried out according to the manufacturer's instructions, using white opaque 96-well plates (Grenier BioOne). All assays were analysed using the Mithras LB 940 Luminometer (Berthold Technologies). Normalized reporter activity was obtained by dividing Firefly luciferase values and Renilla luciferase values (Firefly luciferase:Renilla luciferase) and this was expressed as relative luciferase units (RLU). Luciferase assays in STF cells were performed at least three times on separate occasions (biological replicates) and three technical replicates were carried out each time. For each technical replicate the luminescence value was measured three times.

### **2.10.9.3 HEK293 and STF co-culture TOPFlash assay**

For the co-culture assay, STF cells and HEK293 cells were cultured first separately.  $3 \times 10^5$  HEK293 cells and  $3.5 \times 10^5$  STF cells/well were seeded separately in 6-well plates 24 hours prior to transfection. HEK293 cells were transfected with 480 ng of Norrin plasmid and 600 ng of WT or mutant LGR4 plasmid or/and empty pDEST40 vector. STF cells were transfected with 3 ng of pRL-TK, 240 ng of *FZD4*, 240 ng of *TSPAN12*, 300 ng *LRP5* and 300 ng of WT *LGR4* plasmid or pDEST40. Twenty-four hours post transfection, STF cells and HEK293 cells were dissociated from the plates, using an enzyme-free cell dissociation buffer according to the manufacturer's instructions (Thermo Fisher Scientific). Cells were then mixed at a 1:1 ratio, plated in a 24-well plate and grown for 24 hours before luciferase activity was measured. Fold induction was calculated as Firefly Luciferase/Renilla luciferase ratio and expressed as RLU. Every experiment was performed at least three times on separate occasions (biological replicates) and at least three technical replicates were performed each time. For each technical replicate the luminescence value was measured three times.

### **2.10.10 *In vitro* tube formation angiogenesis assay**

$2 \times 10^4$  HDF cells/well were seeded in a 24-well plate 6 days prior to co-culturing HUVEC on top of the confluent fibroblast layer.

Transient knockdown of HUVEC with the siRNAs of interest was performed as described in section 2.10.6.2. Twenty-four hours after HUVEC siRNA transfection, HUVEC were trypsinized from the 6-well plates and cell density was determined using the Countess™ Cell counter (section 2.10.3).  $8.5 \times 10^3$  HUVEC were seeded on top of the HDF cells in EGM-2 media and the co-culture was kept for 6 days with the media changed every 2 days. Tubule formation was assessed on day 6 using the Cellworks CD31 tubule staining kit (Caltag Medsystems Ltd) according to the manufacturer's protocol. Briefly, cells were washed in PBS and they were fixed for 30 minutes using 70% ethanol that had been kept at  $-20^\circ\text{C}$ . Cells were then washed 3 times with

PBS supplemented with 1% BSA. Incubation with the primary antibody diluted in PBS 1% BSA was performed (mouse anti-human CD31, 1:400, Caltag Medsystems Ltd) for 1 hour at 37°C. Cells were then washed 3 times with 1% BSA in PBS before secondary antibody incubation (goat anti-mouse IgG AP conjugate, 1:500, Caltag Medsystems Ltd) for 1 hour at 37°C. Cells were washed in water before Alkaline Phosphatase (AP) staining was performed using 5-Bromo-4-chloro-3-indolyl phosphate/Nitro blue tetrazolium (BCIP/NBT, Caltag Medsystems Ltd).

Images were taken using an EVOS microscope. A total of 8 images per well were taken and they were analysed using angiogenesis software from ImageJ.

### 2.10.11 Quantitative real-time PCR (qRT-PCR)

RNA extracted from HUVEC cells (section 2.9) was converted into cDNA using M-MLV RT (section 2.2.4). qRT-PCR was performed using TaqMan® Gene Expression Assays (Life Technologies) according to the manufacturer's instructions.

Gene	Species	Reference Sequence	Amplicon length	Exon Boundary	Catalogue number
<i>GAPDH</i>	Human	NM_002037.2	93	6-7	Hs02758991_g1
<i>FZD4</i>	Human	NM_036325.2	74	1-2	Hs00201835_m1
<i>LGR4</i>	Human	NM_018490.2	68	1-2	Hs00173908_m1

**Table 2-3: TaqMan® gene expression assay details for FZD4, LGR4 and GAPDH.**

The TaqMan® gene expression assays consist of a pair of PCR primers and a TaqMan® probe with a reporter dye linked to its 5' end and a minor groove binder together with a non-fluorescent quencher at its 3' end.

The PCR reaction mix was prepared in a volume of 20 µl, containing 10 ng of cDNA, 1 µl of 20X TaqMan® Gene Expression assay, 10 µl of 2X TaqMan®

Gene Expression Master Mix comprising AmpliTaq Gold DNA polymerase, dNTPs and a passive internal reference based on proprietary ROX™ dye (Life Technologies). The final volume was adjusted with RNase-free water. Reactions were carried out in a 96-well standard PCR plate and run on an Applied Biosystems 7300/7500 Real-Time PCR System (Applied Biosystems, Life Technologies). The 96-well plate was run using the TaqMan recommended qPCR cycle, which is composed of 2 minutes at 50°C, followed by a denaturation step at 95°C for 10 minutes, then 95°C for 15 seconds and annealing/extension at 60°C for 1 minute, repeated for 40 cycles.

The output data was analysed using the amplification curves and setting an appropriate threshold for all the samples. Sample comparison was performed using the comparative C<sub>T</sub> ( $\Delta\Delta C_T$ ) method for calculating relative quantitation of gene expression (Peirson *et al.*, 2003), using *GAPDH* as an internal control and normalising the data against *GAPDH* expression.

## **2.10.12 Binding assays**

### **2.10.12.1 Cell surface binding assay**

COS7 cells were seeded in a 12-well plate at a density of  $1.3 \times 10^5$  cells per well and transiently transfected 24 hours later (section 2.10.6.1) with 700 ng of the indicated plasmids. Forty-eight hours post transfection the medium of each well was removed and cells washed twice with Hank's Balanced Salt Solution (HBSS) (Gibco, Life Technologies). 0.5 ml of conditioned media containing WT Norrin fused with alkaline phosphatase was added to each well and the cells incubated at 4°C for 90 minutes. Following this, Norrin conditioned media was removed and a crosslinking reaction was performed for 30 minutes at room temperature. The crosslinking solution was composed of 1.5mM 3,3'-dithiobis[sulphosuccinimidylpropionate] (DTSSP) (Thermo Scientific) and 1M N-2-hydroxyethylpiperazine-N-2-ethane sulphonic acid (HEPES) (Gibco, Life Technologies) in HBSS buffer. The crosslinking reaction was stopped by incubating the cells with 0.1 M hydroxymethyl-aminomethane hydrochloride (Tris-HCl) for 15 minutes at room temperature.

Cells were then washed twice with PBS. Subsequent alkaline phosphatase staining was carried out using 1-Step™ NBT/BCIP (Thermo Scientific) according to the manufacturer's instructions. Alkaline phosphatase stained cells were then rinsed with water and the alkaline phosphatase labelled Norrin binding to the surface of the cells was detected using the EVOS microscope.

#### **2.10.12.2 Cell based binding assay**

$3 \times 10^5$  COS7 cells were seeded in a 6-well plate. 24 hours after seeding, transient transfections were performed (section 2.10.6.1) After a further 24 hours, cells were dissociated from the plates using enzyme-free cell dissociation buffer (Thermo Fisher Scientific) and the cell density calculated using the Countess™ Cell counter (section 2.10.3). For each assay,  $1.7 \times 10^3$  cells were seeded per well of a 96-well plate and grown for 24 hours. Different dilutions of alkaline phosphatase labelled Norrin conditioned media were added to each well and the plate was incubated for 90 minutes at 4°C. After Norrin conditioned media incubation, cells were washed twice with HBSS buffer and alkaline phosphatase detected using the Phospa-Light™ System (Applied Biosystems) according to the manufacturer's instructions. Briefly, cells were lysed for 10 minutes at room temperature and incubated with a mixture of non-placental alkaline-phosphatase inhibitors prior to incubation with CSPD® chemiluminescent substrate. The CSPD substrate produces a luminescent signal when dephosphorylated by alkaline phosphatase and this luminescence signal was measured using a Mithras LB 940 Luminometer (Berthold Technologies).

#### **2.10.13 Live cell imaging using Nikon BioStation IM microscope**

Hek293 cells were seeded in live cell imaging microplates (Ibidi®) 24 hours before transfection. Transfected cells were monitored 24 hours after transfection using IM-Q cell incubator and monitoring system. Before placing the cells in the BioStation IM the media of the cells was changed to CO<sub>2</sub> independent media (Invitrogen). The 20X objective of the inverted

microscope present in the BioStation IM was used to capture the images. Images were collected every 30 seconds for up to 240 minutes. The resulting video and images were analysed using ImageJ.

## 2.11 Immuno-techniques

### 2.11.1 Antibodies

Antibody name	Raised in	Stock concentration	IF dilution	WB dilution (1/x)	Source
Monoclonal Anti-LGR4, clone 8F6	Mouse	0.5mg/ml	-	1/500	Sigma Aldrich
Anti-Human FZD4 polyclonal	Rabbit	1mg/ml	-	1/500	MBL International Corporation
Anti-FZD4 polyclonal	Goat	0.5mg/ml	-	1/500	Abcam
Anti-human Norrin polyclonal	Goat	0.2mg/ml	-	1/500	R&D Systems
Anti-cMyc clone 9E10 polyclonal	Mouse	No data	1/200	1/500	Sigma Aldrich
Anti-6X His monoclonal	Mouse	1.000mg/ml	-	1/1000	Abcam
Anti-CD31 polyclonal	Mouse	No data	1/20	-	Cell Works
Polyclonal Anti-LRP5	Rabbit	0.25mg/ml	-	1/1000	Invitrogen
Polyclonal Anti-TSPAN12	Rabbit	0.5mg/ml	-	1/1000	Sigma Aldrich
Monoclonal Anti- $\beta$ -Actin	Mouse	35.2mg/ml	-	1/1000	Sigma Aldrich
Monoclonal	Mouse	No data	-	1/1000	Invitrogen

Anti-V5

Antigen	Raised in	Conjugate	Stock concentration	IF dilution	WB dilution (1/x)	Source
Mouse IgG	Goat	AlexaFluor 568	2mg/ml	1/1000	-	Invitrogen
Goat IgG	Donkey	AlexaFluor 488	2mg/ml	1/1000	-	Invitrogen
Mouse IgG	Donkey	AlexaFluor 488	2mg/ml	1/1000	-	Invitrogen
Goat IgG	Donkey	AlexaFluor 568	2mg/ml	1/1000	-	Invitrogen
Rat immunoglobulines	Rabbit	HRP	1mg/ml	-	1/1000	Dako Cytomation
Rabbit Immunoglobulines	Goat	HRP	1mg/ml	-	1/1000	Dako Cytomation
Mouse Immunoglobulines	Rabbit	HRP	1mg/ml	-	1/1000	Dako Cytomation

**Table 2-4 A and B: Table 2-4 A (upper table) showing primary antibodies. Table 2-4 B showing secondary antibodies. Names of primary and secondary antibodies. Conjugates of the secondary antibodies are also listed.**

The antibodies have been listed along with the species of animal each antibody was raised in, stock concentration, dilution for immunofluorescence (IF) and western blotting (WB). The commercial source of each antibody is shown.

### 2.11.2 Western Blotting (WB)

Samples containing 10-20 µg of total protein (depending on the assay) were reduced and denatured using 4X NuPAGE LDS sample buffer (106 mM Tris-HCl, 2% lithium dodecyl sulphate (LDS), 10% Glycerol, 0.51 mM EDTA, 0.22 mM SERV A® Blue G250, 0.175 mM Phenol red pH 8.5) and heated to 95°C for 5 minutes. Denatured samples were loaded onto a NuPAGE 4-12% Bis-Tris gel (Invitrogen) along with SeeBlue prestained standard protein marker (Invitrogen), in an X-Cell SureLock electrophoresis tank (Invitrogen) filled with 1X NuPAGE MES Running buffer (Invitrogen). Proteins were separated by electrophoresis at 130V for 90 minutes (unless otherwise indicated). Proteins from the SDS-PAGE gels were transferred onto methanol-activated Invitrolon polyvinylidene fluoride (PVDF) membrane (Invitrogen). The SDS-PAGE gel and PVDF membrane were sandwiched between blotting paper and stacks of sponges, and the full sandwich was soaked in 1X NuPAGE transfer buffer (Invitrogen) containing 10% v/v methanol. The sandwich was assembled onto the X-Cell blot module (Invitrogen). The blot module was filled with 1X NuPAGE transfer buffer and the surrounding tank was filled with ice and distilled water. The transfer module was run at 30V for 90 minutes. After transfer, the PVDF membrane was rinsed with PBST and incubated with western blocking solution (5% w/v non-fat milk powder (Marvel) in PBST) at 4°C overnight with agitation. The membrane was incubated with primary antibody diluted in blocking solution at 4°C with agitation over-night. After 4 rounds of 5 minutes washes in PBST, the membrane was incubated with secondary antibody diluted in blocking solution for 1 hour at room temperature with agitation. After three more rounds of 5 minute washes in PBST, the membrane was rinsed in distilled water and excess liquid allowed to drain away. The membrane was incubated with Femto SuperSignal West Reagent (Pierce) according to the manufacturer's instructions and exposed using the ChemiDoc imaging system and ImageLab software (BioRad) to detect immunopositive bands.

### **2.11.3 Immunofluorescence (IF)**

Cells were grown on sterile coverslips in 6-well plate or in 12-well plates. When 60-80% confluent, cells were washed three times with PBS and fixed in ice-cold methanol for 5 minutes or 2% PFA at room temperature for 20 minutes. PFA fixation was followed by permeabilisation of the cell membrane with 0.1% Triton X-100 in PBS for 5 minutes at RT. Fixed cells were then incubated with blocking solution (3% w/v non-fat milk powder in PBS) for 1 hour at room temperature. Coverslips were inverted in 100µl of primary antibody solution (primary antibody diluted in 1.5% w/v non-fat milk powder in PBS) in humidity chambers for 1 hour at room temperature. Coverslips were rinsed three times for 5 minutes in PBS and inverted onto 100µl of secondary antibody solution (secondary antibody diluted in 1.5% w/v non-fat milk powder in PBS) with 4',6-diamidino-2-phenylindole (DAPI) at a concentration of 1 µg/ml in humidity chambers, away from light, for 1 hour at room temperature. After 3 more 5 minute washes in PBS, coverslips were mounted cell side down onto SuperFrost slides (Fisher Scientific) with Mowiol 4-88 mounting medium (Calbiochem) prepared according to manufacturer's instructions.

For co-localisation experiments, cells were incubated with Norrin conditioned medium for 1 hour at 37°C 48 hours after transfection and prior to being washed and fixed.

## **2.12 Microscopy**

### **2.12.1 Light Microscopy**

Health and confluency of cells was assessed using an Olympus CKX41 bright field microscope and 4x or 10x objective lenses.

### **2.12.2 Confocal microscopy**

Fixed and immunostained cells were visualised using a Nikon A1R confocal laser scanning microscope. Cells were viewed using wide-field

epifluorescence, utilising DAPI blue filter (340-380 nm excitation, 400 nm emission), FITC green filter (460-500 nm excitation, 505 emission) and Texas Red filter (528-553 nm excitation, 565 nm emission). Images were captured using scanning confocal microscopy with 405 nm, 457-514 nm, 561 nm and 642 nm lasers with Nikon NIS-Elements C advanced software (Version 4.11.0).

### **2.12.3 EVOS™ Cell Imaging System**

Transfected cells transfected with fluorescence tagged constructs were monitored using an EVOS FL colour microscope using the GFP filter cube (470 nm excitation and 525 nm emission).

Images from the angiogenesis co-culture and cell surface binding assay were taken using the EVOS XL Core microscope, which presents a transmitted-light system (bright field and phase contrast) using a 4X objective.

### 3 Functional characterization of FEVR-related *LGR4* missense variants using a zebrafish model

#### 3.1 Background

Prior to the work described in this chapter, next generation sequencing technologies had been used to try and identify the autosomal dominant FEVR gene located within the *EVR3* locus on chromosome 11p12-13 (Downey et al., 2001). This work identified a missense variant in *LGR4*, c.188C>T p.(R40W), as the only candidate mutation that segregated with the disease phenotype within the large family used to map the *EVR3* locus. Screening of *LGR4* in the Leeds FEVR cohort identified an additional five putative missense mutations in five unrelated FEVR families/cases; c.933G>C p.(Q311H), c.1289C>T p.(T430M), c.1924G>A p.(E642K), c.2164G>A p.(A722T), c.2248G>A p.(A750T) (unpublished data generated by Dr James Poulter and Mrs. Evangelia Panagiotou, University of Leeds). Pathogenic prediction tools indicated that some of these variants were likely to be pathogenic, but these predictions varied and were very dependent on the prediction tool used (Table 3-1). In addition, the majority of the variants altered evolutionarily conserved amino acids (Figure 3-1). A schematic representation of all the *LGR4* variants can be found in Figure 1-11. At the time this study was initiated, all of the variants were predicted to be rare from the inspection of various SNP and variant databases. Although this data indicated that *LGR4* was the *EVR3* gene, the missense nature of the mutations meant that there was still doubt.

cDNA & protein change	CADD v1.3*	Blosum6 2**	PolyPhen2 (HumVar)	SIFT	Provean
c.118C>T p.(R40W)	32	Score -3	Benign (0.005)	Not Tolerated	Neutral (-0.788)
c.933G>C p.(Q311H)	11.83	Score 0	Benign (0.005)	Tolerated	Neutral (-1.228)
c.1289C>T p.(T430M)	23.5	Score -1	Probably Damaging (0.958)	Tolerated	Neutral (-0.780)
c.1924G>A p.(E642K)	27.8	Score 1	Probably Damaging (0.996)	Not Tolerated	Neutral (-2.402)
c.2164G>A p.(A722T)	18.25	Score -1	Possibly Damaging (0.820)	Tolerated	Neutral (0.594)
c.2248G>A p.(A750T)	29.6	Score -1	Probably Damaging (0.999)	Not Tolerated	Deleterious (-3.212)

**Table 3-1: Summary of bioinformatics analyses undertaken to predict the pathogenic nature of the six *LGR4* missense variants identified in FEVR patients.**

The cDNA and the protein change for each variant is indicated. URLs: PolyPhen2, <http://genetics.bwh.harvard.edu/pph2/> [(Adzhubei et al., 2010)]. This score is based upon its prediction of the possible impact of an amino acid substitution based upon the 3D structural features of the protein and its homologous; SIFT, <http://sift.jcvi.org/> [(Ng and Henikoff, 2003)]. This score classifies amino acid substitutions based upon the evolutionary conservation of the residue within the relevant protein family; Blosum62 [(Henikoff and Henikoff, 1993)]. This score uses alignments between evolutionarily divergent protein sequences; PROVEAN, <http://provean.jcvi.org/> [(Choi et al., 2012)] This score is based upon the amino acid variation within the context of the surrounding sequence. Scaled CADD (Combined Annotation Dependent Depletion) scores generated using version 1.3 <http://cadd.gs.washington.edu> [(Kircher et al., 2014)]. \*A scaled CADD score of 20 means that the variant is amongst the top 1% of deleterious variants in the human genome and a score of 30 means that the variant is in the top 0.1%. \*\*Blosum62 scores range from +3 to -3 and negative scores are more likely to be damaging substitutions.

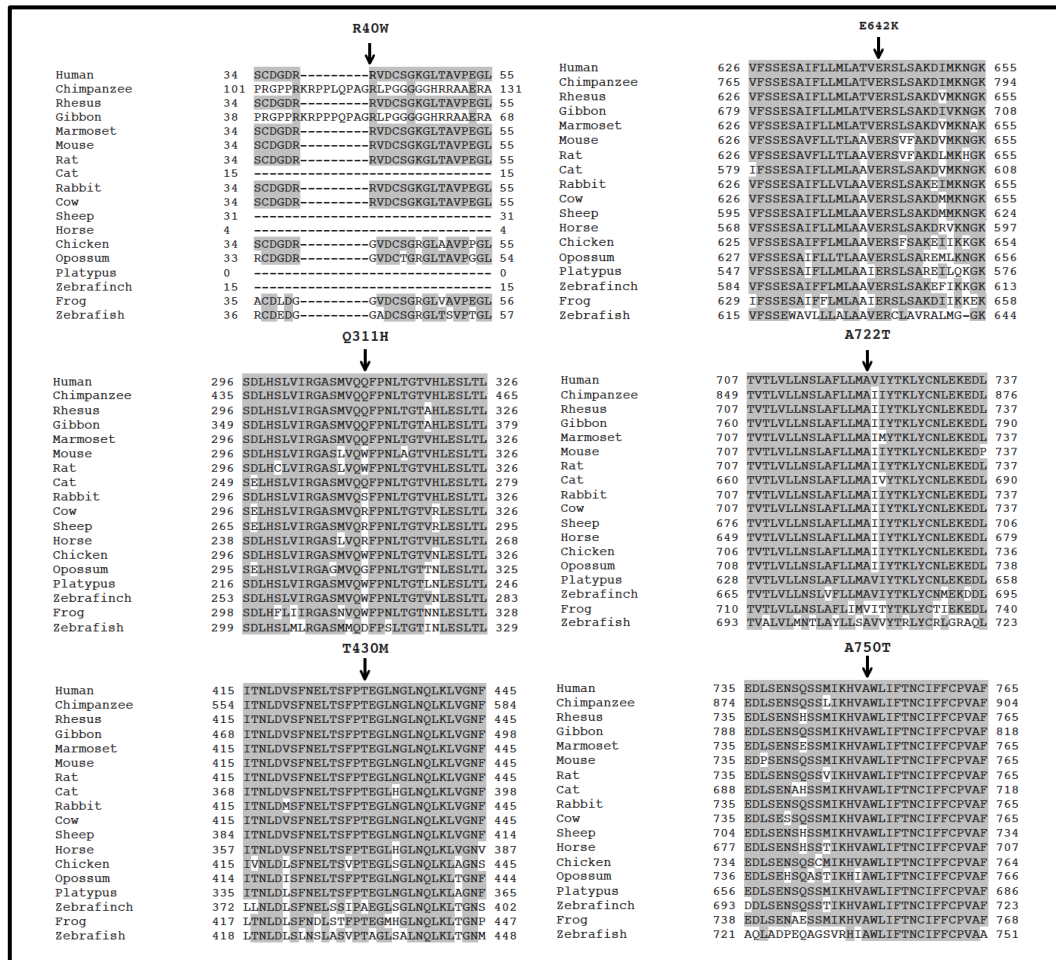


**Figure 3-1: Protein sequence alignment of human LGR4 with its orthologues.**

Alignments were calculated with ClustalW. Accession numbers: Human NP\_060960.2, Chimpanzee XP\_003313024.2, Rhesus Monkey NP\_001252594.1, Gibbon XP\_003254648.2, Marmoset XP\_002755173.1, Mouse NP\_766259.2, Rat NP\_775450.1, Cat XP\_003993169.1, Rabbit XP\_002709069.1, Cow NP\_001192440.1, Sheep XP\_004016773.1, Horse XP\_001502255.1, Chicken XP\_426162.2, Opossum XP\_001380202.1, Platypus XP\_001517774.2, Zebrafish XP\_002194103.2, Frog NP\_001089881.1 and Zebrafish XP\_687184.3. Only 30 amino acid residues surrounding each mutation are shown. Conserved amino acid residues are highlighted.

The aim of this experiment was to undertake an assay to quickly and easily determine if the missense variants altered the function of *LGR4*. Morpholino antisense oligonucleotides (MOs) have been used in zebrafish as a tool to quickly study gene function in early embryo development for over fifteen years (Egger, 2000). Combining the MO knockdown with co-injection of the mRNA sequence of the gene being studied (mRNA rescue), also allows the zebrafish model to be used to verify and study the effects of specific

mutations present in disease genes (Collin et al., 2013; Han et al., 2011; Jin et al., 2015; Wu et al., 2016).

In this study, the zebrafish was used to assess the *LGR4* missense variants using the same ocular vasculature phenotype assay utilised by Collin et al. (2013) to characterise the FEVR related *ZNF408* missense variants. This assay was chosen as it had previously been used to functionally test a causative FEVR missense variant in a new FEVR gene, *ZNF408*. The His455Tyr variant in *ZNF408* was unable to rescue the abnormal vasculature in the fish eye after MO knockdown of *znf408*. For that reason, MOs were used to knockdown *lgr4* in the zebrafish (*Danio rerio*) model and the eye vasculature of the fish was evaluated. Human WT *LGR4* or variant mRNA was then co-injected together with the *lgr4* MO and the eye vasculature of the fish was again evaluated to check for any rescue of the aberrant eye phenotype.

### 3.2 Morpholino antisense oligonucleotide (MOs) design

Two different MOs were designed to knockdown the expression of *lgr4* in zebrafish embryos: a translation blocking MO and a splice blocking MO. To design the MOs, the zebrafish *lgr4* sequence was needed. The zebrafish genome sequence was inspected using the UCSC genome browser (Sep. 2014 (GRCz10/danRer10)) (section 2.5.2). The results showed that there was only one orthologue of *lgr4* in the zebrafish genome but that it had not been annotated. The Zebrafish information network (ZFIN) was also evaluated and confirmed this finding (section 2.8.1). Therefore the *lgr4* gene predicted by *Ensembl* was used (ENS DART00000085419.4) to design the splice and translation blocking MOs (Figure 3-2).



**Figure 3-2: *lgr4* prediction in zebrafish.**

UCSC genome browser assembly for *lgr4* in zebrafish Sep. 2014 (GRCz10/danRer10). Highlighted in maroon is the Ensembl (ENS DART00000085419.4) prediction use to design the MOs for *lgr4*. Data accessed on October 2013.

BLAST alignment (section 2.5.3) of the predicted zebrafish *lgr4* protein with the human LGR4 protein (NP\_060960) showed that the proteins are 59% identical and 72% similar, where conservative substitutions are also included (Appendix 8.1).

The MOs were designed using the Gene Tools MO design service (section 2.8.2). The translation blocking MO (called ATG) was designed against the ATG start codon in exon 1. This MO binds to the 5'-untranslated region (5'-UTR) and includes 20 bases of the coding sequence, and therefore hinders ribosome assembly. The MO sequences were independently checked using BLAT (section 2.5.3) to determine the MO binding site in the zebrafish genome (GRCz10/danRer10) (Figure 3-3, A) and using BLAST to tests for specificity (Figure 3-3, B). The only target found was *lgr4*, with no mismatched targets found for the blocking MO, indicating high specificity of the translation blocking MO.

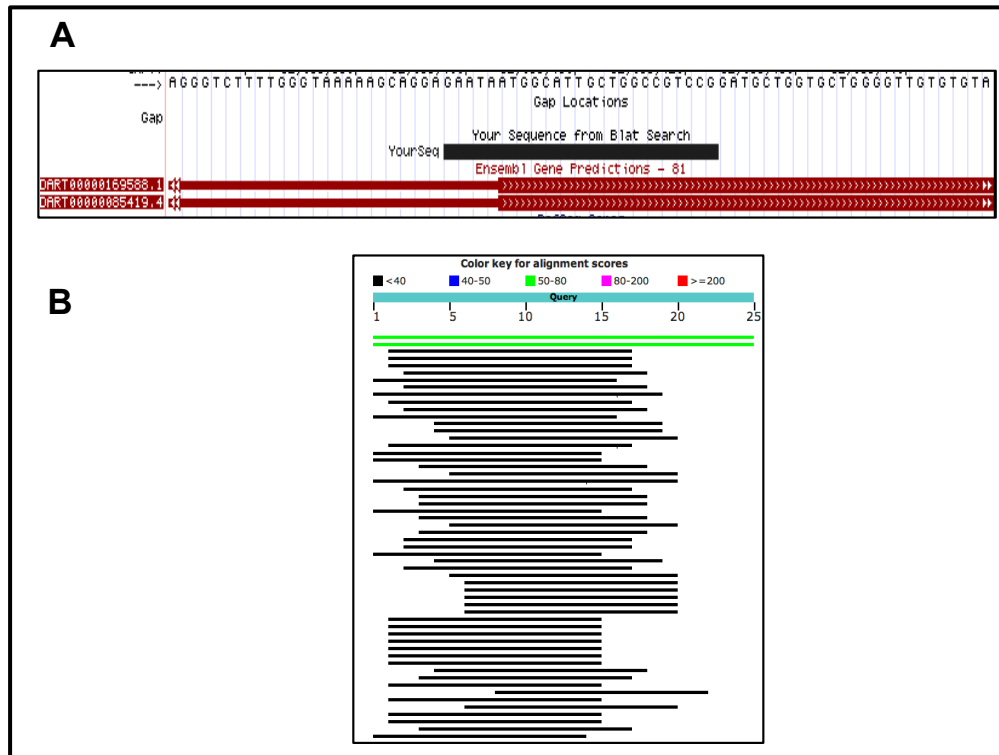


**Figure 3-3: Translational MO design BLAT and BLAST search.**

**A:** Translational ATG MO BLAT search in the Sep. 2014 (GRCz10/danRer10) UCSC genome browser. The translation blocking (ATG) MO sequence is the reverse and complement sequence shown at the top of the image and represented by the black box.

**B:** Translational ATG MO BLAST search. The first green bar represents 100% sequence alignment with *lgr4* from zebrafish (Accession: XM\_682092.8). The second green bar represents 100% alignment with *lgr4* Zebrafish DNA sequence from clone DKEY-288G16 (Accession: BX511109.4). The black bars represent other zebrafish sequences without 100% specificity.

The splice MO (called splice) had to be designed so the resulting mRNA transcript occurred in a frameshift and likely to undergo nonsense-mediated mRNA decay (NMD). Therefore the splice blocking MO had to be designed over an exon that would result in a predicted frameshift and premature termination codon when excluded from the mRNA. The ExPASy translation tool was used to test the outcome of deleting the individual exons of *lgr4*. The first exon to cause a frameshift when deleted was exon 16. Therefore the splice blocking MO was designed against the splice acceptor site of exon 16 (Figure 3-4). The specificity of the splice MO was checked within the zebrafish genome (GRCz10/danRer10) using BLAT (Figure 3-4, A) and BLAST (Figure 3-4, B), and was confirmed to be specific to the *lgr4* locus.

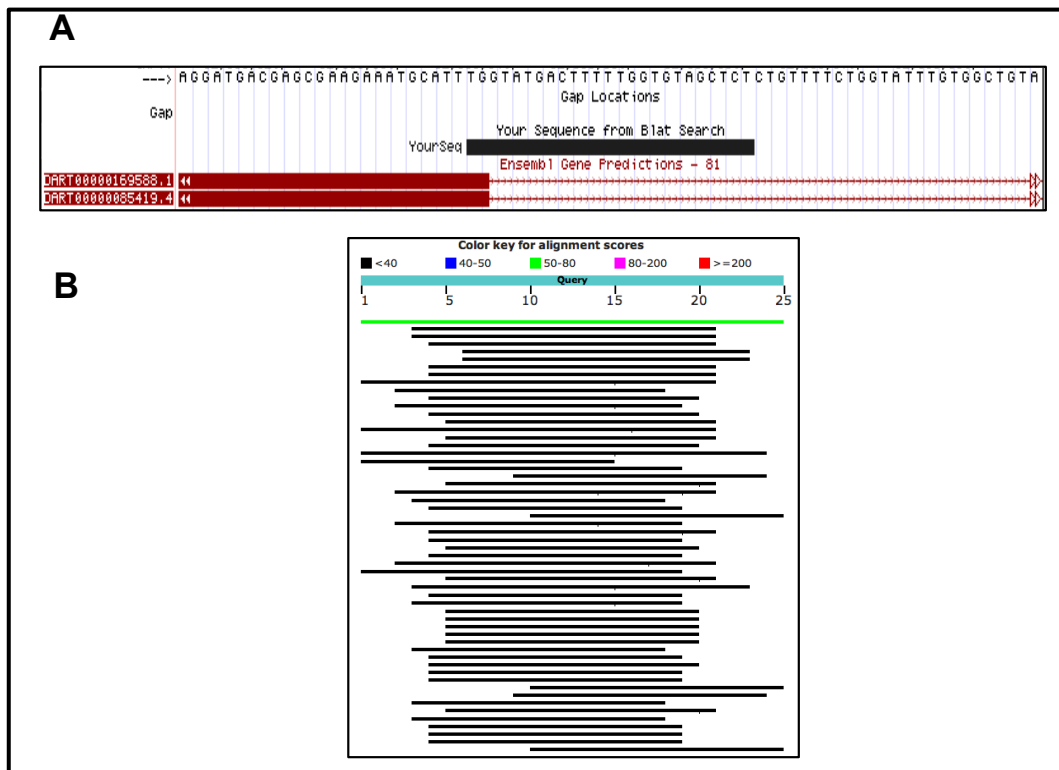


**Figure 3-4: Splice MO design BLAT and BLAST search.**

**A:** Splice MO BLAT search in the Sep.2014 (GRCz10/danRer10) UCSC genome browser. The splicing blocking (splice) MO sequence is the reverse and complement sequence shown at the top of the image and represented by the black box.

**B:** Splice MO BLAST search. The green bar represents 100% sequence alignment with *lgr4* Zebrafish DNA sequence from clone DKEY-288G16 (Accession: BX511109.4). The black bars represent other zebrafish sequences without 100% specificity.

### 3.2.1 MO injection to assess the zebrafish phenotype

MO knockdown of *lgr4* was performed in the *fli1:eGFP* transgenic zebrafish strain, which was obtained from the Zebrafish International Resource Centre (ZIRC) (<http://zebrafish.org> - catalog ID ZL1085). This is a reporter fish line that expresses eGFP under the control of the promoter of the early endothelial marker *fli1*, allowing the visualisation of the blood vessels during embryonic development of the fish (Ellertsdóttir et al., 2010). The endothelial cells of the fish are labelled with eGFP so the vasculature fluoresces green when excited with a 488 nm wavelength laser.

A schematic representation of the experimental procedure is detailed in Figure 3-5. Briefly, this involved injecting individual MOs into 1 or 2-cell stage zebrafish embryos. Four days after injection, the fish were fixed and evaluated under a fluorescent microscope to determine the vasculature phenotype. The Zeiss Axio Imager Z1 fluorescent microscope with an Alexa fluor 488 GFP filter was used for this visualisation.

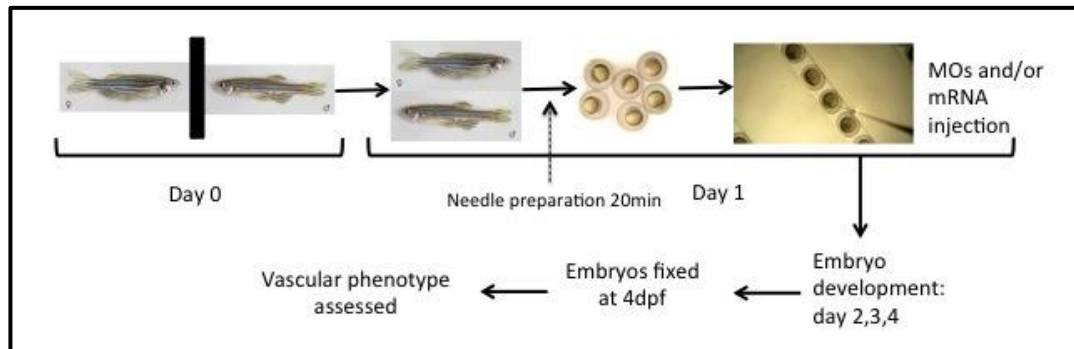


**Figure 3-5: Schematic representation of the experimental procedure carried out in the zebrafish.**

Day 0: one day before the injections male and female fish were kept separately in different tanks overnight. Day 1: male and female fish were put together in the same tank for 20 minutes while the injection needles were prepared. After mating, 1 or 2-cell fish eggs were injected with the MO or with the combined MO/*LGR4* mRNA. Day 2-3: Fish were kept at 37°C. Day 4 post-fertilization (4dpf): morphants were fixed and the vascular phenotype assessed.

### 3.2.1.1 Optimising the *lgr4* morpholino dose-response

The MO dose response experiment was carried out by Dr. Erik de Vrieze (Radboud Medical Centre, Nijmegen, The Netherlands).

To analyse the effects of *lgr4* MO knockdown in zebrafish, and to determine the suitable MO dose to use, different doses of either the splice or the ATG MO were injected into 1 or 2-cell stage zebrafish embryos and the phenotype in a single eye of each embryo was evaluated (Figure 3-6). The classification of the eye phenotype was similar to Collin et al., 2013 and was based on the number of aberrations present in the eye. Eyes were categorised into one of four groups: normal eye, mildly affected, moderately affected or severely

affected (See section 3.2.1.2 below for further explanation of each phenotype). Two controls were used in this experiment. The wildtype (WT) fish control consisted of un-injected fish and was used to control for the survival of the embryos. The second control was a standard negative control from *Gene Tools*. 10 ng of MO directed against a human  $\beta$ -globin intron mutation was used to test for the toxicity of the MOs.

For the splice MO, 1 ng, 4 ng, 6 ng and 8 ng MO doses were tested. The 1 ng dose of *lgr4* splice MO did not have much of an effect, with 98% of fish presenting with a normal eye phenotype, indicating that a higher MO dose was needed. The 8 ng dose of the splice MO had a massive effect with only 22% of the fish presenting with a normal phenotype and 26% of the fish presenting with a severe phenotype. However, the survival rate of these fish decreased dramatically to 77% (Table 3-2), which could be explained by a more severe phenotype of MO resulting in morphant death. The 4 ng dose of splice MO resulted in 63% of the fish eyes having a normal phenotype, but only 1% of the fish presented with a mild phenotype, implying a poor distribution of these fish among the aberrant phenotype classes. However, the 6 ng dose of the *lgr4* splice MO led to approximately 50% of the injected embryos having an abnormal eye phenotype, and these aberrant eye phenotypes were distributed through the three aberrant classes, with 21% of the eyes classified as mild and moderate and 9% of the eyes classified as severe (Figure 3-6, Table 3-2).

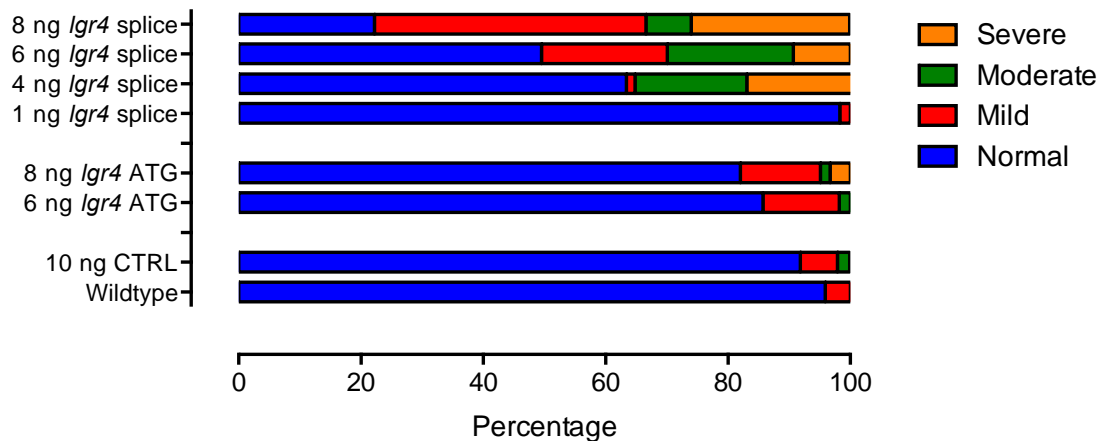


**Figure 3-6: *Igr4* morpholino dose-response results.**

Different doses of splice and ATG MOs were injected into the zebrafish embryos and the eye phenotype was classified as Normal (blue), Mild (red), Moderate (green) or Severe (yellow). Wildtype fish are un-injected fish, which are used to control for the survival of the fish. To control for the toxicity of the MOs, 10 ng of a standard negative control MO directed against a human  $\beta$ -globin intron mutation was injected (10 ng CTRL).

	WT	10 ng Ctrl	6 ng <i>Igr4</i> ATG	8 ng <i>Igr4</i> ATG	1 ng <i>Igr4</i> splice	4 ng <i>Igr4</i> splice	6 ng <i>Igr4</i> splice	8 ng <i>Igr4</i> splice
<b>No. of Embryos</b>	49	52	56	122	60	71	97	54
<b>Normal (%)</b>	96	90	86	82	98	63	50	22
<b>Mild (%)</b>	4	9	12	13	2	1	21	44
<b>Moderate (%)</b>	0	1	2	2	0	19	21	8
<b>Severe (%)</b>	0	0	0	3	0	17	8	26
<b>Fish Survival (%)</b>	95	93	92	90	94	95	92	77

**Table 3-2: Number of embryos analysed, percentage of the fish present with each phenotype and survival numbers of the fish.**

The data is from the *Igr4* MO dose-response experiment. The number of embryos analysed in each category is detailed and the percentage of fish with a normal, mild, moderate or severe phenotype is listed. The survival of the fish was calculated by counting the dead fish before fixation of the fish (4 dpf).

For the ATG (translation blocking) MO, 6 ng and 8 ng doses were tested and both resulted in 86% and 82% of fish having normal eyes respectively. The 6 ng dose of ATG MO led to 12% of the fish presenting with a mild phenotype and only 2% of the fish presenting with a moderate eye phenotype. No fish were found with the severe phenotype. The 8 ng dose of the ATG MO

resulted in 13% of the fish being assigned as mild and 2% with a moderate phenotype. At this dose, 3% of the fish presented with a severe phenotype. The ATG MO appeared to be less efficient when compared to the splice MO, but both MOs resulted in the same aberrant eye phenotype in the fish. The fact that ATG and splice *Igr4* MOs gave the same vascular phenotype in the embryos, indicated that this defect observed was due to the knockdown of *Igr4* and not due to off-target effects of the MOs.

To confirm the effects of the MOs, RNA was extracted from embryos injected with the splice MO and *Igr4* transcript expression was analysed. RT-PCR followed by sequencing confirmed the action of the splice MO and the presence of the splice defect in embryos injected with the splice MO (data not shown, produced by Dr. Erik de Vrieze, Radboud Medical Centre, Nijmegen, The Netherlands).

Based on the results of the MO-dose response experiment, the MO and dose chosen for subsequent experiments was 6 ng of splice *Igr4* MO. The reason for this decision was the good survival rate of the morphants following the injections and because around 50% of the injected embryos displayed an aberrant eye phenotype which was distributed through mild, moderate and severe phenotypes.

#### **3.2.1.2 Classification of the eye phenotype in *Igr4* MO knockdown zebrafish**

With the MO experiment optimised, the experiment was repeated using only 6 ng of splice *Igr4* MO and the fish phenotype was evaluated in order to determine the classification of the different abnormal phenotypes observed.

The embryos were divided into four subclasses based on their ocular vasculature phenotype using a scoring system similar to that developed by Rob Collin and colleagues (Collin et al., 2013) (Figure 3-7). Wild type fish, without any eye vascular defect were classified as normal. In the normal eye, there is a clear inner optic circle (ioc) vessel surrounding the lens and three

vessels connected to it: the optic vein (ov) found at the bottom of the eye and the nasal ciliary artery (nca) and the dorsal ciliary vein (dcv) found at the top of the eye (Figure 3-7, A). The eye vasculature nomenclature used in this study is based on *The Interactive Atlas of Zebrafish Vascular Anatomy* (<http://zfish.nichd.nih.gov/Intro%20Page/intro9.html>). Fish with eye vasculature that differed from the normal phenotype were classified as abnormal and split into three different categories; mild, moderate or severe depending on the number of aberrations present. In the mild phenotype, the number of vessels radiating from the ioc is abnormal or one of the vessels connects with the lens (Figure 3-7, B). The eyes classified as moderate had a combination of two of the aberrations present in the mild phenotype, abnormal number of vessels radiating from the ioc plus a vessel connecting to the lens (Figure 3-7, C). Finally, when there is a clear absence of the ioc, the eyes were categorised as severe phenotype (Figure 3-7, D). From now on, the classification of the fish in the next experiments is based on the eye phenotypes observed and described in Figure 3-7.

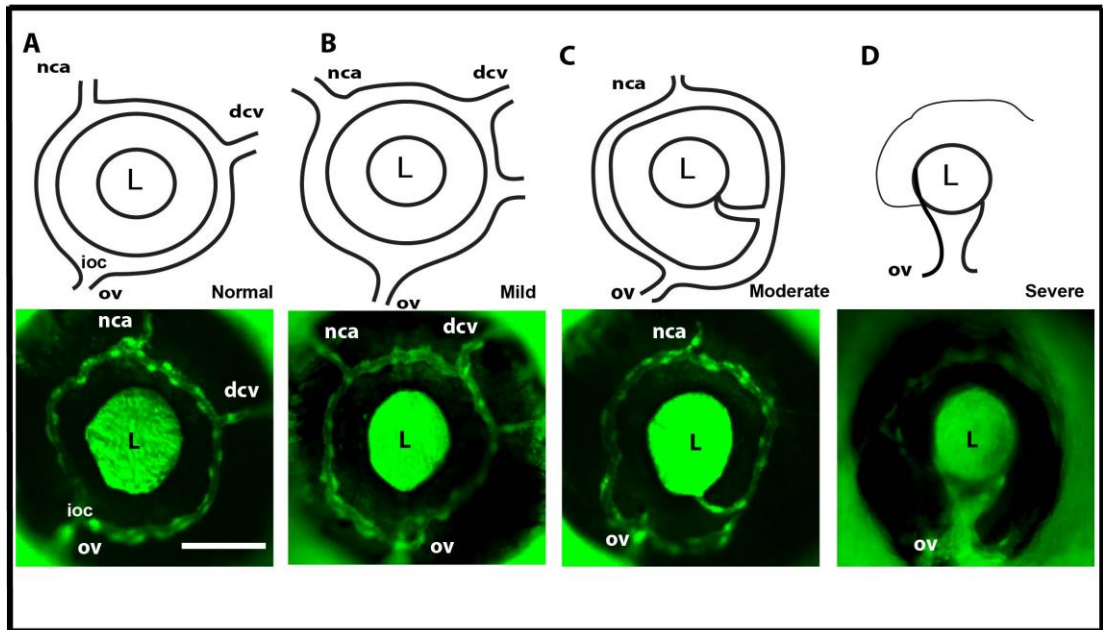


**Figure 3-7: Classification of the eye phenotypes found in *lgr4* MO zebrafish.**

These images are from embryos injected with a 6 ng dose of the *LGR4* Splice MO. In the upper panel are schematic representations of the zebrafish eye vasculature patterns observed in MO-induced knockdown fish. In the lower panel are representative images of GFP labelled vessels in the eyes of *fli1:eGFP* transgenic zebrafish larvae. **A:** Represents normal class or WT phenotype. The ioc is situated around the lens (L) and three vessels radiate from it, the optic vein (ov), the nasal ciliary artery (nca) and the dorsal ciliary vein (dcv). **B:** Eyes classified as a mild phenotype, defined as when the eye presents an aberrant number of vessels radiating from the ioc or a vessel connecting to the lens **C:** Moderate phenotype, defined as when the ioc has an aberrant number of vessels radiating from it plus an abnormal vessel connecting with the lens. **D:** Classification of the eyes as having a severe phenotype, which is defined as when there is an absence of the ioc. Scale bar represents 125 nm.

Only the eyes of the *lgr4* morphants were phenotyped in detail but additional defects were observed in the fish, indicating the presence of additional developmental abnormalities due to MO *lgr4*. For example, the WT fish have a straight body shape but some of the injected fish showed a curved body (Figure 3-8, A). Similarly, vascular abnormalities were also observed in the trunk but these varied in severity (Figure 3-8, B).

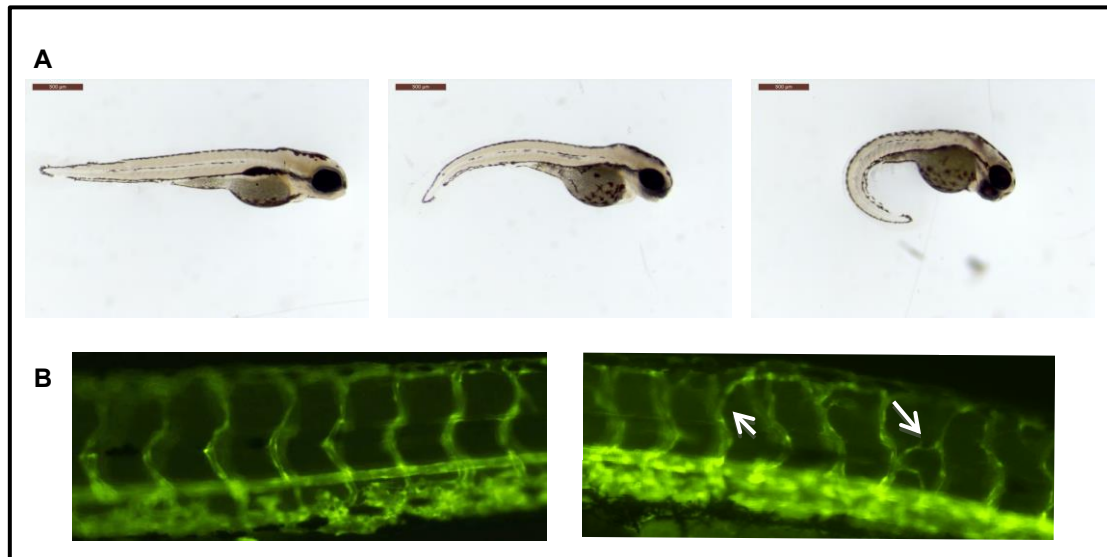


**Figure 3-8: MO *lgr4* morphologies and vascular abnormalities in the trunk.**

**A:** MO *lgr4* fish presented a wide range of body shape morphology. From left to right: straight and normal WT morphology, moderate curve morphology and severe curve morphology. Scale bar = 0.5 mm. **B:** Vascular abnormalities of the fish trunk. The trunk is shown as a lateral view (dorsal side is up). Intersegmental vessels project from the dorsal aorta (bottom horizontal vessel) toward the dorsal longitudinal vessel at the top of the image. In the left, the fish presented normal trunk vasculature. At the right of image B, the trunk presented vascular defects, where the intersegmental vessel branching is disrupted (white arrows).

### 3.3 Creating *LGR4* expression constructs for MO rescue experiments in zebrafish.

In order to functionally characterise the pathogenicity of the missense variants found in *LGR4*, human WT *LGR4* mRNA or mRNA containing one of the candidate *LGR4* variants were co-injected with 6 ng of splice MO to determine if they could rescue the aberrant phenotype found in the fish. For this experiment, expression constructs for WT *LGR4* and the six missense variants were made.

#### 3.3.1 Identification of *LGR4* splice variants

The human genome browser (UCSC GRCh37/hg19) documented only one RefSeq *LGR4* transcript that contained 18 exons and encoded a 951 amino acid protein (NM\_018490) (data accessed October 2013). However, all but

one of the human *LGR4* expression constructs available from plasmid repositories and commercial sources (including DNASU, Addgene) contain an isoform which is missing exon 2. Furthermore, a transcript missing exon 2 (uc001mrk.4) is annotated in the UCSC genes track in the genome browser (hg19 data accessed in October 2013) (Figure 3-9). This variant encodes a protein of 927 amino acids and differs from the RefSeq protein by having one less LRR domain. Therefore, to determine which transcript to use for the rescue experiments, the different *LGR4* isoforms were evaluated in different human tissues.

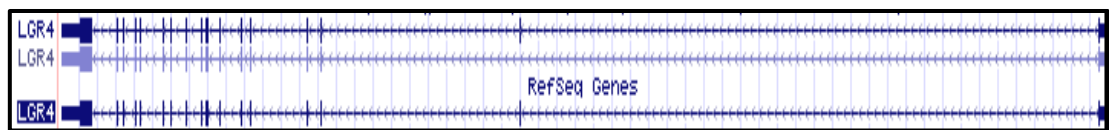


**Figure 3-9: LGR4 transcripts on UCSC Genome Browser (hg.19).**

Only one validated *LGR4* RefSeq transcript is listed but an isoform missing exon 2 (light blue) is predicted under the UCSC genes track. Data accessed on October 2013.

Total RNA from a panel of different human adult and fetal tissues was reversed transcribed into cDNA (section 2.2.4) and PCR amplified with primers for *LGR4* (section 2.2.2). This panel did not contain retinal RNA, therefore ready-made retinal cDNA was purchased from Clontech (Catalog No. 637216) and used for the *LGR4* PCR amplification. The forward primer was designed within exon 1, while the reverse primer was designed within exon 5 (Primer sequences in Appendix 8.3). Thus, the region missing exon 2 could be evaluated. The tissues assayed were: bone marrow, brain, fetal brain, fetal liver, heart, kidney, liver, lung, placenta, prostate, retina, skeletal muscle, spleen, testis, thymus, trachea, uterus, colon, small intestine, spinal cord and stomach. The housekeeping gene *TP53* was used as a positive control for the cDNA (Primer sequences in Appendix 8.3).

The results showed a major PCR product for all the tissues evaluated except for bone marrow, and additional smaller PCR products present in kidney, liver, lung, thymus, and small intestine (Figure 3-10).

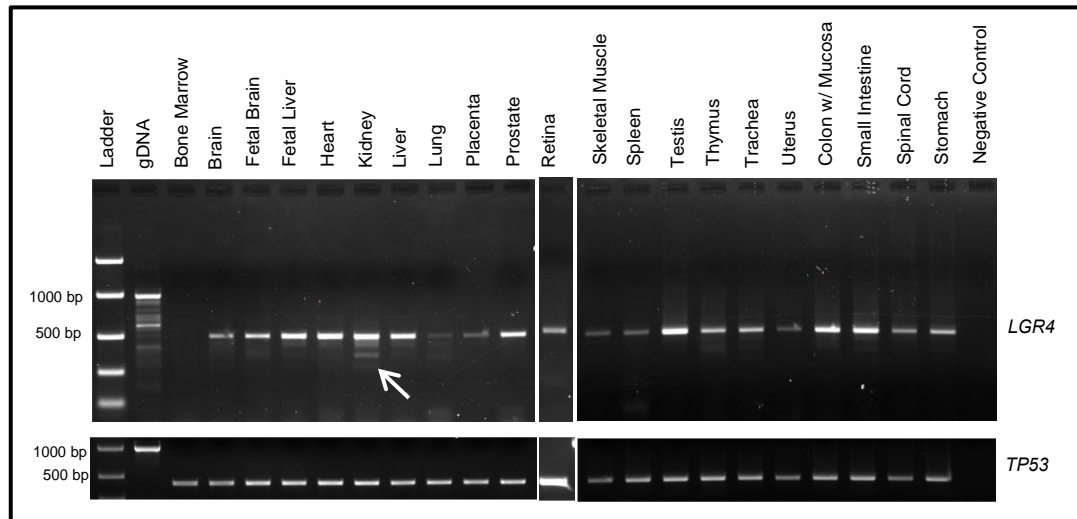


**Figure 3-10: cDNA amplification of *LGR4* in different human tissues.**

Primers located in exon 1 and exon 5 of *LGR4* were used to amplify cDNA created from different human tissues. The larger 488 bp product represents the transcript when the 5 first exons of the RefSeq *LGR4* (NM\_018490) transcript are present. The white arrow highlights the extra PCR products found in human kidney. For the negative control dH<sub>2</sub>O was added instead of cDNA. The *TP53* gene was used as a control for the cDNA. The ladder used is EasyLadder I from Bioline.

The larger PCR product was sequenced (section 2.4) and confirmed to be the 488 bp RT-PCR product produced when the first 5 exons of the RefSeq *LGR4* transcript (NM\_018490) are amplified with the designed primers. This product was found in all the tissues analysed except bone marrow, confirming the wide expression of *LGR4*. The highest levels of *LGR4* expression were found in foetal liver, liver, kidney, heart, prostate, testis, colon and small intestine (Figure 3-10).

Further characterization of the additional smaller *LGR4* RT-PCR products was performed in kidney. The two brightest smaller PCR products found in kidney were gel extracted (section 2.3.2) and cloned into the pCR2.1-TOPO vector (Appendix 8.7) using TOPO-TA cloning technology (section 2.6.1). The upper extra band cloned into pCR2.1-TOPO was named pCR2.1\_kidney\_extra\_band\_1 while the smaller second extra band was named pCR2.1\_kidney\_extra\_band\_2. The inserts from the positive colonies were checked by EcoRI restriction enzyme digestion (section 2.6.2) before being sequenced. Two EcoRI restriction sites are present in the pCR2.1-

TOPO plasmid (Appendix 8.7) flanking the PCR product, but there is no EcoRI restriction site present in the insert, which allows the identification of positive colonies (Figure 3-11).

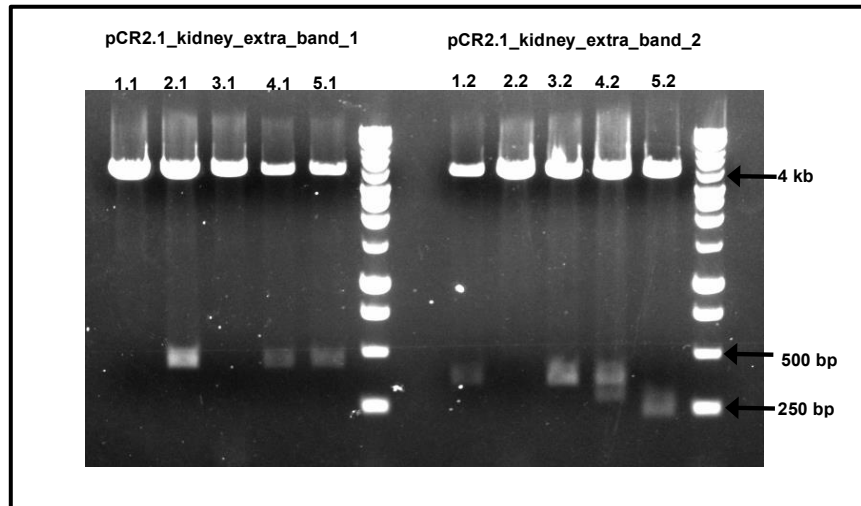


**Figure 3-11: EcoRI digestion of *LGR4* kidney TA-cloning colonies.**

Purified plasmid DNA from 5 single colonies (1 to 5) was digested with EcoRI and electrophoresed in a 1% agarose gel. pCR2.1\_kidney\_extra\_band\_1 represents the larger extra band found in kidney and pCR2.1\_extra\_band\_kidney\_2 the smaller band. The ladder used is GeneRuler 1 kb from Thermo Scientific.

As shown in Figure 3-11, not all the positive colonies contained an insert. For pCR2.1\_kidney\_extra\_band\_1 minipreps 2, 4 and 5 were sequenced using *LGR4* primers (Primer sequences in Appendix 8.6) and all three represented a novel splice variant missing exon 3 (Figure 3-12, C). For pCR2.1\_kidney\_extra\_band\_2 minipreps 3, 4 and 5 were sequenced but only sample 3 gave clean sequence identifying another novel transcript missing exons 2 and 3 (Figure 3-12, D). Minipreps 4.2 and 5.2 did not give clean sequence and the digests show the presence of more than one insert that may explain this. The additional band may be an indication that the miniprep DNA was not derived from a single colony. No transcript missing exon 2 only was identified.

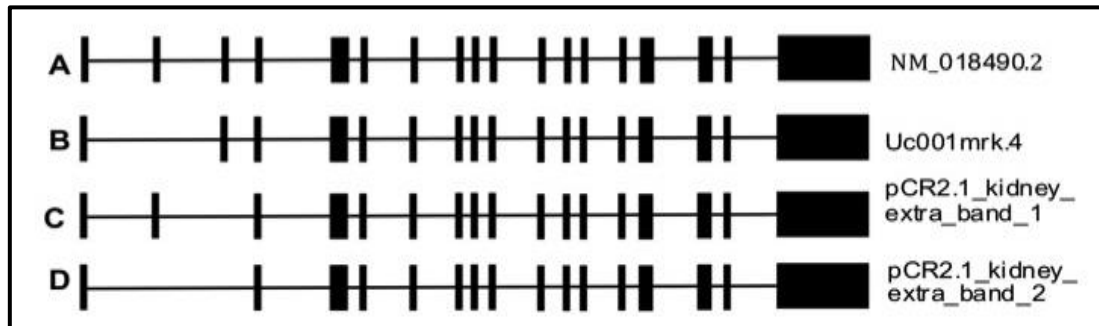


**Figure 3-12: Schematic representation of the *LGR4* transcripts.**

**A:** Schematic representation of *LGR4* main RefSeq transcript (NM\_018490.2). **B:** *LGR4* schematic representation missing exon 2 as described in the Genome browser (Uc001mrk.5). **C:** Novel *LGR4* splice variant identified pCR2.1\_kidney\_extra\_band\_1 missing exon 3. **D:** Novel *LGR4* splice variant identified pCR2.1\_kidney\_extra\_band\_2 missing exon 2 and 3.

After the evaluation of the *LGR4* transcripts in the human tissue panel, it was clear that the *LGR4* RefSeq transcript (Figure 3-12, A) was the predominant transcript in all tissues which expressed *LGR4* and importantly, was the only transcript found in retina (Figure 3-10). Consequently, this was the transcript selected to generate *LGR4* expression constructs and to perform further experiments.

### 3.3.2 Creating a mutation series of expression constructs for *LGR4* by site directed mutagenesis

A commercially available cDNA clone containing the full open reading frame of human *LGR4* (TrueORF Gold, catalogue number RC221345, Origene), in a pCMV6\_Entry mammalian expression vector (Plasmid data in Appendix 8.8) was obtained and used as a template in a site directed mutagenesis (SDM) experiment to generate 6 different constructs each containing one of the missense variants identified previously in the FEVR patients (from now on referred to as variant *LGR4* constructs). The pCMV6\_Entry\_*LGR4* construct (referred in this thesis as pCMV6\_*LGR4*) contains the CMV promoter to allow expression of *LGR4* in mammalian cells and contains a Myc and DDK tag (FLAG tag) at the C-terminus. This allows translation of the

protein without interfering with the N-terminal signal peptide present on LGR4 to target the receptor to the cell membrane.

In order to create the six *LGR4* variant expression constructs, the pCMV6\_*LGR4* construct was used as a template in a series of SDM experiments. The primers were designed using the QuikChange Primer Design tool (section 2.2.1.1) (Primer sequences in Appendix 8.4). The QuikChange Site-Directed Mutagenesis Kit (section 2.6.3) was used initially to introduce the point variants into the pCMV6\_*LGR4* clone. However, no positive colonies were obtained for any of the six different *LGR4* SDM assays, but plenty of colonies were obtained for the positive control pWhitescript. This result suggested that the experimental procedure was working, but that the *LGR4* construct might be difficult to transform. In order to overcome this problem, the QuikChange II XL Site-Directed Mutagenesis Kit was used (section 2.6.3). This kit is specifically optimized for large (>8Kb) and difficult constructs using *Pfu Ultra* High Fidelity Polymerase for high fidelity replication and XL10-Gold ultra competent cells for higher transformation efficiency. The new kit worked for all six variants and the point changes were all successfully introduced onto pCMV6\_*LGR4*. All the constructs were then sequenced (see Appendix 8.6 for primer sequences) to confirm the presence of the missense variants (Figure 3-13) and to check that no other extra changes had been introduced during the PCR amplification step.

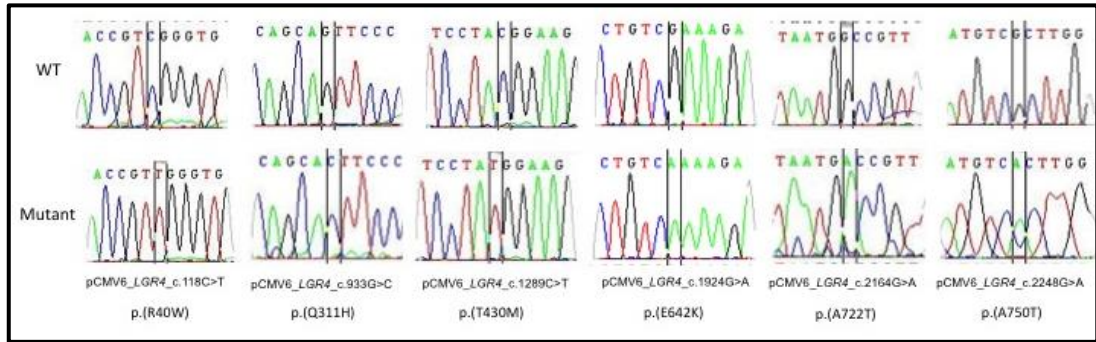


**Figure 3-13: Sequence electropherogram results of all the point changes introduced in pCMV6\_LGR4.**

The WT sequence of the plasmid is presented on the upper panel and the lower panel shows the variant change introduced for each construct by SDM. The cDNA change as well as the protein change is shown for each variant.

The pCMV6\_LGR4 constructs all contain a C-terminal myc and DDK (FLAG) tag. To ensure that the zebrafish rescue experiment was performed with proteins that mimic, as much as possible, the native WT human protein, the SDM experiment (section 2.6.3) was performed again in all six variant constructs, along with the WT construct, in order to introduce a stop codon at the end of the *LGR4* coding sequence (Primer sequences in appendix 8.4). Again, each vector was sequenced (section 2.4) to verify the successful introduction of the stop codon.

At this stage, two sets of pCMV6\_LGR4 (WT and variants) expression constructs had been created: those with a stop codon (closed constructs) and those without the stop codon (fusion constructs). To facilitate vector exchanges for further experiments, these constructs were used to create constructs compatible with the Gateway Technology cloning system (Life Technologies, section 2.6.4). A schematic representation of the Gateway system is shown in Figure 3-14, in which the detailed steps performed to obtain the expression constructs are indicated.

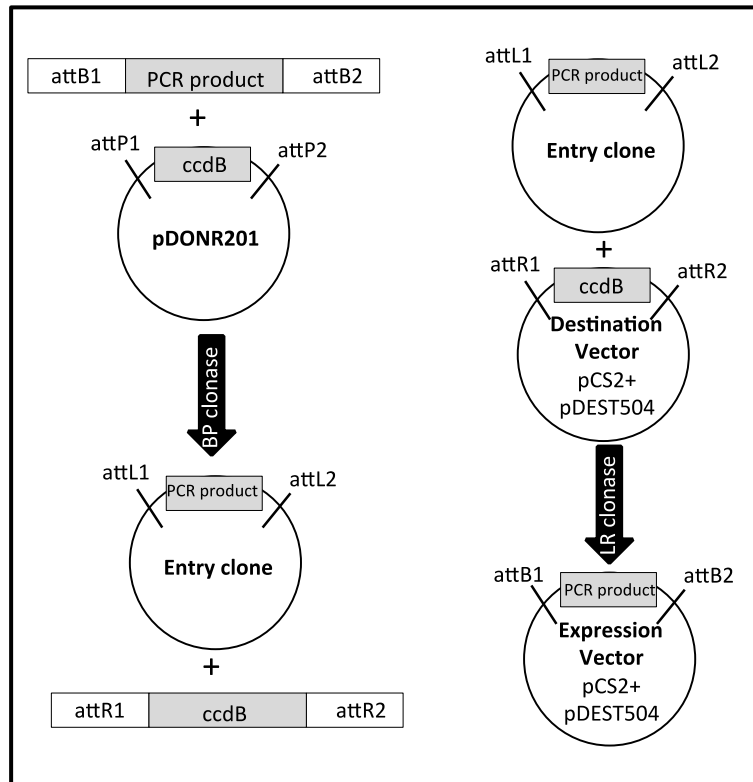


**Figure 3-14: Schematic representation of the Gateway Technology system.**

The PCR product to be cloned is amplified with primers containing the attB sites. The pDONR201 contains the ccdB gene flanked by the attP sites. The entry clone containing the attL sites is created by attB and attP recombination mediated by the BP clonase enzyme. The attB containing expression vector is created by recombination of the attL (entry clone) and attR (destination vector) mediated by the LR clonase enzyme. The destination vectors used to create the *LGR4* expression vectors were pCS2+ (zebrafish rescue experiment) and pDEST504 (further functional experiments described in section 5.5).

For the Gateway cloning system, the first step was to create the *LGR4* entry clones. For this, the pCMV6\_*LGR4* closed constructs (WT and variants) were each used as a template in separate PCR reactions using primers designed to amplify the whole open reading frame of *LGR4*, while introducing flanking attB recombination sites at both sides of the *LGR4* open reading frame-cassette (section 2.6.4). The expression constructs for the zebrafish rescue experiments need to have a zebrafish kozak consensus sequence to ensure efficient translation. For this reason the forward primer used to amplify these plasmids was designed with a zebrafish kozak consensus sequence inserted just after the attB site (gccgccgcc) (Primer sequences in Appendix 8.5). After amplification, the attB-PCR products were checked and excised on an

agarose gel (section 2.3.2) (Figure 3-15). The expected size of the full *LGR4* open reading frame together with the attB sequences is 3065 bp.

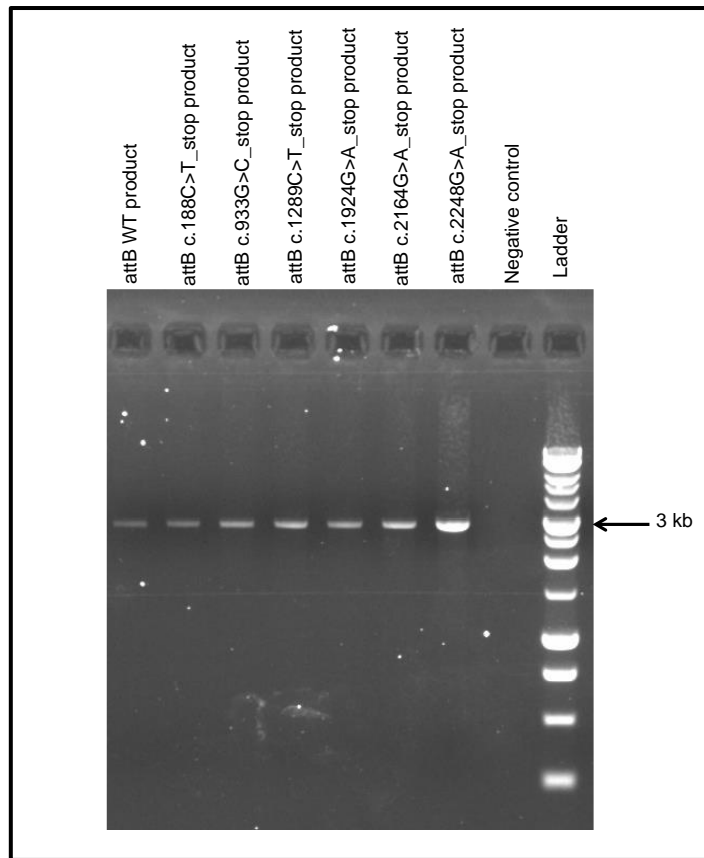


**Figure 3-15: PCR products amplified from pCMV6\_*LGR4* WT or variant clones.**

The expected PCR product size is 3065 bp. The PCR products containing the stop codon at the end of the *LGR4* open reading frame are shown in the gel picture. For the negative control dH<sub>2</sub>O water was added instead of the pCMV6\_*LGR4* template. The ladder used is GeneRuler 1 kb from Thermo Scientific.

After gel verification, the attB-PCR products were extracted from the gel and transferred into the pDONR201 vector using the BP clonase enzyme to create the entry clones (section 2.6.4). The resulting pDONR201\_*LGR4* entry clones were transferred into the chosen destination vector using the LR clonase enzyme to create the expression constructs. The destination vector used for the zebrafish experiments was pCS2+ (Appendix 8.8) (a gift from Dr. Erwin Van Wik). This vector contains the SP6 promoter, allowing *in vitro* RNA synthesis of *LGR4* and the simian CMV IE94 (sCMV) promoter for eukaryotic expression. All the pCS2+\_*LGR4* constructs (variants and WT), were

sequenced (Appendix 8.6) to confirm the presence of the mutations, the TAG stop codon at the end of the *LGR4* open reading frame and to confirm the absence of any extra changes.

### **3.3.3 Linearization of the plasmid, mRNA synthesis and RNA recovery**

After the constructs had been sequenced to verify them, the pCS2+\_*LGR4* expression clones (WT and mutants) were linearized by NotI digestion (section 2.6.2). Digested products were size fractionated on an agarose gel to check for complete digestion and the DNA was extracted from the gel (section 2.3.2). One microgram of the linearized plasmid was used to create the mRNA (section 2.7). The resulting mRNA concentration and the mRNA quality were measured with the nanodrop and confirmed to be optimal for the mRNA rescue experiments in the zebrafish.

## **3.4 Rescue of the aberrant eye phenotype using human WT *LGR4* mRNA**

Once the effect of *Igr4* MO knockdown was confirmed to result in an aberrant eye vasculature phenotype, the next step was to determine if this phenotype could be rescued with the human *LGR4* WT mRNA. The first step was to determine the mRNA WT dose capable of rescuing the phenotype caused by the *Igr4* MO knockdown. For this, different concentrations of mRNA encoding WT human *LGR4* were co-injected along with 6 ng of *Igr4* splice MO into the zebrafish embryos. The different doses of human mRNA tested were 50 pg, 100 pg or 150 pg. Un-injected fish were used as a control to test for the survival of the morphants, and a MO control against human  $\beta$ -globin intron mutation was also used to control for MO toxicity. The fish were blindly scored.

The 100 pg injection of WT mRNA resulted in 85% of the fish having a normal phenotype compared to only 58% when 6 ng *Igr4* splice MO was injected alone (Figure 3-16). The number of fish injected as well as the

percentage of fish present in each phenotype class is shown in Table 3-3. Based on this data, it was decided that the best rescue dose was 100 pg of WT *LGR4* mRNA.

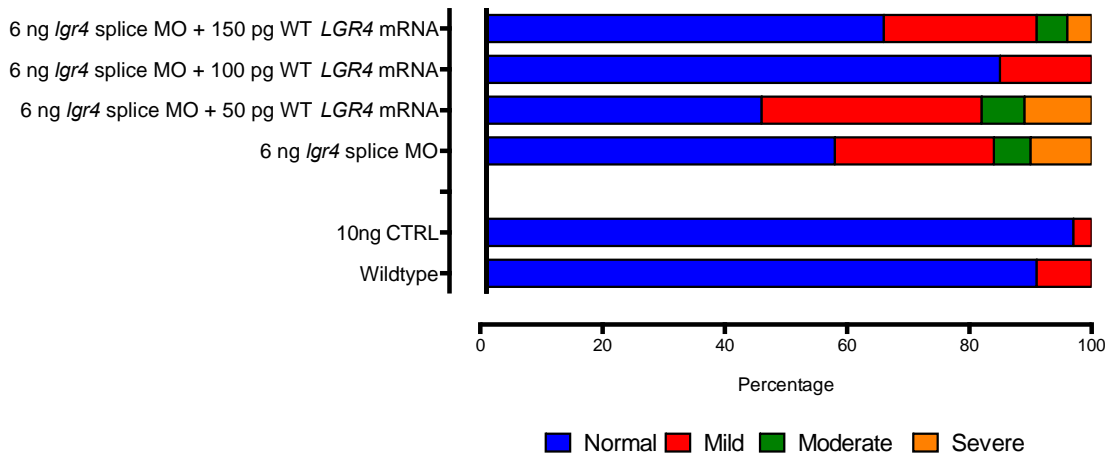


**Figure 3-16: Phenotypic classification of zebrafish larvae when 6 ng of MO *lgr4* was co-injected with 50 pg, 100 pg or 150 pg of WT *LGR4* mRNA.**

Co-injection of *lgr4* MO together with different WT *LGR4* mRNA concentrations (50 pg, 100 pg and 150 pg) was performed in the zebrafish embryo. Two controls were used in this experiment: wildtype corresponds to un-injected fish and 10 ng CTRL corresponds to the human  $\beta$ -globin intron mutation MO control. The percentage of fish categorised as having a normal, mild, moderate or severe phenotype is indicated.

	Un-injected	Control MO	6 ng MO <i>lgr4</i>	6 ng MO <i>lgr4</i> + 50 pg mRNA	6 ng MO <i>lgr4</i> + 100 pg mRNA	6 ng MO <i>lgr4</i> + 150 pg mRNA
Embryos injected	35	39	31	28	29	56
Normal (%)	91	97	58	46	85	66
Mild (%)	9	3	26	36	15	25
Moderate (%)	0	0	6	7	0	5
Severe (%)	0	0	10	11	0	4
Fish Survival (%)	88	90	81	88	84	85

**Table 3-3: Number of embryos analysed, percentage of fish present with each phenotype and fish survival rates.**

The number of fish injected in this experiment was not optimal because the fish did not lay many eggs. A Fisher's exact test was performed to assess significant changes between the different rescue doses. 6 ng MO *lgr4* + 100 pg of *LGR4* mRNA WT was the only dose that gave statistical significance difference (P value= 0.0415) when compared to MO *lgr4* injection alone. The

survival rate of the fish slightly decreased when compared to the experiment performed in Figure 3-6 and Table 3-2 therefore these results needed confirming before testing the *LGR4* variants. For these reasons, the rescue experiment was repeated in a larger number of embryos but this time only the 100 pg dose of WT mRNA was injected as it appeared to perform the best in the pilot experiment (Figure 3-16). The two controls used were the same as previously described: an un-injected WT fish and 10 ng of human  $\beta$ -globin intron mutation control MO. The number of embryos injected and the percentage of eyes present in each phenotype class are detailed in Figure 3-17 and Table 3-4.

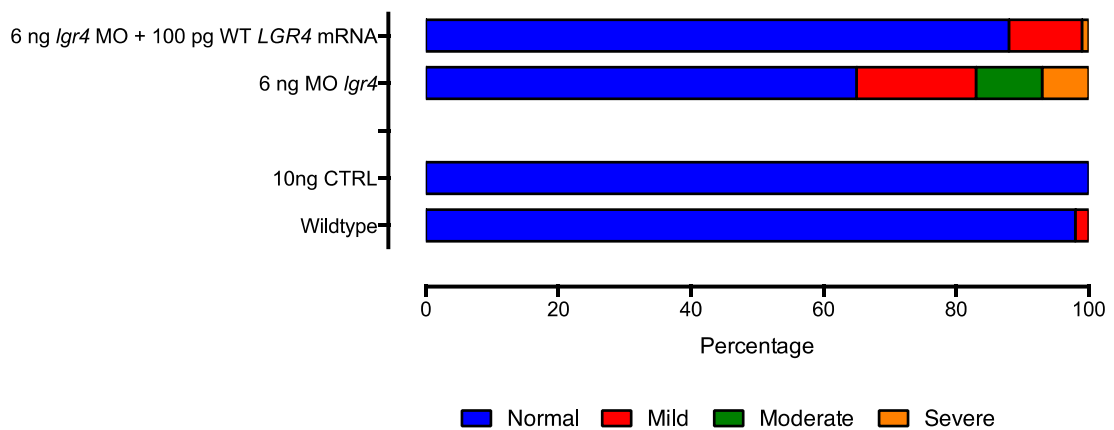


**Figure 3-17: Phenotypic classification of MO-knockdown rescue assays using WT *LGR4* mRNA.**

6 ng of *lgr4* splice MO was co-injected with 100 pg of WT *LGR4* mRNA and the eye phenotypes assessed. Two controls were used: an un-injected WT fish and 10 ng of human  $\beta$ -globin intron mutation control MO. The graph represents the percentage of eyes present in each phenotype class.

	Un-injected	Control MO	6 ng MO <i>lgr4</i>	6 ng MO <i>lgr4</i> + 100 pg mRNA
Embryos injected	42	36	77	73
Normal (%)	98	100	65	88
Mild (%)	2	0	18	11
Moderate (%)	0	0	10	0
Severe (%)	0	0	7	1
Fish Survival (%)	100	100	98	97

**Table 3-4: Number of embryos analysed, percentage of fish present with each phenotype and fish survival rates in the replicate rescue experiment.**

The results from this experiment confirmed that 100 pg of mRNA is a suitable rescue dose. When the *Igr4* splice MO is injected alone only 65% of the fish presented with normal eyes compared to 88% when the WT *LGR4* mRNA is co-injected with the MO. Reassuringly, a Fisher's exact test was performed with the rescue dose data set in Figure 3.17. The P value of the Chi-square test was 0.0030, implying a statistically significant difference between *Igr4* MO group alone and 100 pg of mRNA *LGR4* rescue group, which confirmed the results obtained in Figure 3-16. Overall, the rescued fish tended to be in the mild phenotype class compared to the MO-only injected embryos. This second experiment also confirmed that the vascular defects observed in the fish eyes due to *Igr4* MO knockdown can be rescued by co-injection of human WT *LGR4* mRNA suggesting that the abnormal phenotypes observed in the morphants are due to *Igr4* knockdown and not due to off-target effects of the MO.

#### **3.4.1 Scoring method validation**

For the fish experiments performed to date, only one random eye was scored per fish. To evaluate this strategy, a proportion of the fish from the last experiment (rescue of the phenotype experiment) were re-assessed and this time both eyes of the fish were scored. In total 84 fish (168 eyes) were examined, 50 fish (100 eyes) from the 6 ng MO *Igr4* group and 34 fish (68 eyes) from the 6 ng MO *Igr4* + 100 pg WT *LGR4* mRNA group. The results showed that the phenotypic class assigned to the eyes was discordant in 14.7% (5/34) of fish from the 6 ng MO *Igr4* + 100 pg WT *LGR4* mRNA group and 22% (11/50) of fish that were re-scored in the 6 ng MO *Igr4* category. In total 19% (16/84) of fish scored presented different eye phenotypes. These fish were re-scored and classified into the different eye phenotypes by looking at one random eye and by looking at both eyes to determine if differences in phenotype classifications were observed (Figure 3-18).

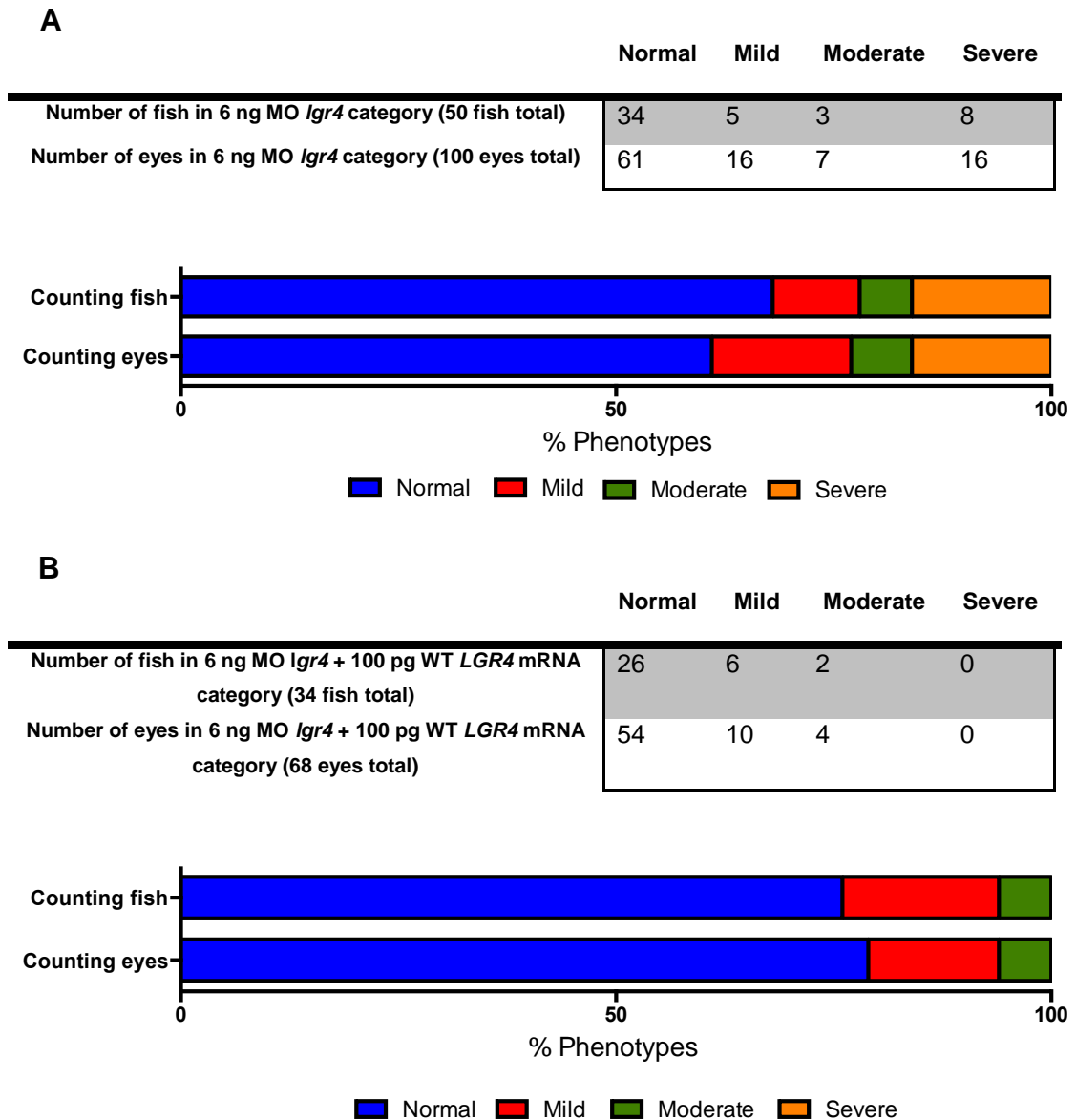


**Figure 3-18: Different eye phenotype classification by scoring fish or by scoring eyes.**

**A:** In total 50 fish (100 eyes) from the 6 ng MO *lgr4* group were scored. The number of fish belonging to each phenotype category is indicated in the table. A schematic diagram of the percentage of fish in each phenotype class is detailed below. **B:** In total 34 fish (68 eyes) from the 6 ng MO *lgr4* + 100 pg WT *LGR4* mRNA group were scored. The number of fish belonging to each phenotype category is indicated in the table. A schematic diagram of the percentage of fish in each phenotype class is detailed below. Fish or eyes abnormalities were classified as normal, mild, moderate or severe.

As detailed in Figure 3-18, differences in phenotype classification were found when only 1 random eye per fish was scored compared to when both eyes were evaluated. These differences were more prominent in the 6 ng MO *lgr4*

category, probably due to the rescue effect of the WT *LGR4* mRNA in the 6 ng MO *lgr4* + 100 pg WT *LGR4* mRNA category, which occurred in about 80% of the fish with normal phenotype and therefore less phenotypic variability. Therefore, for the remaining experiments both eyes of the fish were evaluated in order to assess accurate classification of the eye phenotype in the fish.

Now that the optimal rescue dose and scoring strategy had been determined, the next step was to use this assay to establish if *LGR4* containing one of the missense variants found in the FEVR patients could also rescue the eye phenotype or if they altered the function of LGR4 so it was no longer able to perform this role.

### **3.5 Zebrafish phenotype rescue using *LGR4* mRNA variants**

The MO knockdown rescue assay previously optimised using human WT *LGR4* mRNA (section 3.4) was repeated for each of the different missense variants identified in *LGR4* in the FEVR patients: c.188C>T p.(R40W), c.933G>C p.(Q311H), c.1289C>T p.(T430M), c.1924G>A p.(E642K), c.2164G>A p.(A722T), c.2248G>A p.(A750T). The mRNA generated from each of the pCS2+\_*LGR4* variant constructs (section 3.3.3) was used along with the WT *LGR4* mRNA, which was used as a phenotype rescue control. For each variant being assayed, 100 pg of the relevant *LGR4* mRNA was co-injected into the embryos with 6 ng of *lgr4* splice MO and both eyes of the fish were subsequently blindly scored. The data for this experiment is presented in Figure 3-19 and Table 3-6.

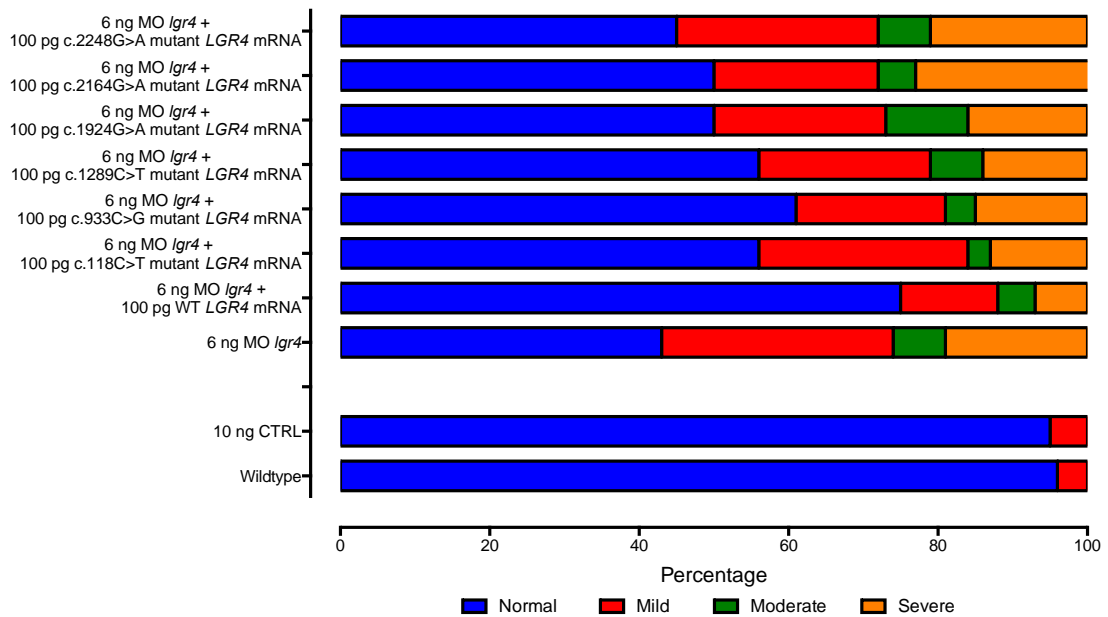


**Figure 3-19: Results of the MO knockdown rescue assays using variant *LGR4* mRNAs.**

6 ng of *Igr4* splice MO was co-injected with 100 pg of WT or variant *LGR4* mRNA and the eye phenotypes assessed. Two controls were used: an un-injected WT fish and 10 ng of human  $\beta$ -globin intron mutation control MO. The graph represents the percentage of eyes present in each phenotype class.

The results show that in MO-only injected embryos, 46% of the eyes were normal but this rose to 77% when WT *LGR4* was co-injected (Figure 3-19 and Table 3-5). This rescue of the phenotype due to WT *LGR4* mRNA resulted in 30% more fish belonging to the normal or WT class, as observed before in the previous experiments (Figure 3-16 and Figure 3-17), suggesting that the experimental procedure is reliable. Similarly, the number of aberrant eyes belonging to mild, moderate and severe phenotype were reduced in the fish co-injected with the human *LGR4* WT mRNA compared to the MO-only injected fish, which was also previously observed and again supports the hypothesis that human *LGR4* WT mRNA is capable of rescuing the MO induced ocular vasculature defects.

	Un- injected	Contr ol MO	6 ng MO <i>lgr4</i>	6 ng MO <i>lgr4</i> + 100 pg WT <i>LGR4</i> mRNA	6 ng MO <i>lgr4</i> + 100 pg c.188C>T <i>LGR4</i> mRNA	6 ng MO <i>lgr4</i> + 100 pg c.933G>C <i>LGR4</i> mRNA	6 ng MO <i>lgr4</i> + 100 pg c.1289C>T <i>LGR4</i> mRNA	6 ng MO <i>lgr4</i> + 100 pg c.1924G>A <i>LGR4</i> mRNA	6 ng MO <i>lgr4</i> + 100 pg c.2164G>A <i>LGR4</i> mRNA	6 ng MO <i>lgr4</i> + 100 pg c.2248G>A <i>LGR4</i> mRNA
<b>Embryos analysed</b>	38	80	70	101	60	62	49	55	67	47
<b>Eyes scored</b>	76	160	140	202	120	124	98	110	134	94
<b>Normal (%)</b>	95	95	46	77	52	57	55	49	44	44
<b>Mild (%)</b>	5	5	31	15	30	20	20	18	26	22
<b>Moderate (%)</b>	0	0	8	5	2	7	16	17	8	4
<b>Severe (%)</b>	0	0	15	3	16	16	9	16	22	30
<b>Fish survival (%)</b>	90	86	84	87	90	83	84	87	86	91

**Table 3-5: Experimental data for the MO knockdown rescue assays using variant *LGR4* mRNAs.**

6 ng of *lgr4* splice MO was injected alone or co-injected with 100 pg of human WT or variant *LGR4* mRNA. The percentages of eyes present in each phenotype class are shown along with the number of embryos injected and the number of eyes scored. Fish were classified as normal, mild, moderate and severe phenotype. Two controls were used: an un-injected WT fish and 10 ng of human  $\beta$ -globin intron mutation control MO. The fish survival is also detailed as a percentage.

Interestingly, none of the *LGR4* missense variants tested were able to rescue the phenotype to the same extent as the human *LGR4* WT mRNA. All the variants tested presented a percentage of normal or WT eyes ranging from 44-57%, similar to the percentage observed when MO *Igr4* is injected alone. The number of aberrant eyes belonging to the mild, moderate and severe phenotype classes did not improve with any of the variant *LGR4* mRNAs, suggesting that the *LGR4* missense variants found in FEVR patients alter the function of the protein in the fish.

### 3.5.1 Statistical analysis

In order to identify if the results obtained from the fish experiments are statistically significant a Fisher's exact test was performed (Taillard ED et al., 2008). This test allows the analysis of contingency tables represented by the frequency distribution of two variables. In the experiment involving a MO knockdown rescue assay using WT or variant *LGR4* mRNAs, the two variables studied are normal eyes or aberrant eyes (mild, moderate and severe phenotype). Two sets of test comparisons were performed. The first test compared the 6 ng MO *Igr4* group with the MO *Igr4* + 100 pg WT or variant *LGR4* mRNA group in order to test if WT or variant *LGR4* mRNA is able to rescue the phenotype. The second test compared the MO *Igr4* + 100 pg WT *LGR4* mRNA group with each of the MO *Igr4* + 100 pg variant *LGR4* mRNA groups in order to test whether the mutants can rescue the phenotype (Table 3-6). The number of normal eyes or aberrant eyes for each group is shown in Table 3-6 and the p value obtained after Fisher's test was performed is also indicated. The null hypothesis is that the proportion of each variable, normal eyes and aberrant eyes, is the same in both groups. Only the WT *LGR4* mRNA rescue group gave a statistically significant difference when compared to the 6 ng MO *Igr4* group. For all the *LGR4* variants, there is no statistical difference, which indicates that the proportion of aberrant and normal eyes in the MO *Igr4* group is not statistically significantly different from that in group treated with variant *LGR4* mRNA. In addition the second Fisher's test performed showed statistically significant difference for all the variants as well as for the MO *Igr4* group from the group treated with WT *LGR4* mRNA.

This data indicates that the WT *LGR4* mRNA is the only mRNA that is able to rescue the observed aberrant fish phenotype.

An additional statistical test was performed using Fisher's contingency test, but in this case, individual comparisons of aberrant eye categories were performed. In the statistical test performed in Table 3-7, the 6 ng MO *lgr4* group was compared to the MO *lgr4* + 100 pg WT or variant *LGR4* mRNA group. The variables are the number of eyes present in the normal group compared to the number of eyes present in the moderate, mild or severe groups separately. This analysis was performed in order to determine if there are statistically significant changes between the aberrant eye categories (moderate, mild and severe). The reason for this is because the aberrant eye categories (moderate, mild and severe) had been mixed in one category in Table 3-6.

As indicated in Table 3-7 the MO *lgr4* + 100 pg WT *LGR4* mRNA group shows a statistically significant difference to the 6 ng MO *lgr4* group in all the aberrant eye categories analysed. In contrast, none of the MO *lgr4* + 100 pg variant *LGR4* mRNA groups presented statistically significant differences in all of the aberrant eye categories analysed. Interestingly, the MO *lgr4* + 100 pg c.933C>T *LGR4* mRNA group and the MO *lgr4* + 100 pg c.2248G>A *LGR4* mRNA group, presented statistically significant differences in the moderate and severe group respectively, when compared to the 6 ng MO *lgr4* group. These results suggest that these two variants might be able to specifically rescue the moderate and the severe phenotype in the fish, even though no rescue was observed for the other aberrant eye categories. This data confirms the results presented in Table 3-6 and suggests that only the MO *lgr4* + 100 pg WT *LGR4* mRNA group is able to rescue the aberrant eye phenotype in all the categories analysed.

	<b>MO <i>Igr4</i></b>	<b>MO <i>Igr4</i> + 100 pg WT <i>LGR4</i> mRNA</b>	<b>MO <i>Igr4</i> + 100 pg c.188C&gt;T <i>LGR4</i> mRNA</b>	<b>MO <i>Igr4</i> + 100 pg c.933G&gt;C <i>LGR4</i> mRNA</b>	<b>MO <i>Igr4</i> + 100 pg c.1289C&gt;T <i>LGR4</i> mRNA</b>	<b>MO <i>Igr4</i> + 100 pg c.1924G&gt;A <i>LGR4</i> mRNA</b>	<b>MO <i>Igr4</i> + 100 pg c.2164G&gt;A <i>LGR4</i> mRNA</b>	<b>MO <i>Igr4</i> + 100 pg c.2248G&gt;A <i>LGR4</i> mRNA</b>
<b>Number of normal eyes</b>	64	155	62	71	54	54	59	41
<b>Number of aberrant eyes</b>	76	47	58	53	44	56	75	53
<b>1- P value (Fisher's test)</b>	NA	< 0.0001 (significant)	0.3840 (ns)	0.0654 (ns)	0.1878 (ns)	0.6118 (ns)	0.8087 (ns)	0.7895 (ns)
<b>2- P value (Fisher's test)</b>	< 0.0001 (significant)	NA	< 0.0001 (significant)	0.0003 (significant)	0.0002 (significant)	< 0.0001 (significant)	< 0.0001 (significant)	< 0.0001 (significant)

**Table 3-6: Number of normal or aberrant eyes present in fish injected with MO *Igr4* or co-injected with the MO *Igr4* and *LGR4* mRNA and Fisher's test P value.**

The number of normal eyes and aberrant eyes is indicated in the table for each fish group analysed. The number of aberrant eyes represents the sum of the eyes classified as mild, moderate and severe phenotype. Fisher test was performed and the P value is indicated in the table. For the 1- Fisher's test MO *Igr4* group was individually compared to each co-injected MO *Igr4* and *LGR4* mRNA group. For the 2- Fisher's test MO *Igr4* and *LGR4* WT mRNA group was individually compared to each MO *Igr4* and *LGR4* variant mRNA group.

	<b>MO <i>lgr4</i></b>	<b>MO <i>lgr4</i> + 100 pg WT <i>LGR4</i> mRNA</b>	<b>MO <i>lgr4</i> + 100 pg c.188C&gt;T <i>LGR4</i> mRNA</b>	<b>MO <i>lgr4</i> + 100 pg c.933G&gt;C <i>LGR4</i> mRNA</b>	<b>MO <i>lgr4</i> + 100 pg c.1289C&gt;T <i>LGR4</i> mRNA</b>	<b>MO <i>lgr4</i> + 100 pg c.1924G&gt;A <i>LGR4</i> mRNA</b>	<b>MO <i>lgr4</i> + 100 pg c.2164G&gt;A <i>LGR4</i> mRNA</b>	<b>MO <i>lgr4</i> + 100 pg c.2248G&gt;A <i>LGR4</i> mRNA</b>
<b>Number of normal eyes</b>	64	155	62	71	54	54	59	41
<b>Number of Moderate eyes</b>	43	31	36	25	20	20	35	43
<b>Number of Mild eyes</b>	11	9	3	8	16	19	10	11
<b>Number of severe eyes</b>	22	7	19	20	8	17	30	22
<b>P value Normal Vs Moderate</b>	NA	<0.0001 (s)	0.6874 (ns)	0.03 (s)	0.0813 (ns)	0.0813 (ns)	0.7719 (ns)	0.4081 (ns)
<b>P value Normal Vs Mild</b>	NA	0.0235 (s)	0.0538 (ns)	0.4661 (ns)	0.2858 (ns)	0.1034 (ns)	0.9999 (ns)	0.4078 (ns)
<b>P value Normal Vs Severe</b>	NA	<0.0001 (s)	0.8576 (ns)	0.5999 (ns)	0.0651 (ns)	0.2519 (ns)	0.8545 (ns)	0.0407 (s)

**Table 3-7: Number of normal, moderate, mild or severe eyes present in fish injected with MO *lgr4* or co-injected with the MO *lgr4* and *LGR4* mRNA and Fisher's test P value.**

The number of eyes for each category is indicated in the table for each group analysed. Fisher's test was performed and the P value is indicated in the table. MO *lgr4* group was individually compared to each co-injected MO *lgr4* and *LGR4* mRNA group for each aberrant eye phenotype category individually (moderate, mild or severe). S= significant and ns= no significant.

### 3.6 Discussion

Determining the pathogenicity of missense variants is a major challenge in genetic research, especially in this data-rich era of next generation sequencing (Frebourg, 2014). In order to prove the pathogenic nature of missense variants, functional studies at the protein level are often required. In the present study, MO-mediated knockdown and mRNA rescue experiments in zebrafish were used to functionally test the *LGR4* missense variants identified in FEVR patients to help determine if they are pathogenic. Six different missense mutations were assessed using this assay and all six were shown to be functionally defective and therefore likely to be disease causing.

The zebrafish MO model system is frequently used for these types of functional studies (Kazanskaya et al., 2008; Lan et al., 2007; Posokhova et al., 2014) and it has previously been used to assess FEVR-related missense mutations (Collin et al., 2013; Wu et al., 2016). MOs offer a quick and cost-effective way to knockdown a gene of interest in zebrafish and this is a major reason for the popularity of this model system. However, there are a number of known flaws with this method that must be controlled for in every experiment.

Traditionally, MO-mediated knockdown in zebrafish was frequently used to determine the phenotype associated with knockdown of a particular gene (Nasevicius & Ekker, 2000; Schauerte et al., 1998). Unfortunately, MO injections in zebrafish can cause variable side effects including MO off-target effects, in which the phenotype observed in the fish is not due to the knockdown of the targeted gene but to the inhibition of an irrelevant gene instead (Wright et al., 2004). A general method to overcome this problem is to utilise two different MOs to target the gene, commonly a translation blocking MO and a splice blocking MO (Eisen and Smith, 2008). If both MOs result in the same phenotype it is more likely that this is due to the knockdown of the targeted gene rather than to off-target effects.

Inconveniently, some off-target effects appear to be common to multiple MOs, such as neuronal cell death driven by the activation of the p53 pathway (Robu et al., 2007). In order to control for these defects, a MO targeting p53 is co-injected with the target gene MO to ensure that the phenotype is not caused by activation of this pathway.

Despite the use of these controls, a recent study by Kok and colleagues showed major discrepancies in zebrafish between MO-induced phenotypes and the mutant phenotypes caused by gene knockout induced by zinc finger nucleases (ZFNs) and transcription activator-like effector nucleases (TALENs) (Kok et al., 2015). Unlike the transient effect of MO-knockdown, which are only effective within the first 5 days of development when injected into one-cell stage embryos (Eisen et al., 2008), ZFNs and TALENS enable permanent gene disruption (Cade et al., 2012; Meng et al., 2008). The Kok study characterised and generated mutant zebrafish lines for 24 genes using ZFNs and TALENs and then compared the phenotypes with the previously published MO-induced phenotypes. Phenotype discordancy was observed in 10 of the mutant lines tested and the authors suggested that MO off-target effects were the likely reason for this variability (Kok et al., 2015). As a result, using MOs to characterise the phenotypic consequences of gene knockdown is controversial and losing popularity.

For these reasons, in this study the MOs were not used to characterise the phenotypic effects of MO-mediated gene knockdown in the zebrafish but to assess variant function and only the ocular vasculature was examined in detail. Nevertheless, knockdown of *lgr4* in zebrafish using MOs resulted in abnormal blood vessels in the eye (Figure 3-7). Both the translation and splice blocking MOs gave the same vascular phenotype, supporting the idea that this phenotype is due to *lgr4* being knocked down and not due to MO off-target effects (Eisen and Smith, 2008). Due to the current experiment combining MO-knockdown with mRNA rescue, the p53 MO control was not used as any phenotypes resulting from activation of the p53 pathway would not be rescued by the mRNA. Reassuringly, co-injection of the human WT

*LGR4* mRNA led to the rescue of the eye vasculature defect, again indicating the specificity of this phenotype to *lgr4* knockdown (Figure 3-17).

It is therefore tempting to speculate that the ocular vascular defects are the result of *lgr4* knockdown. This would indicate that in zebrafish *lgr4* has a role in ocular vasculature development, the same process disrupted in FEVR. This ocular phenotype is also identical to that observed in zebrafish with MO-mediated knockdown of the FEVR genes *ZNF408* and *RCBTB1* (Collin et al., 2013; Wu et al., 2016). If true, this would demonstrate for the first time a functional link between *LGR4* and the development of the vasculature in the fish. Interestingly, MO knockdown of *RSPO3*, a known LGR4 ligand, has been reported to disrupt the normal development of blood vessels in *Xenopus*, which supports the idea of LGR4 signalling being important in vascular development (Kazanskaya et al., 2008). Additionally, mutation in *rspo1* in zebrafish occurs with abnormal vessel development (Gore et al., 2011).

Regarding differences in pathogenicity, the variants present in the transmembrane domain of LGR4 (c.1924G>A p.(E642K), c.2164G>A p.(A722T), c.2248G>A p.(A750T)) seemed to be slightly more severe. These variants occurred of more than 50% of aberrant eyes (Figure 3-19 and Table 3-5). The amino acids substitutions c.2164G>A (p.A722T) and c.2248G>A (p.A750T) change the polarity of the amino acid, non-polar alanine is changed to polar threonine. For c.1924G>A (p.E642K), the negatively charged glutamic acid is changed to a positive lysine. These amino acid substitutions in *LGR4* will therefore change the charge and polarity in the transmembrane region and may consequently result in an aberrant protein assembly in the plasma membrane that may influence the transduction of the signal. The other three variants, c.118C>T (p.R40W), c.933G>C (p.Q311H) and c.1289C>T (p.T430M) are also not capable of rescuing the eye phenotype at the WT levels. These three variants are present in the extracellular LGR4 domain, and they belong to one of the 17LRR domains present in the LGR4 protein. The possible role of these mutations might be regarding the binding affinity of LGR4 with its ligands.

Previous studies in human and mouse suggest that LGR4 plays a widespread role in development and is implicated in a variety of pathologies affecting different organs (Hoshii et al., 2007; Mendive et al., 2006; Weng et al., 2008; Styrkarsdottir et al., 2013; Yi et al., 2013). As only the eye vasculature was fully characterised in the current study, it is not possible to determine if additional defects were present. However, gross morphology in the form of a curved body was observed on many morphants and other vascular defects in the fish trunk were observed indicating that the phenotype was not only limited to the eye.

Ideally, mutant *lgr4* zebrafish would have been generated using ZFNs, TALENs or the more recently developed CRISPR-cas9 technology (Hwang et al., 2013) so the fish could be accurately phenotyped. However, these methods are time consuming and technically demanding and this experiment was focused on being a quick and easy assay. If these models are created in the future it would be interesting to determine if there is phenotypic correlation with the *lgr4* MO phenotype as done in the Kok study (Kok et al., 2015). In addition, considering that the variants assessed in this study are autosomal dominant variants, injection of only WT or variant mRNA of *LGR4* without knocking down endogenous *lgr4* would have been interesting to perform. If that had been the case a possible dominant-negative effect of the mutant proteins inhibiting the function of the endogenous *lgr4* protein could have been explored.

Direct comparison of the zebrafish and the human protein-coding genes reveals that approximately 70% of human genes have at least one zebrafish orthologue (Howe et al., 2013). Although *lgr4* had not been officially annotated in the zebrafish genome, ZFIN predicted a single orthologue and both MOs were designed using this predicted sequence (ENSDART00000085419.4). Different orthologues were predicted for *LGR5* and *LGR6*, the closest paralogues of *LGR4*, indicating that this was the correct transcript. Furthermore, another study investigating *lgr4* expression in zebrafish used the same transcript (Hirose et al., 2011).

The splice MO was designed against exon 16 of the *lgr4* gene (which contains 18 exons in total). Although it is more conventional to design MO against exons earlier in the transcript, removal of earlier exons did not predict the disruption of the open reading frame, which is required to target the transcript for nonsense mediated mRNA decay. Removal of exon 16 however, resulted in a truncated transcript as confirmed by RT-PCR analysis of RNA extracted from splice MO treated embryos. This MO was highly effective at inducing the phenotype in the treated embryos and was therefore chosen for the rescue experiments.

The translation blocking MO was less efficient than the splice MO at producing the aberrant vasculature phenotype. This variability could be due to differences in the binding affinities of the MOs to *lgr4* (He et al., 2005). It could also be due to small sequence differences in the UTR region of *lgr4* derived from the *fli1:eGFP* transgenic zebrafish compared to the Ensembl gene prediction used to design the MO (ENSDART00000085419.4) (Ramis et al., 2007). In order to address this problem, it would have been very useful to sequence *lgr4* in the *fli1:eGFP* strain and use this sequence to design the MOs.

MOs are known to have toxic effects if used at high doses (Bedell et al., 2011; Robu et al., 2007). It is therefore important to balance the amount of MO injected into the cells to ensure that enough is present to knockdown the gene of interest but without causing toxic effects. The MO dose chosen for this study was 6 ng, as at this dose the survival of the fish did not decrease when compared to the MO control (Figure 3-6). This MO amount is consistent with similar studies (Lan et al., 2007; Nasevicius and Ekker, 2000; Vanhollebeke et al., 2015; Wu et al., 2016b). Likewise, the mRNA dose of *LGR4* used for the rescue experiments was determined by performing a dose range rescue experiment and a final dose of 100 pg mRNA was chosen. Again, this quantity is in line with those used in similar studies (Nasevicius and Ekker, 2000; Vanhollebeke et al., 2015). Furthermore, 6 ng of splice MO led to around 50% of the fish with abnormal phenotype, which

is a standard aberrant phenotype range used in MO studies (Bedell et al., 2011).

In the initial experiments in this study, only one eye was scored in each fish. However, it became apparent during the course of the study that around 20% of the fish analysed had discordant phenotypes in each eye (Figure 3-18). Similar discrepancies have been reported before by Yolanda and colleagues when performing phenotypic characterisation of the eye vasculature (Alvarez et al., 2007). One reason that could explain the difference between the eyes could be the unequal distribution of the MO injected in the fish embryo, caused by the timing of the injection being very close to the division of the one cell stage embryo. Similarly, the trunk vascular defects observed in the fish did not always correlate with the presence of ocular vascular defects and again this could be due to the timing of the MO injection. For this reason, in the mRNA rescue experiments the classification of the fish was based exclusively in the eye phenotype found in both eyes.

The rescue experiments were performed by co-injecting mRNA encoding human LGR4 into the zebrafish. Human LGR4 is 58% identical to zebrafish *lgr4* and 71% similar. Despite these differences between the human and zebrafish proteins, the functional assay performed in this chapter aims to determine if the human variants are pathogenic by performing a direct comparison between WT *LGR4* mRNA and variant *LGR4* mRNA, with only one amino acid change difference between both transcripts.

For the rescue experiments it was important to use the right isoform of *LGR4*. Although only one RefSeq version of *LGR4* was annotated at the time of this experiment, almost all the *LGR4* constructs commercially available were missing exon 2 of this transcript. Initial experiments therefore focused on determining which was the major *LGR4* transcript and specifically, which one was the major transcript present in the retina. PCR primers designed to amplify both *LGR4* isoforms were used to amplify cDNA from a variety of human tissues. The results showed that *LGR4* is widely

expressed, being present in every tissue except bone marrow (Figure 3-10). Similar broad expression patterns of *Lgr4* have been reported for mouse and zebrafish (Hirose et al., 2011; Mazerbourg et al., 2004). The major transcript in every tissue was the full-length RefSeq transcript and this was therefore used for the rescue experiments. No major isoforms missing only exon 2 were detected. However, two novel splice variants were characterized in kidney, one missing exon 3 and another missing exons 2 and 3. Similar sized transcripts were observed in liver, lung, thymus and small intestine but these were very faint and not characterised. Additional different sized fainter transcripts were also detected in kidney, lung, liver, colon and small intestine and it is possible that one of these corresponds to the splice variant missing exon 2 but these were not characterised as this was beyond the scope of this study. Interestingly, on the latest version of the UCSC Genome Browser (hg38 accessed Oct 2016), the transcript missing exon 2 has been reviewed and is now annotated as a RefSeq transcript (NM\_001346432.1).

*LGR4* contains 18 exons. The first exon encodes the signal peptide and the N-terminal LRR domain (LRRNT). The 17 LRR domains remaining in the *LGR4* structure are encoded by exons 2 to 17 and finally exon 18 encodes the seven transmembrane domains and the intracellular regions (Figure 1-11). As the LRR domains have been implicated in ligand binding (Loh et al., 2001; Rajashankar et al., 2013), the possible role of the splice variants missing exon 2, exon 3, and exons 2 and 3, might be related to the binding affinity of *LGR4* with its ligand(s). However, no further characterization of these variants has been performed to determine their specific roles. An additional *Lgr4* splice variant encoding only the *Lgr4* ectodomain (*Lgr4*-ED) has been reported in mouse testis (Hsu et al., 2014). This transcript was not identified in this study but the PCR primers used for the RT-PCR would not detect its presence. It has been proposed that the *Lgr4*-ED isoform could play a role as an antagonist of *Lgr4* modulating *Lgr4* signalling (Hsu et al., 2014). Truncated receptors lacking their transmembrane region and serving as dominant-negative antagonists to the full-length receptor have been described before in G-protein coupled receptors and specifically in *LGRs* receptors (You et al., 2000).

In summary, in this chapter the six *LGR4* variants identified in FEVR patients were investigated using a functional assay consisting of MO-mediated knockdown of *lgr4*, followed by mRNA rescue with either WT or variant human *LGR4* mRNA. None of the six variant mRNAs were able to rescue the ocular vasculature phenotype induced in the fish but the WT mRNA showed significant rescue. Therefore using this assay, all six variants appeared to impair the function of *LGR4* providing evidence that they are pathogenic.

## 4 Investigating the effects of *LGR4* missense variants on the Norrin- $\beta$ -Catenin signalling pathway

### 4.1 Background

Chapter 3 showed that the six *LGR4* missense variants identified in FEVR patients appear to alter the normal function of LGR4 by failing to restore the correct development of the ocular vasculature in the zebrafish embryo. In this chapter, further functional assessment of the missense variants was undertaken to provide additional evidence that they cause FEVR and to provide some insight into their pathological effect.

The majority of mutations underlying FEVR are in genes that encode components of the Norrin- $\beta$ -Catenin signalling pathway (section 1.4.2). Given that LGR4 is reported to play a role in the closely related Wnt- $\beta$ -Catenin signalling pathway (section 1.6.3), the aim of this experiment was to investigate if LGR4 also participated in the Norrin- $\beta$ -Catenin signalling pathway and if the FEVR-related LGR4 missense variants affected this interaction.

A popular, well established method that has been used for over 20 years to assess  $\beta$ -Catenin signalling, particularly in the context of Wnt activation, is the TOPflash assay (Molenaar et al., 1996). This is a reporter-based assay which measures the activation of the signalling pathway using a luciferase TOPflash reporter construct. This construct contains the *Firefly* luciferase reporter gene under the control of seven copies of the wild-type TCF binding sites known as the SuperTOPflash (referred to in this thesis as a TOPflash) (Xu et al., 2004). Therefore, in cells which contain this reporter, pathway activation will trigger  $\beta$ -Catenin to translocate into the nucleus and form complexes with TCF leading to the transcription of the *Firefly* luciferase gene and ultimately a luminescence signal can be measured.

Missense variants in FEVR genes have been characterized using the TOPflash assay in many studies (Fei et al., 2014; Qin et al., 2008; Xu et al., 2004; Zhang et al., 2011). In the majority of these studies, cells that express the FZD4-LRP5-TSPAN12 receptor complex are stimulated with Norrin and the levels of signalling are assessed by measuring the luminescence triggered by  $\beta$ -Catenin translocating into the nucleus and activating the *Firefly* luciferase gene (Figure 4-1). In this chapter a similar strategy was undertaken using LGR4.

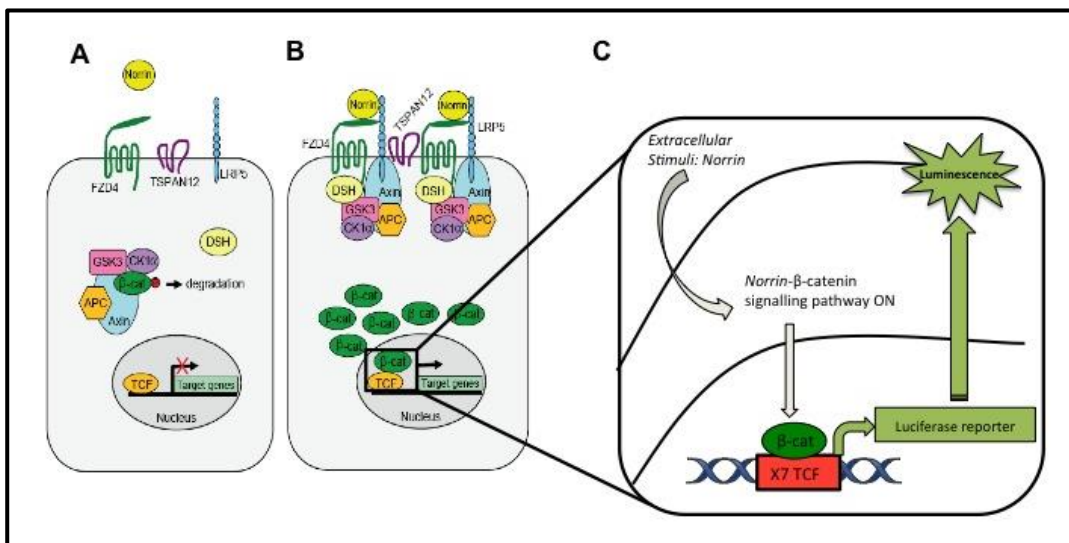


**Figure 4-1: Measuring activation of the Norrin- $\beta$ -Catenin signalling pathway using the TOPflash reporter construct.**

**A:** When Norrin is not bound to the FZD4-LRP5-TSPAN12 receptor complex,  $\beta$ -Catenin is degraded and the target genes are not transcribed. **B:** When Norrin binds to the FZD4-LRP5-TSPAN12 receptor complex,  $\beta$ -Catenin accumulates in the cytoplasm and translocates into the nucleus where it interacts with the transcription factor TCF, leading to the transcription of target genes. **C:** In the TOPflash reporter assay,  $\beta$ -Catenin will translocate into the nucleus, interact with TCF and bind to the 7 copies of the TCF binding sites to activate the luciferase reporter gene and thus produce a luminescence signal that can be measured. Figure adapted with permission from Dr. Carmel Toomes.

## 4.2 Identification of a suitable cell line in which to perform the TOPflash assay

To perform the TOPflash assay a suitable cell line was needed. The plan was to use endogenous copies of the Norrin receptor complex (*FZD4*, *LRP5* and *TSPAN12*) and to transiently transfect cells with the TOPflash construct and *LGR4*. The signalling pathway would be activated by the addition of Norrin to the media. Therefore, a variety of different cell lines were investigated to determine if they expressed the required proteins.

Total RNA from 12 different human cell lines (section 2.10.1) was reversed transcribed into cDNA (section 2.2.4) and PCR amplified with specific primers (Appendix 8.3) to test for the expression of *LGR4* and the Norrin- $\beta$ -Catenin signalling pathway components: *FZD4*, *LRP5*, *TSPAN12* and *NDP* (Norrin). *TP53* expression was also assessed as a control for cDNA synthesis.

The following cell lines were tested: MCF7 (breast adenocarcinoma), RPE1 (retinal pigment epithelium), serum starved (SS) RPE1, U2OS (osteosarcoma), HB2 (breast epithelial), HRT18 (colorectal carcinoma), HCT116 (intestinal adenocarcinoma), HT29 (colon adenocarcinoma), SW480 (colon adenocarcinoma), differentiated (diff) and undifferentiated (undiff) SH-SY5Y (neuroblastoma), MCF10A (epithelial cell line derived from human fibrocystic mammary tissue), HDF (human dermal fibroblasts) and HEK293 (human embryonic kidney).

The optimum cell line would express *FZD4*, *LRP5* and *TSPAN12* but would not express *NDP* or *LGR4*. The results indicated that the cell lines with high expression levels of *FZD4*, *LRP5*, *TSPAN12* but not expressing *NDP* were differentiated SH-SY5Y, RPE1 and HEK293 cells (Figure 4-2). Unfortunately, all these cell lines expressed *LGR4*.

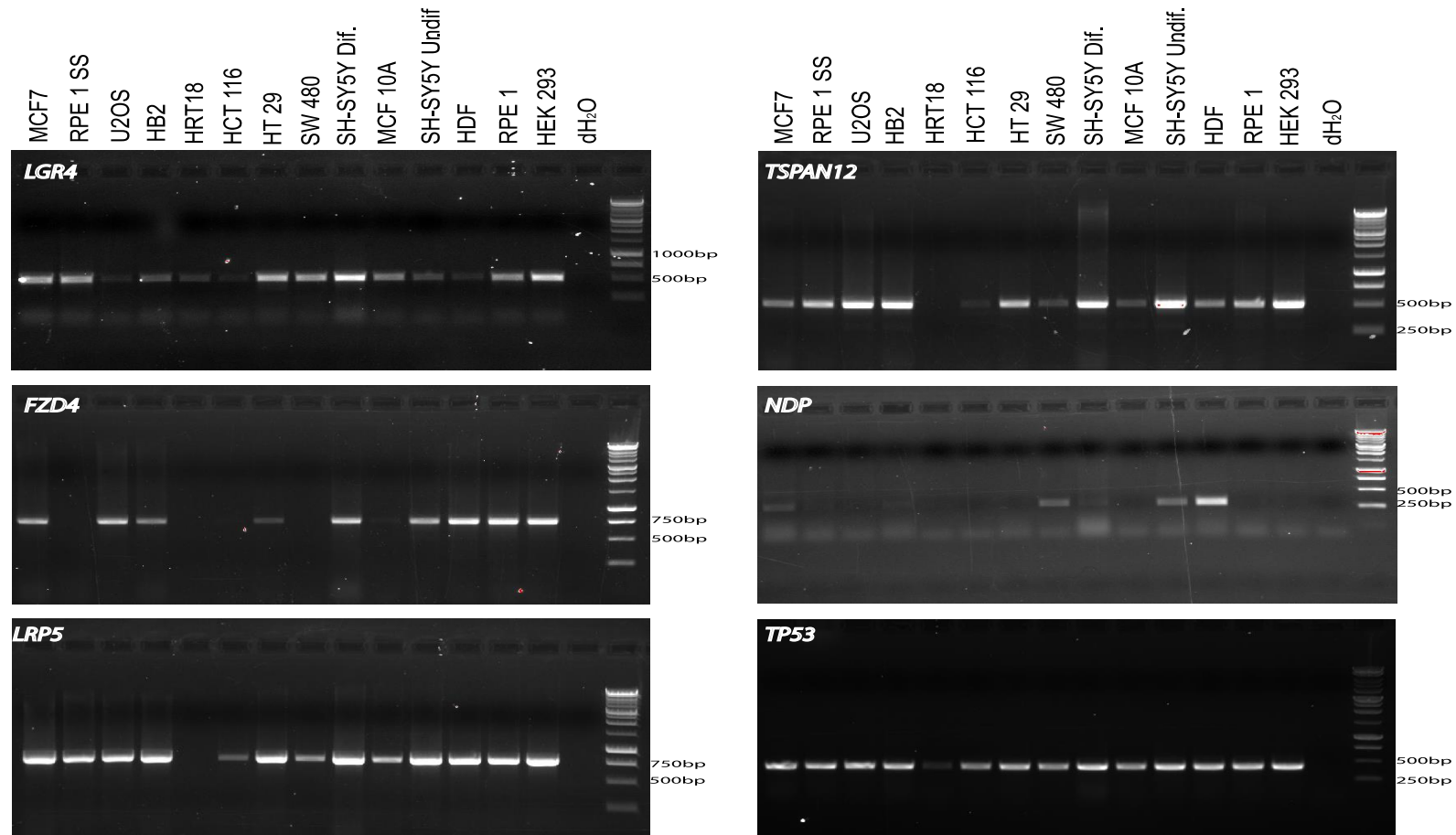


**Figure 4-2: Expression of *LGR4* and Norrin signalling pathway components in a panel of cell lines.**

*LGR4*, *FZD4*, *LRP5*, *TSPAN12* and *NDP* mRNA expression was evaluated in the cell lines indicated. *TP53* was used as a control. For the negative control dH<sub>2</sub>O was added instead of cDNA. The correct sizes of the PCR products are 488bp for *LGR4*, 745bp for *FZD4*, 747bp for *LRP5*, 499bp for *TSPAN12*, 299bp for *NDP* and 400bp for *TP53*. The ladder used is GeneRuler 1Kb.

At this point in the experiment, a HEK293 cell line stably transfected with the “Super TOPFlash” construct (STF) was obtained as a kind gift from Professor Jeremy Nathans (John Hopkins University, USA) (Xu et al., 2004). The use of these STF cells would reduce experimental variability as the TOPflash reporter construct wouldn’t have to be transiently transfected into the cells. STF cells are derived from HEK293 cells; consequently the gene expression profile is expected to be the same. To check that this assumption was correct, the expression of *LGR4* and the Norrin- $\beta$ -Catenin pathway components were evaluated in the STF cells.

As expected, STF cells also expressed *FZD4*, *LRP5*, *TSPAN12* and *LGR4* but they did not express *NDP* (Figure 4-3). Therefore, STF cells seemed to be the most appropriate cell line in which to perform the TOPflash assay.

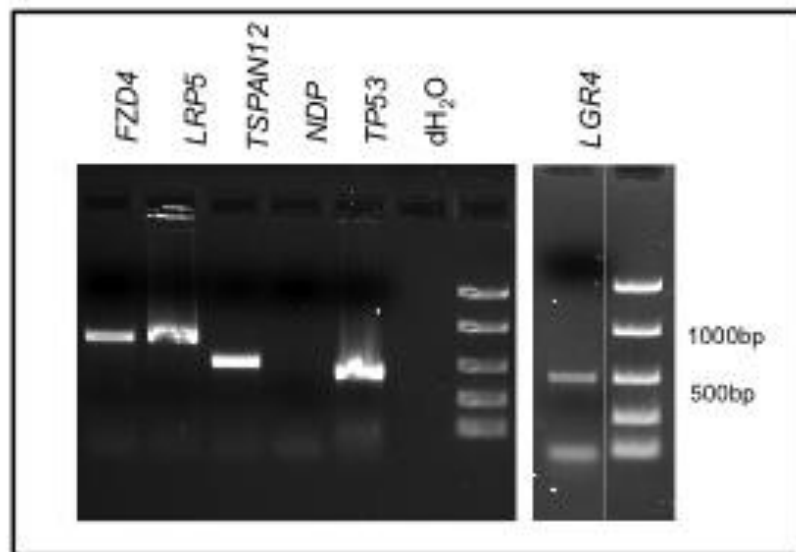


**Figure 4-3: cDNA expression of *LGR4* and the Norrin signalling pathway components in STF cells.**

*FZD4*, *LRP5*, *TSPAN12*, *NDP* and *LGR4* expression was evaluated. *TP53* was used as a positive control. For the negative control *dH<sub>2</sub>O* was added instead of cDNA. The correct sizes of the PCR products are 488bp for *LGR4*, 745bp for *FZD4*, 747bp for *LRP5*, 499bp for *TSPAN12*, 299bp for *NDP* and 400bp for *TP53*. The ladder used is EasyLadder I.

### 4.3 Topflash assay using recombinant human Norrin (rhNorrin)

The first attempt to develop the TOPflash assay in STF cells was to use endogenous levels of the Norrin- $\beta$ -Catenin pathway components present in STF cells and to control pathway activation by adding Norrin into the culture media. Recombinant human Norrin (rhNorrin) (R&D systems) was used for this assay as it had been used previously in the study for the identification and characterization of *TSPAN12* as a new component of the Norrin- $\beta$ -Catenin pathway (Junge et al., 2009).

RhNorrin was reconstituted at a final concentration of 250 $\mu$ g/ml in sterile 4mM HCl. The STF cells were incubated with rhNorrin overnight prior to performing the luciferase assay (section 2.10.9.1). The luciferase assay used to measure *Firefly* activity was the single luciferase assay (Luciferase Assay System, Promega). STF cells were stimulated with rhNorrin at concentrations ranging from 50ng/ml to 250ng/ml. The concentration range was chosen based on those used by Junge et al., (2009). Three control groups were also evaluated. "Control" cells were native STF cells without Norrin media. This control group measures background  $\beta$ -Catenin pathway activation levels in STF cells. "Control HCl" cells are STF cells incubated with 4mM HCl, the carrier used for rhNorrin. This control group rules out any consequences of adding HCl to the STF cells. The third control was "Wnt3a conditioned media", which was used as a positive control for  $\beta$ -Catenin pathway activation (Farin et al., 2016; J. Hao et al., 2013; Kishida et al., 1999).

Unfortunately, the results obtained were inconsistent and not reproducible (Figure 4-4). Despite attempts to optimise with different concentrations (50-1000ng/ml) of rhNorrin and different batches of recombinant protein, a reliable assay could not be developed. If it had been successful, this method would have reduced the need to transfect the STF cells with multiple constructs which is a well-known cause of variability in TOPflash assays. However, as the assay could not be optimised, the well-established and

broadly utilized method of transfecting all the  $\beta$ -Catenin pathway components into the STF cells was used (Fei et al., 2014; Qin et al., 2008; Smallwood et al., 2007; Xu et al., 2004; Zhang et al., 2011; Ke et al., 2013).

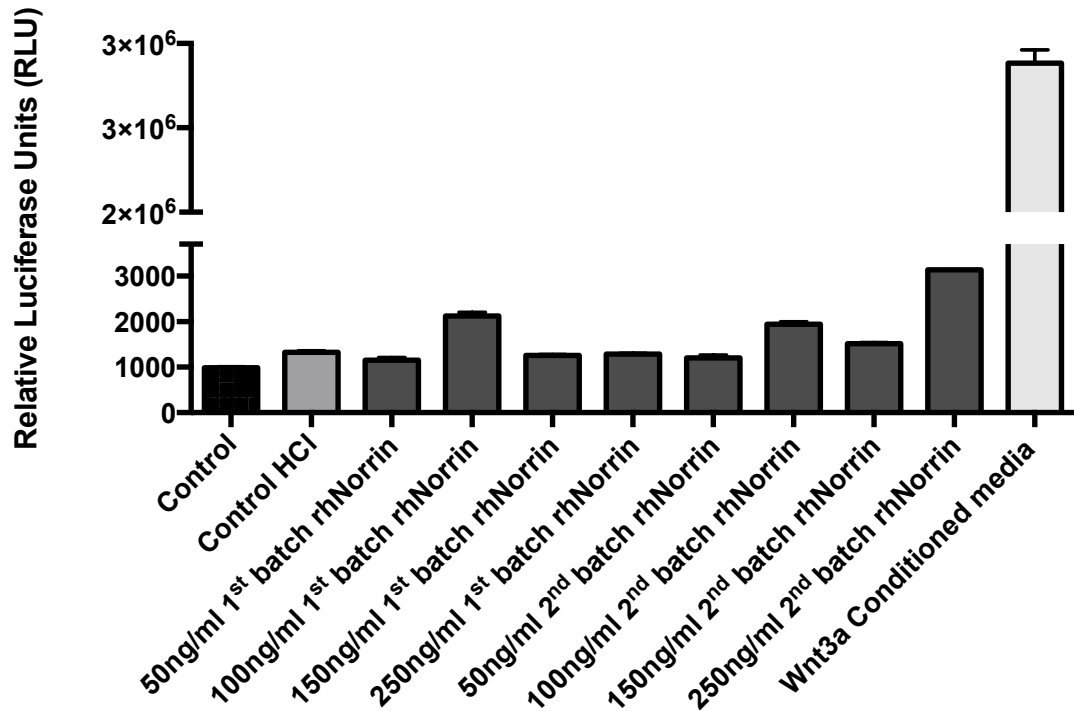


**Figure 4-4: TOPflash assay in STF cells activated using 50, 100, 150 and 250ng/ml of human recombinant Norrin.**

Luciferase activity was measured and expressed as Relative Luciferase Units (RLU). “Control” cells are STF cells without Norrin added into the medium. “Control HCl” cells are STF cells with HCl (Norrin carrier) but no Norrin. Recombinant human Norrin (rhNorrin) was added 16 to 18 hours prior to performing the luciferase assay. Two different recombinant Norrin batches, 1<sup>st</sup> batch and 2<sup>nd</sup> batch were used at concentrations ranging from 50ng/ml to 250ng/ml. Wnt3a conditioned media was added onto the cells 16 to 18 hours prior to measure luciferase activity as a positive control. Error bars show standard error of the mean.

#### **4.4 TOPflash assay transfecting Norrin- $\beta$ -Catenin pathway components into STF cells**

##### **4.4.1 Creating expression constructs for the TOPflash assay.**

The aim of this experiment was to create expression constructs for the known components of the Norrin- $\beta$ -Catenin pathway in order to transiently transfect them into the STF cells to perform the TOPflash assay.

Parent clones for *FZD4* (pCR-BluntII-topo-*FZD4*, parent clone accession: BC114527), *LRP5* (pCR-XL-Topo-*LRP5*, parent clone accession: BC150595) and *TSPAN12* (pBluescriptR-*TSPAN12*, parent clone accession: BC031265) containing the entire ORF of the genes of interest were purchased from *Transomic Technologies* (Huntsville, USA). Each of these clones was sequence verified (section 2.4) to ensure they were full length and contained no variants in the coding sequence (Primer sequences in Appendix 8.6). The results showed the presence of common synonymous SNPs in *LRP5* and *TSPAN12* and a rare missense variant in *TSPAN12*, c.170C>T p.(S57L) (Table 4-1). The inserts of these clones were used as templates to facilitate the introduction of these genes into plasmids compatible with Gateway technology (section 2.6.4).

	Accession number	SNP id	Variant allele Frequency	Genetic variant	Protein variant
<b><i>FZD4</i></b>	BC114527	NA	NA	NA	NA
<b><i>LRP5</i></b>	BC150595	rs545382	113469 / 126394	c.1647 T>C	p.(F549F)
		rs556442	84517 / 125834	c.3357 G>A	p. (V1119V)
<b><i>TSPAN12</i></b>	BC031265	rs1785293	NA	c.170 C>T	p.(S57L)
		rs41623	101755 / 126384	c.765 G>T	p.(P255P)

**Table 4-1: Variants present in the cDNA clones purchased from Transomic technologies.**

The variants present in the cDNA clones compared to the reference sequences are listed. Reference sequence: *FZD4* (NM\_012193.3), *LRP5* (NM\_002335.3) and *TSPAN12* (NM\_012338). The frequency data was obtained from or USCS genome browser Dec. 2013 (GRCh38/hg38) accessed on October 2016.

PCR amplification using attB-tagged primers was performed using each parental clone as a template (Appendix 8.5). An entry clone for each gene was then created by transferring the attB-tagged PCR product into a donor vector (pDONR201) using BP clonase (Invitrogen) (section 2.6.4). Subsequently, SDM was performed on the *TSPAN12* entry clone (pDONR201\_*TSPAN12*) to correct the rare missense variant (p.S57L) identified (Primer sequences in Appendix 8.4). Each entry clone was sequenced to ensure that no errors had been introduced during the PCR amplification stage and to ensure that the SDM experiment had worked (Sequencing primers in Appendix 8.6).

The destination vector chosen to create the expression clones was pDEST40 (Invitrogen). This expression vector contains a C-terminal V5 epitope and 6x His-tag, to facilitate the detection and purification of the fusion protein, and a cytomegalovirus (CMV) promoter for high-level expression in mammalian cells (Appendix 8.8). The *FZD4*, *LRP5* and *TSPAN12* ORF in the entry clones were transferred to the pDEST40 plasmid using the LR clonase enzyme (section 2.6.4). All expression constructs were sequenced verified and confirmed to have the whole ORF of the gene in frame with the tag at the C-terminal end of the sequence (Sequencing primers in Appendix 8.6).

A human Norrin construct was provided as a gift from Professor Jeremy Nathans (John Hopkins University, USA). The AP-3myc-Norrin expression vector contains alkaline phosphatase (AP) and 3 myc epitopes at the N-terminal (Xu et al 2004). The resulting AP fusion protein can be secreted at high levels into the culture medium and thus be detected by either the AP activity assay or by Western Blot (WB).

An expression construct for WT human *LGR4* (pCMV6\_*LGR4*-WT), and the corresponding variant *LGR4* constructs had previously been created by SDM (section 3.3.2).

#### 4.4.2 Validation of the expression constructs

The aim of this experiment was to verify the protein expression of the constructs by expressing them in mammalian cells and detecting the proteins by WB.

HEK293 cells were separately transfected (section 2.10.6.1) with pDEST40\_ *FZD4*, pDEST40\_ *LRP5*, pDEST40\_ *TSPAN12* or empty vector pDEST40. Cells treated with Lipofectamine2000 only were used as a negative control (C-). Forty-eight hours after transfection, protein extraction was performed (section 2.10.7) and cell lysates were analysed by WB using either an anti-His antibody or anti-V5 antibody to target the pDEST40 fusion protein or by using antibodies specific for the protein of interest (Figure 4-5). The C-terminal tag on the pDEST40 fusion protein was predicted to be 4.5 kDa.

The molecular weight of LRP5 (NP\_002326) was predicted to be 179 kDa by the ExPASy ProtParam tool. The predicted molecular weight without the signal peptide (3.09 kDa) and adding the C-terminal tag would occur in a fused protein of 180 kDa. A band of this size was obtained with both the anti-His and anti-V5 antibody (Figure 4-5, A) and anti-LRP5 antibody (Figure 4-5, B) confirming the expression of the LRP5 fusion protein. In both blots, a larger second LRP5 specific band was detected which most likely represented dimers or oligomers of LRP5 (Figure 4-5).

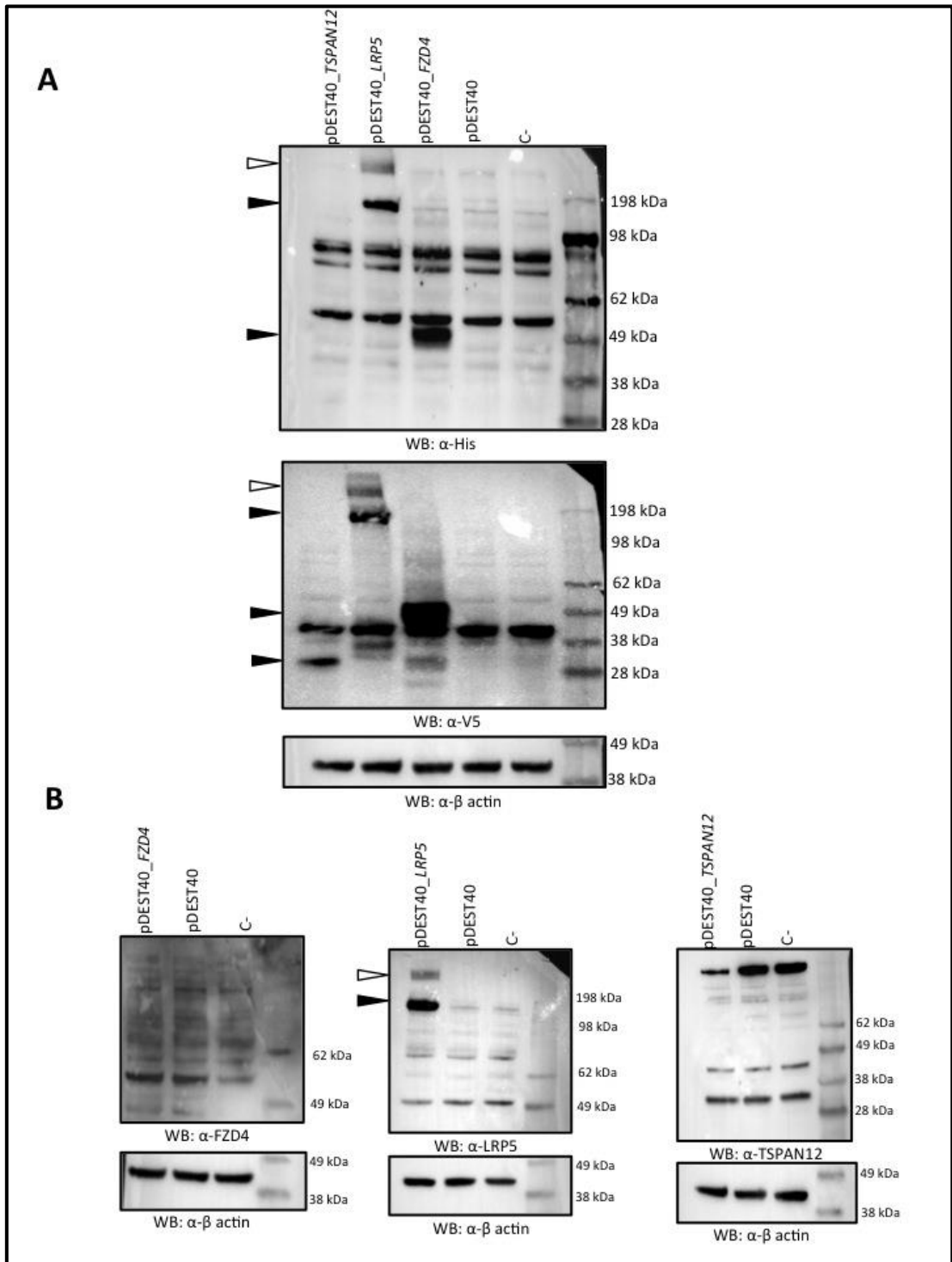


**Figure 4-5: Western blots to confirm the expression of the pDEST40 fusion proteins.**

HEK293 cells were transfected with pDEST40, pDEST40\_FZD4, pDEST40\_LRP5 and pDEST40\_TSPAN12 plasmids and the resulting cell lysates were evaluated by WB. **A:** WB of pDEST40, pDEST40\_FZD4, pDEST40\_LRP5 and pDEST40\_TSPAN12 incubated with an antibody raised against the His-tag or the V5-tag present in the pDEST40 fusion proteins. **B:** Separate WBs of pDEST40 and pDEST40\_fusion protein incubated with antibodies against the target proteins FZD4, LRP5 and TSPAN12. C- indicates lysate from HEK293 cells

treated with lipofectamine2000 only (negative control). Black arrows correspond to expression of the fused proteins. White arrows correspond to dimers or oligomers of the fused protein. Each blot was probed with an anti- $\beta$  actin (42 kDa) antibody to control for protein loading. Ladder used was SeeBlue Plus2 Prestained standard.

The ExPASy ProtParam tool predicted TSPAN12 to have a molecular weight of 35 kDa (NP\_036470). When the C-terminal tag was added the fused protein was predicted to be 39.5 kDa. A band around 35 kDa size was detected by the anti-TSPAN12 antibody in all the samples analysed, but not specific band for pDEST40\_TSPAN12 was detected (Figure 4-5, B). TSPAN12 expression was not detected by the anti-His antibody, but detection was obtained using the anti-V5 antibody even though a smaller size than expected was obtained (Figure 4-5, A). The sequence of the expression construct was double-checked and confirmed to be the full ORF for TSPAN12 in frame with the C-terminal tag.

The ExPASy ProtParam tool predicted a molecular weight of 59.8 kDa for FZD4 (NP\_036325) and 60.7 kDa for FZD4 without the signal peptide (3.6 kDa) fused with the C-terminal tag. However, a specific band smaller than this was detected by the anti-His and anti-V5 antibodies (Figure 4-5, A). No specific band was detected with the anti-FZD4 antibody (Figure 4-5, B). The sequence of the expression construct was double-checked and confirmed to be the full length for FZD4 in frame with the C-terminal tag.

Unfortunately, TSPAN12 and FZD4 expression constructs were not completely verified by WB, due to smaller discrepancies in the size of the fused protein. However as the sequence of the full ORF for the expression constructs were correct, and assuming that WB is not a precise determination of molecular sizes, these constructs were used for the functional experiments in this chapter and Chapter 5, which further validated the functioning of both fused proteins.

Next, the expression of the WT and variant pCMV6\_LGR4 fusion proteins were verified in HEK293 cells using the same method. LGR4 is predicted to

be 104 kDa using NP\_060960 as a reference sequence. The fused protein without the signal peptide (2.2 kDa) and fused to the C-terminal tag (2.8 kDa) was still predicted to be 104.6 kDa. Bands of the correct size were detected with an anti-LGR4 antibody confirming the expression of the fusion protein. However, a larger doublet was also observed (Figure 4-6). These higher bands corresponded in size to LGR4 dimers and oligomers (white arrow). Different expression levels of LGR4 were detected on the blot but these were not present in duplicate experiments indicating that they are due to experimental variability in expression levels.

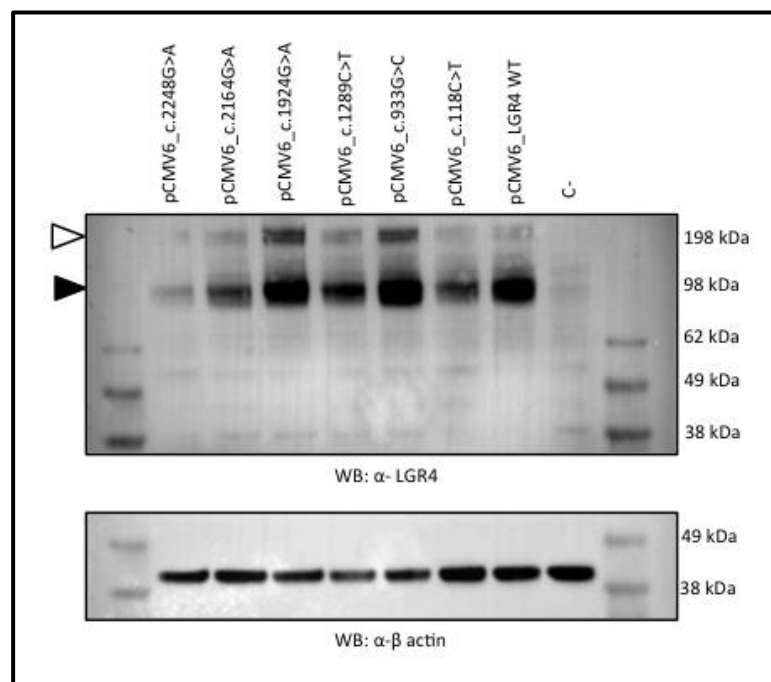


**Figure 4-6: Western blot to confirm the expression of the LGR4 fusion proteins.**

HEK293 cells were transfected with WT or variant pCMV6\_LGR4 constructs and the resulting cell lysates were evaluated by WB and probed with an anti-LGR4 antibody. C- indicates lysate from HEK293 cells treated with lipofectamine2000 only (negative control). Black arrows correspond to expression of LGR4 fused proteins. White arrows correspond to dimers or oligomers of LGR4 proteins. Each blot was probed with an anti-β actin (42 kDa) antibody to control for protein loading. Ladder used was SeeBlue Plus2 Prestained standard.

A similar experiment was performed to validate the Ap-3myc-Norrin vector. HEK293 cells were transfected with the Norrin expression vector but protein extraction was performed at 4 different time points following transfection: 18

hours, 24 hours, 48 hours and 72 hours. The reason for investigating the different time points was to determine the optimal time needed for the cells to express Norrin. Duplicate WBs were probed with either anti-Myc antibody or with anti-Norrin antibody (Figure 4-7).

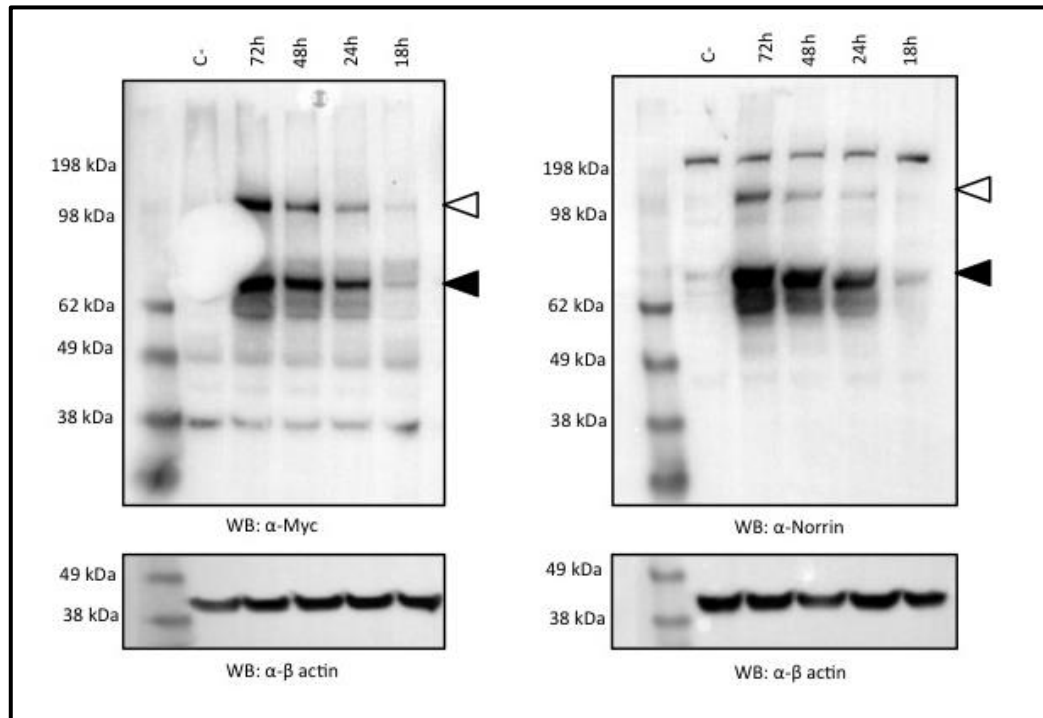


**Figure 4-7: Western blot to confirm the expression of the AP-Norrin fusion protein.**

HEK293 cells were transfected with AP-3myc-Norrin plasmid and protein extraction was performed at 4 different time points: 72h, 48h, 24h and 18h post transfection. The resulting cell lysates were evaluated by WB and probed with an anti-Myc antibody (left panel) and anti-Norrin antibody (right panel). C- indicates lysate from HEK293 cells treated with lipofectamine2000 only (negative control). Black arrows correspond to expression of Norrin. White arrows correspond to dimers or oligomers of Norrin. Each blot was probed with an anti- $\beta$  actin (42 kDa) antibody to control for protein loading. Ladder used was SeeBlue Plus2 Prestained standard.

The results showed that Norrin expression was detected at all the time points tested, but as expected the expression levels increased gradually over time. Norrin is predicted to have a molecular weight of 15 kDa according to the ExPASy ProtParam prediction tool (NP\_000257) but the signal peptide is not included in the AP construct so its size is predicted to be 12.8 kDa. The AP tag present in the vector is predicted to be 57 kDa and the Myc tag also

present is predicted to be 1.2 kDa. Therefore, the predicted size of the fusion protein is 71 kDa, which corresponded to the size of the bands detected with both anti-Myc and anti-Norrin antibodies (Figure 4-7). Both antibodies also detected a second target which suggests dimerization of Norrin (white arrows).

In summary, expression constructs for Norrin, LRP5, LGR4 and all six LGR4 variants were created and expression verified using WB, ready for use in the TOPflash assay. FZD4 and TSPAN12 expression constructs, which gave smaller band sizes on WB than predicted for molecular weight, were sequence verified and their use in further functional experiments suggested that both fused proteins were working correctly.

#### **4.4.3 Elucidating if LGR4 plays a role in Norrin- $\beta$ -Catenin signalling**

The aim of this experiment was to optimise the TOPflash assay so that it could be used to assess if LGR4 played a role in the Norrin- $\beta$ -Catenin pathway, and if the FEVR-related *LGR4* variants had any effect on this role.

The assay was performed as originally described by Xu et al. (2004). Briefly, all the components of the pathway (LRP5, FZD4, Norrin, TSPAN12) and LGR4 were transiently transfected into STF cells. A *Renilla* transfection control was used in all experiments (pRL-TK). Each well was transfected with the same amount of DNA (400ng per well). To control for this, empty pDEST40 vector was added in the place of any expression constructs omitted from the reaction. The assay was performed in 24-well plates and cells were 70-80% confluent prior to transfection. Cell lysis was performed 48 hours after transfection and *Renilla* and *Firefly* luciferase levels were determined using the Dual Luciferase reporter assay (Promega). The *Firefly* signal was normalized to the *Renilla* signal for every well and pathway activation levels were expressed as relative luciferase units (RLU) using the *Firefly/Renilla* ratio (section 2.10.9.2). Every assay was performed in

triplicate, and each experiment was independently replicated on at least four separate occasions, unless stated otherwise in the text.

LGR4 is well reported to form complexes with Frizzled receptors and LRP5/6 co-receptors to activate  $\beta$ -Catenin signalling through the binding of an R-spondin (RSPO) ligand (Carmon et al., 2011; Glinka et al., 2011; Lau et al., 2011; Ruffner et al., 2012). A single controversial study has also shown that Norrin can substitute for RSPO to activate  $\beta$ -Catenin signalling in the presence of LGR4 and LRP5 receptors (Deng et al., 2013). Therefore, in this experiment, different combinations of the Norrin receptor complex were tested to determine whether LGR4 enhances the Norrin- $\beta$ -Catenin pathway and which combination of receptors is needed for this enhancement (Figure 4-8).

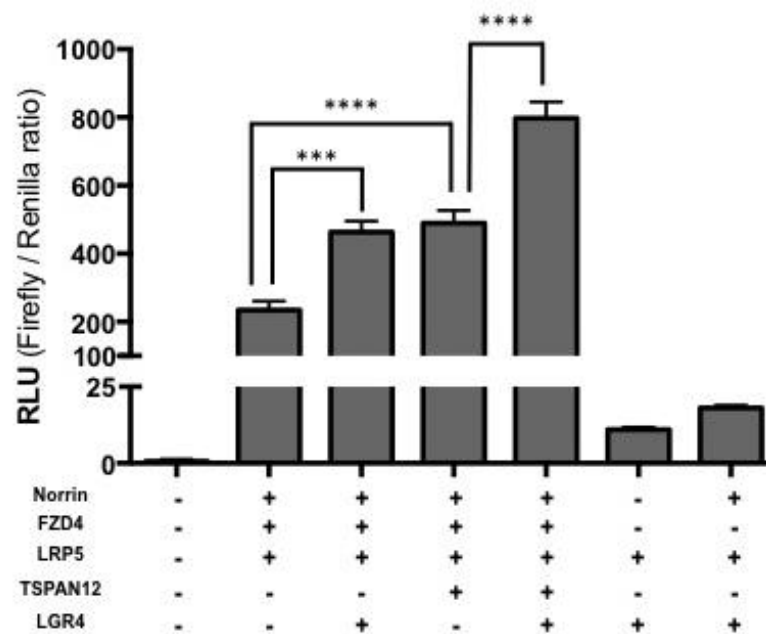


**Figure 4-8: TOPflash assay in STF cells transfected with different Norrin pathway components.**

STF cells were transfected with different combinations of plasmids as indicated. 48 hours after transfection the dual luciferase reporter assay was performed to measure TOPflash activation levels. Values are recorded as relative luciferase units (RLU) and are expressed as Firefly/Renilla ratio. \*\*\*: p value  $\leq 0.001$ ; \*\*\*\*: p value  $\leq 0.0001$  Error bars show standard error of the mean. An ANOVA Tukey's multiple comparison test was performed. The results were made in triplicate with at least 4 biological replicates per condition, except for column 6 and 7 where only one biological replicate was performed.

The results showed the significant enrichment of the TOPflash reporter activation levels when *LGR4* was present. This increase in TOPflash levels occurred either when TSPAN12 expression was not present (column 3 and column 4) or when TSPAN12 expression was present (column 5 and column 6). The highest activation of the TOPflash reporter was obtained when all the Norrin receptor complex components were transfected together, suggesting that the highest LGR4 enrichment of the pathway occurs when all the Norrin pathway components are present in the cells (as TSPAN12 is specific to the Norrin- $\beta$ -Catenin pathway and has no effect on Wnt/ $\beta$ -Catenin signalling (Junge et al., 2009)) (Figure 4-8). These results suggest that LGR4 plays a role in the Norrin- $\beta$ -Catenin signalling pathway. However, unlike the data presented in the study by Deng and colleagues (2013), there was no statistically significant difference when only LRP5, LGR4 and Norrin were overexpressed in the cells (Column 6 and 7).

Transfection of *FZD4* into the cells resulted in a massive increase in pathway activation, which provides evidence that the FZD4 fusion protein is being expressed and can mediate Norrin signalling. Similarly, *TSPAN12* transfection also resulted in an increase in TOPflash levels, as previously reported by Junge et al. (2009), even though this increase was not as pronounced as with FZD4, as TSPAN12 is an auxiliary protein enhancing Norrin pathway and not the main receptor of the pathway (Junge et al., 2009).

#### **4.4.3.1 Investigating the effects of the *LGR4* missense variants on the Norrin- $\beta$ -Catenin signalling pathway**

The aim of this experiment was to determine if the missense variants identified in *LGR4* in FEVR patients had any effect on Norrin- $\beta$ -Catenin signalling. As the largest increase in TOPflash output was obtained when STF cells were transfected with *FZD4*, *LRP5*, *TSPAN12*, *Norrin* and *LGR4* (section 4.4.3), this combination of receptors was used in this experiment using the same method. The assay was performed using either the WT *LGR4* construct or one of the different *LGR4* variant constructs to see if and

how these variants altered the TOPflash signal. Every assay was performed in triplicate, and each experiment was independently replicated on at least three separate occasions. The pooled data was subjected to statistical analysis using the GraphPad Prism 6 one-way ANOVA test.

The results confirmed the increase in TOPflash signal with the addition of WT LGR4 (Figure 4-9) as previously found (Figure 4-8). Three of the FEVR-related variants, present in the binding domain of LGR4 showed a statistically significant reduction in TOPflash activation: c.118C>T p.(R40W), c.933G>C p.(Q311H) and c.1289C>T p.(T430M). The variants present in the transmembrane domain of LGR4 showed no significant difference: c.1924G>A p.(E642K), c.2164G>A p.(A722T), c.2248G>A p.(A750T) (Figure 4-9).

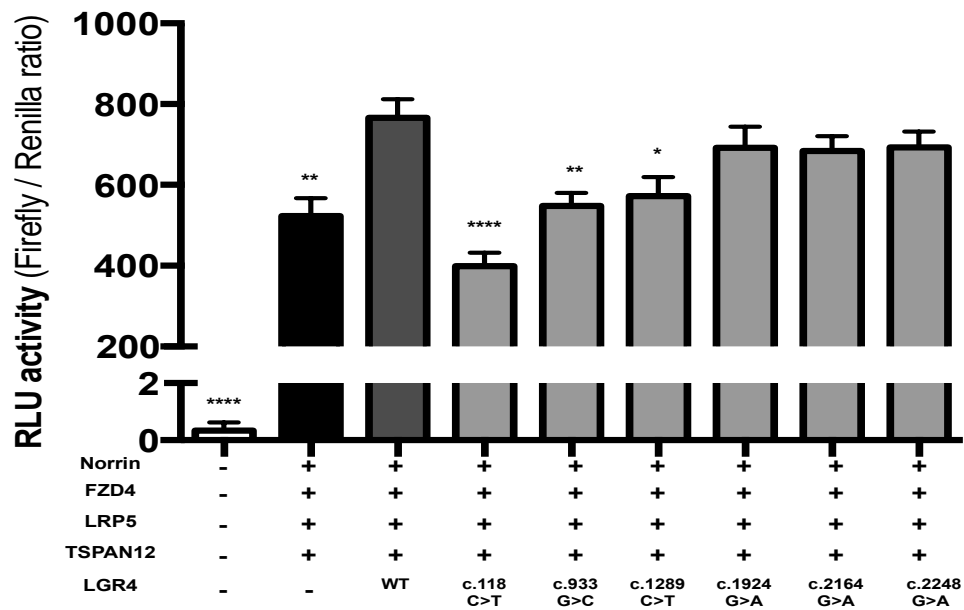


**Figure 4-9: TOPflash assay to assess the effect of *LGR4* variants on Norrin- $\beta$ -Catenin signalling.**

STF cells were transfected with Norrin pathway components and WT/variant LGR4 and luciferase levels were measured 48 hours after transfection. Values are given as relative luciferase units (RLU) and are expressed as *Firefly/Renilla* ratios. The nucleotide change for the *LGR4* missense variants is indicated for each bar. \*:  $p \leq 0.05$ ; \*\*:  $p \leq 0.01$ ; \*\*\*\*:  $p \leq 0.0001$ . Error bars show standard error of the mean. An ANOVA test was performed comparing column 3 (WT *LGR4*) to the rest of the conditions tested. The results were made in triplicate with four biological replicates.

#### 4.4.3.2 Genetic update on *LGR4* Variants.

At this stage of the project, further genetic studies were performed by Evangelia Panagiotou (University of Leeds) on five of the FEVR patients with *LGR4* variants (all except the *EVR3* family). WES was undertaken in these patients to exclude the possibility that they harboured a mutation in another FEVR gene. This analysis revealed that the patient with the c.1924G>A p.(E642K) *LGR4* variant also contained a heterozygous whole exon deletion in *TSPAN12*. This deletion had previously been missed as it was not detectable by Sanger sequencing.

Furthermore, the frequency data for the c.2248G>A p.(A750T) *LGR4* variant had been updated, which was now reported as a polymorphism (allele frequency >1%) in the East Asian population (ExAC database) (Table 4-2).

Population	Allele Count	Allele Number	Number homozygotes	Allele frequency
East Asian	146	8654	1	0.01687
South Asian	2	16512	0	0.0001211
European	1	66736	0	1.498e-05
African	0	10396	0	0
Finnish	0	6614	0	0
Latino	0	11574	0	0
Other	0	908	0	0
<b>Total</b>	<b>149</b>	<b>121394</b>	<b>1</b>	<b>0.001227</b>

**Table 4-2: Population frequencies from ExAC Browser Beta database for the *LGR4* variant c.2248G>A p.(A750T).**

Different populations are listed. Allele count, allele number and number of homozygotes with this variant is indicated. The allele frequencies for individual populations is indicated. The c.2248G>A p.(A750T) variant occurred with an allele frequency of 0.01687 in the East Asian population, indicating this variant as a polymorphism in the Asian population.

In light of these updates, the *LGR4* variants c.1924G>A p.(E642K) and c.2248G>A p.(A750T) were excluded from further experiments as they are unlikely to be Mendelian alleles causing FEVR.

#### **4.4.4 Investigating the effects of the *LGR4* missense variants on R-spondin signalling**

LGR4 is an established receptor for RSPO ligands (RSPO1-4) and ligand binding potentiates  $\beta$ -Catenin signalling in a Wnt dependent manner through Frizzled-LRP5/6 complexes (Carmon et al., 2011; Glinka et al., 2011; Lau et al., 2011; Ruffner et al., 2012). The aim of this experiment was to determine whether or not the missense variants found in *LGR4* also alter RSPO signalling or if they only specifically affect Norrin signalling.

This experiment was performed the same way as described for the Norrin- $\beta$ -Catenin TOPflash assay (section 4.4.3) but recombinant RSPO1 (Life Technologies) reconstituted in sterile distilled water was added in place of Norrin into the culture media 16 to 18 hours before the luminescence values were recorded (Ruffner et al., 2012).

Initially, the assay was optimised to determine the optimal concentration of recombinant RSPO1 needed to activate TOPflash signalling. Affinity purification mass spectrometry-based experiments identified LGR4 binding to RSPOs and LRP5/6 (De Lau et al., 2011), so for this reason this combination of receptors and ligand was tested. Based on the study performed by Ruffner and colleagues, recombinant RSPO1 was added at concentrations ranging from 50ng/ml to 1000ng/ml (Ruffner et al., 2012) (Figure 4-10).

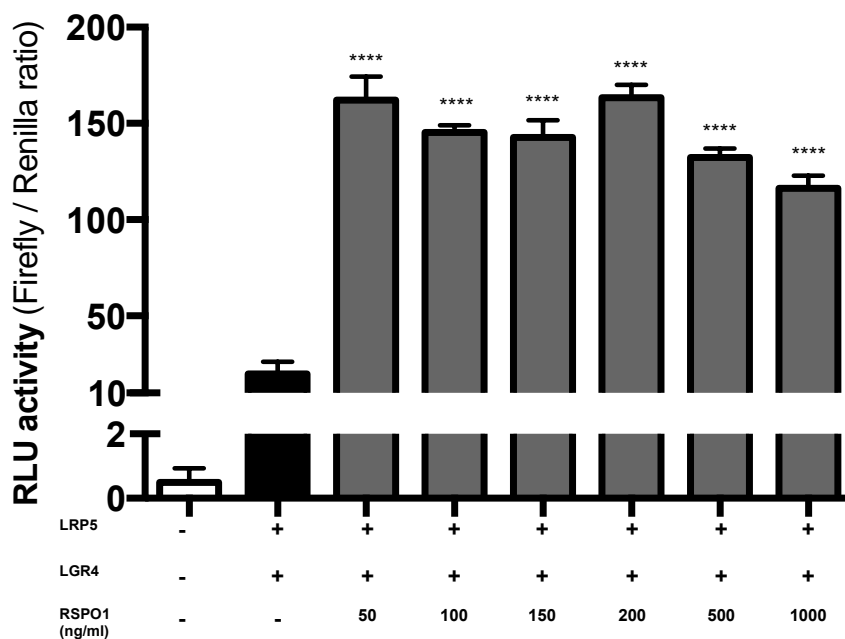


**Figure 4-10: TOPflash assay to determine the optimum RSP01 concentration required to activate  $\beta$ -Catenin signalling.**

STF cells were transfected with LRP5 and LGR4 plasmids and approximately 30 hours later recombinant RSP01 was added to the culture media and a further 16-18 hours later luciferase levels were measured (48 hours post transfection). Recombinant RSP01 was added at concentrations ranging from 0 to 1000ng/ml. Values are given as relative luciferase units (RLU) and are expressed as *Firefly/Renilla* ratios. Error bars show standard error of the mean. \*\*\*\*:  $p \leq 0.0001$ . An ANOVA test was performed comparing Column 2 (no RSP01 added) to the rest of the conditions tested. The results were made in triplicate with one biological replicate.

The results clearly showed that recombinant RSP01 is able to trigger  $\beta$ -Catenin signalling through LGR4 and LRP5. Statistically significant increases in pathway activation were observed with all the different concentrations of RSP01 tested (Figure 4-10). RSP01 concentration dependent pathway activation was not obtained using increasing amounts of RSP01. This suggests that 50 ng/ml of recombinant RSP01 is enough to activate the pathway to the maximum level (Ruffner et al., 2012) and this concentration was used in further experiments.

To assay the effects of the *LGR4* variants on RSP01/LGR4/LRP5 signalling, the assay was repeated substituting the WT *LGR4* construct for one of the variant *LGR4* constructs and using 50 ng/ml of recombinant RSP01.

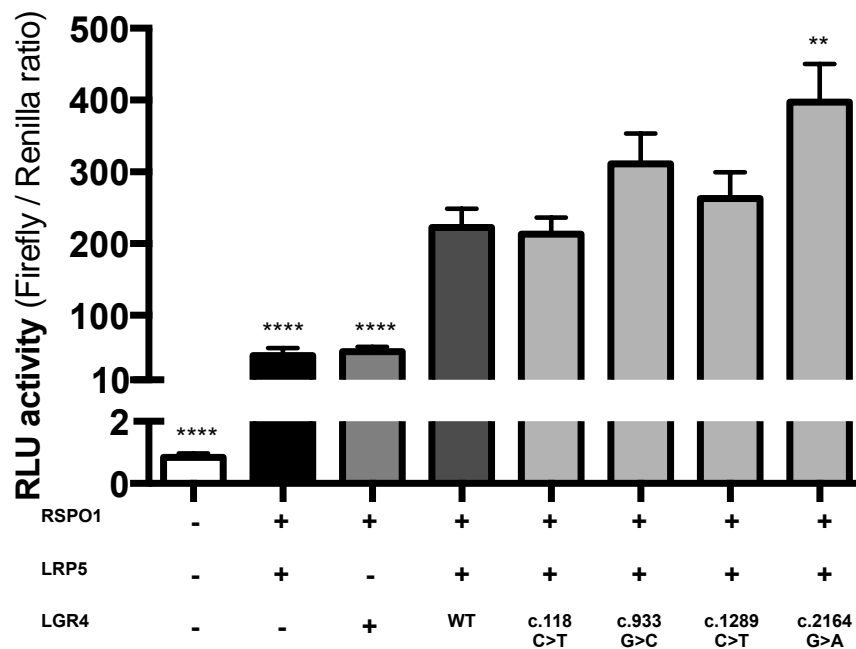


**Figure 4-11: TOPflash assay to determine if the *LGR4* variants alter RSP01- $\beta$ -Catenin signalling.**

STF cells were transfected with *LRP5* and *LGR4* plasmids and approximately 30 hours later recombinant RSP01 was added to the culture media and a further 16-18 hours later luciferase levels were measured (48 hours post transfection). Recombinant RSP01 was added at a concentration of 50ng/ml. Values are given as relative luciferase units (RLU) and are expressed as *Firefly/Renilla* ratios. Error bars show standard error of the mean. An ANOVA test was performed comparing column 4 (WT *LGR4*) to the rest of the conditions tested. Only significant changes are shown. \*\*:  $p \leq 0.01$ ; \*\*\*\*:  $p \leq 0.0001$ . The results were performed in triplicate with seven biological replicates.

The results show that three of the *LGR4* variants had no effect on RSP01 mediated activation of  $\beta$ -Catenin signalling (Figure 4-11). These variants are all located in the LRR extracellular binding domain (c.118C>T p.(R40W), c.933G>C p.(Q311H) and c.1289C>T p.(T430M) of *LGR4* and were the variants which previously were shown to cause a reduction in Norrin- $\beta$ -Catenin signalling (Figure 4-9). Interestingly, the fourth variant located within the fifth transmembrane domain of *LGR4*, c.2164G>A p.(A722T), which previously did not show any effect on Norrin signalling (Figure 4-9), produced a statistically significant increase in RSP01 mediated  $\beta$ -Catenin signalling.

## 4.5 Discussion

The Norrin- $\beta$ -Catenin signalling pathway is believed to be the major pathway affected by FEVR mutations (section 1.5). LGR4 is known to modulate the Wnt- $\beta$ -Catenin signalling pathway (section 1.6.3), which is closely related to, and shares many components with, the Norrin- $\beta$ -Catenin signalling pathway. Therefore, in the present study, LGR4 was investigated to see if it participated in Norrin- $\beta$ -Catenin signalling and if the FEVR-related *LGR4* missense variants affected this signalling. The results support a role for LGR4 in Norrin-mediated  $\beta$ -Catenin signalling and also indicate that the three FEVR-related missense mutations located in the extracellular domain (ligand binding domain) reduce this signalling.

The well-established TOPflash assay was used for these experiments. The TOPflash assay is a reporter assay used to investigate levels of  $\beta$ -Catenin signalling. It was developed over 20 years ago to test  $\beta$ -catenin's interaction with the TCF/LEF family of transcription factors (Molenaar et al., 1996) and since then it has been broadly used to help characterise key components in Wnt- $\beta$ -catenin signalling (Blitzer and Nusse, 2006; Korinek et al., 1997; Mikels and Nusse, 2006; Smallwood et al., 2007).

The majority of published TOPflash experiments involve overexpressing different pathway components, or mutant forms of these components, followed by measuring pathway activation (Chang et al., 2015; Fei et al., 2014; Hao et al., 2012; Junge et al., 2009; Kaykas et al., 2004; Qin et al., 2008; Smallwood et al., 2007; Xu et al., 2004; Zhou & Nathans, 2014). However, the TOPflash assay is notoriously variable in its outputs. This has been attributed to the random uptake of different plasmids by cells which are transfected with multiple constructs and to varying transfection efficiencies (Hollon and Yoshimuraty, 1989). To overcome this variability, the initial experimental design planned to use native levels of the pathway components and recombinant Norrin. At the start of this experiment, the TOPflash stably transfected HEK293 cell line (STF) were not available so a variety of other

cell lines were investigated to determine if they were suitable for this assay. Ideally, the cell line would express *FZD4*, *LRP5* and *TSPAN12* but not express *NDP* or *LGR4*. All the cell lines tested expressed *LGR4* but this was not unexpected given the fact that *LGR4* is widely expressed (Chapter 3, Figure 3-10) (Schoore et al., 2005; Yi et al., 2013). Nevertheless, three cell lines all fulfilled the remaining criteria; differentiated SHSY-5Y, RPE1 and HEK293. The differentiated nature of the SHSY-5Y cells meant that these would be technically difficult to use for the experiment but RPE1 and HEK293 were both suitable. However, after all this work, a TOPflash stably transfected HEK293 cell line (STF) which expressed the TOPflash Renilla reporters became available (gift from Jeremy Nathans, John Hopkins University, USA). Using these cells reduced the need to transfect in the TOPflash reporter construct and they also showed the same expression profile as HEK293 cells (Figure 4-3) making them the ideal cell line for this experiment.

Pathway activation was attempted using rhNorrin but despite multiple attempts this was unsuccessful. This was unexpected as the same recombinant Norrin had successfully been used by others to perform the TOPflash assay (Junge et al., 2009, Wu et al., 2016). While the studies by both Junge and Wu did not use endogenous levels of the receptor complex, the Wnt3A control used in the current study indicated using endogenous levels of the receptors was not the issue (Figure 4-4).

Given the significant amount of time already spent trying to optimise this assay, the decision was made to use the tried and tested method developed by Jeremy Nathan's team (Xu et al., 2004). This involved transfecting individual expression constructs for the receptors (*LRP5*, *FZD4*, *TSPAN12* and *LGR4*) into the STF cells with the ligand provided by transfecting the cells with a secreting alkaline phosphatase tagged Norrin expression construct. This assay worked first time and although there was the expected variability in the size of the TOPflash outputs, similar trends were found among the biological replicates and the cell viability was consistently high. To overcome this variability, multiple repetitions were made and the

luminescence values of individual experiments were pooled together and presented as a single data set (Schagat et al., 2007) with standard error of mean bars indicating the variation between individual experiments.

Before the TOPflash assay was used to investigate the *LGR4* variants, different combinations of the known Norrin receptor complex components were tested in order to determine which combinations gave the best pathway enhancement when *LGR4* was co-expressed (Figure 4-8). For all the receptor combinations tested an increase in pathway activation was found when *LGR4* was co-transfected, even though to obtain statistically significance difference the presence of FZD4 was required in the receptor complex. The best and the highest statistically significant enhancement of the TOPflash output was observed when all the known Norrin pathway components (FZD4, LRP5, TSPAN12, NDP) were co-transfected with *LGR4*. This result suggests that LGR4 has a role in Norrin- $\beta$ -Catenin signalling but the precise function of LGR4 in this pathway is unknown. Determining the exact role of individual components in a signalling pathway requires further and more detailed characterisation of the molecular pathway using other functional assays such as co-immunoprecipitations, binding assays, mass spectrometry or crystal structures of the receptor complex (Junge et al., 2009; Lau et al., 2011; Xie et al., 2013; Xu et al., 2004; Ke et al., 2013; Xu et al., 2013).

This result is inconsistent with those presented by Deng and colleagues who described LGR4 binding to Norrin and enhancing Norrin- $\beta$ -Catenin signalling in the presence of LGR4 and only LRP5 or LRP6 without the addition of FZD4 or TSPAN12 (Figure 4-12) (Deng et al., 2013).

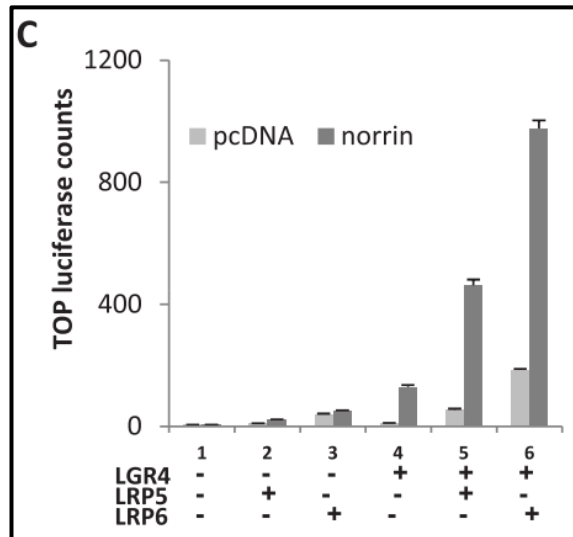


**Figure 4-12: Norrin stimulation of LGR4-mediated Wnt signalling is augmented by LRP5 and LRP6.**

Norrin stimulation of LGR4-mediated Wnt signaling is augmented by LRP5 and LRP6. HEK293T cells were transfected with plasmids encoding TOPFLASH with or without norrin, LGR4, LRP5 and/or LRP6, as described above, before luciferase assays. Image used with permission from the Journal of Cell Science (Deng et al., 2013).

In the present study, the same combination of LGR4, LRP5 and Norrin were used to activate the TOPflash assay and although a slight increase in TOPflash activation was observed it was not statistically significant (Figure 4.8). In the experiment described in this study, transfection of *FZD4* and *TSPAN12* was essential to achieve significant activation of the TOPflash reporter and Deng and colleagues never included FZD4 or TSPAN12 in an assay with LGR4. Although there were slight differences in the methodology used for the TOPflash assay between the studies, these do not explain the huge discrepancies. Other experiments described in the Deng study could not be replicated in this study and these will be discussed in more detail in Chapter 5.

After determining the optimum combination of pathway components to co-transfect with *LGR4* to induce the largest increase in TOPflash signalling, the assay was repeated using the *LGR4* FEVR-related missense variants to determine if they altered Norrin signalling. Similar strategies have been used

previously to assess mutations in FEVR genes (Fei et al., 2014; Qin et al., 2008; Xu et al., 2004; Zhang et al., 2011).

During this study, two of the original six variants were excluded as Mendelian mutations; c.1924G>A p.(E642K) was excluded as the patient with this variant was found to have a large exon-spanning deletion in *TSPAN12* and c.2248G>A p.(A750T) was excluded as its frequency was updated to 1% in the East Asian population and it was therefore re-classified as a polymorphism (Collins et al., 2002). Furthermore, this last variant has been recently associated with central obesity in the eastern China population (Zou et al., 2016), which confirmed the use of the correct criteria used to exclude this variant for further studies. Of the remaining four mutations, the three located in the extracellular LRR domain (c.118C>T p.(R40W), c.933G>C p.(Q311H) and c.1289C>T p.(T430M)) all led to a reduction in TOPflash activation but the one located in the transmembrane domain, c.2164G>A p.(A722T), showed no alteration in signalling levels (Figure 4-9). The level of reduction in TOPflash signal was variable among the three extracellular mutations, with the lowest level being found with the *EVR3* variant, c.118C>T p.(R40W). Similar differential levels in TOPflash signalling have been reported before with missense mutations in other FEVR-causative genes including *FZD4*, *LRP5* and *NDP* (Qin et al., 2008; Xu et al., 2004, Fei et al., 2014, Zhang et al., 2011). This suggests that even a moderate reduction in Norrin signalling can underlie FEVR, although as this is an artificial cell based assay this is only an informed hypothesis.

The LRR domain is believed to be the site of ligand binding (Kajava, 1998; Xu et al., 2013). It is therefore interesting to speculate that the mechanism by which the *LGR4* variants in the LRR domain cause reduced activation of the TOPflash reporter is by altering ligand, and specifically Norrin binding. Similar mutations in the extracellular cysteine-rich domain (CRD) of *FZD4* have been shown to reduce Norrin signalling due to impaired binding with Norrin (Qin et al., 2008; Robitaille et al., 2002; Zhang et al., 2011). However, additional experiments are required to investigate this hypothesis (see Chapter 5).

#### 4.5.1 Investigation of LGR4 variants on RSPO1 signalling

LGR4, and its closely related family members LGR5 and LGR6, are receptors for the RSPO family of ligands (RSPO1-4) (Carmon et al., 2011; Glinka et al., 2011; Lau et al., 2011; Ruffner et al., 2012). All four RSPOs are reported to bind LGR4 (Carmon et al., 2011) and the site of interaction is the LRR domain (Xu et al., 2013). Therefore, the FEVR-related *LGR4* variants were also assessed to see if they abrogate RSPO signalling. For this experiment only RSPO1 was investigated. Its interaction with LGR4 is well characterised (Carmon et al., 2011; Glinka et al., 2011), and all RSPOs have a similar structure and are likely to interact with LGR4 in a similar manner (Carmon et al., 2011; De Lau, Snel, & Clevers, 2012). Although biologically RSPOs form a complex with LGR4/5/6 and ZNRF3/RNF43 (Hao et al., 2012; Xie et al., 2013), to simplify this experiment, due to the reported binding and interaction of LGR4 with RSPOs and LRP5/6 (Lau et al., 2011) the basic components of RSPO1, LRP5 and LGR4 were used to trigger TOPflash activation.

Recombinant RSPO1 was used to trigger TOPflash activation in accordance to published studies (Carmon et al., 2011; Ruffner et al., 2012). The results showed no significant difference in TOPflash activation between WT LGR4 and the three FEVR-related missense variants located in the LRR domain (Figure 4-11), which had previously been shown to cause a reduction in Norrin induced activation of TOPflash. These results suggest that these variants do not have any effect on RSPO1's interaction with LGR4 and have a specific effect on Norrin signalling. Clearly, the remaining three RSPO ligands (RSPO2-4) were not assessed in this experiment so caution must be made in extrapolating these results. Similarly, LGR4 has recently been shown to be a receptor for RANKL, regulating osteoclast differentiation (Luo et al., 2016) but the effects of the missense variants on this interaction have not been investigated. However, the mutations only affecting Norrin- $\beta$ -catenin signalling is consistent with the limited phenotype observed in the FEVR patients.

Due to the multiple roles of LGR4 in development (section 1.7.2) and the different phenotypes observed with *RSPO* mutations in humans (section 1.6.3), other phenotypes would have been expected in the FEVR patients if the *LGR4* variants had an effect on *RSPO*(2-4) or RANKL interaction. In the study by Styrkarsdottir et al. (2013), a nonsense mutation in *LGR4* is the cause of low bone mineral density and a wide range of phenotypes similar to those observed in *Lgr4* mutant mice (Kato et al., 2006; Luo et al., 2009; Mazerbourg et al., 2004; Mendive et al., 2006; Styrkarsdottir et al., 2013; Yamashita et al., 2009). The phenotypes observed in these patients are probably due to the extended role of LGR4 and *RSPO* in development. Therefore, the fact that the patients in this study only have a retinal phenotype, suggests it is most likely that these variants should have an effect in Norrin signalling but no effect should be expected with the other LGR4 ligands described. This is only a theory as it has not been assessed in this thesis.

Unexpectedly, an increase in *RSPO*1 mediated TOPflash activation was observed for the FEVR *LGR4* variant located in the transmembrane domain, c.2164G>A p.(A722T). This was the only variant (apart from the two variants removed from the study), that didn't show any effect on Norrin- $\beta$ -Catenin signalling TOPflash output. The mechanism by which this variant is causing the increase in TOPflash output is unknown and whether it is related to the FEVR phenotype remains to be determined, but it is an interesting observation worthy of further investigation. The crystal structure of *RSPO*1 binding to LGR4 has been reported and showed that ligand binding to LGR4 does not induce significant conformational changes in LGR4 (Xu et al., 2013). This suggests that changes caused by this variant in the oligomerisation state or orientation of the receptor at the cell membrane could have an effect on the ability of the LGR4 7TM GPCR to transduce a signal at the cell surface. Alternatively the switch in the polarity of the protein, changing a non-polar alanine to polar threonine in the transmembrane region, may result in aberrant protein assembly in the plasma membrane that may also influence the transduction of the signal (Lv et al., 2011; McClellan et

al., 2001). Similarly, an *LGR4* mutation with an amino acid substitution changing from polar to non-polar p.(T755I) at the transmembrane domain of *LGR4* resulted in an increase in intracellular cAMP and upregulation of the cAMP-PKA-CREB signalling pathway (Song et al., 2008), confirming the possible effect of *LGR4* transmembrane variants in signal transduction (Xu et al., 2013).

During the course of this experiment, expression constructs were created for *FZD4*, *LRP5*, *TSPAN12* and *LGR4*, and an AP-tag construct of *NDP* was obtained as a gift from Prof. Jeremy Nathans (John Hopkins University, USA). The sequence of all of these constructs was checked and verified and attempts were made to confirm the expression of the fusion proteins by western blotting. Expression for all fused proteins was confirmed using WB. *LGR4*, *LRP5* and *NDP* all showed bands at the expected size but larger bands were also detected. These larger bands probably represented dimers or oligomers as these have previously been described for all three proteins (Chen et al., 2014; Hao et al., 2012; Ke et al., 2013; Yi et al., 2013). However, it is also possible that the larger bands represent heterodimerization products of the proteins assessed, as has been previously described for *LRP6* (Lee et al., 2014).

Expression of *TSPAN12* was observed by western blot when using the anti-V5 antibody. However *TSPAN12* detection was not obtained with either anti-His or anti-*TSPAN12* antibodies. The absence of *TSPAN12* detection with anti-His antibody could be explained due to the specific structural conformation of the fusion protein masking the His tag and avoiding detection of the fused protein with an anti-His antibody (Feldman et al., 2006). Expression of *FZD4* was detected with anti-His and anti-V5 antibody, but no detection was observed with anti-*FZD4* antibody. The detection of the fused protein with an antibody against the C-terminal tag of the fused protein suggested that these proteins were in frame with the tag, as confirmed by sequencing of the full ORF of the fusion protein.

The WB band size obtained for TSPAN12 with the V5 antibody and for FZD4 with both the His antibody and the V5 antibody was slightly smaller than expected. An explanation that could clarify this fact is the presence of TM domains (4 in TSPAN12 and 7 in FZD4) in these proteins. TM domains are very hydrophobic domains, which in association to detergents may influence the molecular weight of a transmembrane protein as much as  $\sim\pm 50\%$  from its predicted molecular weight (Rath et al., 2009). This phenomenon, in which a polypeptide migrates anomalously to a position on a gel that does not correspond to its molecular weight is known as “gel shifting” and it commonly occurs with transmembrane proteins (Rath and Deber, 2012). Shirai and colleagues (2008) showed that 45% of 301 proteins they tested diverged by more than 5% from their predicted molecular weight in a motility analysis (Shirai et al., 2008). Another example is found with the GPCR receptor rhodopsin, the molecular weight of which is predicted to be 39kDa, but it is detected as a 30kDa protein (Frank RN et al., 1975). Therefore, the smaller molecular size obtained for FZD4 and TSPAN12 could be the result of the hydrophobic nature of the TM domains of the protein. It is also important to note that the SeeBlue2 prestained ladder used is not accurate enough to determine precise molecular weights. Even though smaller molecular sizes were detected for these two proteins, the function of the protein was observed when the expression construct was transfected into cells during the TOPflash experiments described here, and further validation is achieved in Chapter 5.

In summary, in this chapter LGR4 was investigated to see if it participates in Norrin- $\beta$ -Catenin signalling and if the six FEVR-related *LGR4* missense variants affected this signalling, suggesting a disease mechanism in these patients. After the genetic update on the *LGR4* variants (section 4.4.3.2), two of the variants were discarded as Mendelian alleles causing FEVR and only the four remaining variants were assessed in further experiments. The results indicate that LGR4 does potentiate Norrin signalling but the mechanism for this modulation is currently unknown. Three FEVR-related missense mutations located in the ligand-binding domain of LGR4 caused a reduction in TOPflash output compared to the WT LGR4 when cells were

stimulated with Norrin, but these variants showed no effect on RSPO1's ability to activate the TOPflash reporter. A further missense variant located in the transmembrane domain showed no effect on the TOPflash assay when the cells were stimulated with Norrin but it caused an increase in signalling when RSPO1 was used to stimulate the cells. At this point of the study evidence for the transmembrane variant as a possible cause underlying FEVR has not yet been achieved. These results provide compelling evidence for the pathogenic nature of three of the FEVR-associated variants in *LGR4* and provide further evidence that *LGR4* is a new FEVR disease gene.

## 5 Investigating the role of LGR4 in angiogenesis and the interaction of Norrin and LGR4

### 5.1 Background

FEVR is primarily characterised by retinal angiogenesis defects (section 1.4.1). Therefore, if the missense variants identified in *LGR4* are causing FEVR, this implies that LGR4 plays a role in angiogenesis. Similarly, the results in Chapter 3 show a retinal vascular defect in the *lgr4* morpholino knockdown zebrafish models (section 3.2.1.2) and the results in Chapter 4 point towards LGR4 playing a role in the Norrin- $\beta$ -Catenin signalling pathway which controls angiogenesis (section 1.5.4). Therefore in this part of the study, the role of LGR4 in angiogenesis was examined using an *in vitro* organotypic angiogenesis assay.

The TOPflash results presented in Chapter 4 suggest that LGR4 enhances Norrin- $\beta$ -Catenin signalling but the precise mechanism of this enhancement is unknown. Furthermore, the FEVR-related variants located in the binding-domain of LGR4 showed a reduced level of activation of this pathway when cells were activated with Norrin but they did not show any difference in TOPflash activation when the cells were treated with the canonical LGR4 ligand, RSPO1 (section 4.4.3.1 and section 4.4.4). These results suggest that these FEVR-related *LGR4* variants only affect Norrin-mediated signalling. The fact that these variants are located in the binding domain of LGR4 implies that this may be a site of Norrin-LGR4 interaction. In this chapter, cell-based assays, including localisation studies, co-culture assays and alkaline phosphatase (AP) binding assays, were performed to investigate this potential Norrin-LGR4 interaction and any affects the FEVR-related *LGR4* variants may have on it.

## **5.2 *In vitro* organotypic co-culture angiogenesis assay**

To determine if *LGR4* is involved in angiogenesis, an *in vitro* organotypic angiogenesis assay was performed. The organotypic model used was developed by Bishop and colleagues and consists of human vascular endothelial cells (HUVECs) co-cultured on a layer of human dermal fibroblasts (HDFs) (Bishop et al., 1999). The fibroblasts act as a scaffold for the endothelial cells and secrete stromal matrix components. This enables the endothelial cells to form capillary-like tubule structures which closely resemble the capillary bed found *in vivo* (Donovan et al., 2001). Using this model it is possible to investigate the proliferation, migration and differentiation of endothelial cells into tubules. In this experiment, the assay was performed on HUVECs which had been transfected with siRNAs targeting *LGR4* and *FZD4* to knock-down its expression.

### **5.2.1 Validation of *FZD4* and *LGR4* knockdown in siRNA treated HUVECs**

RT-PCR confirmed that both *LGR4* and *FZD4* mRNAs were expressed in HUVECs, along with the Norrin- $\beta$ -Catenin pathway specific transcripts *NDP* and *TSPAN12*, indicating that the proteins are also expressed in these cells (Primer sequences Appendix 8.3) (Section 2.2.4) (Figure 5-1).

WB was first attempted to validate *LGR4* and *FZD4* protein knockdown in the HUVECs treated with siRNAs. The anti-*FZD4* and anti-*LGR4* antibodies were first validated in protein extracts from HUVEC WT cells. A range of different quantities of total protein from HUVEC were analysed by WB (5, 10, 15 and 20 $\mu$ g of HUVEC total protein) (section 2.11.2). The results showed that the anti-*FZD4* antibody was not detecting *FZD4* (59 kDa) (Figure 5-2), confirming the results obtained previously for this antibody (Figure 4-5). The WB result for the anti-*LGR4* antibody showed multiple nonspecific bands but none appeared to correspond to the predicted size of *LGR4* (104 kDa) (Figure 5-2). This *LGR4* antibody had previously specifically detected *LGR4* in a WB of HEK293 cell lysates (Figure 4-6). However, these cells were transfected

with pCMV6\_ *LGR4* expression constructs, indicating that the endogenous levels of *LGR4* present in HUVECs was below the detectable range for this WB assay.

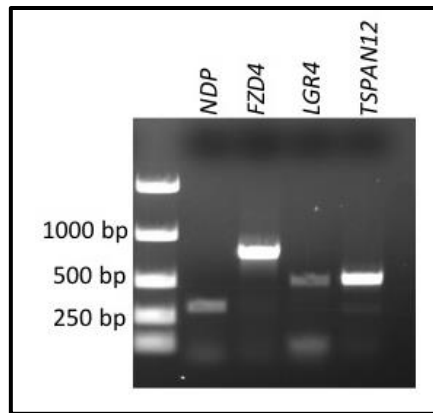


**Figure 5-1: Confirmation of *FZD4* and *LGR4* mRNA expression in WT HUVECs.**

Total RNA from HUVECs was extracted and reverse transcribed into cDNA. RT-PCR for *FZD4*, *LGR4*, *TSPAN12* and *NDP* was performed to assess expression of these genes in the cells. The correct sizes of the PCR products are 299bp for *NDP*, 745bp for *FZD4*, 488bp for *LGR4* and 499bp for *TSPAN12*. The ladder used is EasyLadder I.

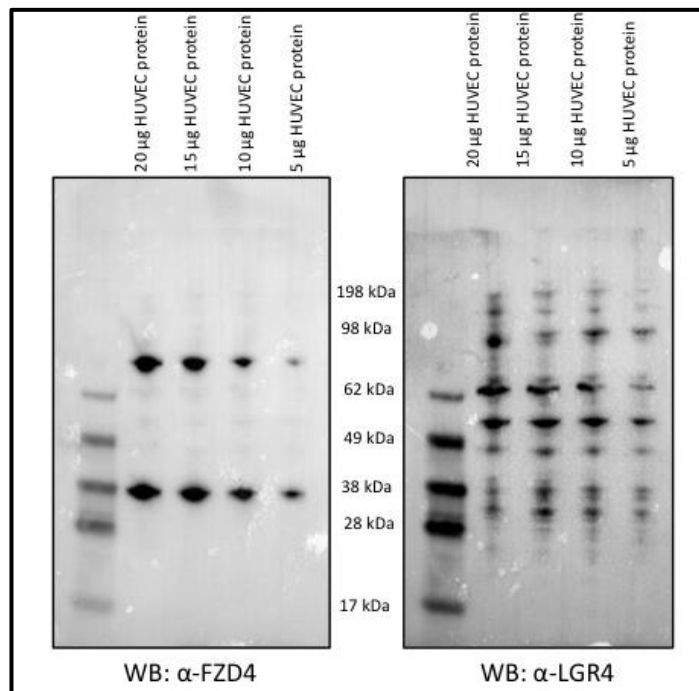


**Figure 5-2: Western blot of HUVEC protein extract incubated with anti-FZD4 or anti-LGR4 antibodies.**

Different concentrations (5, 10, 15 and 20μg) of whole protein extract from WT HUVECs were size fractionated and blotted with anti-FZD4 antibody (left) or with anti-LGR4 antibody (right). Expected size for FZD4 is 59 kDa and for LGR4 is 104 kDa. The ladder used was SeeBlue Plus2 Prestained standard.

In light of these results, validation of *FZD4* and *LGR4* knockdown by siRNA was performed using real-time quantitative PCR (RT- qPCR) (Figure 5-3).

### 5.2.2 Validation of *FZD4* and *LGR4* knockdown using RT- qPCR

RT-qPCR was used to validate the siRNA knockdown of *FZD4* and *LGR4* in HUVECs. Total RNA from the siRNA treated HUVECs (Mock, *NT1* siRNA, *FZD4* siRNA and *LGR4* siRNA) was extracted (section 2.9) 72 hours after siRNA transfection and reverse transcribed into cDNA (section 2.2.4). RNA was extracted from the three replica experiments and RT-qPCR was performed for each experiment individually (total of 3) using TaqMan assays (section 2.10.11). The results were then mixed together and are represented in Figure 5-3.

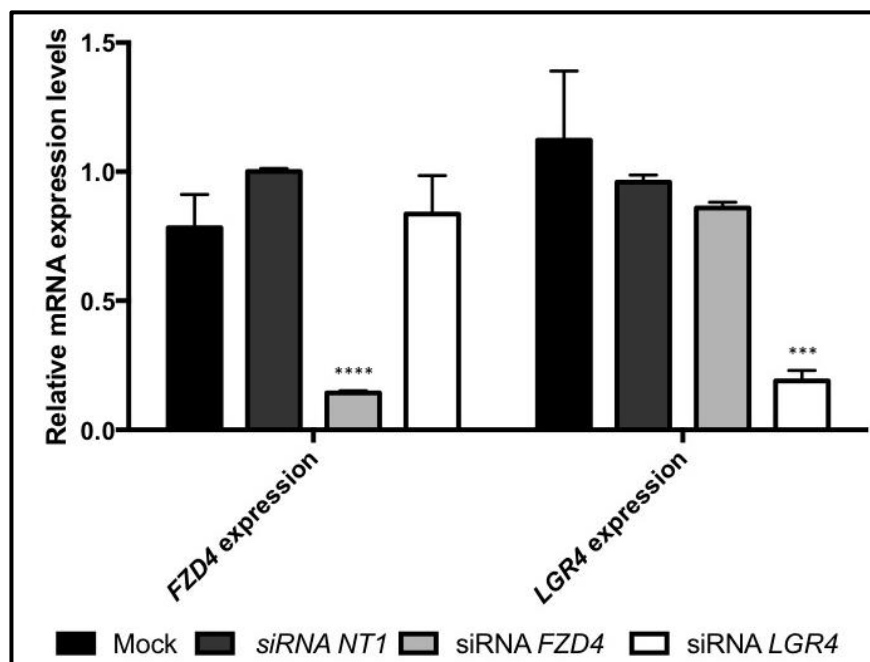


**Figure 5-3: Relative mRNA expression levels of *FZD4* and *LGR4* in siRNA treated HUVECs.**

*FZD4* and *LGR4* expression was evaluated using RT-qPCR in all the siRNA treated HUVECs used in the tubule formation angiogenesis assays. RT-qPCR was performed separately for the three independent replica assays and pooled in the graph. An ANOVA test was performed and statistical values are assigned to changes compared to *NT1* siRNA \*\*\*\* $p < 0.0001$ , \*\*\* $p < 0.001$ . Error bars show standard error of the mean.

The results show that *FZD4* and *LGR4* mRNA expression was decreased by 86% (0.1429/1.001) and 80% (0.1894/0.9595) respectively in the HUVEC samples treated with *FZD4* and *LGR4* siRNAs compared to the *NT1* siRNA treated cells. These mRNA results infer that the *FZD4* and *LGR4* protein levels were also reduced in the siRNA treated HUVECs and suggest that the phenotype observed in the tubule formation assay in Figure 5-4 is due to *FZD4* and *LGR4* being knocked-down in HUVEC

### **5.2.3 HDF-HUVEC co-culture angiogenesis assay**

The co-culture assay was performed as described in section 2.10.10. Briefly, HDFs were cultured to confluence in a 24-well plate for 6 days before HUVECs were seeded on top. Prior to seeding on the HDFs, the HUVECs were seeded in a 6-well plate and siRNA transfection was performed (section 2.10.6.2). Twenty-four hours after siRNA transfection, HUVECs were detached from the 6-well plate and seeded on top of the fibroblasts. The HDF-HUVEC co-culture was kept for 6 days. Tubule formation was visualised using a primary antibody against CD31 (PECAM-1) and an AP-coupled anti-CD31 secondary antibody, followed by immunohistochemical detection using NBT/BCIP. The assay was repeated in three independent experiments, and three replicates per condition were performed in every independent experiment. The conditions tested were: mock transfection control with WT HUVECs (Mock), HUVECs with scrambled non-targeting siRNA pool #1 (*NT1*), HUVECs with *FZD4* siRNA (positive control, (Ye et al., 2009)) and HUVECs with *LGR4* siRNA. Tubule formation was analysed using the ImageJ angiogenesis software and measurements recorded included the number of tubules, total tubule length and number of tubule junctions. The undifferentiated cell clusters were manually detected and the area calculated using ImageJ. The quantification of each characteristic was performed individually. Eight pictures per well were evaluated and the full data set for the three independent experiments was pooled together and analysed using One-way ANOVA Tukey's multiple comparisons test. Significance values were generated compared to the *NT1* siRNA control.

Representative images of the tubule formation assay are shown in Figure 5-4. The results showed that the HUVECs differentiated into tubular structures on the fibroblasts matrix. The mock transfection control and *NT1* siRNA control HUVECs both differentiated into long, branching tubular structures. However, the *FZD4* siRNA and *LGR4* siRNA treated HUVECs both showed a reduction in the formation of the tubular assemblies compared to *NT1* siRNA control. Specifically they showed a reduction in total tubule length, 32% (29852/43636) for *FZD4* and 36% (27713/43636) for *LGR4*; a reduction in the number of tubules, 31% (174.8/255.1) for *FZD4* and 42% (147.8/255.1) for *LGR4*; and a reduction in the number of tubule junctions, 39% (122.6/201.8) for *FZD4* and 46% (108.6/201.8) for *LGR4* (Figure 5-4).

Knockdown of *FZD4* in HUVECs also resulted in clusters of undifferentiated endothelial cells (Friis et al., 2005). Similar but less pronounced clusters were also observed for the *LGR4* siRNA treated HUVECs. The automated ImageJ angiogenesis software was not able to detect these clusters so the outline of the clusters was manually added to the images and the area calculated with ImageJ. This result showed an increase in total cluster area of 1514% (10.11mm<sup>2</sup>/ 0.6263mm<sup>2</sup>) for *FZD4* and an increase of 670% (4.826mm<sup>2</sup>/ 0.6263mm<sup>2</sup>) for *LGR4*. These results suggest that knockdown of *LGR4* (or *FZD4*) results in a decrease in endothelial differentiation and tubule formation.

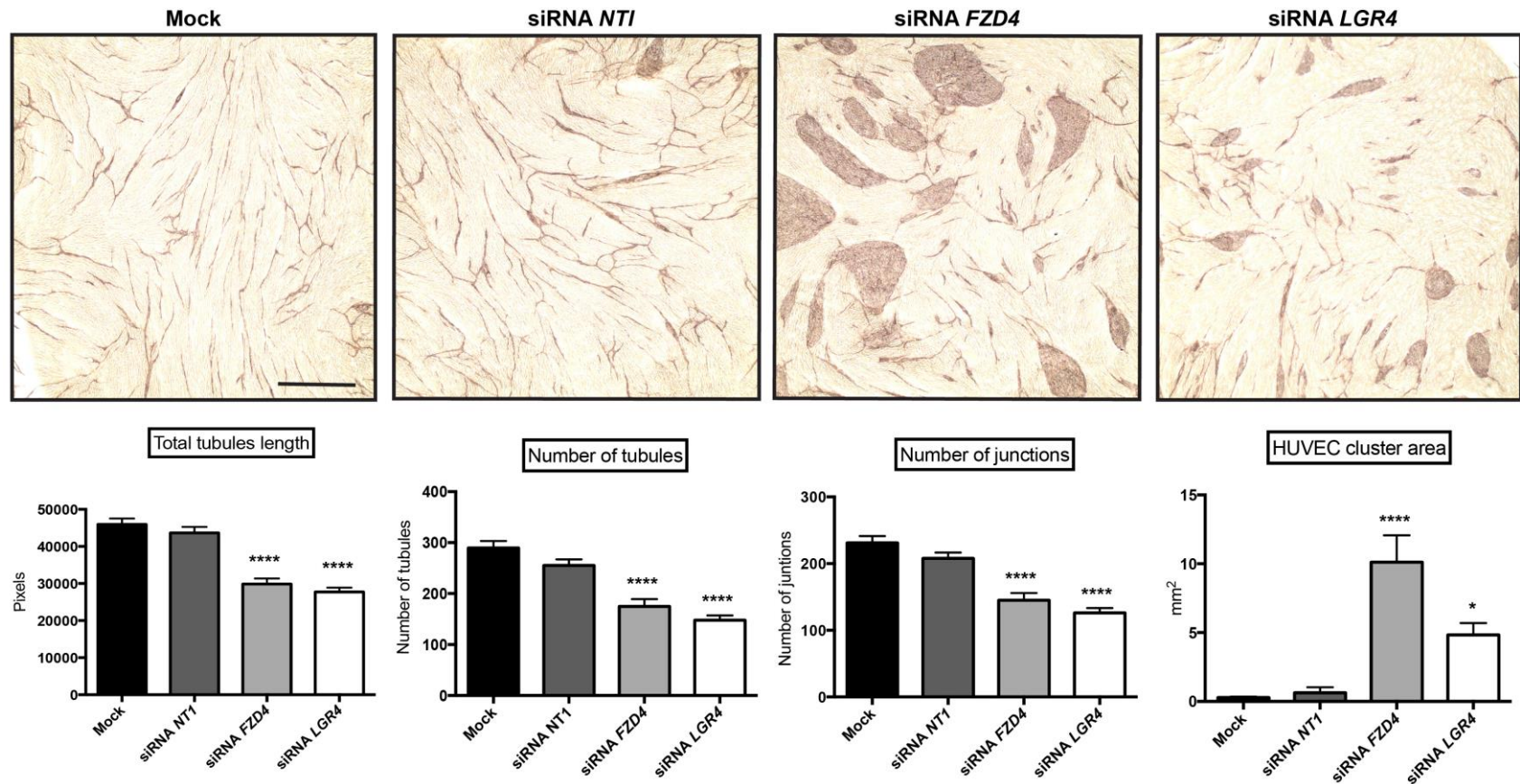


**Figure 5-4: HDF and HUVEC co-culture tubule formation assay. Quantification of tubule length, number of tubules, number of tubule junctions and area of undifferentiated HUVEC clusters.**

HDF-HUVEC co-culture was kept for 6 days. The degree of angiogenesis was determined by assessing the extent of tubule formation after 6 days: quantifying the total tubule length, the number of tubules, the number of tubule junctions and the area of undifferentiated HUVEC clusters. The conditions analysed were mock transfection, corresponding to WT HUVECs, *NT1* (scramble siRNA), *FZD4* siRNA and *LGR4* siRNA transfected HUVECs. \*\*\*\* $p < 0.0001$ , \* $p < 0.05$  using two-way ANOVA followed by Tukey's multiple comparison test. The significance shown is compared against *NT1* siRNA. Scale bar = 1 mm.

### **5.3 Investigating Norrin binding to WT and variant LGR4**

The aim of the following experiments was to investigate the mechanism by which LGR4 enhances the Norrin- $\beta$ -Catenin pathway, and how the FEVR *LGR4* variants disrupt this. There are a number of different possible mechanisms, but the location of three of the four FEVR variants in the extracellular binding domain of LGR4 raises the possibility that Norrin binds LGR4 and that this interaction is abolished or diminished by these three FEVR variants. Alternatively, these *LGR4* variants might result in aberrant binding of Norrin to LGR4, which could result in Norrin being sequestered away and thus being unavailable to bind to the FZD4, LRP5 and TSPAN12 receptor complex and activate Norrin- $\beta$ -Catenin signalling.

#### **5.3.1 Investigating Norrin binding to WT and variant LGR4 in co-culture assays**

In the following experiment, these last two hypotheses were investigated by performing a TOPflash assay in a co-culture of HEK293 and STF cells (HEK293 cells stably transfected with TOPflash) (Section 2.10.9.3). Briefly, HEK293 cells were transfected with Norrin only or with Norrin and WT or variant *LGR4*. Simultaneously, STF cells were transfected with *LGR4*, *LRP5*, *TSPAN12* and *FZD4* but no Norrin. All the expression constructs were those used in the TOPflash assays in chapter 4 (section 4.4.2). Twenty-four hours after transfection, the cells were combined together and plated in a 1:1 ratio and 24 hours later luciferase values were measured (section 2.10.9.3) (Figure 5-5).

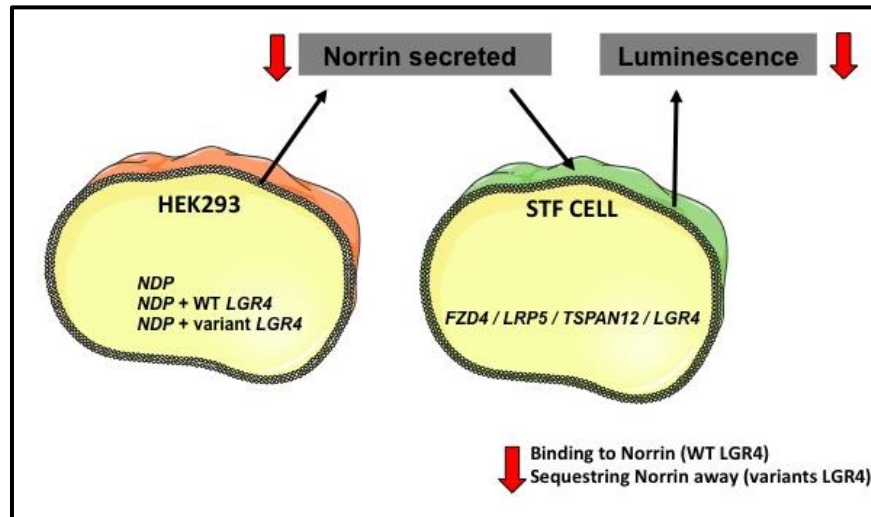


**Figure 5-5: Schematic representation of the co-culture experiment.**

HEK293 cells were transfected with *NDP* (Norrin) or with *NDP* and WT or variant *LGR4*. STF cells were transfected with *FZD4*, *LRP5*, *TSPAN12* and *LGR4*. Twenty-four hours after transfection, cells were mixed together (1:1) and incubated for a further 24 hours. Luminescence values were measured 48 hours after transfection. If WT or variant *LGR4* receptors are binding to Norrin on the HEK293 cell surface, a decrease in luminescence will be recorded in the STF cells due to less Norrin being available to bind to the *FZD4*/*LRP5*/*TSPAN12*/*LGR4* receptor complex (red arrow).

Norrin has been shown to have paracrine and autocrine activity (Xu et al., 2004). Therefore, Norrin secreted from HEK293 cells can bind to the receptor complex on the neighbouring STF cells and trigger pathway activation which will result in an increase in TOPflash luminescence. However, if WT or variant *LGR4* is co-transfected with Norrin in the HEK293 cells, these proteins can also bind to the available Norrin on the surface of the HEK293 cells and sequester it away from the neighbouring STF cells causing a reduction in TOPflash signalling and luminescence.

The four *LGR4* variants and WT *LGR4* were independently assessed using this co-culture assay. The results show that the highest activation of the TOPflash reporter in the STF cells is found when only Norrin was transfected into the neighbouring HEK293 cells (Figure 5-6). This result confirms the paracrine activity of Norrin described by Xu et al., (2004).

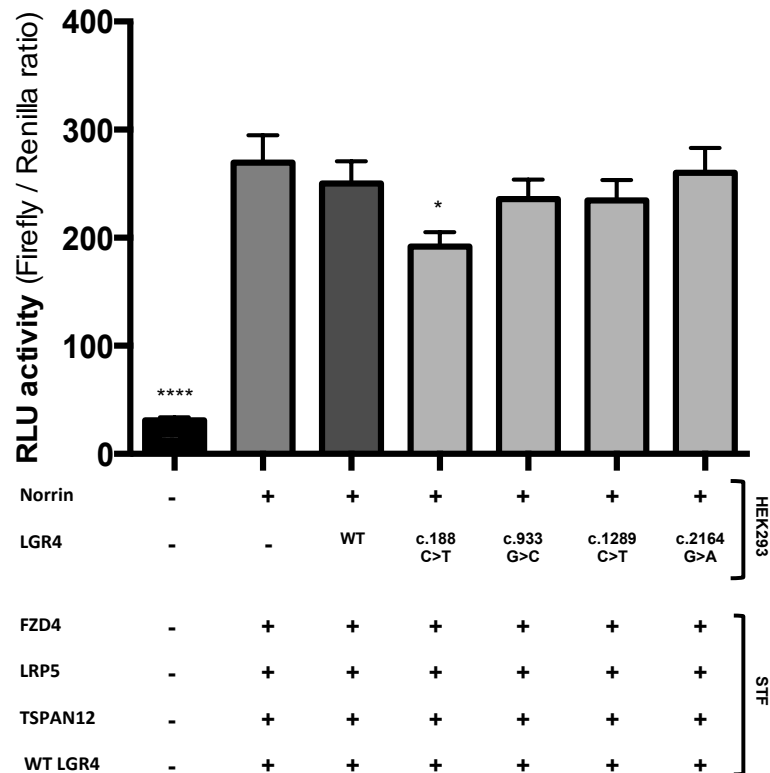


**Figure 5-6: TOPflash luciferase assay in HEK293-STF co-culture.**

STF and HEK293 cells were transfected separately with the indicated plasmids. A 1:1 mixture of the cells was plated together 24 hours after transfection. Twenty-four hours later RLU activity was measured. Values are given as relative luciferase units (RLU) and are expressed as *Firefly/Renilla* ratio. The nucleotide change for the *LGR4* missense variants is indicated for each bar. Only significant changes are shown. \*:  $p \leq 0.05$ ; \*\*\*\*:  $p \leq 0.0001$ . Error bars show standard error of the mean. An ANOVA test was performed comparing HEK293 cells transfected with Norrin only (column 2) to the rest of the conditions tested. The results were made in triplicate with 4 biological replicates per condition.

When WT *LGR4* was co-transfected with Norrin into the HEK293 cells, there was a small reduction in TOPflash activation but this was not statistically significant. The three FEVR-related *LGR4* variants located in the binding domain showed a further small decrease in signalling but only with one of these variants the reduction was statistically significant, the EVR3 variant (c.118C>T p.(R40W)). The remaining *LGR4* variant, present in the transmembrane domain (c.2164G>A p.(A722T)), showed the same level of TOPflash signalling as WT *LGR4*. This result is consistent with the EVR3 variant, and to a lesser extent the c.933G>C

p.(Q311H) and c.1289C>T p.(T430M) variants, aberrantly binding Norrin and preventing it from activating the TOPflash reporter in the neighbouring STF cells by binding to FZD4, LRP5 and TSPAN12.

### **5.3.2 Investigating Norrin binding to WT and variant LGR4 using an AP cell surface binding assay**

Further investigation of the interaction between WT and variant LGR4 and Norrin was performed using AP staining based assay. Binding assays using AP-tagged ligands have been widely used to characterise receptor ligand binding. Examples include, LGR4 binding to RSPOs and syndecans (Glinka et al., 2011; Ohkawara et al., 2011) and FZD4 binding to Norrin (Xu et al., 2004; Qin et al., 2008; Smallwood et al. 2007). In this experiment the same method was used as in Xu et al 2004 (Hsieh et al., 1999). Briefly, AP-3myc-Norrin conditioned medium was prepared (section 2.10.5). Experimental and biological repetitions for all the binding assays were performed with the same batch of Norrin conditioned medium for consistency. Cos7 cells were transfected with the indicated plasmids for 48 hours and incubated with Norrin conditioned medium for 90 minutes at 4°C. Crosslinker solution was added for 30 minutes at room temperature. After washing, cells were stained using NBT/BCIP (section 2.10.12.1).

The *LGR4* expression constructs used to perform this experiment were the WT and variant pCMV6\_*LGR4* plasmids used and validated in Chapter 4. Binding of Norrin to FZD4 (pDEST40\_*FZD4*) was used as a positive control (Xu et al., 2004). Binding assays using pDEST40\_*LRP5* and pDEST40\_*TSPAN12* were also performed to allow comparison between LGR4 and other co-receptors of the Norrin receptor complex. pDEST40 empty vector was used as a negative control. All the assays were performed in three independent biological replicates and a minimum of two technical replicates were performed for each condition.

Representative images of the results are shown in Figure 5-7 and Figure 5-8. Norrin binding to the cell surface is indicated by a brown/purple stain. The results showed intense AP staining at the surface of cells transfected with the positive control *FZD4*, confirming the reliability of the experimental procedure and replicating the results previously reported by Xu et al., 2004. Similarly, the empty vector negative control (pDEST40) did not show AP staining.

The FEVR-related variants present in the LGR4 binding domain (c.118C>T p.(R40W), c.933G>C p.(Q311H) and c.1289C>T p.(T430M)) all showed marginally higher levels of AP-Norrin staining compared to WT LGR4, except for the EVR3 variant (c.118C>T p.(R40W)) which showed intense staining similar to that seen for FZD4 (Figure 5-7). The LGR4 variant present in the transmembrane domain (c.2164G>A p.(A722T)) had a similar level of intense AP-Norrin staining as WT LGR4.

Comparative levels of AP-Norrin staining were obtained for cells transfected with WT LGR4, LRP5 or TSPAN12. This staining was weak but was consistently stronger than the empty vector negative control (Figure 5-8). These results suggest that WT LGR4 does not bind Norrin with the same strength as its main receptor FZD4, but it does show some level of interaction and this interaction appears to be increased by the EVR3 variant (c.118C>T p.(R40W)) and potentially the other two variants in the binding domain.

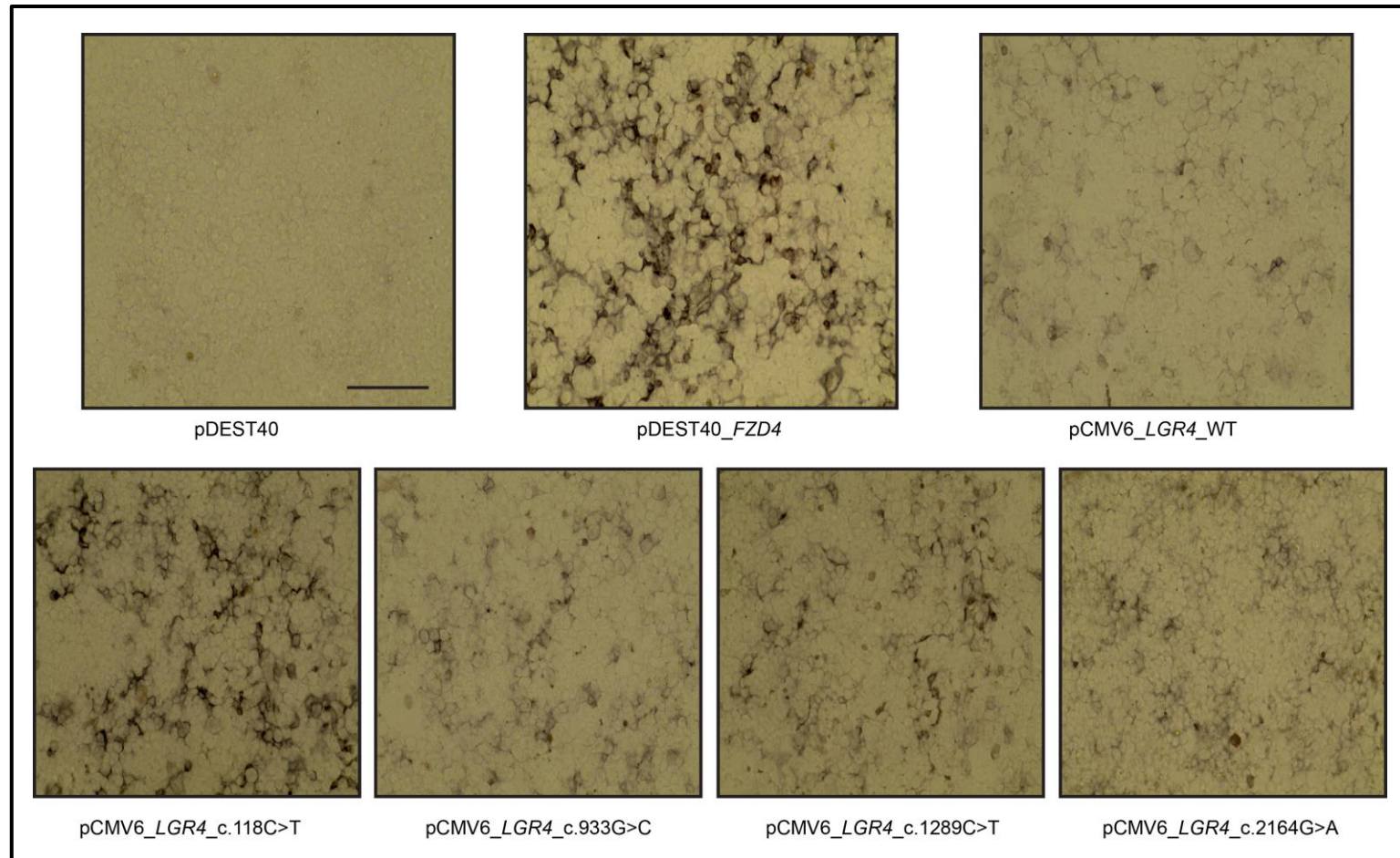


**Figure 5-7: Cell surface binding assay of WT and variant LGR4 with AP-Norrin.**

Cos7 cells were transfected with the indicated plasmids and incubated with AP-3myc-Norrin conditioned medium containing Norrin protein fused to alkaline phosphatase. pDEST40 empty vector was used as a negative control and pDEST40\_FZD4 vector was used as a positive control. pCMV6\_LGR4 expression constructs were used to determine Norrin binding to WT or variant LGR4. AP-Norrin staining at the cell surface of the transfected cells results in black/purple staining. Scale bar = 250 $\mu$ m.

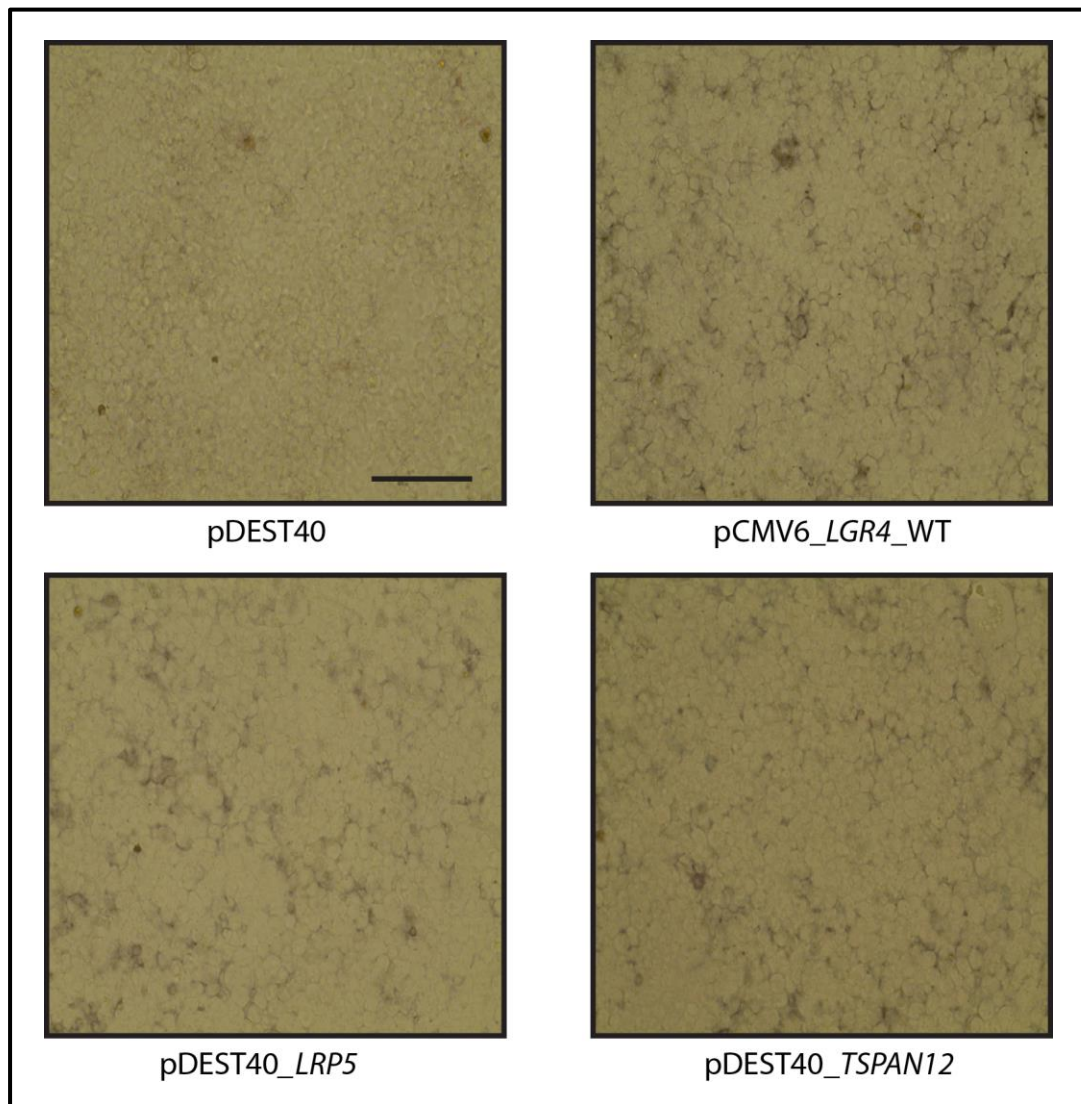


**Figure 5-8: Cell surface binding assay comparing the binding of AP-Norrin to LGR4, LRP5 and TSPAN12.**

Cos7 cells were transfected with the indicated plasmids and incubated with AP-3myc-Norrin conditioned medium containing Norrin fused to alkaline phosphatase. pDEST40 empty vector was used as a negative control. pCMV6\_LGR4, pDEST40\_LRP5 and pDEST40\_TSPAN12 were used to determine Norrin binding to each receptor. Scale bar = 250  $\mu$ m.

To quantitate the level of binding observed between Norrin and LGR4, the same AP binding assay was performed, but this time the level of cellular Norrin (bound to the cell surface or internalised) was measured using an AP chemiluminescent reporter assay. Cos7 cells were transfected with the indicated plasmids for 48 hours. Cells were then incubated with different

dilutions of Norrin conditioned medium (100%, 80%, 60%, 40%, 20% and 0%) for 90 minutes at 4°C. The cells were then lysed and the cellular AP was measured using the Phospha Light System (Applied Biosystems) (section 2.10.12.2). All experiments were performed in duplicate and replicated at least 4 times unless stated in the text. Data were analysed using two-way ANOVA followed by Tukey's multiple comparison test using GraphPad 6 Prism software.

The results of the assay are presented in Figure 5-9. The results show that the assay worked with the positive control, FZD4, showing much higher levels of cellular Norrin compared to the empty vector. The level of cellular Norrin also increased incrementally with increasing concentrations of AP-3myc-Norrin conditioned media, although saturation was not observed. The results also replicated the trends observed in the cell surface AP staining assay (Figure 5-7 and Figure 5-8). The EVR3 variant form of LGR4, c.118C>T p.(R40W), clearly shows a highly significant increase in the level of cellular Norrin compared to WT LGR4. Indeed, the levels are almost as high as the FZD4 levels. The other FEVR variants located in the binding domain of LGR4, c.933G>C p.(Q311H) and c.1289C>T p.(T430M), showed weaker but increased levels of Norrin at higher concentrations of AP-3myc-Norrin condition medium but none of these were statistically significant. The FEVR variant in the transmembrane domain of LGR4, c.2164G>A p.(A722T), showed no difference to WT LGR4.

The results also confirmed a significant increase in cellular Norrin in cells transfected with LRP5 and TSPAN12 compared to empty vector. However, the increased level of Norrin in cells transfected with WT LGR4 did not show any significance.

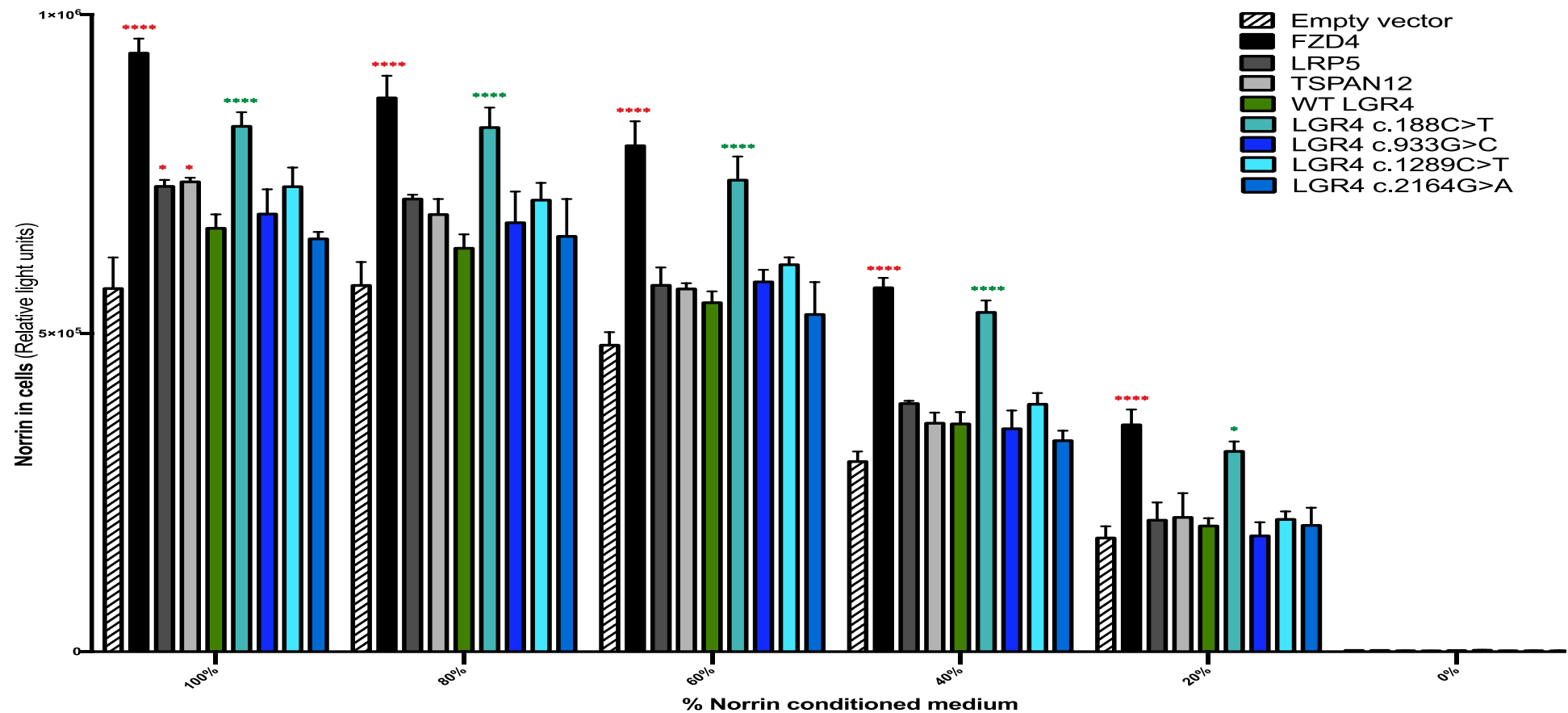


**Figure 5-9: Quantification of AP-Norrin binding assay.**

Cos7 cells were transfected with the indicated plasmids and incubated with different dilutions of AP-3myc-Norrin conditioned medium. Cellular associated AP-Norrin was measured using the Phospha Light System. The graph shows the results for 100%, 80%, 60%, 40%, 20% and 0% dilutions of AP-3myc-Norrin conditioned media for all the receptors tested. Red stars show significance compared to the empty vector (hatched columns) and green stars show significance compared to WT LGR4 (green column). \*: p value  $\leq 0.5$ ; \*\*\*\*: p value  $\leq 0.0001$ . Error bars show standard error of the mean. An ANOVA Tukey's multiple comparison test was performed. The assays were made in duplicate with at least 4 biological replicates per condition, except for LRP5 and TSPAN12 in where two biological replicates were performed.

### 5.3.3 Replicating the study by Deng et al 2013.

The results obtained in this study did not replicate the results of the binding assays reported by Deng and colleagues which showed that Norrin bound to LGR4 with similar affinities to the Norrin-FZD4 interaction (Deng et al., 2013). A significant difference between the two experimental designs was the temperature; the current study performed the binding assays at 4°C to avoid internalization and recycling of the receptor complex (Blitzer and Nusse, 2006), whereas the Deng study performed the binding assay at room temperature. Therefore the assay was replicated in its entirety to the experiment of the Deng study. All experimental procedures were kept the same but the temperature was changed to room temperature. FZD4, WT LGR4 and the c.118C>T p.(R40W) LGR4 variant (EVR3) were investigated (Figure 5-10).

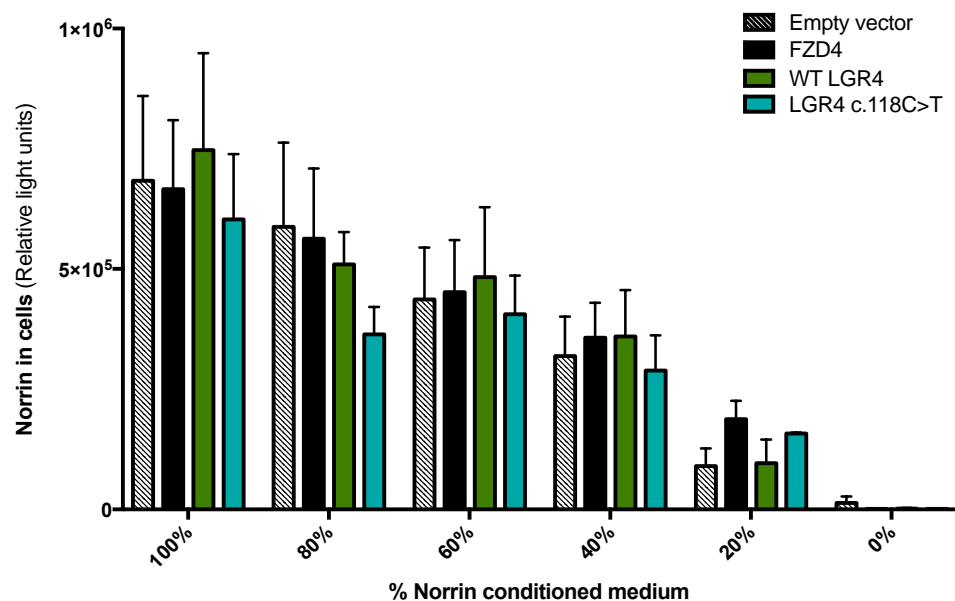


**Figure 5-10: AP-Norrin binding assay performed at room temperature.**

Cos7 cells were transfected with the indicated plasmids and incubated with different dilutions of AP-3myc-Norrin conditioned medium. Cellular associated AP-Norrin was measured using the Phospha Light System. The graph shows 100%, 80%, 60%, 40%, 20% and 0% of Norrin conditioned medium for all the conditions tested. Error bars show standard error of the mean. An ANOVA Tukey's multiple comparison test was performed. The assay was performed in duplicate with two biological replicates per condition.

The results differed drastically from those previously obtained by performing the assay at 4°C (Figure 5-9). In the room temperature experiment there was no difference found between the levels of cellular Norrin measured in the negative control (empty vector) and the positive control (FZD4) for any of the Norrin medium dilutions tested. This indicates that the experimental procedure is not working.

#### **5.4 Investigating any effects on LGR4 localisation caused by the FEVR-related *LGR4* variants**

In parallel to the above experiments, a comparison between the location of WT and variant LGR4 was undertaken in cells to evaluate if the FEVR-associated missense variants caused mislocalisation of the protein or a reduction in the amount of protein being transported to the cell membrane. Expression constructs for WT and variant LGR4 were made using Gateway technology (section 2.6.4) as described in Chapter 3. The original destination expression vector used was pDEST47, which creates a fusion protein with a C-terminal GFP tag. However, fluorescence was not obtained for any of the WT or variant LGR4 constructs made using this vector indicating that the structure of the fusion protein hinders the GFP activity (data not shown) (Stepanenko et al., 2008). Therefore the backbone of the LGR4 constructs was switched to a destination expression vector with a C-terminal eYFP (yellow fluorescence protein) tag, pDEST504 (Roepman et al., 2005).

HEK293 cells growing on coverslips were transiently transfected with either the WT pDEST504\_ *LGR4* construct or one of the variant LGR4 expression constructs (section 2.10.6.1). Forty-eight hours after transfection, the cells were fixed and imaged using a Nikon A1R laser-scanning confocal microscope (section 2.12.2). Over one hundred cells were analysed from duplicate experiments for each construct. For all five constructs, YFP signals were observed, confirming that the LGR4 fusion proteins were correctly being translated and expressed in the HEK293 cells (Figure 5-11).

LGR4 is a membrane receptor and WT LGR4 and all four variant LGR4 expression constructs were located at the cell membrane as expected (Figure 5-11). Unfortunately, all the constructs also formed large clusters in the cytoplasm of the cells. For some of the transfected cells, the signal from the fusion protein located in the cytoplasm was so strong that it often concealed the presumptive LGR4 localisation at the cell membrane. Nevertheless, no differences were found between the localisation of WT or variant LGR4 fusion proteins in HEK293 cells, indicating that the FEVR variants do not cause mislocalisation of LGR4. Unfortunately, the expression of the aggregates of fusion protein prevented any quantification of the amounts of fusion protein present at the cell membrane so no direct comparison between WT and FEVR-related variant LGR4 localisation was possible.

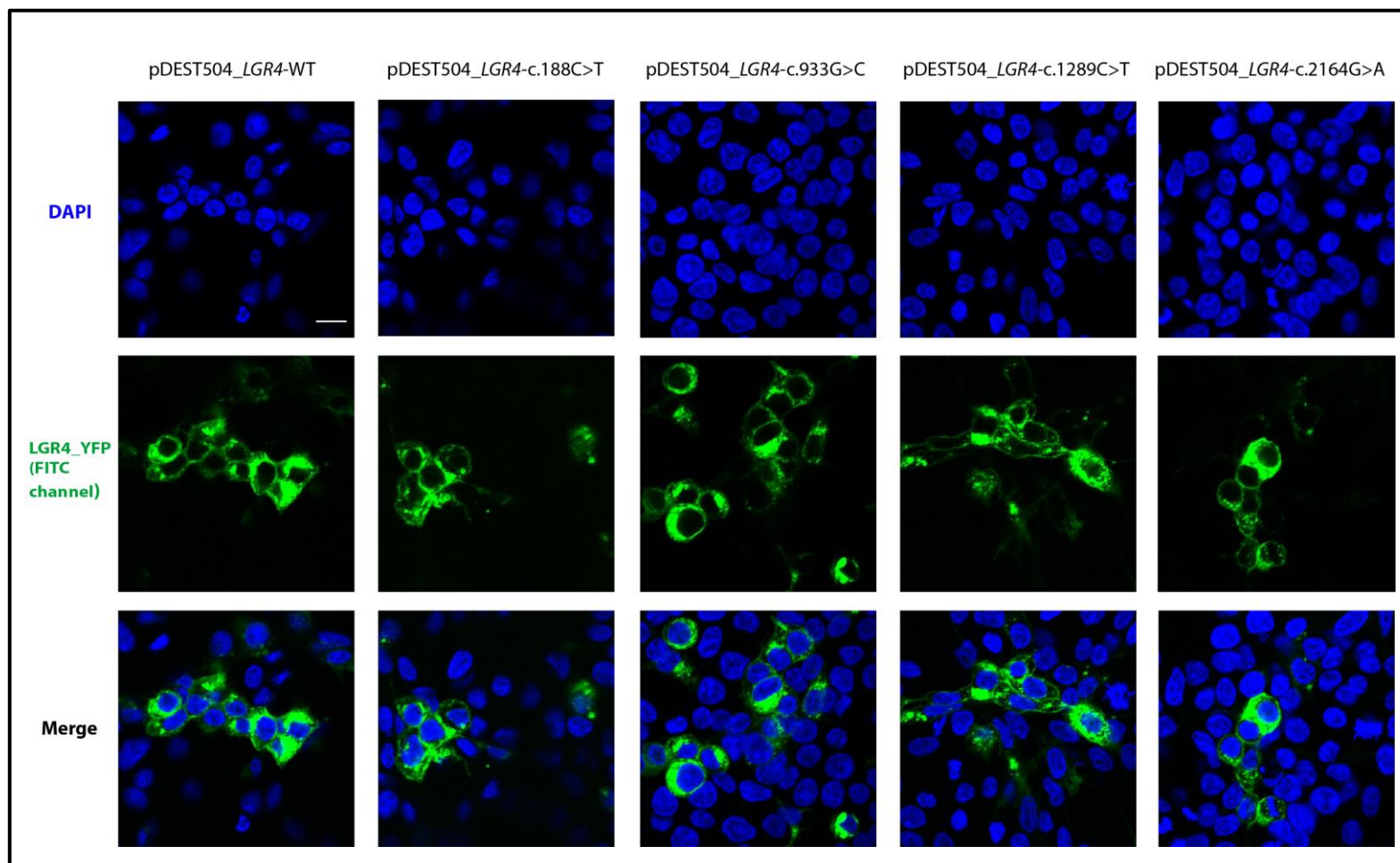


**Figure 5-11: Confocal images of HEK293 cells transfected with pDEST504\_LGR4 expression constructs showing LGR4 localisation.**

Cells transfected with pDEST504\_LGR4 expression constructs were fixed 48 hours after transfection. Images were taken using Nikon A1R confocal microscope. Nuclei were stained with DAPI. LGR4-YFP expression and localisation is shown in green using the FITC channel. Scale bar = 20  $\mu$ m.

Alongside this experiment, live-cell imaging of the LGR4-YFP fusion protein was also undertaken to evaluate any localisation differences between the WT and FEVR-related variant LGR4 fusion proteins. Time-lapse imaging was performed using a Nikon BioStation IM live cell screening system (section 2.10.13). The incubation chamber of the Biostation IM fits 2.5 cm imaging plates separated into 4 quadrants (HiQ plates). Therefore, the first run evaluated HEK293 cells transfected with WT pDEST504\_ *LGR4*. Imaging started 24 hours after transfection and images were captured every 30 seconds for up to 240 minutes.

The results also showed the presence of aggresomes, similar to the data obtained from the previous experiment. Figure 5-12 shows stills taken from the time-lapse movie at time points spanning 0-150 minutes. The full movie can be viewed on YouTube or in the attached data file ([https://www.youtube.com/watch?v=33CrZYA\\_-iU&feature=youtu.be](https://www.youtube.com/watch?v=33CrZYA_-iU&feature=youtu.be)). At zero minutes, the LGR4-YFP fusion protein is being expressed in the cytoplasm of the cell and the start of LGR4-YFP protein aggregates formation can be observed. With increasing time, the expression of LGR4-YFP intensifies and the number of intracellular aggregates increases. Membrane detection was not visible in this experiment. This may be due to the reduced sensitivity of the BioStation compared to the confocal microscope compounded by the intensity of the aggresome signal limiting detection of the fainter membrane staining. Given this result, this experiment was abandoned and the FEVR-related *LGR4* variants were not assessed using this method.

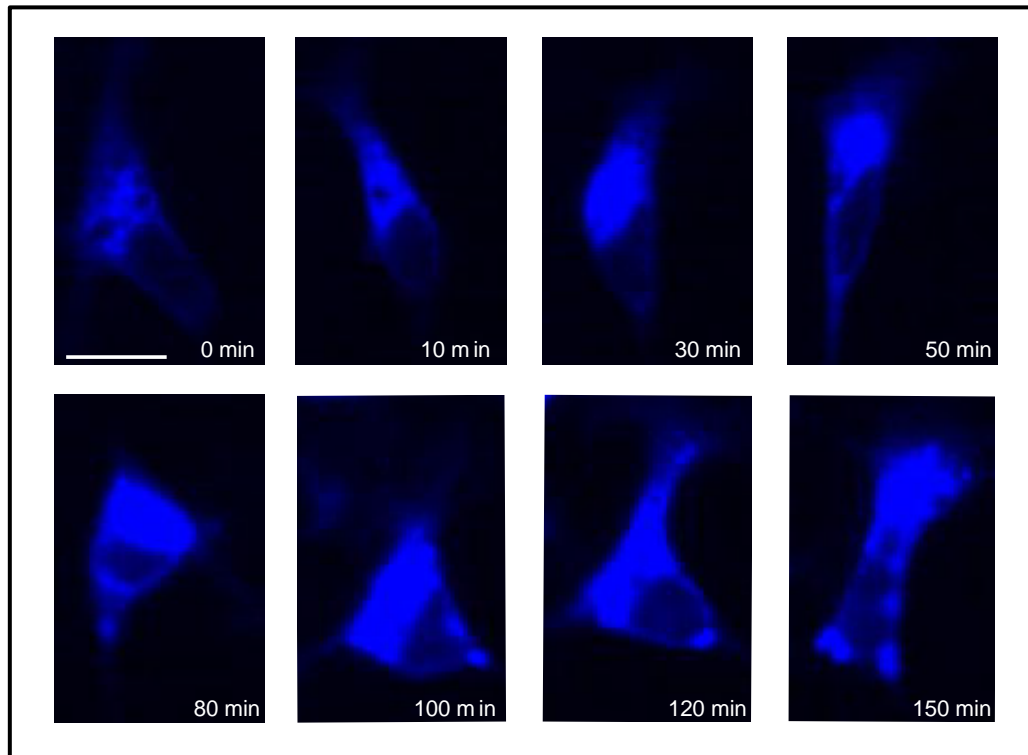


**Figure 5-12: Live-cell imaging of HEK293 cells transfected with WT pDEST504\_LGR4.**

Movie stills from live cell imaging of HEK293 cells 24 hours after transfection with pDEST504\_LGR4-WT. The images show aggresome formation between 0 and 150 minutes. The full movie is available on the accompanying data file or at [https://www.youtube.com/watch?v=33CrZYA\\_-iU&feature=youtu.be](https://www.youtube.com/watch?v=33CrZYA_-iU&feature=youtu.be)). Scale bar = 5  $\mu$ m.

## 5.5 LGR4 and Norrin co-localisation assay

Co-localisation studies have been widely used in research in order to determine if two molecules could belong to the same structural complex by comparing the subcellular distribution of two fluorescently labelled molecules (Dunn et al., 2011). If both molecules reside at the same physical location they will co-localise together and there will be a detectable overlap in their fluorescent signals (Linse and James, 2007). In this experiment this technique was used to determine if LGR4/variant-LGR4 and Norrin co-localise at the cell membrane to provide evidence that they are part of the same protein complex.

For this experiment, conditioned media obtained from cells transfected with AP-3myc-Norrin was used as the source of Norrin (AP-3myc-Norrin

conditioned medium), as recombinant human Norrin had not worked previously in the TOPflash assay (section 4.3). To validate the use of AP-3myc-Norrin conditioned media, the co-localisation experiment was performed with FZD4 first as this is the established receptor for Norrin (Xu et al., 2004). The pDEST40\_ *FZD4* expression construct created and validated in Chapter 4 was used. This construct creates an FZD4 fusion protein with a C-terminal His and V5 tag (Appendix 8.8).

HEK293 cells were grown to 70% confluence on coverslips and transfected with pDEST40\_ *FZD4*. Forty-eight hours after transfection, cells were incubated with AP-3myc-Norrin conditioned medium for one hour at 37°C (section 2.11.3). Following this, cells were fixed, permeabilised and immunostained with mouse anti-His and goat anti-Norrin primary antibodies. Secondary antibodies used were donkey anti-mouse Alexa Fluor 488 (green for FZD4 staining) and donkey anti-goat Alexa Fluor 568 (red for Norrin staining). Two controls were used for the co-localisation experiment. For the first control, the primary antibody was omitted but the secondary antibody incubation was performed as normal (secondary only control). For the second control, the cells were transfected with empty vector prior to immunostaining (empty vector control).

The results confirmed that the AP-3myc-Norrin conditioned media was suitable for this assay (Figure 5-13). As expected, FZD4 (green) and Norrin (red) localised predominantly at the cell membrane. Norrin only co-localised with FZD4 at the plasma membrane of cells overexpressing FZD4 (yellow). The lack of staining in cells transfected with pDEST40\_ *FZD4* and incubated with Ap-3myc-Norrin conditioned medium, but immunostained without the primary antibodies, confirmed the specificity of the antibodies used for this experiment. Similarly, the absence of Norrin co-localisation with pDEST40 empty vector, demonstrated that Norrin and FZD4 co-localisation at the cell membrane is specific.

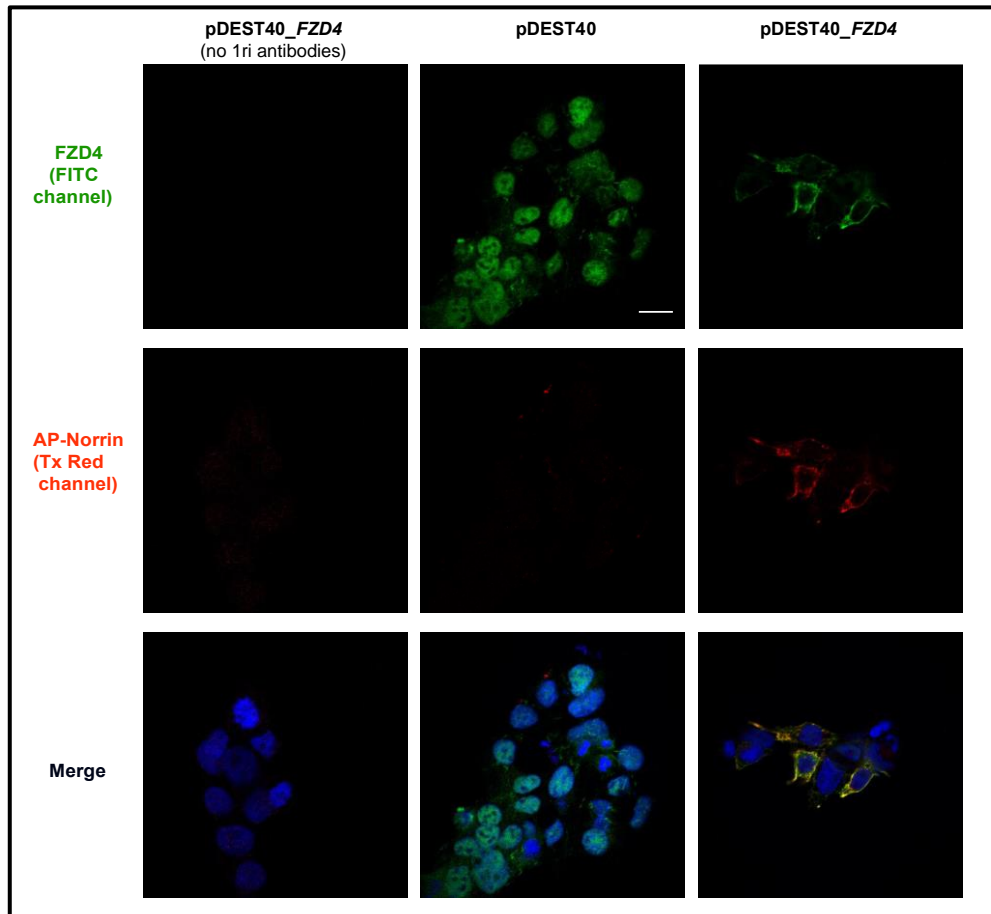


**Figure 5-13: Co-localisation of FZD4 and Norrin in HEK293 cells by immunofluorescence microscopy.**

HEK293 cells were transfected with either pDEST40 empty plasmid or pDEST40\_FZD4. 48 hours after transfection cells were incubated with AP-3myc-Norrin conditioned medium (AP-Norrin) for 1 hour at 37°C, fixed and immunostained. Images show FZD4 in green (FITC channel) and Norrin in red (Tx Red channel). Nuclei are stained with DAPI. Co-localisation of Norrin with FZD4 is found at the cell membrane of the cells (yellow). Nuclei are blue (DAPI). Absence of co-localisation is found in the two controls used for this experiment. Scale bar = 20 µm.

Next the experiment was repeated for WT and variant LGR4 fusion proteins. HEK293 cells were grown to confluence on coverslips and transfected with the WT or variant pDEST504\_LGR4 (YFP-tagged) expression constructs. Forty-eight hours after transfection, cells were incubated with Norrin conditioned medium for one hour at 37°C (section 2.11.3). Following this, cells were fixed, permeabilised and immunostained for Norrin using mouse anti-Myc primary antibody followed by goat anti-mouse Alexa Fluor 568 secondary antibody. For each condition, a minimum of 100 positive cells

were analysed over three replicate experiments. The same two controls were used as performed for the FZD4 co-localisation experiment: the secondary only control and the empty vector control (Figure 5-14).

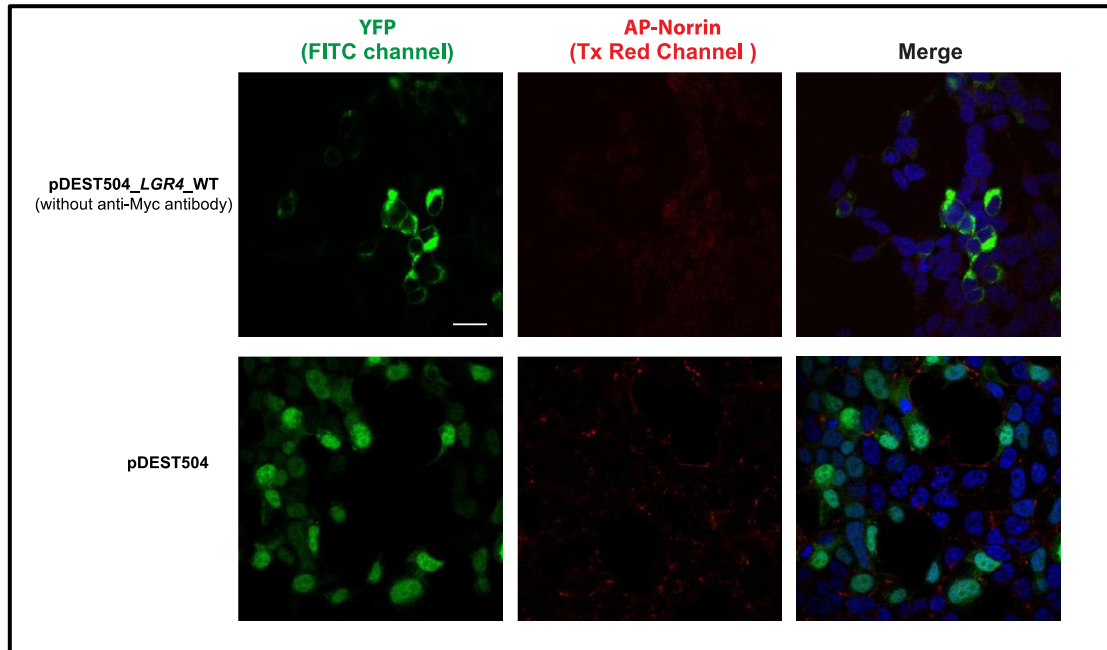


**Figure 5-14: Confocal images of the two controls used for the co-localisation of LGR4 and Norrin experiment.**

The first control experiment (secondary only) was cells transfected with pDEST504\_LGR4-WT and incubated with AP-3myc-Norrin conditioned medium (AP-Norrin). These cells were not incubated with primary anti-Myc antibody prior to incubating with the secondary antibody Alexa Fluor 568 (upper panel). The second control used were cells transfected with the empty vector pDEST504 and primary and secondary antibody incubations were performed (lower panel). Images were taken using the FITC channel for YFP detection and the Tx Red channel for Alexa Fluor 568 detection. Nuclei are blue (DAPI). Scale bar = 20  $\mu$ m.

Representative images of AP-3myc-Norrin and LGR4 co-localisation in HEK293 cells are shown in Figure 5-15. LGR4 localised at the cell membrane (green) of transfected cells, but strong LGR4 localisation was also found in the cytoplasm of the positive transfected cells, where it seemed to form LGR4 aggregates. Comparable cellular localisations were observed for both WT and variant LGR4 fusion proteins confirming the results obtained previously (Figure 5-11).

Norrin was localised at the cell membrane of cells expressing LGR4-YFP (red) (Figure 5-15) but was not observed in the control cells expressing empty YFP vector (Figure 5-15). Co-localisation of WT and variant LGR4 fusion proteins with Norrin was predominantly found at the cell membrane (yellow), but for some of the cells intracellular co-localisation was also observed. As previously mentioned, the strong fluorescent signal from the cytoplasmic aggregates of LGR4-YFP often impeded the examination of membrane localisation. Therefore the co-localisation of LGR4 with Norrin at the cell membrane was highly dependant on whether LGR4 was localised at the cell membrane or within cytoplasmic aggregates. For this reason, quantification of Norrin and LGR4 co-localisation at the cell membrane could not be performed using automated software such as coloc on ImageJ.

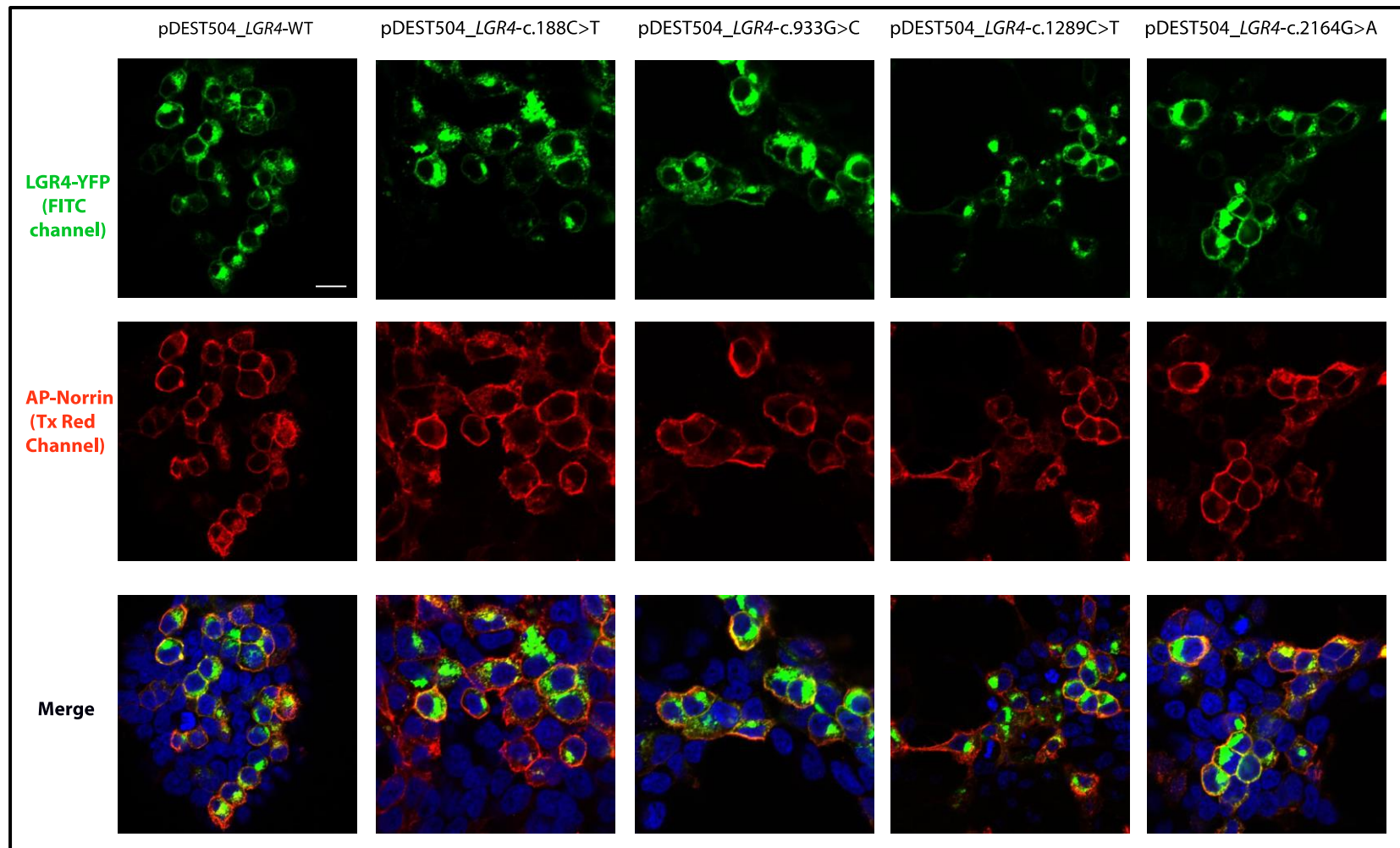


**Figure 5-15: Co-localisation of LGR4-YFP and AP-3myc-Norrin in HEK293 cells analysed by confocal microscopy.**

HEK293 cells were transfected with WT or variant pDEST504\_LGR4. 48 hours after transfection AP-3myc-Norrin conditioned medium (AP-Norrin) was added onto the cells for 1 hour at 37°C. Images show LGR4 in green (FITC channel) and Norrin in red (Tx Red channel). Nuclei are blue (DAPI). Scale bar = 20 µm.

## 5.6 Discussion

The data presented in chapters 3 and 4 on the function of LGR4, and the effects of the FEVR-related variants on this function, provide compelling evidence that *LGR4* is a new FEVR disease gene. In this chapter, further evidence was gathered to support this hypothesis and to provide preliminary data on the disease mechanism. A key role for LGR4 in angiogenesis was demonstrated using siRNA-mediated knockdown of *LGR4* in an *in vitro* organotypic endothelial tube formation assay. Furthermore, a variety of different methods were used to investigate the binding and co-localisation of LGR4 and Norrin. Although the results are incomplete, the data clearly points towards an increased binding affinity between Norrin and the EVR3 variant form of LGR4, providing initial insight into the disease mechanism.

LGR4 has been linked to multiple developmental processes (section 1.7.2) but it has not previously been implicated in vascular development. To investigate this, an organotypic angiogenesis assay was performed. An angiogenesis assay was chosen as the phenotype in FEVR patients and FEVR mouse models points towards a defect in angiogenic sprouting rather than a defect in vasculogenesis (section 1.3.4.2 and section 1.4.2).

The assay chosen was that developed by Bishop and colleagues and consisted of HUVECs co-cultured on a layer of HDF (Bishop et al., 1999). The extracellular matrix (ECM) has a huge role in the angiogenesis as it provides the physiological substrate for the endothelial cells and influences many processes including proliferation, differentiation, signal transduction, gene expression and cell and tissue morphology (Adams and Alitalo, 2007). Although a variety of different artificial substrates are frequently used in angiogenesis assays, including Matrigel™, gelatin, collagen and fibronectin, the organotypic model using HDF is believed to be the closer to the physiologically angiogenesis process (Hetheridge et al., 2011). In this model, the fibroblasts act as a scaffold for the endothelial cells and secrete stromal matrix components. This enables the endothelial cells to proliferate and

differentiate to form capillary-like tubule structures which closely resemble capillaries *in vivo* (Donovan et al., 2001).

Originally the angiogenesis co-culture experiment was performed by plating HUVEC and HDF cells together and co-culturing for 15 days (Sorrell et al., 2007). This procedure was recently modified to shorten the experiment to allow the effects of siRNA-mediated gene silencing to be investigated using this assay (Jones et al., 2009; Mavria et al., 2006; Scott et al., 2008). In the new method, HUVECs are plated on top of a confluent layer of fibroblasts and tubule formation is assessed after 5-6 days (Mavria et al., 2006). This shortened version of the organotypic assay was used in the present study and has been widely used to investigate signalling pathways that control angiogenesis by other teams (Jones et al., 2009; Kaur et al., 2011; Mavria et al., 2006; Ye et al., 2009).

The investigation of siRNA-mediated knockdown of *LGR4* using this model showed a decrease in the ability of the cells to form a capillary network evidenced by a reduction in the length and number of tubules, a reduction in the number of tubule branch points and an increase in the presence of undifferentiated endothelial cell clusters (Figure 5-4). All of these effects were similar to those observed in the positive control, cells with siRNA-mediated knockdown of *FZD4*, with the exception of the undifferentiated clusters which was more pronounced in *FZD4*-siRNA cells. These findings show that *LGR4* plays a role in angiogenesis. The similarity between the defects observed in both the *FZD4* and *LGR4* siRNA treated cells is striking and points towards an underlying common defect. Although further experiments are needed to verify this statement, the association of both proteins with the FEVR phenotype and the Norrin- $\beta$ -Catenin pathway provides additional evidence that this may be the case.

Although the key pathological feature in FEVR is a defect in the development of the retinal vasculature, surprisingly few cell-based angiogenesis assays have been performed on the FEVR disease genes. This is because the majority of studies have focused on phenotyping humans with FEVR and

knockout mice models (section 1.4) (Xu et al., 2004; Richter et al., 1998; Kato et al., 2002; Junge et al., 2009; Poulter et al., 2010; Robitaille et al., 2002; Toomes et al., 2004). However, a couple of assays have been reported. Retinal endothelial cells (REC) derived from *Fzd4*<sup>-/-</sup> mice were shown to impair the formation of capillary like structures *in vitro* (Ye et al., 2009). Similarly, antagonising antibodies targeting Norrin caused a reduction in total tubular length and branch point number in an endothelial cell line during *in vitro* angiogenesis assay (Planutis et al., 2014). Although these assays were not the same as the one used in this study, they do show that the FEVR disease genes show defects in similar angiogenesis assays.

The HUVEC clusters observed in the *LGR4* and *FZD4*-siRNA treated cells are not typically observed in angiogenesis assays which is why automated software was not available to quantitate them (Staton et al., 2009). These clusters are reported to be endothelial cells that have not been able to differentiate into tubular-like structures (Friis et al., 2005). Similar clusters were observed in the *Fzd4*<sup>-/-</sup> REC angiogenesis assays previously performed (Ye et al., 2009). Interestingly, these HUVEC clusters are similar to the ball-like clusters of endothelial cells found in the inner plexiform layer (IPL) of *Fzd4*<sup>-/-</sup> mice, in which the terminating sprouts in RECs cause clusters (Ye et al., 2009). It is possible that these clusters represent an inability of the cells to respond to signals triggering angiogenesis, maybe directly as a result of defects in Norrin- $\beta$ -Catenin signalling or from other pathways downstream of this pathway. Further studies are required to investigate this possibility and to determine if they are seen in similar assays performed with other FEVR disease genes.

Although this study is the first one to show a direct role for LGR4 in angiogenesis, RSPO/Wnt signalling has been shown to be pro-angiogenic in endothelial cells and to promote angiogenesis via VEGF (Caruso et al., 2015; Gore et al., 2011; Kazanskaya et al., 2008). Furthermore, VEGF is known to be a downstream transcriptional target of  $\beta$ -Catenin (Zhang et al. 2001; Easwaran et al., 2003). These studies support a role for LGR4 in vasculature

development but additional studies will be required to unravel the specific molecular signals and pathways involved.

The siRNA gene silencing of *LGR4* is a model for a recessive null allele (assuming efficient levels of knockdown). This therefore may not be a suitable model for the *LGR4*-related FEVR variants which are all heterozygous missense changes. However, the cellular model should be representative of the *Lgr4* knockout mouse. These mice often die embryonically or in the perinatal period and display many developmental defects (Hoshii et al., 2007; Mazerbourg et al., 2004; Mendive et al., 2006; Schoore et al., 2005) (section 1.7.2). However, no defects in the vasculature of these mice have been reported. This may be because the defects haven't been looked for and are subtle, as observed in other FEVR disease gene mouse models (section 1.4.2). Alternatively, the animals may have so many other anomalies that the vasculature defects were present but were not reported. Therefore it would be beneficial to investigate the *Lgr4*<sup>+/-</sup> and *Lgr4*<sup>-/-</sup> mice to look at the retinal vasculature in greater detail. This may provide clues to aid in deciphering the mechanism of the FEVR *LGR4* variants.

In order to investigate the possibility of an interaction between Norrin and *LGR4*, and any affect the FEVR-related *LGR4* variants had on this interaction, a variety of different cell-based binding assays were performed. The first assay was a co-culture assay based on a similar experiment used to confirm Norrin as a ligand for FZD4 (Xu et al., 2004). This assay takes advantage of the autocrine and paracrine activity of Norrin (Xu et al., 2004) and involves culturing STF cells transfected with the Norrin receptor components alongside HEK293 cells transfected with either AP-Norrin alone or a combination of AP-Norrin and WT or variant *LGR4* (Figure 5-5). The experiment was designed to assay if *LGR4* is binding to Norrin or if the *LGR4* variants are aberrantly binding Norrin and sequestering it away so that it is no longer available to trigger the TOPflash assay in the neighbouring cells.

The results of this co-culture experiment showed a statistically significant reduction in TOPflash activation when the *EVR3* variant (c.118C>T

p.(R40W)) was co-transfected with Norrin in comparison to cells transfected with WT *LGR4* and Norrin. However, none of the other variants showed the same effect (Figure 5-6). These results suggest that the EVR3 variant is aberrantly binding to Norrin resulting in less Norrin being secreted into the medium to activate the TOPflash reporter in the neighbouring STF cells.

In order to further investigate a potential interaction between Norrin and *LGR4*, and to confirm the increased binding observed with the EVR3 variant, a second cell based binding assay was undertaken using AP-tagged Norrin. Binding assays using AP-tagged ligands have been broadly used to investigate receptor-ligand interactions between Wnt signalling components and their ligands (Glinka et al. 2011; Ohkawara et al. 2011; Xu et al. 2004; Qin et al. 2008; Smallwood et al. 2007; Junge et al. 2009; Wei et al., 2007). Therefore, this method seemed appropriate to analyse binding of *LGR4* to Norrin.

In concordance with the results from the TOPflash co-culture assay, the cell-surface AP-staining assay also showed increased binding of the EVR3 variant (c.118 C>T p.(R40W)) to Norrin (Figure 5-7). The level of binding was similar to that observed for the Norrin-FZD4 interaction and when quantified using the AP-chemiluminescence assay, this increase in binding was highly significant compared to WT *LGR4* (Figure 5-9). A slight increase in AP-staining was observed for two additional variants located in the *LGR4* binding domain (c.933G>C p.(Q311H) and c.1289C>T p.(T430M)) (Figure 5-7) but these were not statistically significant (Figure 5-9).

These results show that the level of Norrin binding observed in the AP-binding assays correlates inversely with the levels of TOPflash activation previously observed for these variants in chapter 4 (Figure 4-9). The EVR3 variant had the strongest binding affinity and the lowest level of TOPflash activation. Similarly, the other variants in the *LGR4* extracellular domain had reduced levels of TOPflash activation when compared to WT *LGR4* and they also showed slightly higher levels of Norrin binding. In contrast, WT *LGR4* and the variant present within the transmembrane domain of *LGR4*,

c.2164G>A p.(A722T) showed similar levels of TOPflash activation and Norrin binding. These findings suggest that the reduction in TOPflash activation found with the variants present in the LGR4 binding domain are due to the aberrant binding of these variant forms of LGR4 to Norrin. Therefore, a possible hypothesis for the disease mechanism of these variants is that they aberrantly bind Norrin and this results in a decrease in Norrin signalling (see chapter 6 for further discussion). However, at present, statistical proof of increased Norrin binding is only available for the EVR3 variant and further evidence is needed before any conclusions can be drawn. There are, however, examples in the literature which show a similar mechanism of increased binding between receptor and ligand as the cause of disease (Warren et al. 2015; Choi et al. 2004; Wimmers et al. 2016).

An interesting observation from the AP-staining experiment is that there was a weak but clear increase in staining observed between WT LGR4 and the empty vector control (Figure 5-7). This level of staining was similar to that observed between Norrin and LRP5 and TSPAN12 (Figure 5-8). However, when this interaction was quantitated using AP-chemiluminescence, only the interactions between TSPAN12 and LRP5 were confirmed to be statistically significant at the higher concentration levels of Norrin conditioned media. The interaction between WT LGR4 and Norrin failed to reach significance even though it can clearly be seen in the AP-staining assay (Figure 5-7 and Figure 5-8). This result may be influenced by the transient nature of the interaction between Norrin and WT LGR4 and it is worth noting that the AP-staining assay used a protein crosslinking agent whereas the chemiluminescent assay didn't. This technical difference might explain why an increased signal is clearly visible in the stained cells but is not evident in the quantification assay. Clearly additional studies are needed to investigate the possibility that LGR4 interacts with Norrin, albeit in a weak or transient manner. If LGR4 is forming part of a receptor complex with FZD4, LRP5 and TSPAN12, then stable interactions may not be evident without factoring in these co-receptors into the experimental design. Similar inconsistent results were found in earlier studies investigating the ligands and binding sites for LRP5/6 and this

is also undoubtedly due to the fact that these proteins function as co-receptors (Kikuchi et al., 2007; Nam et al., 2006; Wei et al., 2007).

The crystal structure of the LRR domain of LGR4 bound to RSPO1 has been determined and the results showed no difference in the structural conformation of the bound and unbound LGR4 LRR domain leading the authors to conclude that unlike other members of the LGR family of receptors, LGR4 (along with the closely related LGR5 and LGR6) does not undergo a conformational change upon initial ligand binding to strengthen the interaction (Xu et al., 2013). This result indicates the importance of the amino acid residues in the LRR domain as any variation may alter the conformation of the binding domain or the affinity for the ligand-receptor interaction and thus have a profound affect on the function of the receptor. It is possible that any interaction between Norrin and LGR4 may act in a similar manner.

Despite RSPO and “potentially” Norrin binding to the LRR domain of LGR4, evidence suggest that this is not to the same interface. Dr Narcis Fernandez-Fuentes (Aberystwyth University) has modelled the interaction of Norrin and LGR4 based on the published crystal structures and this data shows that RSPO and Norrin appear to interact with LGR4 at different interfaces and the FEVR-related variants are located in the Norrin interface (unpublished data). This finding is consistent with the WT levels of TOPflash activation obtained when the FEVR-related LGR4 variants were treated with RSPO1 (Figure 4-11). In addition, LGR4 and RSPO1 mutagenesis studies were performed as part of the Xu study to confirm the RSPO1 and LGR4 interaction sites deduced from the crystal structure (Xu et al., 2013). This data showed that Asn114, Asp137, Ala181, Thr183 and Val204 were all key LGR4 amino acid residues required for RSPO1-mediated signalling and these are not near the FEVR-related variants investigated in this study. In the future it would be interesting to determine the crystal structure of Norrin and LGR4 and perform similar mutagenesis studies.

From the data obtained in this study it is not clear if LGR4 is a receptor for Norrin. However, it is clear that the results in this thesis do not agree with

those generated by Deng and colleagues which show that LGR4 is a receptor for Norrin (Deng et al., 2013). The binding assays performed in the current study were performed at 4°C in order to stop the internalisation and recycling of the receptor complex (Schlessinger et al., 1978; Blitzer & Nusse, 2006). This is the temperature used in the majority of binding assays and in all of the published studies investigating Norrin and RSPO binding (Xu et al. 2004; Junge et al. 2009; Glinka et al. 2011; Smallwood et al. 2007; Wei et al., 2007; Ohkawara et al., 2011). However, given the importance of this result to this study the assay was repeated at room temperature. Consistent with the Deng study, at room temperature strong binding of LGR4 to Norrin was observed. However, the controls for this experiment did not work making the data unreliable. Norrin showed strong binding to the empty vector (negative control) and there was no difference in the level of Norrin bound to FZD4 (positive control) compared to the empty vector (Figure 5-10). Furthermore, when using higher dilutions of Norrin conditioned media (100% and 80%) the empty vector showed higher levels of binding to Norrin than FZD4. This suggests that the experimental procedure at room temperature is not accurate for determining Norrin binding. An additional difference between Deng and colleagues study and the assay performed in this thesis is the Norrin conditioned medium used. In Deng study, Norrin conditioned medium was obtained in serum free medium and it was concentrated and diluted in PBS prior to perform the binding assays, whereas in this study Norrin conditioned medium was obtain in 10% serum complete medium (section 2.10.5). The difference in Norrin conditioned medium preparation could also explain the discrepancies obtained in this thesis when compared to Deng et al. (2013) study. For that reason, it would have been interesting to obtain Norrin conditioned medium in the same way as in the Deng study and to perform the binding assays at room temperature and 4 degrees. If that had been the case, it could have been possible to determine if such differences observed in Figure 5-9 at 4 degrees and Figure 5-10 at room temperature using serum Norrin conditioned medium are reproducible in serum free Norrin conditioned medium.

Localisation and co-localisation studies were undertaken to determine if the FEVR-related *LGR4* variants altered the localization of LGR4 or any interaction with Norrin compared to the WT protein. Co-localisation studies have been broadly used in order to determine if two proteins are located in the same part of the cell (Dunn et al., 2011). Ligand-receptor co-localisation studies are frequently performed by labelling each protein with a different fluorophore. This allows images to be taken of the individual proteins by using appropriate filters on a fluorescence microscope. Co-localisation can then be assessed by studying the overlap of the two protein signals (Morrison et al., 2003; Lachmanovich et al. 2003; Parmryd et al. 2003). In this study, this technique was undertaken to study the co-localisation of LGR4 and Norrin to determine if they are situated together at the cell membrane and support the hypothesis that they form a receptor-ligand complex.

Unfortunately these were ill-fated experiments. The first experiment used a C-terminal GFP fusion protein but unfortunately the fusion protein did not fluoresce indicating that the Cycle 3 GFP activity or structure was compromised by the addition of LGR4 (Corish et al., 1999; Nicholls & Hardy, 2013). The constructs were therefore all switched to create an LGR4-YFP fusion protein series and although these proteins did fluoresce, they formed clumps.

The formation of dimers and oligomers with YFP fusion proteins is a known phenomenon and results in misfolding of the protein which causes aggregates formation (Campbell *et al.* 2002; Zacharias *et al.* 2002). These aggregates form distinctive circular structures localised next to the nucleus of the cell and distributed around the cytoplasm (García-mata et al., 1999; Johnston et al., 1998). This phenotype resembled the LGR4-YFP fusion protein localisation found in this study (Figure 5-11 and Figure 5-15). Nevertheless, membrane localisation was observed for all the LGR4 variants indicating that the variants do not stop the receptor trafficking to the plasma membrane, a result that was expected given the RSPO1 TOPflash results

(section 4.4.4). However, the presence of multiple aggresomes impaired the detailed analysis and quantification of the proteins.

Similarly, all of the LGR4-YFP fusion proteins co-localised with Norrin predominantly at the cell membrane although some co-localisation was also found in the cytoplasm which may represent internalised ligand-receptor complex (Carmon et al., 2012; Cruciat & Niehrs, 2013; Blitzer and Nusse 2006; Niehrs and Acebron 2010) (Figure 5-15). No differences were observed between the WT and variant forms of LGR4. Again however, the formation of aggresomes prevented any detailed analysis or quantification of this co-localisation. Nevertheless, this result suggests that LGR4 and Norrin associate within the same structural complex in the cells. The control for this experiment used an FZD4-His fusion protein and this smaller tag caused no aggresome formation (Figure 5-13). Therefore the constructs need to be switched to a third expression construct such as pDEST40 and the assay repeated to enable the interactions of Norrin with the mutants to be properly assessed. In addition, it would be good to look at the co-localisation of WT LGR4 and the FEVR-related variant forms of LGR4 with additional proteins including FZD4, TSPAN12 and LRP5 to try and build up a full picture of where this protein is located in relation to the Norrin receptor complex. Similar co-localisation studies using LGR4 with the ligands RSPOs and RANKL have successfully been performed and used to provide evidence that these are ligand-receptor pairs (Carmon et al., 2011; Glinka et al., 2011; Luo et al., 2016; Ruffner et al., 2012). Similarly, this technique has been used previously to investigate the effects of FZD4 FEVR mutations on the localisation and interaction of FZD4 with Norrin (Milhem et al. 2014; K. Zhang et al. 2011; Kaykas et al. 2004).

In summary, in this chapter the role of LGR4 in vasculature development was assessed using an *in vitro* organotypic assay. The results confirmed that LGR4 appears to play a role in this biological process and that this role is similar to that of FZD4. Norrin-LGR4 binding assays were also undertaken and although no concrete evidence was obtained to show that LGR4 was a receptor for Norrin, the assay clearly showed that the EVR3 mutation

induced an increase in the binding affinity between Norrin and LGR4 and this is likely to be the pathogenic mechanism of this mutation. Finally, LGR4 appeared to co-localise with Norrin at the cell membrane supporting the close association of these proteins. Furthermore, no defects in protein localisation or Norrin co-localisation were observed for the *LGR4* variants although this assay needs repeating. Taken together, this data shows that *LGR4* is the gene mutated in the EVR3 family and *LGR4* is confirmed as a new autosomal dominant FEVR gene.

## 6 General discussion

### 6.1 Key findings of this thesis

The aim of the work described in this thesis was to determine if *LGR4* was the autosomal dominant FEVR gene located in the EVR3 locus. Next generation sequencing had previously identified a missense variant in *LGR4* in a member of the EVR3 family. Subsequent screening of *LGR4* in a cohort of FEVR patients had identified a further 5 missense variants. However, as all six *LGR4* variants were missense changes it was impossible to confirm with absolute certainty whether the variants were disease causing mutations or rare benign variants. Therefore, in this study WT *LGR4* was functionally characterised to provide evidence to support its role as an FEVR disease gene and the *LGR4* missense variants were functionally assessed to gather evidence to support their pathogenic nature.

The main conclusion of this work is that *LGR4* is the *EVR3* gene. However, this conclusion cannot be drawn for every variant assessed in this study. Two of the six variants were withdrawn as Mendelian disease alleles (section 4.4.3.2). Of the remaining four variants, only the EVR3 variant, c.118C>T p.(R40W), clearly looked pathogenic in all the different assays investigated: zebrafish MO-knockdown and rescue (section 3.5), TOPflash assay of Norrin- $\beta$ -Catenin signalling (section 4.4.3.1) and ligand-receptor binding assays (section 5.3.1 and section 5.3.2). The two additional variants in the *LGR4* binding domain, c.933G>C p.(Q311H) and c.1289C>T p.(T430M), also looked pathogenic in the zebrafish MO assay (section 3.5) and the TOPflash assay of Norrin- $\beta$ -Catenin signalling (section 4.4.3.1). However, the data for the binding assays was less convincing and did not show significant differences from WT *LGR4* (section 5.3.2). Finally, the variant in the transmembrane domain of *LGR4*, c.2164G>A p.(A722T), only looked pathogenic on the zebrafish MO assay (section 3.5).

In addition to this data on the *LGR4* variants, functional assessment of *LGR4* also provided evidence that it plays a role in the biological pathway implicated in FEVR and in the development process disrupted in FEVR. *LGR4* knockdown in an *in vitro* assay of angiogenesis showed, for the first time, that *LGR4* plays a role in vasculature development (section 5.2) and TOPflash assays support a functional role for *LGR4* in Norrin-mediated  $\beta$ -Catenin signalling (section 4.4.3).

The major concern of this thesis is the zebrafish assay used in Chapter 3. This assay was designed as a quick and cost effective assay to assess the functional impact of the missense variants. The conclusion drawn at the end of this chapter is that all six variants are pathogenic. However, subsequent to this finding, two of the variants were withdrawn as candidate Mendelian disease alleles (section 4.4.3.2). A large deletion in *TSPAN12* was identified in the patient with the c.1924G>A p.(E642K) variant and the c.2248G>A p.(A750T) variant was shown to be a polymorphism. At first glance this result would indicate that this assay is not a reliable test, however the situation is a little more complicated and requires further investigation.

Although FEVR is always described as a Mendelian single gene disorder there is growing evidence that the inheritance pattern is more complex. This theory stems from the marked variation in disease expression observed between members of the same family (Benson, 1995; Toomes et al., 2004b). Although variable expression is a common occurrence in genetic disease (Lobo, 2008), there are not many disorders where the contrast is so different. At the mild end of the spectrum, individuals are asymptomatic and are often unaware that they have the disorder until a relative with severe disease is diagnosed, prompting a molecular test or a clinical investigation (fluorescein angiography). However, at the severe end of the spectrum, children might suffer a total retinal detachment or retinal dysplasia and be registered blind from birth. This observation has led to speculation that FEVR may be a bi-allelic or digenic disorder, or that modifier genes may influence the phenotype (Poulter et al., 2012).

Data supporting this hypothesis is still anecdotal, however mutations in *TSPAN12*, *LRP5* and *FZD4* all underlie dominant and recessive forms of FEVR and the recessive forms of the disease are always at the severe end of the phenotypic spectrum, whereas the dominant forms show a more variable expression (Poulter et al., 2010; Toomes et al., 2004b). This observation suggests that the mutations may have an additive effect and this has been confirmed for *TSPAN12* and *LRP5* (Poulter et al., 2012; Carmel Toomes personal communication). Although in these examples both mutant alleles reside in the same gene, it is possible that the mutant alleles are in different genes. Indeed, potential digenic inheritance has been reported in FEVR patients but again the data supporting this is weak due to the small size of the families investigated and the missense nature of the disease alleles (Qin et al., 2005; Nikopoulos et al., 2010). However, preliminary unpublished data from the Leeds Vision Research team supports this digenic inheritance theory (Carmel Toomes personal communication). Given the potential for an FEVR patient to have two mutant alleles, care must be taken when disregarding the c.1924G>A p.(E642K) allele simply because a further change was identified in *TSPAN12*. Similarly, although the c.2248G>A p.(A750T) variant has been shown to have a frequency of 1% in Asians, it could potentially be a modifier allele. Polymorphisms in *LRP5* have been shown to alter the function of the protein, and many of them are associated with normal variation in bone mineral density and show defects in the TOPflash assay (Qin et al., 2008). Indeed, some of these *LRP5* “polymorphisms” appear to be candidate modifier alleles for FEVR severity (Carmel Toomes personal communication). Given this additional data it is therefore possible that the two variants dropped from this study may play a role in the disease and this may explain why they looked pathogenic in the zebrafish assay. As such, these variants were not excluded as FEVR alleles but were excluded as “Mendelian disease alleles”. This phrase was chosen as currently, the evidence for digenic inheritance is preliminary and unpublished and FEVR is still described as a Mendelian disorder in the literature and in a clinical setting. Therefore, although the zebrafish MO-assay looks unreliable, it cannot be totally disregarded at the moment.

## 6.2 LGR4's role in the Norrin- $\beta$ -Catenin signalling pathway

The results in this thesis provide compelling evidence that LGR4 plays a role in the Norrin- $\beta$ -Catenin signalling pathway. However, the precise mechanism underlying this interaction is still not established and requires further investigation. A schematic representation of a suggested possible role of LGR4 in Norrin signalling is represented in Figure 6-1. In the presence of the canonical ligands (Norrin and RSPO), Norrin binds to FZD4 receptor complex and Norrin pathway is activated. Additionally, RSPO binds to its receptor LGR4 and RNF43/ZNRF3 avoiding the membrane clearance of FZD4 and LRP5, which consequently boosts Norrin signalling pathway (Figure 6-1 A).

On the other hand, in the absence of Norrin, Norrin pathway remains inactivated due to  $\beta$ -Catenin degradation in the cytoplasm (section 1.5.3). Furthermore, the absence of RSPO triggers ubiquitination and degradation of FZD4 and LRP5 receptors by the RNF43/ZNRF3 pair, which would consequently occur in a reduction of signalling (Figure 6-1 B) (section 1.6.3.1). A question that still remains unsolved with the data presented in this thesis is whether LGR4 belongs to the Norrin receptor complex or it is in close proximity to the receptor complex regulating Norrin pathway. In addition, whether Norrin can bind to LGR4 WT in a similar way than Norrin might transiently bind to LRP5 and TSPAN12 is still not clear and needs further investigation (see below).

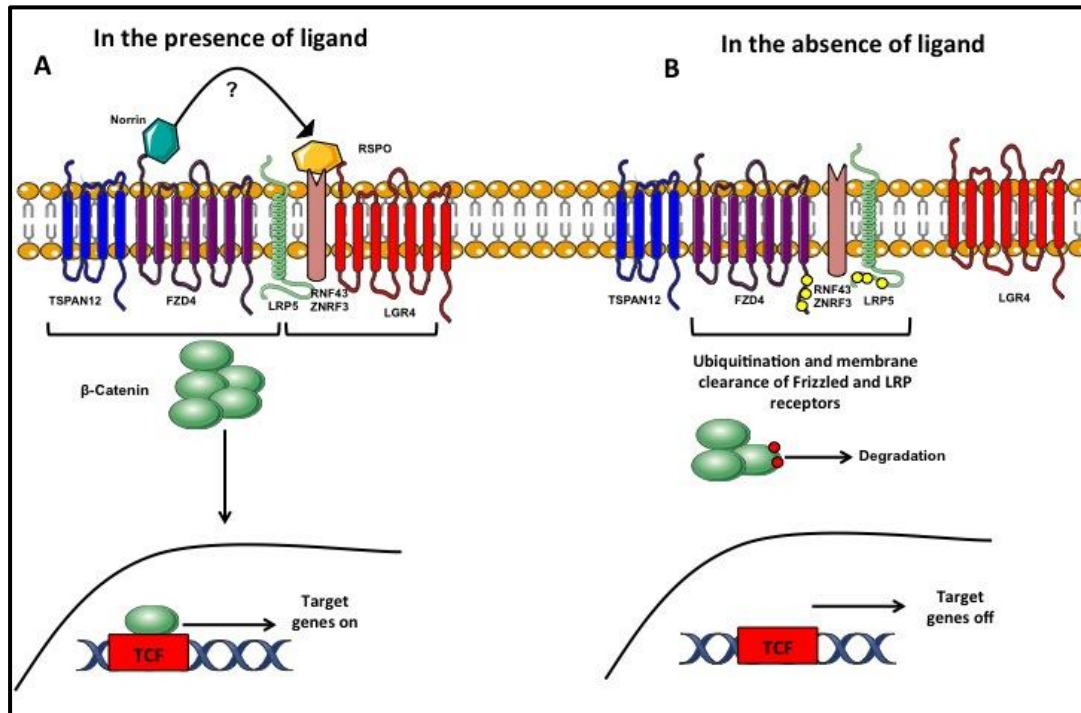


**Figure 6-1: Schematic diagram of the suggested role of LGR4 in Norrin signalling.**

**A:** In the presence of ligand, Norrin binds to FZD4 receptor complex to transduce the signal. RSPO binds to LGR4 receptor and RNF43/ZNRF3 avoiding ubiquitination and membrane clearance of FZD4 and LRP5 receptors. It is unclear whether Norrin can also bind to LGR4 WT receptor to activate Norrin pathway. The presence of ligand occurs in  $\beta$ -Catenin accumulation in the cytoplasm, which will translocate into the nucleus interacting with the TCF transcription factor to turn the target genes on. **B:** In the absence of ligand, Norrin pathway will remain inactive due to  $\beta$ -Catenin phosphorylation and degradation in the cytoplasm. The absence of RSPO binding to LGR4 occurs in the ubiquitination of FZD4 and LRP5 receptors by the RNF43/ZNRF3 pair, which are cleared out of the cell membrane. Consequently, the target genes remain off.

The simplest interpretation of the TOPflash data is that LGR4 is a component of the Norrin receptor complex along with FZD4, TSPAN12 and LRP5. The missense variants in the binding domain of LGR4 could therefore be impairing Norrin binding to this receptor complex and result in a reduction in TOPflash activation. This is the same mechanism described for the effect of FEVR mutations located in the binding domain of *FZD4* (Qin et al., 2008; Xu et al., 2004; Zhang et al., 2011). Interestingly, The AP-binding assay results for LGR4 and Norrin did not confirm an interaction between these molecules with statistical significance, although a slight increase in binding above

background levels was observed (section 5.3.2). The AP-staining methods showed that Norrin bound to LGR4 with a similar intensity as it bound to LRP5 and TSPAN12. Previous studies have described binding between LRP5 and Norrin (Chang et al., 2015; Ke et al., 2013) and TSPAN12 binding to Norrin has also been observed (personal communication from Dr. Harald Junge in the Wnt Signalling meeting Brno, September 2016). Therefore, the weak-binding result observed between LGR4 and Norrin may simply reflect the technical limitations of the current method to detect rapid transient binding. Additional studies are therefore required to confirm if this is the case. Dr Junge used proximity PCR ligation assays to investigate the TSPAN12–Norrin interaction so this would be a good method to use (Koos et al., 2014).

The co-localisation experiments showed Norrin and LGR4 localised together at the plasma membrane (Figure 5-15). These results could be interpreted as a ligand receptor interaction and again these studies need repeating with a fusion protein without a YFP tag to overcome the aberrant clustering observed and to facilitate the quantification of these interactions.

Previous work by Deng and colleagues has shown that Norrin is a ligand for LGR4 (Deng et al., 2013). However, the data in the present study did not replicate this result (section 4.4.3 and section 5.3.2) and its not clear if the authors used appropriate controls for their experiments from their manuscript. As such, the data in the Deng study should be treated with caution until an independent group repeats them. Despite this, the Deng study did present data showing that LGR4 potentiates TOPflash activation when cells are stimulated with Norrin, and this conclusion was obtained in the current study (section 4.4.3).

However, this simplistic view is complicated when the TOPflash results are viewed alongside the ligand-binding results obtained for the EVR3 variant, which shows a dramatic increase in binding affinity between Norrin and this mutant form of LGR4 (Figure 5-9). An alternative hypothesis could be that the increased affinity of Norrin for the LGR4 EVR3 mutant is a result of the ligand not binding to its target binding site correctly and this subsequently

causing a deficit in the signal transduction initiated upon Norrin binding (Figure 6-2 A). This disruption could be by preventing the dimerisation of Norrin or the receptor complex (Chang et al., 2015; Ke et al., 2013), or alternatively, by inhibiting a conformational change in the receptor required for signal activation (Milhem et al., 2014).

A completely different explanation could be that LGR4 is not a component of the Norrin receptor complex and the FEVR variants located in the LGR4 binding domain cause LGR4 to aberrantly bind Norrin and prevent it from binding to its true target, the receptor complex formed by FZD4, LRP5 and TSPAN12. This would result in a decrease in TOPflash activation as found with the FEVR mutants in the binding domain.

LGR4 plays a role in regulating Wnt signalling by triggering the membrane clearance and subsequent degradation of frizzled receptor complexes. It does this through a negative feedback regulation mechanism mediated by LGR4-RSPO and ZNRF3/RNF43 (section 1.6.3). It is therefore possible that LGR4 plays a similar role in regulating Norrin signalling. The aberrant binding of Norrin to the LGR4 binding domain variants could inhibit the binding of RSPO to LGR4 and this could result in increased membrane clearance of FZD4 from the cell membrane and result in a decrease in Norrin-mediated TOPflash activation (Figure 6-2 B).

On the other hand, the LGR4 variant present in the transmembrane domain presented an increase in TOPflash output when using RSPO1 as a ligand, but no differences were found when Norrin was used as a ligand. This variant could induce a conformational change in LGR4 receptor having an effect on the ability of LGR4 to transduce RSPO1 signal at the cell surface (Xu et al., 2013) (Figure 6-2 C). The switch in the polarity of the protein, changing a non-polar alanine to polar threonine in the transmembrane region, may result in aberrant protein assembly in the plasma membrane that may increase RSPO1 transduction of the signal (Lv et al., 2011; McClellan et al., 2001).

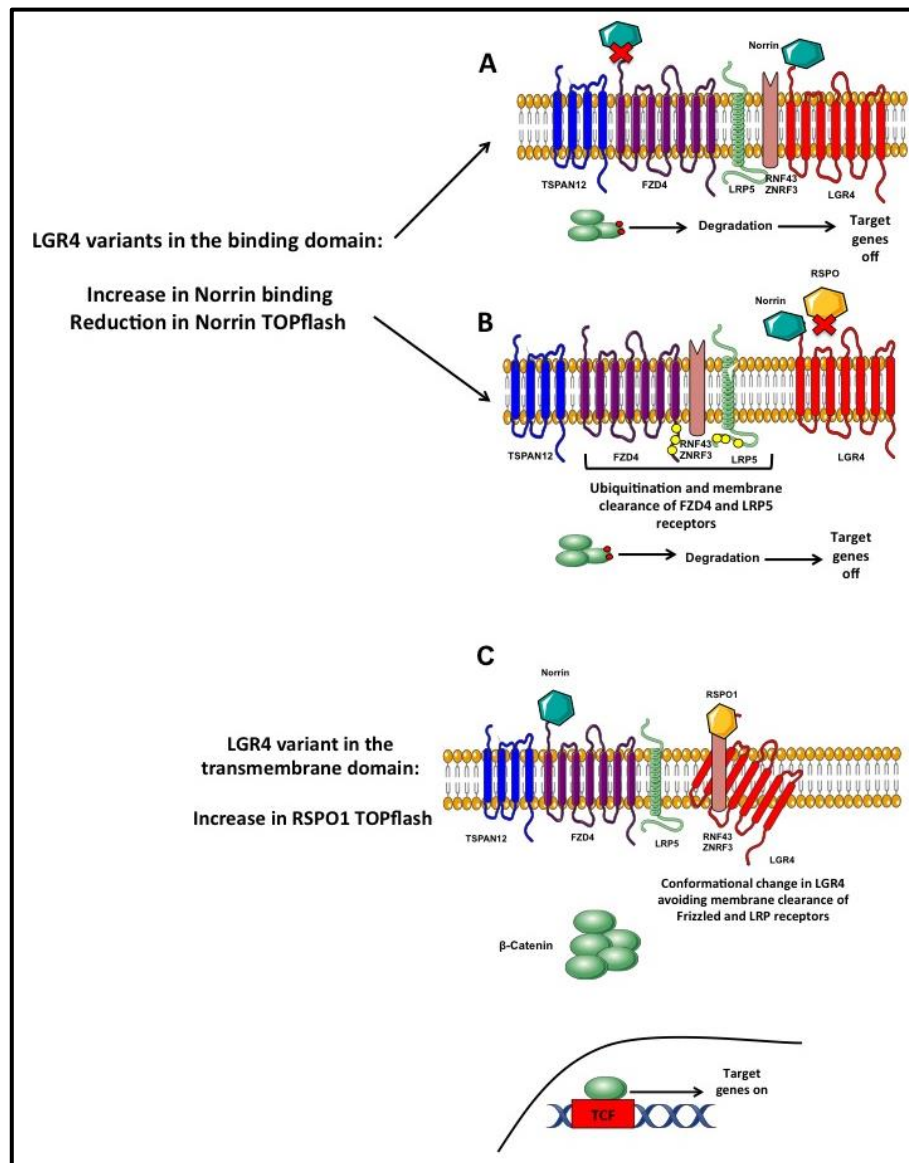


**Figure 6-2: Schematic diagram suggesting different possible pathogenic mechanism of action for the LGR4 variants.**

At the top of the figure the LGR4 variants in the binding domain presenting increase Norrin binding and decrease Norrin TOPflash output could be explain by two mechanisms. **A:** The increase in Norrin binding for LGR4 is impairing Norrin binding to its FZD4 receptor complex. This would occur in degradation of  $\beta$ -Catenin and reduction in Norrin signalling. **B:** Norrin binding to LGR4 impairs RSPO binding to LGR4. The absence of RSPO binding to LGR4 and RNF43/ZNRF3 occurs in ubiquitination and membrane clearance of FZD4 and LRP5 receptors, which would also occur in reduction in Norrin signalling. **C:** The LGR4 variant in the transmembrane domain could induce a conformational change of the LGR4 receptor at the cell membrane due to the aminoacid polarity change. This change might avoid the membrane clearance of Frizzled and LRPs receptors, which would consequently occur in an increase in canonical signalling.

Clearly, this is all speculation and the different hypotheses need to be investigated further. Therefore, at this point of the study, it cannot be determined if LGR4 is a co-activator or co-receptor of the Norrin pathway or if it is negatively regulating the Norrin pathway through RSPO and RNF43/ZNRF3. GPR124 has been shown to be a co-activator of FZD4 to activate Wnt signalling and control angiogenesis and blood brain barrier (BBB) integrity during brain development (Zhou et al., 2014). This finding suggests that co-activators of Wnt signalling might be especially important in the vascular biology of the central nervous system and that accurate and detailed role of LGR4 in this pathway needs to be further characterised.

### **6.3 Verifying pathogenic missense variants**

Determining the pathogenic nature of missense mutations has always been a difficulty in disease gene identification studies and in molecular diagnostic laboratories. However, with the advent of next generation sequencing (NGS) technologies this problem has increased substantially (Goldstein et al., 2013). Whole exome sequencing (WES) identifies between 20,000 and 30,000 single nucleotide variants (SNVs) and 40% of these will result in a non-synonymous amino acid substitution (Stitzel et al., 2011). A major challenge of human genetics in this era of NGS is distinguishing and prioritising disease causing variants from this large amount of genetic variation (Masica and Karchin, 2016).

Large amounts of resources have been spent in trying to develop and improve computational methods to determine the impact of missense variants. Many different tools have been developed and each uses a slightly different algorithm in its predictions. For example, one of the most popular prediction tools used at the moment is CADD (Combined Annotation Dependent Depletion) which combines diverse annotations including conservation, frequency, functional data, structure etc., into a single score (Kircher et al., 2014). However, despite many recent advances in the prediction software, different tools often reach different conclusions making it

difficult to interpret the results (Hicks et al., 2011; Thusberg et al., 2011, Masica & Karchin, 2016). Furthermore, the prediction tools normally only focus on the amino acid substitution encoded by the variant, and this can often miss other outcomes of SNV such as splicing defects (Bellingham et al., 2015; Gonzalez-paredes et al, 2015). The EVR3 mutation identified and verified in this study, p.(R40W), was predicted to be pathogenic by three tools but benign by two. Similarly, the p.(A750T) variant shown to be a polymorphism was predicted to be pathogenic by all five tools (see Table 3-1 for *LGR4* missense variants).

Clearly these *in silico* prediction tools are not reliable and they must be used with caution, especially in a diagnostic setting. As a result, there is a growing need for functional assays that can reliably characterise variants of unknown significance (VUS) (Goldstein et al., 2013). However, it's clear from the results of this study that functional studies can be very time consuming and also don't give clear-cut reliable results. Therefore considerable efforts must be made by the scientific community to development high-throughput robust functional assays. Without such tools, all the benefits of having a molecular diagnosis will not be available to patients with inconclusive diagnostic reports. This is a particular problem for FEVR as this disorder is heterogeneous, has a large number of asymptomatic mutation carriers who are often found in "control" cohorts and has genes with large numbers of rare SNV such as *LRP5*.

A well-known example that reflects the importance and utility of reliable functional tests is *BRCA1*. Individuals with mutations in *BRCA1* have an increased risk of developing breast and ovarian cancer (Miki et al., 1994). VUS in *BRCA1* such as intronic variants, in-frame deletions/insertions and missense variants cannot be directly classified as pathogenic without the use of functional tests (Millot et al., 2012). Therefore, Woods and colleagues developed functional tests for *BRCA1* and showed that if this was incorporated into a clinical diagnostic setting it would reduce by 86% the number of VUS (Woods et al., 2016).

## 6.4 The impact of this study

The identification of *LGR4* as a new autosomal dominant FEVR gene has impact at multiple levels. The scientific impact of this study is that it increases the understanding of the molecular pathways and processes that control normal and abnormal retinal blood vessel development. This will aid the development of therapies and treatments for FEVR but also for other disorders of the retinal vasculature including retinopathy of prematurity, diabetic retinopathy and age-related macular degeneration.

The great thing about genetic studies is that the identification of a new disease gene can immediately be translated by facilitating molecular diagnostic testing. The FEVR disease genes are already part of the UK Genetic Testing network enabling accredited NHS testing of FEVR patients and their families (<https://ukgtn.nhs.uk>). Based on the results in this study, *LGR4* will now be included in this service. The identification of a family's mutation allows accurate genetic counselling and can identify asymptomatic mutation carriers without the need of expensive and invasive eye tests (fluorescein angiography). This is particularly important for FEVR as this disorder has a large number of asymptomatic patients (Toomes, Downey, 1993 [updated 2008]). Identifying asymptomatic mutation carriers allows these individuals to be targeted for routine ophthalmic evaluations and enable sight-saving preventative treatments to be administered at the first signs of retinal traction.

Another example of FEVR patient care being influenced by a molecular test is seen in patients with *LRP5* mutations. *LRP5* mutations cause a reduction in bone mineral density (BMD) and patients can suffer from osteopenia or osteoporosis (Downey et al., 2006; Ferrari et al., 2004; Toomes et al., 2004). These bone defects are often only diagnosed by DEXA scan and FEVR patients with *LRP5* mutations are now routinely referred for bone scans and treated with bisphosphates if necessary (Toomes, Downey, 1993 [updated 2008]). Excitingly, a similar treatment option may be relevant to *LGR4* FEVR

patients. Two members of the EVR3 family have been shown to have reduced BMD but it is unclear if this is age-related as both patients were middle aged females (Mr David Mansfield personal communication). BMD data is currently being gathered in further EVR3 family members to determine if this association is related to the *LGR4* mutation. However, the role of LGR4 in regulating osteoclast differentiation and bone resorption provides additional evidence that there may be a bone phenotype associated with LGR4 (Luo et al., 2016).

A molecular diagnosis also opens up the possibility for interventions such as embryo selection. At present, carriers of serious genetic disorders are able to choose to actively exclude the possibility of passing on their inherited disease to their offspring by undergoing *in vitro* fertilisation (IVF) and pre-implantation genetic diagnosis (PIGD) of embryos. In this method, zygotes are screened for the mutations prior to implantation (Tur-Kaspa et al., 2010). This technique has been used to select healthy embryos where both parents were carrying *ABCA4* mutations which can cause Stargardt's disease (Sohrab et al., 2010) and Norrie disease is currently listed as an approved disorder. Clearly there are ethical implications associated with this technology and the Human Fertilisation and Embryology Authority (HFEA) tightly regulate it. For example, it has been argued that deafness is not a disability but more of a culture with its own language (Nunes, 2006), opening the debate on what is considered a disability.

A final advantage of a molecular diagnosis in FEVR patients is the opportunity to take part in clinical trials; patients usually require a genetically confirmed mutation before they can be enrolled on a trial. Furthermore, one of the main problems in developing therapies is having cohorts of molecularly diagnosed patients available for clinical trials for rare diseases. As such, patient registry databases are currently being created to facilitate the development of therapies ([http://www.eurordis.org/sites/default/files/publications/Factsheet\\_registries.pdf](http://www.eurordis.org/sites/default/files/publications/Factsheet_registries.pdf)). An FEVR database is currently being curated by the Leeds Vision Research team.

## 6.5 The treatment of FEVR.

Currently the treatment of FEVR is primarily focused on preventing the secondary complications that develop in a subset of patients as a result of retinal ischemia. Treatments include prophylactic cryotherapy or argon laser photocoagulation to halt the development of new abnormal blood vessels and to prevent retinal detachments (Shukla et al., 2003). The use of anti-VEGF therapies has also been trialled but with limited improvements (Henry et al., 2015; Quiram et al., 2008; Tagami et al., 2008). However, the ultimate aim is to translate all the FEVR molecular discoveries made in recent years into a cure for patients.

The eye field is leading the way in developing new treatments for genetic disorders. Gene replacement therapy using an adeno-associated viral vector (AAV) has been used for the treatment of Leber Congenital Amaurosis (LCA) (Weleber et al., 2016) and choroideremia (Maclaren et al., 2014). Even though this approach seems to be somewhat effective for some genes, the major challenge remains in the cargo capacity of the AAV viruses (5 kb) and the lifespan of the treatment (Trapani et al., 2014).

Recently, the CRISPR/cas9 system has been developed to enable the direct editing of genes. Gene correction using this system occurs by replacing the mutation through homologous recombination with a portion of the WT gene. This approach has been successfully used in a rat model of autosomal dominant retinitis pigmentosa (RP) (Bakondi et al., 2016). A similar strategy has also been performed in a mouse model of RP, although in this case the mutated allele was knocked-out first followed by the introduction of the WT coding sequence, providing a mutation-independent editing approach (Latella et al., 2016). The use of CRISPR/Cas9 editing in a cellular model of LCA has also shown promising results by correcting a deep intronic splicing mutation in *CEP290* (Ruan et al., 2017). Clearly these are exciting results from a technology which is still in its infancy but there are still challenges to

overcome including off-target effects, low targeting efficiency and unknown long term clinical impacts (Baltimore et al., 2015).

The use of induced pluripotent stem cells (iPSCs) has also gained popularity over the last few years. iPSC-derived retinal transplants have successfully been transplanted into the degenerated retina of mice and primates (Assawachananont et al., 2014; Shirai et al., 2015). These transplanted cells have been shown to form direct contact with the host cells, demonstrating their full integration (Mandai et al., 2017). In humans, clinical trials are currently underway investigating the efficacy of transplanting RPE cells generated from iPSC in patients with age related macular degeneration (Reardon and Cyranoski, 2014) (<http://www.thelondonproject.org/>). The application of the CRISPR/cas9 editing system in combination with iPSC technology is an exciting prospect. The combination of these technologies has recently been reported to correct a pathogenic RP mutation in patient-derived iPSC (Bassuk et al., 2016). Therefore, these therapies offer promising opportunities for the future treatment of many genetic diseases.

The prospect of using treatments like these for a developmental disease like FEVR is challenging. Gene replacement or gene editing therapies may require very early treatment, possibly even *in utero* and current guidelines prohibit the culture of genetically modified human embryos beyond seven days post fertilisation (Callaway, 2016). The possibility of using CRISPR technology for genetic editing in human embryos, or even adults, opens a complex ethical debate. Ethical arguments against gene editing are complicated due to the clear benefit of correcting serious genetic defects. However, even if these ethical barriers were overcome, would FEVR be considered a serious genetics disease, especially given the high number of asymptomatic cases?

Alternatively, the use of cell therapies or pharmacological products may provide a treatment for FEVR patients. Cell therapies would restore or replace the underdeveloped retinal vasculature and research into this field is giving some promising results. Injection of marrow-derived endothelial

precursor cells into the vitreous of retinal degeneration mice restored their damaged retinal vasculature (Otani et al., 2002). More recently, CD34+ endothelial precursor cells have been shown to incorporate into the pre-existing retinal vasculature and abrogate the ischemic damage observed in a mouse model of retinal vasculopathy (Park et al., 2012). Based on these successful results, a phase 1 clinical study is currently on going using autologous CD34+ cells derived from the bone marrow of the patient to treat retinal ischemia and degeneration. Initial results show no safety concerns and the treatment appears feasible but the full data will not be available until later in 2017 (Park et al., 2015). Similarly, many different drugs are being investigated as a treatment for FEVR or related retinopathies (see ClinicalTrials.gov).

In conclusion, research into FEVR genetics leads to improvements in the counselling, diagnosis, management and treatment of patients and will ultimately lead to therapies. The work in this thesis adds to these benefits by confirming that *LGR4* is a new gene mutated in autosomal dominant FEVR. This work highlights the utility of combining different functional tests in order to elucidate the pathogenic nature of missense mutations, but also shows that there is much more work needed in this area to create robust, quick assays which can be translated into a diagnostic setting. Furthermore, the identification of LGR4 as a new component of the Norrin- $\beta$ -Catenin signalling pathway helps unravel this complex pathway. This will hopefully lead to an increased understanding of the molecules and pathways controlling retinal angiogenesis and help define new therapies for FEVR and other disorders of the retinal vasculature.

## 7 References

- Adaimy, L., Chouery, E., Me, H., Mroueh, S., Nicolas, E., Belguith, H., Mazancourt, P. De, 2007. Mutation in WNT10A Is Associated with an Autosomal Recessive Ectodermal Dysplasia: The Odonto-onycho-dermal Dysplasia. *American journal of human genetics* **81**, 821–828.
- Adams, R.H., Alitalo, K., 2007. Molecular regulation of angiogenesis and lymphangiogenesis. *Nature Reviews* **8**, 464–478.
- Adzhubei, I.A., Schmidt, S., Peshkin, L., Ramensky, V.E., Gerasimova, A., Bork, P., Kondrashov, A.S., Sunyaev, S.R., 2010. A method and server for predicting damaging missense mutations. *Nature* **7**, 2009–2010.
- Ai, M., Heeger, S., Bartels, C.F., Schelling, D.K., 2005. Clinical and Molecular Findings in Osteoporosis-Pseudoglioma Syndrome. *American journal of human genetics* **77**, 741–753.
- Alexandre, C., Baena-lopez, A., Vincent, J., 2014. Patterning and growth control by membrane - tethered Wingless. *Nature* **505**, 180–185.
- Alvarez, Y., Cederlund, M.L., Cottell, D.C., Bill, B.R., Ekker, S.C., Torres-Vazquez, J., Weinstein, B.M., Hyde, D.R., Vihtelic, T.S., Kennedy, B.N., 2007. Genetic determinants of hyaloid and retinal vasculature in zebrafish. *BMC developmental biology* **7**, 114–131.
- Aoki, M., Mieda, M., Ikeda, T., Hamada, Y., Nakamura, H., Okamoto, H., 2007. R-spondin3 is required for mouse placental development. *Developmental Biology* **301**, 218–226.
- Ashton, N., 1970. Retinal angiogenesis in the human embryo. *Brit Med Bull* **26**, 103–106.
- Assawachananont, J., Mandai, M., Okamoto, S., Yamada, C., Eiraku, M., Yonemura, S., Sasai, Y., Takahashi, M., 2014. Transplantation of Embryonic and Induced Pluripotent Stem Cell-Derived 3D Retinal Sheets into Retinal Degenerative Mice. *Stem Cell Reports* **2**, 662–674.
- Avila-fernandez, A., Perez-carro, R., Corton, M., Lopez-molina, M.I., Campello, L., Garanto, A., Fernandez-sanchez, L., Duijkers, L., Lopez, M.A., Riveiro-alvarez, R., Rodrigues, L., Da, J., Sanchez-alcudia, R.,

- Martin-garrido, E., Reyes, N., Garcia-garcia, F., Dopazo, J., Garcia-sandoval, B., Collin, R.W.J., Cuenca, N., Ayuso, C., 2015. Whole-exome sequencing reveals ZNF408 as a new gene associated with autosomal recessive retinitis pigmentosa with vitreal alterations. *Human molecular genetics* **24**, 4037–4048.
- Bakondi, B., Lv, W., Lu, B., Jones, M.K., Tsai, Y., Kim, K.J., Levy, R., Akhtar, A.A., Breunig, J.J., Svendsen, C.N., Wang, S., 2016. In Vivo CRISPR / Cas9 Gene Editing Corrects Retinal Dystrophy in the S334ter-3 Rat Model of Autosomal Dominant Retinitis Pigmentosa. *Official journal of the American Society of Gene & Cell Therapy* **24**, 556–563.
- Baltimore, B.D., Berg, P., Botchan, M., Carroll, D., Charo, R.A., Church, G., Corn, J.E., Daley, G.Q., Doudna, J.A., Fenner, M., Greely, H.T., Jinek, M., Puck, J., Sternberg, S.H., 2015. A prudent path forward for genomic engineering and germline gene modification. *Science* **348**, 9–12.
- Bamashmus, M. a, Downey, L.M., Inglehearn, C.F., Gupta, S.R., Mansfield, D.C., 2000. Genetic heterogeneity in familial exudative vitreoretinopathy; exclusion of the EVR1 locus on chromosome 11q in a large autosomal dominant pedigree. *The British journal of ophthalmology* **84**, 358–63.
- Bassett, E.A., Tokarew, N., Allemanno, E.A., Mazerolle, C., Morin, K., Mears, A.J., Mcneill, B., Ringuette, R., Campbell, C., Smiley, S., Pokrajac, N.T., Dubuc, A.M., Ramaswamy, V., Northcott, P.A., Remke, M., Monnier, P.P., Potter, D., Paes, K., Kirkpatrick, L.L., 2016. Norrin / Frizzled4 signalling in the preneoplastic niche blocks medulloblastoma initiation. *eLife* **8**, 1–27.
- Bassuk, A.G., Zheng, A., Li, Y., Tsang, S.H., Mahajan, V.B., 2016. Precision Medicine : Genetic Repair of Retinitis Pigmentosa in Patient- Derived Stem Cells. *Scientific reports* **10**, 1–6.
- Beck, L., D'amore, P.A., 1997. Vascular development: cellular and molecular regulation. *FASEB* **11**, 365–373.
- Bedell, V.M., Westcot, S.E., Ekker, S.C., 2011. Lessons from morpholino-based screening in zebrafish. *Briefings in functional genomics* **10**, 181–8.
- Bellingham, J., Davidson, A.E., Aboshiha, J., Simonelli, F., Bainbridge, J.W., Michaelides, M., Spuy, J. Van Der, 2015. Investigation of Aberrant

- Splicing Induced by AIPL1 Variations as a Cause of Leber Congenital Amaurosis. *Investigative Ophthalmology and Visual Science* **56**, 7784–7793.
- Benson, W.E., 1995. Familial exudative vitreoretinopathy. *Transactions of the American Ophthalmological Society* **93**, 473–521.
- Berger, W., Meindl, A., Pol, T.J.R. van de, Cremers, F.P.M., Ropers, H.H., Döerner, C., Monaco, A., Bergen, A.A.B., Lebo, R., Warburg, M., Zergollern, L., Lorenz, B., Gal, A., Bleeker-Wagemakers, E.M., Meitinger, T., 1992. Isolation of a candidate gene for Norrie disease by positional cloning. *Nature Genetics* **1**, 246–250.
- Berger, W., Pol, D. Van De, Bächner, D., Oerlemans, F., Winkens, H., Hameister, H., Wieringa, B., Hendriks, W., Ropers, H., 1996. An animal model for Norrie disease (ND): gene targeting of the mouse ND gene. *Human molecular genetics* **5**, 51–59.
- Bhanot, P., Brink, M., Samos, C.H., Hsieh, J.C., Wang, Y., Macke, J.P., Andrew, D., Nathans, J., and Nusse, R., 1996. A new member of the frizzled family from Drosophila functions as a Wingless receptor. *Nature* **382**, 225–230.
- Bhanot P, Brink M, Samos CH, Hsieh JC, Wang Y, Macke JP, Andrew D, Nathans J, N.R., 1996. A new member of the frizzled family from Drosophila functions as Wingless receptor.
- Bilic, J., Huang, Y., Davidson, G., Zimmermann, T., Cruciat, C., Bienz, M., Niehrs, C., 2007. Wnt Induces LRP6 Signalosomes and Promotes Dishevelled-Dependent LRP6 Phosphorylation. *Science* **316**, 2–6.
- Blaydon, D.C., Ishii, Y., Toole, E.A.O., Unsworth, H.C., Teh, M., Ru, F., Tidman, N., Sinclair, C., Moss, C., Watson, R., Berker, D. De, Wajid, M., Christiano, A.M., Kelsell, D.P., 2006. The gene encoding R-spondin 4 ( RSPO4 ), a secreted protein implicated in Wnt signaling , is mutated in inherited anonychia. *Nature genetics* **38**, 1245–1248.
- Blitzer, J.T., Nusse, R., 2006. A critical role for endocytosis in Wnt signaling. *BMC Cell Biology* **10**, 1–10.
- Brown, N.L., Patel, S., Brzezinski, J., Glaser, T., 2001. Math5 is required for retinal ganglion cell and optic nerve formation. *Development* **128**, 2497–2508.

- Cade, L., Reyon, D., Hwang, W.Y., Tsai, S.Q., Patel, S., Khayter, C., Joung, J.K., Sander, J.D., Peterson, R.T., Yeh, J.J., 2012. Highly efficient generation of heritable zebrafish gene mutations using homo- and heterodimeric TALENs. *Nucleic acids research* **40**, 8001–8010.
- Cai, J., Nelson, K.C., Wu, M., Jr, P.S., Jones, D.P., 2000. Oxidative Damage and Protection of the RPE. *Progress in retinal and eye research* **19**, 205–221.
- Callaway, Fe., 2016. UK scientists gain licence to edit genes in human embryos. *Nature* **530**, 7588.
- Campbell, M., Nguyen, A.T.H., Kiang, A., Tam, L.C.S., Gobbo, O.L., Kerskens, C., Ni, S., Humphries, M.M., Farrar, G., Kenna, P.F., Humphries, P., 2009. An experimental platform for systemic drug delivery to the retina. *Proceedings of the National Academy of Sciences of the United States of America* **106**, 17817–17822.
- Campbell, R.E., Tour, O., Palmer, A.E., Steinbach, P.A., Baird, G.S., Zacharias, D.A., Tsien, R.Y., 2002. A monomeric red fluorescent protein. *Proceedings of the National Academy of Sciences of the United States of America* **99**, 7877–7882.
- Canny, C.L., Oliver, G.L., 1976. Fluorescein angiographic findings in familial exudative vitreoretinopathy. *Archives of ophthalmology* **94**, 1114–20.
- Carmeliet, P., 2003. Angiogenesis in health and disease. *Nature medicine* **9**, 653–660.
- Carmeliet, P., Ferreira, V., Breier, G., Pollefeyt, S., Kieckens, L., Gertsensteins, M., Fahrig, M., Eberhardt, C., Declercq, C., Pawling, J., Moons, L., Collen, D., Risau, W., Nagy, A., 1996. Abnormal blood vessel development and lethality in embryos lacking a single VEGF allele. *Nature* **380**, 435–439.
- Carmon, K.S., Gong, X., Lin, Q., Thomas, A., Liu, Q., 2011. R-spondins function as ligands of the orphan receptors LGR4 and LGR5 to regulate Wnt /  $\beta$  -catenin signaling. *Proceedings of the National Academy of Sciences of the United States of America* **108**, 2–7.
- Carmon, K.S., Lin, Q., Gong, X., Thomas, A., Liu, Q., 2012. LGR5 Interacts and Cointernalizes with Wnt Receptors to Modulate Wnt/ $\beta$ -Catenin Signaling. *Molecular and Cellular Biology* **32**, 2054–2064.

- Caruso, M., Ferranti, F., Scheri, K.C., Dobrowolny, G., 2015. R-Spondin 1/Dickkopf-1/Beta-Catenin Machinery Is Involved in Testicular Embryonic Angiogenesis. *Plos One* **10**, 1–25.
- Chan-ling, T., Mcleod, D.S., Hughes, S., Baxter, L., Chu, Y., Hasegawa, T., Luty, G.A., 2004. Astrocyte – Endothelial Cell Relationships during Human Retinal Vascular Development. *Investigative Ophthalmology and Visual Science* **45**, 2020–2032.
- Chang, T., Hsieh, F., Zebisch, M., Harlos, K., Elegheert, J., Jones, E.Y., 2015. Structure and functional properties of Norrin mimic Wnt for signalling with Frizzled4, Lrp5/6, and proteoglycan. *eLife* **4**, 1–27.
- Chen, J., Stahl, A., Krah, N.M., Seaward, M.R., Dennison, R.J., Sapienza, P., Hua, J., Hatton, C.J., Juan, A.M., Aderman, C.M., Willett, K.L., Guerin, K.I., Mammoto, A., Campbell, M., Smith, L.E.H., 2011. Wnt Signaling Mediates Pathological Vascular Growth in proliferative retinopathy. *Circulation* **124**, 1871–1881.
- Chen, J., Stahl, A., Krah, N.M., Seaward, M.R., Joyal, J., Aimee, M., Hatton, C.J., Aderman, C.M., Dennison, R.J., Willett, K.L., Sapienza, P., Smith, L.E.H., 2012. Retinal Expression of Wnt-Pathway Mediated Genes in Low-Density Lipoprotein Receptor-Related Protein 5 ( Lrp5 ) Knockout Mice. *PloS one* **7**, 1–10.
- Chen, J., Yan, H., Ren, D., Yin, Y., Li, Z., He, Q., Wo, D., Ho, M.S., Chen, Y., Liu, Z., Yang, J., Liu, S., Zhu, W., 2014. LRP6 dimerization through its LDLR domain is required for robust canonical Wnt pathway activation. *Cellular Signalling* **26**, 1068–1074.
- Chen, W., Chen, W., Berge, D., Brown, J., Ahn, S., Hu, L.A., Miller, W.E., Caron, M.G., Barak, L.S., Nusse, R., Lefkowitz, R.J., 2003. Dishevelled 2 Recruits  $\beta$ -Arrestin 2 to Mediate Wnt5A-Stimulated Endocytosis of Frizzled 4. *Science* **301**, 1391–1394.
- Chen, Z.-Y., Battinelli, E.M., Fielder, A., Bunday, S., Sims, K., Breakefield, X.O., Craig, I.W., 1993. A mutation in the Norrie disease gene (NDP) associated with X-linked familial exudative vitreoretinopathy. *Nature genetics* **5**, 180–183.
- Choi, W., Zibae, S., Jakes, R., Serpell, L.C., Davletov, B., Crowther, R.A., Goedert, M., 2004. Mutation E46K increases phospholipid binding and

- assembly into filaments of human alpha-synuclein. *FEBS letters* **576**, 363–368.
- Choi, Y., Sims, G.E., Murphy, S., Miller, J.R., Chan, A.P., 2012. Predicting the Functional Effect of Amino Acid Substitutions and Indels. *PloS one* **7**, 1–13.
- Chu, Y., Hughes, S., Chan-ling, T., Building, A., 2001. Differentiation and migration of astrocyte precursor cells (APCs) and astrocytes in human fetal retina: relevance to optic nerve coloboma. *The FASEB journal* **15**, 2013–2015.
- Clevers, H., Nusse, R., 2012. Wnt/ $\beta$ -catenin signaling and disease. *Cell* **149**, 1192–1205.
- Collin, R.W.J., Nikopoulos, K., Dona, M., Gilissen, C., Hoischen, A., Boonstra, F.N., Poulter, J. a, Kondo, H., Berger, W., Toomes, C., Tahira, T., Mohn, L.R., Blokland, E. a, Hatterschijt, L., Ali, M., Groothuismink, J.M., Duijkers, L., Inglehearn, C.F., Sollfrank, L., Strom, T.M., Uchio, E., van Nouhuys, C.E., Kremer, H., Veltman, J. a, van Wijk, E., Cremers, F.P.M., 2013. ZNF408 is mutated in familial exudative vitreoretinopathy and is crucial for the development of zebrafish retinal vasculature. *Proceedings of the National Academy of Sciences of the United States of America* **110**, 9856–61.
- Collins, J., Schwartz, C., 2002. Detecting Polymorphisms and Mutations in Candidate Genes. *American journal of human genetics* **1250**, 1251–1252.
- Coppieters, F., Ascari, G., Dannhausen, K., Nikopoulos, K., Meunier, I., Peelman, F., Karlstetter, M., Xu, M., Tsilimbaris, M.K., Tsika, C., Blazaki, S. V, Vergult, S., Farinelli, P., Laethem, T. Van, Bauwens, M., Bruyne, M. De, Chen, R., Langmann, T., 2016. Isolated and Syndromic Retinal Dystrophy Caused by Biallelic Mutations in RCBTB1, a Gene Implicated in Ubiquitination. *American journal of human genetics* **99**, 470–480.
- Corish, P., Tyler-Smith, C., 1999. Attenuation of green fluorescent protein half-life in mammalian cells. *Protein engineering* **12**, 1035–1040.
- Costa, G., Harrington, K.I., Lovegrove, H.E., Page, D.J., Chakravartula, S., Bentley, K., Herbert, S.P., 2016. Asymmetric division coordinates collective cell migration in angiogenesis. *Nature Cell Biology* **18**, 1292–

1301.

- Cruciat, C.-M., Niehrs, C., 2013. Secreted and transmembrane Wnt inhibitors and activators. *Cold Spring Harb Perspect Biol* **5**, 1–26.
- D. Scott McLeod, Takuya Hasegawa, Tarl Prow, Carol Merges, and G.L., 2006. The Initial Fetal Human Retinal Vasculature Develops by Vasculogenesis. *Dev Dyn.* **235**, 3336–3347.
- Dann, C.E., Hsieh, J., Rattner, A., Sharma, D., 2001. Insights into Wnt binding and signalling from the structures of two Frizzled cysteine-rich domains. *Nature* **412**, 86–90.
- Deng, C., Reddy, P., Cheng, Y., Luo, C.-W., Hsiao, C.-L., Hsueh, A.J.W., 2013. Multi-functional norrin is a ligand for the LGR4 receptor. *Journal of cell science* **126**, 2060–8.
- Diehl, A.G., Zarepari, S., Qian, M., Khanna, R., Angeles, R., Gage, P.J., 2006. Extraocular Muscle Morphogenesis and Gene Expression Are Regulated by Pitx2 Gene Dose. *Investigative Ophthalmology and Visual Science* **47**, 1785–1793.
- Donovan, D., Brown, N.J., Bishop, E.T., Lewis, C.E., 2001. Comparison of three in vitro human “angiogenesis” assays with capillaries formed in vivo. *Angiogenesis* **4**, 113–121.
- Downey, L.M., Bottomley, H.M., Sheridan, E., Ahmed, M., Gilmour, D.F., Inglehearn, C.F., Reddy, a, Agrawal, a, Bradbury, J., Toomes, C., 2006. Reduced bone mineral density and hyaloid vasculature remnants in a consanguineous recessive FEVR family with a mutation in LRP5. *The British journal of ophthalmology* **90**, 1163–7.
- Downey, L.M., Keen, T.J., Roberts, E., Mansfield, D.C., Bamashmus, M., Inglehearn, C.F., 2001. A new locus for autosomal dominant familial exudative vitreoretinopathy maps to chromosome 11p12-13. *American journal of human genetics* **68**, 778–81.
- Dumont, D.J., Jussila, L., Taipale, J., Lymboussaki, A., Mustonen, T., Pajusola, K., Breitman, M., Alitalo, K., Carmeliet, P., Shalaby, F., Ferrara, N., Davis-Smyth, T., Korpelainen, E.I., Alitalo, K., Park, J.E., Sawano, A., Olofsson, B., Jeltsch, M., Oh, S.J., Joukov, V., Lee, J., Achen, M.G., Eichmann, A., Kaipainen, A., Kukk, E., Puri, M.C., Sabin, F.R., Risau, W., Vecchi, A., Rossant, J., Hiratsuka, S., Visvader, J.E.,

- Fujiwara, Y., Orkin, S.H., Wang, L.C., Carmeliet, P., Wojnowski, L., Sato, T.N., Wang, H.U., Chen, F.-F., Anderson, D.J., Oshima, M., Oshima, H., Taketo, M.M., Suri, C., Lindahl, P., Kuo, C.T.K., 1998. Cardiovascular failure in mouse embryos deficient in VEGF receptor-3. *Science* **282**, 946–9.
- Dunn, K.W., Kamocka, M.M., McDonald, J.H., 2011. A practical guide to evaluating colocalization in biological microscopy. *American journal of physiology* **300**, 723–742.
- Duplaa, C., Jaspard, B., Moreau, C., Amore, P.A.D., 1999. Identification and Cloning of a Secreted Protein Related to the Cysteine-Rich Domain of Frizzled Evidence for a Role in Endothelial Cell Growth Control. *Circulation Research* **84**, 1433–1445.
- Dyer, M.A., Cepko, C.L., 2001. Regulating proliferation during retinal development. *Nature reviews. Neuroscience* **2**, 333–342.
- Easwaran, V., Lee, S.H., Inge, L., Guo, L., Goldbeck, C., Garrett, E., Wiesmann, M., Garcia, P.D., Fuller, J.H., Chan, V., Randazzo, F., Gundel, R., Warren, R.S., Escobedo, J., Aukerman, S.L., Taylor, R.N., Fantl, W.J., 2003.  $\beta$ -Catenin Regulates Vascular Endothelial Growth Factor Expression in Colon Cancer. *Cancer Research* **63**, 3145–3153.
- Eisen, J.S., Smith, J.C., 2008. Controlling morpholino experiments: don't stop making antisense. *Development* **135**, 1735–43.
- Ekker, S.C., 2000. Morphants: a new systematic vertebrate functional genomics approach. *Yeast* **17**, 302–306.
- Ellertsdóttir, E., Lenard, A., Blum, Y., Krudewig, A., Herwig, L., Affolter, M., Belting, H.-G., 2010. Vascular morphogenesis in the zebrafish embryo. *Developmental biology* **341**, 56–65.
- Exome Aggregation Consortium, M.L., Karczewski, K.J., Eric V Minikel, Samocha, K.E., Banks, E., Timothy Fennell, O'Donnell, A.H.L., Ware, J.S., Hill, A.J., Ber, L.O., Peloso, G.M., Poplin, R., Rivas, M.A., Ruano-Rubio, V., Ruderfer, D.M., Shakir, K., Stenson, P.D., Stevens, C., Thomas, B.P., Tiao, G., Tusie-Luna, M.T., Weisburd, B., Won, H.-H., Yu, D., Altshuler, D.M., Ardissino, D., B, M., Watkins, H.C., Wilson, J.G., Daly, M.J., MacArthur, D.G., 2015. Analysis of protein-coding genetic variation in 60,706 humans 2. *Nature* **536**, 285–291.

- Fantin, A., Vieira, J.M., Gestri, G., Denti, L., Schwarz, Q., Prykhozhij, S., Peri, F., Wilson, S.W., Ruhrberg, C., 2010. Tissue macrophages act as cellular chaperones for vascular anastomosis downstream of VEGF-mediated endothelial tip cell induction. *Blood* **116**, 829–841.
- Farin, H.F., Jordens, I., Mosa, M.H., Basak, O., Korving, J., Tauriello, D.V.F., Punder, K. De, Angers, S., Peters, P.J., Maurice, M.M., Clevers, H., 2016. Visualization of a short-range Wnt gradient in the intestinal stem-cell niche. *Nature* **530**, 340–343.
- Fei, P., Zhang, Q., Huang, L., Xu, Y., Zhu, X., Tai, Z., Gong, B., Ma, S., Yao, Q., Li, J., Zhao, P., Yang, Z., 2014. Identification of two novel LRP5 mutations in families with familial exudative vitreoretinopathy. *Molecular vision* **20**, 395–409.
- Feldman, L., Davis, K.L., Komel, R., Sytkowski, A.J., 2006. Variability in the immunodetection of His-tagged recombinant proteins. *Analytical Biochemistry* **359**, 216–223.
- Ferrari, S.L., Deutsch, S., Choudhury, U., Chevalley, T., Bonjour, J.-P., Dermitzakis, E.T., Rizzoli, R., Antonarakis, S.E., 2004. Polymorphisms in the low-density lipoprotein receptor-related protein 5 (LRP5) gene are associated with variation in vertebral bone mass, vertebral bone size, and stature in whites. *American journal of human genetics* **74**, 866–75.
- Folkman, J., 2007. Angiogenesis: an organizing principle for drug discovery? *Nature Reviews* **6**, 273–286.
- Fong, G.-H., Rossant, J., Gershenstein, M., Breltman, M.L., 1995. Role of the Flt-1 receptor tyrosine kinase in regulating the assembly of vascular endothelium. *Nature* **376**, 66–70.
- Frebourg, T., 2014. The Challenge for the Next Generation of Medical. *Human mutation* **35**, 909–911.
- Friis, T., Engel, A., Klein, B.M., Rygaard, J., Houen, G., 2005. Levamisole inhibits angiogenesis in vitro and tumor growth in vivo. *Angiogenesis* **8**, 25–34.
- Frojmark, A.-S., Schuster, J., Sobol, M., Entesarian, M., Kilander, M.B.C., Gabrikova, D., Nawaz, S., Baig, S.M., Schulte, G., Klar, J., Dahl, N., 2011. Mutations in Frizzled 6 Cause Isolated Autosomal-recessive Nail Dysplasia. *American journal of human genetics* **88**, 852–860.

- Fruttiger, M., 2007. Development of the retinal vasculature. *Angiogenesis* **10**, 77–88.
- Fruttiger, M., 2001. Development of the Mouse Retinal Vasculature : Angiogenesis Versus Vasculogenesis. *Investigative Ophthalmology and Visual Science* **43**, 522–527.
- Fruttiger, M., Calver, A.R., Kru, W.H., Mudhar, H.S., Michalovich, D., Takakura, N., Nishikawa, S.I., Richardson, W.D., 1996. PDGF Mediates a Neuron – Astrocyte Interaction in the Developing Retina. *Neuron* **17**, 1117–1131.
- Fruttiger, M., Calver, A.R., Richardson, W.D., 2000. Platelet-derived growth factor is constitutively secreted from neuronal cell bodies but not from axons. *Current Biology* **10**, 1283–1286.
- Gal, M., Levanon, E.Y., Hujeirat, Y., Khayat, M., Pe'er, J., Shalev, S., 2014. Novel mutation in TSPAN12 leads to autosomal recessive inheritance of congenital vitreoretinal disease with intra-familial phenotypic variability. *American journal of medical genetics* **23**, 1–7.
- Gale, N.W., Dominguez, M.G., Noguera, I., Pan, L., Hughes, V., Valenzuela, D.M., Murphy, A.J., Adams, N.C., Lin, H.C., Holash, J., Thurston, G., Yancopoulos, G.D., 2004. Haploinsufficiency of delta-like 4 ligand results in embryonic lethality due to major defects in arterial and vascular development. *Proceedings of the National Academy of Sciences of the United States of America* **101**, 15949–54.
- García-mata, R., Bebök, Z., Sorscher, E.J., Sztul, E.S., Cell, P.J.T.J., To, B., 1999. Characterization and Dynamics of Aggresome Formation by a. *The Journal of Cell Biology* **146**, 1239–1254.
- Gariano, R.F., 2003. Cellular mechanisms in retinal vascular development. *Progress in Retinal and Eye Research* **22**, 295–306.
- Gariano, R.F., Iruela-arispe, M.L., Hendrickson, A.E., 1994. Vascular Development in Primate Retina: Comparison of Lamina Plexus Formation in Monkey and Human. *Investigative Ophthalmology and Visual Science* **35**, 3442–3455.
- Gerhardt, H., Golding, M., Fruttiger, M., Ruhrberg, C., Lundkvist, A., Abramsson, A., Jeltsch, M., Mitchell, C., Alitalo, K., Shima, D., Betsholtz, C., 2003. VEGF guides angiogenic sprouting utilizing endothelial tip cell

- filopodia. *J. Cell Biol.* **161**, 1163–1178.
- Gilmour, D.F., 2015. Familial exudative vitreoretinopathy and related retinopathies. *Eye* **29**, 1–14.
- Glinka, A., Dolde, C., Kirsch, N., Huang, Y.-L., Kazanskaya, O., Ingelfinger, D., Boutros, M., Cruciat, C.-M., Niehrs, C., 2011. LGR4 and LGR5 are R-spondin receptors mediating Wnt/ $\beta$ -catenin and Wnt/PCP signalling. *EMBO reports* **12**, 1055–61.
- Goldstein, B., Takeshita, H., Mizumoto, K., Sawa, H., Hill, C., Carolina, N., 2006. Wnt Signals Can Function as Positional Cues in Establishing Cell Polarity. *Developmental Cell* **10**, 391–396.
- Goldstein, D.B., Allen, A., Keebler, J., Margulies, E.H., 2013. Sequencing studies in human genetics: design and interpretation. *Nature reviews. Genetics* **14**, 460–470.
- Gong, Y., Bourhis, E., Chiu, C., Stawicki, S., Dealmeida, V.I., Liu, B.Y., Cao, T.C., Carano, R.A.D., Ernst, J.A., Solloway, M., Rubinfeld, B., Hannoush, R.N., Wu, Y., Polakis, P., Costa, M., 2010. Wnt Isoform-Specific Interactions with Coreceptor Specify Inhibition or Potentiation of Signaling by LRP6 Antibodies. *PloS one* **5**, e12682.
- Gong, Y., Slee, R.B., Fukai, N., Rawadi, G., Roman-Roman, S., Reginato, a M., Wang, H., Cundy, T., Glorieux, F.H., Lev, D., Zacharin, M., Oexle, K., Marcelino, J., Suwairi, W., Heeger, S., Sabatakos, G., Apte, S., Adkins, W.N., Allgrove, J., Arslan-Kirchner, M., Batch, J. a, Beighton, P., Black, G.C., Boles, R.G., Boon, L.M., Borrone, C., Brunner, H.G., Carle, G.F., Dallapiccola, B., De Paepe, a, Floege, B., Halfhide, M.L., Hall, B., Hennekam, R.C., Hirose, T., Jans, a, Jüppner, H., Kim, C. a, Keppler-Noreuil, K., Kohlschuetter, a, LaCombe, D., Lambert, M., Lemyre, E., Letteboer, T., Peltonen, L., Ramesar, R.S., Romanengo, M., Somer, H., Steichen-Gersdorf, E., Steinmann, B., Sullivan, B., Superti-Furga, a, Swoboda, W., van den Boogaard, M.J., Van Hul, W., Vikkula, M., Votruba, M., Zabel, B., Garcia, T., Baron, R., Olsen, B.R., Warman, M.L., 2001. LDL receptor-related protein 5 (LRP5) affects bone accrual and eye development. *Cell* **107**, 513–23.
- Gonzalez-paredes, F.J., Ramos-trujillo, E., Claverie-martin, F., 2015. Three exonic mutations in polycystic kidney disease-2 gene (PKD2) alter

- splicing of its pre-mRNA in a minigene system. *Gene* **578**, 117–123.
- Gore, A. V., Swift, M.R., Cha, Y.R., Lo, B., Mckinney, M.C., Li, W., Castranova, D., Davis, A., Mukoyama, Y., Weinstein, B.M., 2011. Rspo1 / Wnt signaling promotes angiogenesis via Vegfc / Vegfr3. *Development* **4886**, 4875–4886.
- Graw, J., 2003. The genetic and molecular basis of congenital eye defects. *Nature reviews. Genetics* **4**, 876–888.
- Gu, X., Neric, N.J., Crabb, J.S., Crabb, J.W., Bhattacharya, S.K., Rayborn, M.E., Hollyfield, J.G., Bonilha, V.L., 2012. Age-Related Changes in the Retinal Pigment Epithelium (RPE). *PloS one* **7**, e38673.
- Hackett, S.F., Wiegand, S., Yancopoulos, G., Campochiaro, P.A., 2002. Angiopoietin-2 Plays an Important Role in Retinal Angiogenesis. *Journal of Cellular Physiology* **187**, 182–187.
- Halfter, W., Willem, M., Mayer, U., 2005. Basement Membrane – Dependent Survival of Retinal Ganglion Cells. *Investigative ophthalmology & visual science* **46**, 1000–1009.
- Han, C., Yan, D., Belenkaya, T.Y., Lin, X., 2005. Drosophila glypicans Dally and Dally-like shape the extracellular Wingless morphogen gradient in the wing disc. *Development* **132**, 667–679.
- Han, Y., Mu, Y., Li, X., Xu, P., Tong, J., Liu, Z., 2011. Grhl2 deficiency impairs otic development and hearing ability in a zebrafish model of the progressive dominant hearing loss DFNA28. *Human molecular genetics* **20**, 3213–3226.
- Hao, H.-X., Xie, Y., Zhang, Y., Charlat, O., Oster, E., Avello, M., Lei, H., Mickanin, C., Liu, D., Ruffner, H., Mao, X., Ma, Q., Zamponi, R., Bouwmeester, T., Finan, P.M., Kirschner, M.W., Porter, J. a, Serluca, F.C., Cong, F., 2012. ZNRF3 promotes Wnt receptor turnover in an R-spondin-sensitive manner. *Nature* **485**, 195–200.
- Hao, J., Ao, A., Zhou, L., Murphy, C.K., Frist, A.Y., Keel, J.J., Thorne, C. a, Kim, K., Lee, E., Hong, C.C., 2013. Selective small molecule targeting  $\beta$ -catenin function discovered by in vivo chemical genetic screen. *Cell reports* **4**, 898–904.
- Hasegawa, T., Mcleod, D.S., Prow, T., Merges, C., Grebe, R., Lutty, G.A., 2008. Vascular Precursors in Developing Human Retina. *Investigative*

*Ophthalmology and Visual Science* **49**, 2178–2192.

- Hauser, F., Nothacker, H., Grimmelikhuijzen, C.J.P., Ø, D.-C., 1997. Molecular Cloning , Genomic Organization , and Developmental Regulation of a Novel Receptor from *Drosophila melanogaster* Structurally Related to Members of the Thyroid-stimulating Hormone , Follicle-stimulating Hormone , Luteinizing Hormone / Choriogonadotropin. *The Journal of biological chemistry* **272**, 1002–1010.
- He, J., Liu, X., Zhang, S., Liu, G., Hnatowich, D.J., 2005. Affinity Enhancement Bivalent Morpholinos for Pretargeting: Surface Plasmon Resonance Studies of Molecular Dimensions. *Bioconjugate Chem.* **16**, 1098–1104.
- Hellström, M., Phng, L.K., Gerhardt, H., 2007. VEGF and Notch signaling: the yin and yang of angiogenic sprouting. *Nature* **1**, 133–136.
- Henikoff, S., Henikoff, J.G., 1993. Performance Evaluation of Amino Acid Substitution Matrices. *Proteins: Structure, Function and Genetics* **61**, 49–61.
- Henry, C.R., Sisk, R.A., Tzu, J.H., Albin, T.A., Davis, J.L., Murray, T.G., Berrocal, A.M., 2015. Long-term follow-up of intravitreal bevacizumab for the treatment of pediatric retinal and choroidal diseases. *Journal of AAPOS* **19**, 541–548.
- Hetheridge, C., Mavria, G., Mellor, H., 2011. Uses of the in vitro endothelial – fibroblast organotypic co-culture assay in angiogenesis research. *Advances in the Cellular and Molecular Biology of Angiogenesis* **39**, 1597–1600.
- Hicks, S., Wheeler, D.A., Plon, S.E., Å, M.K., 2011. Prediction of Missense Mutation Functionality Depends on Both the Algorithm and Sequence Alignment Employed. *Human mutation* **32**, 661–668.
- Hirose, K., Shimoda, N., Kikuchi, Y., 2011. Expression patterns of *Igr4* and *Igr6* during zebrafish development. *Gene Expression Patterns* **11**, 378–383.
- Hollon, T., Yoshimuraty, F.M.K., 1989. Variation in Enzymatic Transient Gene Expression Assays. *Analytical Biochemistry* **418**, 411–418.
- Hoon, M., Okawa, H., Santana, L. Della, Wong, R.O.L., 2014. Functional architecture of the retina : Development and disease. *Progress in Retinal*

*and Eye Research* **42**, 44–84.

- Hoshii, T., Takeo, T., Nakagata, N., Takeya, M., Araki, K., Yamamura, K., 2007. LGR4 regulates the postnatal development and integrity of male reproductive tracts in mice. *Biology of reproduction* **76**, 303–13.
- Howe, K., Clark, M.D., Torroja, C.F., Torrance, J., Berthelot, C., Muffato, M., Collins, J.E., Humphray, S., McLaren, K., Matthews, L., McLaren, S., Sealy, I., Caccamo, M., White, S., Chow, W., Kilian, B., Churcher, C., Scott, C., Barrett, J.C., Koch, R., Zhou, Y., Gu, Y., Yen, J., Vogel, J., Eyre, T., Redmond, S., Banerjee, R., Chi, J., Fu, B., Langley, E., Maguire, S.F., Laird, G.K., Lloyd, D., Kenyon, E., Donaldson, S., Sehra, H., Almeida-king, J., Loveland, J., Trevanion, S., Jones, M., Quail, M., Willey, D., Hunt, A., Burton, J., Sims, S., Mclay, K., Plumb, B., Davis, J., Clee, C., Oliver, K., Clark, R., Riddle, C., Elliot, D., Threadgold, G., Harden, G., Ware, D., Begum, S., Mortimore, B., Kerry, G., Heath, P., Phillimore, B., Tracey, A., Corby, N., Dunn, M., Johnson, C., Wood, J., Clark, S., Pelan, S., Griffiths, G., Smith, M., Glithero, R., Howden, P., Barker, N., Lloyd, C., Stevens, C., Harley, J., Holt, K., Panagiotidis, G., Lovell, J., Beasley, H., Henderson, C., Gordon, D., Auger, K., Wright, D., Collins, J., Raisen, C., Dyer, L., Leung, K., Robertson, L., Ambridge, K., Leongamornlert, D., Mcguire, S., Gilderthorp, R., Griffiths, C., Manthravadi, D., Nichol, S., Barker, G., Whitehead, S., Kay, M., Brown, J., Murnane, C., Gray, E., Humphries, M., Sycamore, N., Barker, D., Saunders, D., Wallis, J., Babbage, A., Hammond, S., Mashreghi-mohammadi, M., Barr, L., Martin, S., Wray, P., Ellington, A., Matthews, N., Ellwood, M., Woodmansey, R., Clark, G., Cooper, J.D., Tromans, A., Grafham, D., Skuce, C., Pandian, R., Andrews, R., Harrison, E., Kimberley, A., Garnett, J., Fosker, N., Hall, R., Garner, P., Kelly, D., Bird, C., Palmer, S., Gehring, I., Osoegawa, K., Zhu, B., Rapp, A., Widaa, S., Rogers, J., Stemple, D.L., 2013. The zebrafish reference genome sequence and its relationship to the human genome. *Nature* **496**, 2–8.
- HP, N., Grimmelikhuijzen, C., 1993. Molecular cloning of a novel, putative G protein-coupled receptor from sea anemones structurally related to members of the FSH, TSH, LH/CG receptor family from mammals.

- Biochemical and biophysical research communications* **197**, 1062–1069.
- Hsieh, J.C., Kodjabachian, L., Rebert, M.L., Rattner, A., Smallwood, P.M., Samos, C.H., Nusse, R., Dawid, I.B., and Nathans, J., 1999. Biochemical characterization of Wnt-Frizzled interactions using a soluble, biologically active vertebrate Wnt protein. *Proceedings of the National Academy of Sciences of the United States of America* **96**, 3546–3551.
- Hsu, P.-J., Wu, F.-J., Kudo, M., Hsiao, C.-L., Hsueh, A.J.W., Luo, C.-W., 2014. A naturally occurring lgr4 splice variant encodes a soluble antagonist useful for demonstrating the gonadal roles of lgr4 in mammals. *PloS one* **9**, e106804.
- Hsu, S.Y., Kudo, M., Chen, T., Nakabayashi, K., Bhalla, A., Spek, P.J. Van Der, Duin, M. Van, Hsueh, A.J.W., Biology, R., 2000. The Three Subfamilies of Leucine- Rich Repeat-Containing G Protein- Coupled Receptors (LGR): Identification of LGR6 and LGR7 and the Signaling Mechanism for LGR7. *Molecular Endocrinology* **14**, 1257–1271.
- Hsu, S.Y., Liang, S., Hsueh, A.J.W., 1998. Characterization of Two LGR Genes Homologous to Gonadotropin and Thyrotropin Receptors with Extracellular Leucine-Rich Repeats and a Transmembrane Region. *Molecular Endocrinology* **12**, 1830–1845.
- Hsu, S.Y., Nakabayashi, K., Nishi, S., Kumagai, J., Kudo, M., Sherwood, O.D., Hsueh, A.J.W., 2002. Activation of Orphan Receptors by the Hormone Relaxin. *Science* **932**, 671–675.
- Hughes, S., Yang, H., Chan-ling, T., 2000. Vascularization of the Human Fetal Retina : Roles of Vasculogenesis and Angiogenesis. *Investigative ophthalmology & visual science* **45**, 1217–1228.
- Hwang, W.Y., Fu, Y., Reyon, D., Maeder, M.L., Tsai, S.Q., Sander, J.D., Peterson, R.T., Yeh, J.J., Joung, J.K., 2013. Efficient genome editing in zebrafish using a CRISPR-Cas system. *Nature biotechnology* **31**, 2012–2014.
- Ishikawa, T., Tamai, Y., Zorn, A.M., Yoshida, H., Seldin, M.F., Nishikawa, S., Taketo, M.M., 2001. Mouse Wnt receptor gene Fzd5 is essential for yolk sac and placental angiogenesis. *Development* **33**, 25–33.
- Jakobsson, L., Franco, C.A., Bentley, K., Collins, R.T., Ponsioen, B., Aspalter, I.M., Busse, M., Thurston, G., Medvinsky, A., Schulte-merker,

- S., Gerhardt, H., 2010. Endothelial cells dynamically compete for the tip cell position during angiogenic sprouting. *Nature Cell Biology* **12**, 943–953.
- Janda, C.Y., Waghray, D., Levin, A.M., Thomas, C., Garcia, K.C., 2012. Structural Basis of Wnt Recognition by Frizzled. *Science* **337**, 2–9.
- Jansson, L., Kim, G.S., Cheng, A.G., 2015. Making sense of Wnt signaling — linking hair cell regeneration to development. *Frontiers in Cellular Neuroscience* **9**, 1–12.
- Jeays-ward, K., Hoyle, C., Brennan, J., Dandonneau, M., Alldus, G., Capel, B., Swain, A., 2003. Endothelial and steroidogenic cell migration are regulated by WNT4 in the developing mammalian gonad. *Development* **2**, 3663–3670.
- Jiang, X., Charlat, O., Zamponi, R., Yang, Y., Cong, F., 2015. Dishevelled Promotes Wnt Receptor Degradation through Recruitment of ZNRF3 / RNF43 E3. *Molecular Cell* **58**, 522–533.
- Jiang, X., Cong, F., 2016. Novel Regulation of Wnt Signaling at the Proximal Membrane Level. *Trends in Biochemical Science* **41**, 773–783.
- Jiao, X., Ventruto, V., Trese, M.T., Shastry, B.S., Hejtmancik, J.F., 2004. Autosomal recessive familial exudative vitreoretinopathy is associated with mutations in LRP5. *American journal of human genetics* **75**, 878–84.
- Jin, C., Yin, F., Lin, M., Li, H., Wang, Z., Weng, J., 2008. GPR48 Regulates Epithelial Cell Proliferation and Migration by Activating EGFR during Eyelid Development. *Investigative ophthalmology & visual science* **49**, 4245–4253.
- Jin, L., Jiang, Q., Wu, Z., Shao, C., Zhou, Y., Yang, L., Uitto, J., Wang, G., 2015. Genetic Heterogeneity of Pseudoxanthoma Elasticum: The Chinese Signature Profile of ABCC6 and ENPP1 Mutations. *Journal of Investigative Dermatology* **135**, 1294–1302.
- Johnston, J.A., Ward, C.L., Kopito, R.R., 1998. Aggresomes: A Cellular Response to Misfolded Proteins. *The Journal of Cell Biology* **143**, 1883–1898.
- Jones, M.C., Caswell, P.T., Roberts, M., Simon, T., Gampel, A., Mellor, H., Norman, J.C., Glasgow, G., 2009. VEGFR1 (Flt1) Regulates Rab4

- Recycling to Control Fibronectin Polymerization and Endothelial Vessel Branching. *Traffic* **10**, 754–766.
- Jr, J.P., Janku, F., 2014. Pharmacology & Therapeutics Molecular targets for cancer therapy in the PI3K / AKT / mTOR pathway. *Pharmacology and Therapeutics* **142**, 164–175.
- Jun Yamashita, Hiroshi Itoh, Masanori Hirashima, Minetaro Ogawa, Satomi Nishikawa, Takami Yurugi, Makoto Naito, K.N.& S.-I.N., 2000. Flk1-positive cells derived from embryonic stem cells. *Nature* **408**, 92–96.
- Junge, H.J., Yang, S., Burton, J.B., Paes, K., Shu, X., French, D.M., Costa, M., Rice, D.S., Ye, W., 2009. TSPAN12 regulates retinal vascular development by promoting Norrin- but not Wnt-induced FZD4/beta-catenin signaling. *Cell* **139**, 299–311.
- Kajava, A. V, 1998. Structural Diversity of Leucine-rich Repeat Proteins. *J. Mol. Biol.* **277**, 519–527.
- Kato, M., Patel, M.S., Levasseur, R., Lobov, I., Chang, B.H., Li, D.A.G., Hartmann, C., Li, L., Hwang, T., Brayton, C.F., Lang, R.A., Karsenty, G., Chan, L., 2002. Cbfa1 -independent decrease in osteoblast proliferation, osteopenia, and persistent embryonic eye vascularization in mice deficient in Lrp5, a Wnt coreceptor. *The Journal of Cell Biology* **157**, 303–314.
- Kato, S., Matsubara, M., Mohri, T., Yasuaki, M., Kazama, I., Hatano, R., Umezawa, A., Nishimori, K., 2006. Leucine-Rich Repeat-Containing G Protein-Coupled Receptor-4 (LGR4, Gpr48) Is Essential for Renal Development in Mice. *Nephron Exp Nephrol* **104**, 63–76.
- Kato, S., Mohri, Y., Matsuo, T., Ogawa, E., Umezawa, A., Okuyama, R., Nishimori, K., 2007. Eye-open at birth phenotype with reduced keratinocyte motility in LGR4 null mice. *FEBS letters* **581**, 4685–90.
- Kaur, S., Leszczynska, K., Abraham, S., Scarcia, M., Hiltbrunner, S., Marshall, C.J., Mavria, G., Bicknell, R., Heath, V.L., 2011. RhoJ / TCL Regulates Endothelial Motility and Tube Formation and Modulates Actomyosin Contractility and Focal Adhesion Numbers. *Arterioscler Thromb Vasc Bio* **31**, 657–664.
- Kay, J.N., Finger-baier, K.C., Roeser, T., Staub, W., Baier, H., 2001. Retinal Ganglion Cell Genesis Requires Iakritz , a Zebrafish atonal Homolog.

*Neuron* **30**, 725–736.

Kaykas, A., Yang-snyder, J., Héroux, M., Shah, K. V, Bouvier, M., Moon, R.T., 2004. Mutant Frizzled 4 associated with vitreoretinopathy traps wild-type Frizzled in the endoplasmic reticulum by oligomerization.

*Nature Cell Biology* **6**, 52–58.

Kazanskaya, O., Glinka, A., Barrantes, B., Stannek, P., Niehrs, C., Wu, W., 2004. R-Spondin2 Is a Secreted Activator of Wnt /  $\beta$ -Catenin Signaling and Is Required for *Xenopus* Myogenesis. *Developmental Cell* **7**, 525–534.

Kazanskaya, O., Ohkawara, B., Herout, M., Wu, W., Maltry, N., Augustin, H.G., Niehrs, C., 2008. The Wnt signaling regulator R-spondin 3 promotes angioblast and vascular development. *Development* **135**, 3655–3664.

Ke, J., Harikumar, K.G., Erice, C., Chen, C., Gu, X., Wang, L., Parker, N., Cheng, Z., Xu, W., Williams, B.O., Melcher, K., Miller, L.J., Xu, H.E., 2013. Structure and function of Norrin in assembly and activation of a Frizzled 4-Lrp5/6 complex. *Genes & development* **27**, 2305–19.

Kent, W.J., Sugnet, C.W., Furey, T.S., Roskin, K.M., Pringle, T.H., Zahler, A.M., Haussler, D., 2002. The Human Genome Browser at UCSC. *Genome Research* **12**, 996–1006.

Khan, A.O., Lenzner, S., Bolz, H.J., 2016. A family harboring homozygous *FZD4* deletion supports the existence of recessive *FZD4*-related familial exudative vitreoretinopathy. *Ophthalmic Genetics* **6810**, 1–3.

Khan, K., Logan, C. V, McKibbin, M., Sheridan, E., Elçioğlu, N.H., Yenice, O., Parry, D. a, Fernandez-Fuentes, N., Abdelhamed, Z.I. a, Al-Maskari, A., Poulter, J. a, Mohamed, M.D., Carr, I.M., Morgan, J.E., Jafri, H., Raashid, Y., Taylor, G.R., Johnson, C. a, Inglehearn, C.F., Toomes, C., Ali, M., 2012. Next generation sequencing identifies mutations in Atonal homolog 7 (ATOH7) in families with global eye developmental defects. *Human molecular genetics* **21**, 776–83.

Kikuchi, A., Yamamoto, H., Kishida, S., 2007. Multiplicity of the interactions of Wnt proteins and their receptors. *Cellular Signalling* **19**, 659–671.

Kikuchi, A., Yamamoto, H., Sato, A., Matsumoto, S., 2011. New Insights into

the Mechanism of Wnt Signaling Pathway Activation, International Review of Cell and Molecular Biology. Elsevier Inc.

- Kim, K., Kakitani, M., Zhao, J., Oshima, T., Tang, T., Binnerts, M., Liu, Y., Boyle, B., Park, E., Emtage, P., Funk, W.D., Tomizuka, K., 2005. Mitogenic Influence of Human R-Spondin1 on the Intestinal Epithelium. *Science* **309**, 1256–1260.
- Kimelman, D., Xu, W., 2006.  $\beta$ -Catenin destruction complex: insights and questions from a structural perspective. *Oncogene* **25**, 7482–7491.
- Kircher, M., Witten, D.M., Jain, P., Roak, B.J.O., Cooper, G.M., Shendure, J., 2014. A general framework for estimating the relative pathogenicity of human genetic variants. *Nature genetics* **46**, 310–315.
- Kishida, M., Koyama, S., Kishida, S., Matsubara, K., Nakashima, S., 1999. Axin prevents Wnt-3a-induced accumulation of  $\beta$ -catenin. *Oncogene* **18**, 979–985.
- Kok, F.O., Shin, M., Ni, C., Gupta, A., Grosse, A.S., Impel, A. Van, Kirchmaier, B.C., Peterson-maduro, J., Kourkoulis, G., Male, I., Desantis, D.F., Sheppard-tindell, S., Ebarasi, L., Betsholtz, C., Schulte-merker, S., Wolfe, S.A., Lawson, N.D., 2015. Reverse Genetic Screening Reveals Poor Correlation between Morpholino-Induced and Mutant Phenotypes in Zebrafish. *Developmental Cell* **32**, 97–108.
- Koo, B., Spit, M., Jordens, I., Low, T.Y., Stange, D.E., Wetering, M. Van De, Es, J.H. Van, Mohammed, S., Heck, A.J.R., Maurice, M.M., Clevers, H., 2012. Tumour suppressor RNF43 is a stem-cell E3 ligase that induces endocytosis of Wnt receptors. *Nature* **488**, 665–669.
- Koos, B., Andersson, L., Clausson, C.-M., Grannas, K., Klaesson, A., Cane, G., Söderberg, O., 2014. Analysis of Protein Interactions in situ by Proximity Ligation Assays. *Topics in Microbiology and Immunology* **377**, 111–126.
- Korinek, V., Korinek, V., Barker, N., Morin, P.J., Wichen, D. Van, Weger, R. De, Kinzler, K.W., Vogelstein, B., Clevers, H., 1997. Constitutive Transcriptional Activation by a  $\beta$ -Catenin – Tcf Complex in APC  $-/-$  Colon Carcinoma. *Science* **275**, 1784–1787.
- Krebs, L.T., Xue, Y., Norton, C.R., Shutter, J.R., Maguire, M., Sundberg, J.P., Gallahan, D., Closson, V., Kitajewski, J., Callahan, R., Smith, G.H.,

- Stark, K.L., Gridley, T., 2000. Notch signaling is essential for vascular morphogenesis in mice. *Genes & development* **14**, 1343–1352.
- Kudo, M., Chen, T., Nakabayashi, K., Hsu, S.Y., Hsueh, A.J.W., 2000. The Nematode Leucine-Rich Coupled Receptor (LGR) Protein Homologous to Vertebrate Gonadotropin and Thyrotropin Receptors is Constitutively Activated in Mammalian Cells. *Molecular Endocrinology* **14**, 272–284.
- Kuhl, M., Geis, K., Sheldahl, L.C., Pukrop, T., Moon, R.T., Wedlich, D., 2001. Antagonistic regulation of convergent extension movements in *Xenopus* by Wnt/ $\beta$ -catenin and Wnt/ Ca<sup>2+</sup> signaling. *Mechanisms of Development* **106**, 61–76.
- Lachmanovich E, Shvartsman DE, Malka Y, Botvin C, Henis YI, W.A., 2003. Co-localization analysis of complex formation among membrane proteins by computerized fluorescence microscopy: application to immunofluorescence co-patching studies. *Journal of Microscopy* **212**, 122–131.
- Lan, F., Bayliss, P.E., Rinn, J.L., Whetstine, J.R., Wang, J.K., Chen, S., Iwase, S., Alpatov, R., Issaeva, I., Canaani, E., Roberts, T.M., Chang, H.Y., Shi, Y., 2007. A histone H3 lysine 27 demethylase regulates animal posterior development. *Nature* **449**, 689–94.
- Lang, R.A., Bishop, J.M., 1993. Macrophages Are Required for Cell Death and Tissue Remodeling in the Developing Mouse Eye. *Cell* **74**, 453–462.
- Latella, M.C., Teresa, M., Salvo, D., Cocchiarella, F., Benati, D., Grisendi, G., Comitato, A., Marigo, V., Recchia, A., 2016. In vivo Editing of the Human Mutant Rhodopsin Gene by Electroporation of Plasmid-based CRISPR / Cas9 in the Mouse Retina. *Molecular Therapy* **5**, 1–12.
- Lau, W. De, Barker, N., Low, T.Y., Koo, B., Li, V.S.W., Teunissen, H., Kujala, P., Haegebarth, A., Peters, P.J., Wetering, M. Van De, Stange, D.E., Es, J.E. Van, Guardavaccaro, D., Schasfoort, R.B.M., Mohri, Y., Nishimori, K., Mohammed, S., Heck, A.J.R., Clevers, H., 2011. Lgr5 homologues associate with Wnt receptors and mediate R-spondin signalling. *Nature* **476**, 293–297.
- Lau, W.B.M. De, Snel, B., Clevers, H.C., 2012. The R-spondin protein family. *Genome biology* **13**, 242–252.

- Lee, E., Salic, A., Kruger, R., Heinrich, R., Kirschner, M.W., 2003. The Roles of APC and Axin Derived from Experimental and Theoretical Analysis of the Wnt Pathway. *PLoS Biology* **1**, 116–132.
- Lee, K., Shin, Y., Cheng, R., Park, K., Hu, Y., McBride, J., He, X., 2014. Receptor heterodimerization as a novel mechanism for the regulation of Wnt/ $\beta$ -catenin signaling. *Journal of cell science* **127**, 4857–4869.
- Leod, D.S.M.C., Hasegawa, T., Prow, T., Merges, C., Luty, G., 2006. The Initial Fetal Human Retinal Vasculature Develops by Vasculogenesis. *Developmental dynamics* **235**, 3336–3347.
- Li, Y., Muller, B., Fuhrmann, C., van Nouhuys, C.E., Laqua, H., Humphries, P., Schwinger, E., Gal, A., 1992. The autosomal dominant familial exudative vitreoretinopathy locus maps on 11q and is closely linked to D11S533. *American journal of human genetics* **51**, 749–754.
- Liang, F., Yue, J., Wang, J., Zhang, L., Fan, R., Zhang, H., Zhang, Q., 2015. GPCR48/LGR4 promotes tumorigenesis of prostate cancer via PI3K/Akt signaling pathway. *Medical Oncology* **32**, 2–11.
- Linse, S., James, P., 2007. Methods for the detection and analysis of protein – protein interactions. *Proteomics* **7**, 2833–2842.
- Lobo, I., 2008. Same genetic mutation, different genetic disease phenotype. *Nature Education* **1**, 64.
- Lobov, I.B., Rao, S., Carroll, T.J., Vallance, J.E., Ito, M., Ondr, J.K., Kurup, S., Glass, D.A., Patel, M.S., Shu, W., Morrissey, E.E., McMahon, A.P., Karsenty, G., Lang, R.A., 2006. WNT7b mediates macrophage-induced programmed cell death in patterning of the vasculature. *Nature* **437**, 417–421.
- Loh, E.D., Broussard, S.R., Kolakowski, L.F., 2001. Molecular characterization of a novel glycoprotein hormone G-protein-coupled receptor. *Biochemical and biophysical research communications* **282**, 757–64.
- Luhmann, U.F.O., Lin, J., Acar, N., Lammel, S., Feil, S., Grimm, C., Seeliger, M.W., Hammes, H.-P., Berger, W., 2005. Role of the Norrie disease pseudoglioma gene in sprouting angiogenesis during development of the retinal vasculature. *Investigative ophthalmology & visual science* **46**, 3372–3382.

- Luo, J., Yang, Z., Ma, Y., Yue, Z., Lin, H., Qu, G., Huang, J., Dai, W., Li, C., Zheng, C., Xu, L., Chen, H., Wang, J., Li, D., Siwko, S., Penninger, J.M., Ning, G., Xiao, J., Liu, M., 2016. LGR4 is a receptor for RANKL and negatively regulates osteoclast differentiation and bone resorption. *Nature medicine* **22**, 539–546.
- Luo, J., Zhou, W., Zhou, X., Li, D., Weng, J., Yi, Z., Cho, S.G., Li, C., Yi, T., Wu, X., Li, X.-Y., de Crombrughe, B., Höök, M., Liu, M., 2009. Regulation of bone formation and remodeling by G-protein-coupled receptor 48. *Development* **136**, 2747–2756.
- Lv, M., Wang, J., Wang, X., Zuo, T., Zhu, Y., Kong, W., Yu, X., 2011. Polarity Changes in the Transmembrane Domain Core of HIV-1 Vpu Inhibits Its Anti-Tetherin Activity. *PloS one* **6**, e20890.
- Maclaren, R.E., Groppe, M., Barnard, A.R., Cottrill, C.L., Tolmachova, T., Seymour, L., Clark, K.R., During, M.J., Cremers, F.P.M., Black, G.C.M., Lotery, A.J., Downes, S.M., Webster, A.R., Seabra, M.C., 2014. Retinal gene therapy in patients with choroideremia: initial findings from a phase 1 / 2 clinical trial. *Lancet* **6736**, 1–9.
- Mandai, M., Fujii, M., Hashiguchi, T., Sunagawa, G.A., Ito, S., Sun, J., Kaneko, J., Sho, J., Yamada, C., Takahashi, M., 2017. iPSC-Derived Retina Transplants Improve Vision in rd1 End-Stage Retinal-Degeneration Mice. *Stem Cell Reports* **8**, 69–83.
- Mao, J., Wang, J., Liu, B., Pan, W., Farr, G.H., Flynn, C., Yuan, H., Takada, S., Kimelman, D., Li, L., Wu, D., York, N., 2001. Low-Density Lipoprotein Receptor-Related Protein-5 binds to Axin and Regulates the Canonical Wnt Signaling Pathway. *Molecular Cell* **7**, 801–809.
- Maria Carolina Florian, Kalpana J. Nattamai, Karin Dorr, Gina Marka, Bettina Uberle, Virag Vas, Christina Eckl, Immanuel Andra, Matthias Schiemann, Robert A. J. Oostendorp, Karin Scharffetter-Kochanek, Hans Armin Kestler, Y.Z.& H.G., 2013. A canonical to non-canonical Wnt signalling switch in haematopoietic stem-cell ageing. *Nature* **503**, 392–396.
- Martinez, J.J., Toledo, F.J., Fernandez, E., Ferrandez, J.M., 2008. A retinomorph architecture based on discrete-time cellular neural networks using reconfigurable computing. *Neurocomputing* **71**, 766–775.

- Masica, D.L., Karchin, R., 2016. Towards Increasing the Clinical Relevance of In Silico Methods to Predict Pathogenic Missense Variants. *PLoS computational biology* **12**, 1–16.
- Mavria, G., Vercoulen, Y., Yeo, M., Paterson, H., Karasarides, M., Marais, R., Bird, D., Marshall, C.J., 2006. ERK-MAPK signaling opposes Rho-kinase to promote endothelial cell survival and sprouting during angiogenesis. *Cancer Cell* **9**, 33–44.
- Mazerbourg, S., Bouley, D.M., Sudo, S., Klein, C. a, Zhang, J. V, Kawamura, K., Goodrich, L. V, Rayburn, H., Tessier-Lavigne, M., Hsueh, A.J.W., 2004. Leucine-rich repeat-containing, G protein-coupled receptor 4 null mice exhibit intrauterine growth retardation associated with embryonic and perinatal lethality. *Molecular endocrinology* **18**, 2241–54.
- Mcclellan, D.A., Mccracken, K.G., 2001. Estimating the Influence of Selection on the Variable Amino Acid Sites of the Cytochrome b Protein Functional Domains. *Mol. Biol. Evol* **18**, 917–925.
- McEwen, D.G., Peifer, M., 2000. Wnt signaling : Moving in a new direction. *Current Biology* **10**, 562–564.
- McLeod, D.S., Lutty, G.A., Wajer, S.D., Flower, R.W., 1987. Visualization of a Developing Vasculature. *Microvascular Research* **269**, 257–269.
- Meitinger T, Meindl A, Bork P, Rost B, Sander C, Haasemann M, M.J., 1993. Molecular modelling of the Norrie disease protein predicts a cystine knot growth factor tertiary structure. *Nature genetics* **5**, 376–380.
- Mendive, F., Laurent, P., Van Schoore, G., Skarnes, W., Pochet, R., Vassart, G., 2006. Defective postnatal development of the male reproductive tract in LGR4 knockout mice. *Developmental biology* **290**, 421–34.
- Meng, X., Noyes, M.B., Zhu, L.J., Lawson, N.D., Wolfe, S.A., 2008. Targeted gene inactivation in zebrafish using engineered zinc-finger nucleases. *Nature biotechnology* **26**, 695–701.
- Mikels, A.J., Nusse, R., 2006. Purified Wnt5a Protein Activates or Inhibits  $\beta$ -Catenin–TCF Signaling Depending on Receptor Context. *PLoS Biology* **4**, e115.
- Miki, Y., Swensen, J., Shattuck-eidens, D., Futreal, P.A., Harshman, K., Tavtigian, S., Liu, Q., Cochran, C., Bennett, L.M., Ding, W., Bell, R., Rosenthal, J., Hussey, C., Tran, T., McClure, M., Frye, C., Hattier, T.,

- Phelps, R., Haugen-strano, A., Katcher, H., Yakumo, K., Gholami, Z., Shaffer, D., Stone, S., Bayer, S., Wray, C., Bogden, R., Dayananth, P., Ward, J., Tonin, P., Narod, S., Bristow, P.K., Norris, F.H., Helvering, L., Morrison, P., Rosteck, P., Lai, M., Barrett, J.C., Lewis, C., Neuhausen, S., Cannon-albright, L., Goldgar, D., Wiseman, R., Kamb, A., Skolnick, M.H., 1994. Strong Candidate for the Breast and Ovarian Cancer Susceptibility Gene BRCA1. *Science* **266**, 66–71.
- Milhem, R.M., Ben-Salem, S., Al-Gazali, L., Ali, B.R., 2014. Identification of the cellular mechanisms that modulate trafficking of frizzled family receptor 4 (FZD4) missense mutants associated with familial exudative vitreoretinopathy. *Investigative Ophthalmology and Visual Science* **55**, 3423–3431.
- Millot, G., Carvalho, M.A., Caputo, S.M., Vreeswijk, M.P.G., 2012. A Guide for Functional Analysis of BRCA1 Variants of Uncertain Significance (VUS). *Human mutation* **33**, 1526–1537.
- Moffat, L.L., Robinson, R.E., Bakoulis, A., Clark, S.G., 2014. The conserved transmembrane RING finger protein PLR-1 downregulates Wnt signaling by reducing Frizzled , Ror and Ryk cell-surface levels in *C . elegans*. *Development* **6**, 617–628.
- Molenaar, M., Wetering, M. Van De, Oosterwegel, M., Peterson-maduro, J., Godsave, S., Korinek, V., Roose, J., 1996. XTcf-3 Transcription Factor Mediates  $\beta$ -Catenin-Induced Axis Formation in *Xenopus* Embryos. *Cell* **86**, 391–399.
- Monkley, S.J., Delaney, S.J., Pennisi, D.J., Christiansen, J.H., Wainwright, B.J., 1996a. Targeted disruption of the Wnt2 gene results in placentation defects. *Development* **3353**, 3343–3353.
- Monkley, S.J., Delaney, S.J., Pennisi, D.J., Christiansen, J.H., Wainwright, B.J., 1996b. Targeted disruption of the Wnt2 gene results in placentation defects. *Development* **122**, 3343–3353.
- Morrison, I.E.G., Karakikes, I., Barber, R.E., Ferna, N., Cherry, R.J., 2003. Detecting and Quantifying Colocalization of Cell Surface Molecules by Single Particle Fluorescence Imaging. *Biophysical Journal* **85**, 4110–4121.
- Mudhar, H.S., Pollock, R.A., Wang, C., Stiles, C.D., Richardson, W.D., 1993.

- PDGF and its receptors in the developing rodent retina and optic nerve. *Development* **552**, 539–552.
- Nam, J., Turcotte, T.J., Smith, P.F., Choi, S., Yoon, J.K., 2006. Mouse cristin/R-spondin family proteins are novel ligands for the frizzled 8 and LRP6 receptors and activate  $\beta$ -catenin-dependent gene expression. *The Journal of biological chemistry* **281**, 13247–13257.
- Nam, J.S., Turcotte, T.J., Smith, P.F., Choi, S., Jeong, K.Y., 2006. Mouse cristin/R-spondin family proteins are novel ligands for the frizzled 8 and LRP6 receptors and activate  $\beta$ -catenin-dependent gene expression. *Journal of Biological Chemistry* **281**, 13247–13257.
- Nasevicius, A., Ekker, S.C., 2000. Effective targeted gene “knockdown” in zebrafish. *Nature genetics* **26**, 216–20.
- Nathans, J., 1999. The Evolution and Physiology of Human Color Vision : Insights from Molecular Genetic Studies of Visual Pigments. *Neuron* **24**, 299–312.
- Ng, P.C., Henikoff, S., 2003. SIFT : predicting amino acid changes that affect protein function. *Nucleic acids research* **31**, 3812–3814.
- Nicholls, S.B., Hardy, J.A., 2013. Structural basis of fluorescence quenching in caspase activatable-GFP. *Protein Science* **22**, 247–257.
- Nickle, B., Robinson, P.R., 2007. The opsins of the vertebrate retina : insights from structural, biochemical, and evolutionary studies. *Cellular and Molecular Life Science* **64**, 2917–2932.
- Nikopoulos, K., Gilissen, C., Hoischen, A., van Nouhuys, C.E., Boonstra, F.N., Blokland, E. a W., Arts, P., Wieskamp, N., Strom, T.M., Ayuso, C., Tilanus, M. a D., Bouwhuis, S., Mukhopadhyay, A., Scheffer, H., Hoefsloot, L.H., Veltman, J. a, Cremers, F.P.M., Collin, R.W.J., 2010a. Next-generation sequencing of a 40 Mb linkage interval reveals TSPAN12 mutations in patients with familial exudative vitreoretinopathy. *American journal of human genetics* **86**, 240–7.
- Nikopoulos, K., Venselaar, H., Collin, R.W.J., Riveiro-Alvarez, R., Boonstra, F.N., Hoymans, J.M.M., Mukhopadhyay, A., Shears, D., van Bers, M., de Wijs, I.J., van Essen, A.J., Sijmons, R.H., Tilanus, M. a D., van Nouhuys, C.E., Ayuso, C., Hoefsloot, L.H., Cremers, F.P.M., 2010b. Overview of the mutation spectrum in familial exudative vitreoretinopathy

- and Norrie disease with identification of 21 novel variants in FZD4, LRP5, and NDP. *Human mutation* **31**, 656–66.
- Nunes, R., 2006. Deafness, genetics and dysgenics. *Med Health Care Philos* **9**, 25–31.
- Ohkawara, B., Glinka, A., Niehrs, C., 2011. Rspo3 Binds Syndecan 4 and Induces Wnt/PCP Signaling via Clathrin-Mediated Endocytosis to Promote Morphogenesis. *Developmental Cell* **20**, 303–314.
- Ohlmann, A., Scholz, M., Goldwich, A., Chauhan, B.K., Hudl, K., Ohlmann, A. V, Zrenner, E., Berger, W., Seeliger, M.W., Tamm, E.R., 2005. Ectopic Norrin Induces Growth of Ocular Capillaries and Restores Normal Retinal Angiogenesis in Norrie Disease Mutant Mice. *The Journal of neuroscience* **25**, 1701–1710.
- Otani, A., Kinder, K., Ewalt, K., Otero, F.J., Shimmel, P., Friedlander, M., 2002. Bone marrow–derived stem cells target retinal astrocytes and can promote or inhibit retinal angiogenesis. *Nature medicine* **8**, 1004–1010.
- Ozawa, M., Baribault, H., Kemler, R., 1989. The cytoplasmic domain of the cell adhesion molecule uvomorulin associates with three independent proteins structurally related in different species. *The EMBO Journal* **8**, 1711–1717.
- Park, S.S., Bauer, G., Abedi, M., Pontow, S., Panorgias, A., Jonnal, R., Zawadzki, R.J., Werner, J.S., Nolta, J., 2015. Intravitreal Autologous Bone Marrow CD34+ Cell Therapy for Ischemic and Degenerative Retinal Disorders: Preliminary Phase 1 Clinical Trial Findings. *Investigative Ophthalmology and Visual Science* **56**, 81–89.
- Park, S.S., Caballero, S., Bauer, G., Shibata, B., Roth, A., Fitzgerald, P.G., Forward, K.I., Zhou, P., Mcgee, J., Telander, D.G., Grant, M.B., Nolta, J.A., 2012. Long-Term Effects of Intravitreal Injection of NOD-SCID Mice with Acute Ischemia-Reperfusion Injury. *Investigative Ophthalmology and Visual Science* **53**, 986–994.
- Parma, P., Radi, O., Vidal, V., Chaboissier, M.C., Dellambra, E., Valentini, S., Guerra, L., Schedl, A., Camerino, G., 2006. R-spondin1 is essential in sex determination, skin differentiation and malignancy. *Nature genetics* **38**, 1304–1309.
- Parmryd, I., Adler, J., Patel, R., Magee, A.I., 2003. Imaging metabolism of

- phosphatidylinositol 4, 5-bisphosphate in T-cell GM1-enriched domains containing Ras proteins. *Experimental Cell Research* **285**, 27–38.
- Patel-hett, S., Amore, P.A.D., 2011. Signal transduction in vasculogenesis and developmental angiogenesis. *Int.J. Dev. Biol* **55**, 353–363.
- Peirson, S.N., Butler, J.N., Foster, R.G., 2003. Experimental validation of novel and conventional approaches to quantitative real-time PCR data analysis. *Nucleic acids research* **31**, 1–7.
- Peters, S., Lamah, T., Kokkinou, D., 2006. Melanin Protects Choroidal Blood Vessels against Light Toxicity. *Z Naturforsch C* **61**, 427–433.
- Pinson, K.I., Brennan, J., Monkley, S., Avery, B.J., 2000. An LDL-receptor-related protein mediates Wnt signalling in mice. *Nature* **407**, 1998–2001.
- Planutis, K., Planutiene, M., Holcombe, R.F., 2014. A novel signaling pathway regulates colon cancer angiogenesis through Norrin. *Scientific reports* **4**, 5630–5635.
- Posokhova, E., Shukla, A., Seaman, S., Volate, S., Hilton, M.B., Wu, B., Morris, H., Swing, D. a, Zhou, M., Zudaire, E., Rubin, J.S., St Croix, B., 2014. GPR124 Functions as a WNT7-Specific Coactivator of Canonical beta-Catenin Signaling. *Cell Reports* **10**, 123–130.
- Poulter, J. a, Ali, M., Gilmour, D.F., Rice, A., Kondo, H., Hayashi, K., Mackey, D. a, Kearns, L.S., Ruddle, J.B., Craig, J.E., Pierce, E. a, Downey, L.M., Mohamed, M.D., Markham, A.F., Inglehearn, C.F., Toomes, C., 2010. Mutations in TSPAN12 cause autosomal-dominant familial exudative vitreoretinopathy. *American journal of human genetics* **86**, 248–253.
- Poulter, J. a, Davidson, A.E., Ali, M., Gilmour, D.F., Parry, D. a, Mintz-Hittner, H. a, Carr, I.M., Bottomley, H.M., Long, V.W., Downey, L.M., Sergouniotis, P.I., Wright, G. a, MacLaren, R.E., Moore, A.T., Webster, A.R., Inglehearn, C.F., Toomes, C., 2012. Recessive mutations in TSPAN12 cause retinal dysplasia and severe familial exudative vitreoretinopathy (FEVR). *Investigative ophthalmology & visual science* **53**, 2873–2879.
- Provis, J.M., 2001. Development of the Primate Retinal Vasculature. *Progress in retinal and eye research* **20**, 800–821.
- Qin, M., Hayashi, H., Oshima, K., Tahira, T., Hayashi, K., Kondo, H., 2005. Complexity of the genotype-phenotype correlation in familial exudative

- vitreoretinopathy with mutations in the LRP5 and/or FZD4 genes. *Human mutation* **26**, 104–12.
- Qin, M., Kondo, H., Tahira, T., Hayashi, K., 2008a. Moderate reduction of Norrin signaling activity associated with the causative missense mutations identified in patients with familial exudative vitreoretinopathy. *Human genetics* **122**, 615–23.
- Qin, M., Kondo, H., Tahira, T., Hayashi, K., 2008b. Moderate reduction of Norrin signaling activity associated with the causative missense mutations identified in patients with familial exudative vitreoretinopathy. *Human Genetics* **122**, 615–623.
- Quiram, P.A., Drenser, K.A., Lai, M.M., Jr, A.C., Trese, M.T., 2008. Treatment of vascularly active familial exudative vitreoretinopathy with pegaptanib sodium (Macugen). *Retina* **28**, 8–12.
- Ramis, J.M., Collart, C., Smith, J.C., 2007. Xnrs and Activin Regulate Distinct Genes during Xenopus Development: Activin Regulates Cell Division. *PloS one* **2**, e213.
- Ranchod, T.M., Ho, L.Y., Drenser, K. a, Capone, A., Trese, M.T., 2011. Clinical presentation of familial exudative vitreoretinopathy. *Ophthalmology* **118**, 2070–5.
- Rath, A., Deber, C.M., 2012. Correction factors for membrane protein molecular weight readouts on sodium dodecyl sulfate-polyacrylamide gel electrophoresis. *Analytical Biochemistry* **434**, 67–72.
- Rath, A., Glibowicka, M., Nadeau, V.G., Chen, G., Deber, C.M., 2009. Detergent binding explains anomalous SDS-PAGE. *Proceedings of the National Academy of Sciences of the United States of America* **106**, 1760–1765.
- Reardon, S., Cyranoski, D., 2014. Japan stem-cell trial stirs envy. *Nature* **513**, 7–8.
- Rehm, H.L., Zhang, D.-S., Brown, M.C., Burgess, B., Halpin, C., Berger, W., Morton, C.C., Corey, D.P., Chen, Z.-Y., 2002. Vascular defects and sensorineural deafness in a mouse model of Norrie disease. *The Journal of neuroscience* **22**, 4286–4292.
- Reis, M., Liebner, S., 2013. Wnt signaling in the vasculature. *Experimental Cell Research* **319**, 1317–1323.

- Richter, M., Gottanka, J., May, C.A., Welge-luissien, U., Berger, W., Lutjendrecoll, E., 1998. Retinal Vasculature Changes in Norrie Disease Mice. *Investigative Ophthalmology and Visual Science* **39**, 2450–2457.
- Rijsewijk, F., 1987. The Drosophila Homolog of the Mouse Mammary Oncogene int-1 Is Identical to the Segment Polarity Gene wingless. *Cell* **50**, 649–657.
- Robitaille, J., MacDonald, M.L.E., Kaykas, A., Sheldahl, L.C., Zeisler, J., Dubé, M.-P., Zhang, L.-H., Singaraja, R.R., Guernsey, D.L., Zheng, B., Siebert, L.F., Hoskin-Mott, A., Trese, M.T., Pimstone, S.N., Shastry, B.S., Moon, R.T., Hayden, M.R., Goldberg, Y.P., Samuels, M.E., 2002. Mutant frizzled-4 disrupts retinal angiogenesis in familial exudative vitreoretinopathy. *Nature genetics* **32**, 326–30.
- Robitaille, J.M., Gillett, R.M., LeBlanc, M. a., Gaston, D., Nightingale, M., Mackley, M.P., Parkash, S., Hathaway, J., Thomas, A., Ells, A., Traboulsi, E.I., Héon, E., Roy, M., Shalev, S., Fernandez, C. V., MacGillivray, C., Wallace, K., Fahiminiya, S., Majewski, J., McMaster, C.R., Bedard, K., 2014. Phenotypic Overlap Between Familial Exudative Vitreoretinopathy and Microcephaly, Lymphedema, and Chorioretinal Dysplasia Caused by KIF11 Mutations. *JAMA Ophthalmology* **132**, 1393–1399.
- Robitaille, J.M., Wallace, K., Zheng, B., Beis, M.J., Samuels, M., Hoskin-mott, A., 2009. Phenotypic Overlap of Familial Exudative Vitreoretinopathy (FEVR) with Persistent Fetal Vasculature (PFV) Caused by FZD4 Mutations in two Distinct Pedigrees. *Ophthalmic genetics* **30**, 23–30.
- Robu, M.E., Larson, J.D., Nasevicius, A., Beiraghi, S., Brenner, C., Farber, S. a, Ekker, S.C., 2007. P53 Activation By Knockdown Technologies. *PLoS genetics* **3**, e78.
- Roepman, R., Letteboer, S.J.F., Arts, H.H., Beersum, S.E.C. Van, Lu, X., Krieger, E., Ferreira, P.A., Cremers, F.P.M., 2005. Interaction of nephrocystin-4 and RPGRIP1 is disrupted by nephronophthisis or Leber congenital amaurosis-associated mutations. *Proceedings of the National Academy of Sciences of the United States of America* **51**, 18520–18525.
- Ruan, G., Barry, E., Yu, D., Lukason, M., Cheng, S.H., Scaria, A., 2017.

- CRISPR / Cas9-Mediated Genome Editing as a Therapeutic Approach for Leber Congenital Amaurosis 10. *Molecular Therapy* **25**, 1–11.
- Ruffner, H., Sprunger, J., Charlat, O., Leighton-Davies, J., Grosshans, B., Salathe, A., Zietzling, S., Beck, V., Therier, M., Isken, A., Xie, Y., Zhang, Y., Hao, H., Shi, X., Liu, D., Song, Q., Clay, I., Hintzen, G., Tchorz, J., Bouchez, L.C., Michaud, G., Finan, P., Myer, V.E., Bouwmeester, T., Porter, J., Hild, M., Bassilana, F., Parker, C.N., Cong, F., 2012. R-Spondin potentiates Wnt/ $\beta$ -catenin signaling through orphan receptors LGR4 and LGR5. *PloS one* **7**, e40976.
- Saint-geniez, M., Maharaj, A.S.R., Walshe, T.E., Tucker, B.A., Sekiyama, E., Kurihara, T., Darland, D.C., Young, M.J., Amore, P.A.D., 2008. Endogenous VEGF Is Required for Visual Function: Evidence for a Survival Role on Müller and Photoreceptors. *PloS one* **3**, e3554.
- Schafer, N.F., Luhmann, U.F.O., Feil, S., Berger, W., 2008. Differential Gene Expression in NdpH-Knockout Mice in Retinal Development. *Investigative Ophthalmology and Visual Science* **50**, 906–916.
- Schagat, T., Paguio, A., Kopish, K., 2007. Normalizing genetic reporter assays: Approaches and considerations for increasing consistency and statistical significance. *Promega Corporation* **17**, 9–12.
- Schauerte, H.E., Eeden, F.J.M. Van, Fricke, C., Odenthal, J., Strähle, U., 1998. Sonic hedgehog is not required for the induction of medial floor plate cells in the zebrafish. *Development* **125**, 2983–2993.
- Schlessinger, J., Shechter, Y., Mark, C., Pastant, I.R.A., 1978. Direct visualization of binding, aggregation, and internalization of insulin and epidermal growth factor on living fibroblastic cells. *Proceedings of the National Academy of Sciences of the United States of America* **75**, 2659–2663.
- Schnitzer, J., 1987. Retinal astrocytes: their restriction to vascularized parts of the mammalian retina. *Neuroscience Letters* **78**, 29–34.
- Schoore, V., Mendive, F., Roland, G., Vassart, G., 2005. Expression pattern of the orphan receptor LGR4 / GPR48 gene in the mouse. *Histochem Cell Biol* **124**, 35–50.
- Scott, A.N., Hetheridge, C., Reynolds, A.R., Nayak, V., Hodivala-dilke, K., Mellor, H., 2008. Farnesyltransferase inhibitors target multiple

- endothelial cell functions in angiogenesis. *Angiogenesis* **11**, 337–346.
- Shalaby, F., Rossant, J., Yamaguchi, T.P., Gertsenstein, M., Wu, X.-F., Brechtman, M.L., Schuh, A.C., 1995. Failure of blood-island formation and vasculogenesis in Flk-1-deficient mice. *Nature* **376**, 62–66.
- Shastri, B.S., Pendergast, S.D., Hartzler, M.K., Liu, X., Trese, M.T., 1997. Identification of Missense Mutations in the Norrie Disease Gene Associated With Advanced Retinopathy of Prematurity. *Arch. Ophthalmol.* **115**, 651–655.
- Shawber, C.J., Funahashi, Y., Li, C., Kitajewski, J., 2005. Wnt/ $\beta$ -catenin signaling induces proliferation, survival and Interleukin-8 in human endothelial cells. *Angiogenesis* **8**, 43–51.
- Shirai, A., Matsuyama, A., Hashimoto, A., Arai, R., Komatsu, Y., 2008. Global Analysis of Gel Mobility of Proteins and Its Use in Target Identification. *The Journal of biological chemistry* **283**, 10745–10752.
- Shirai, H., Mandai, M., Matsushita, K., Kuwahara, A., Yonemura, S., 2015. Transplantation of human embryonic stem cell-derived retinal tissue in two primate models of retinal degeneration. *Proceedings of the National Academy of Sciences of the United States of America* **22**, 81–90.
- Shukla, D., Singh, J., Sudheer, G., Soman, M., John, R.K., Ramasamy, K., Perumalsamy, N., 2003. Familial exudative vitreoretinopathy (FEVR). Clinical profile and management. *Indian Journal of Ophthalmology* **51**, 323–328.
- Silbert, M., Gunwood, A.S., 2000. Persistent hyperplastic primary vitreous. *Clinical Eye and Vision Care* **12**, 131–137.
- Siwko, S., Lai, L., Weng, J., Liu, M., 2013. Lgr4 in ocular development and glaucoma. *Journal of ophthalmology* **2013**, 987494.
- Smallwood, P.M., Williams, J., Xu, Q., Leahy, D.J., Nathans, J., 2007. Mutational Analysis of Norrin-Frizzled4 Recognition. *The Journal of biological chemistry* **282**, 4057–4068.
- Smet, F. De, Segura, I., Bock, K. De, Hohensinner, P.J., Carmeliet, P., 2009. Mechanisms of Vessel Branching Filopodia on Endothelial Tip Cells Lead the Way. *Arterioscler Thromb Vasc Biol.* **29**, 639–649.
- Sohrab, M.A., Allikmets, R., Guarnaccia, M.M., Smith, R.T., 2010. Preimplantation Genetic Diagnosis for Stargardt Disease. *American*

*Journal of Ophthalmology* **149**, 651–655.

- Song, H., Luo, J., Luo, W., Weng, J., Wang, Z., Li, B., Li, D., Liu, M., 2008. Inactivation of G-protein-coupled receptor 48 (Gpr48/Lgr4) impairs definitive erythropoiesis at midgestation through down-regulation of the ATF4 signaling pathway. *The Journal of biological chemistry* **283**, 36687–97.
- Sorrell, J.M., Baber, M.A., Caplan, A.I., 2007. A self-assembled fibroblast-endothelial cell co-culture system that supports in vitro vasculogenesis by both human umbilical vein endothelial cells and human dermal microvascular endothelial cells. *Cells Tissues Organs* **186**, 157–168.
- Staton, C.A., Reed, M.W.R., Brown, N.J., 2009. A critical analysis of current in vitro and in vivo angiogenesis assays. *Int. J. Exp. Path* **90**, 195–221.
- Stenman, J.M., Rajagopal, J., Carroll, T.J., Ishibashi, M., McMahon, J., McMahon, A.P., Every, 2008. Canonical Wnt Signaling Regulates Organ-Specific Assembly and Differentiation of CNS Vasculature. *Science* **322**, 1247–1250.
- Stepanenko, O. V., Verkhusha, V. V., Kuznetsova, I.M., N., V.U., Turoverov, K.K., 2008. Fluorescent Proteins as Biomarkers and Biosensors: Throwing Color Lights on Molecular and Cellular Processes. *Curr Protein Pept Sci* **9**, 338–369.
- Stitzel, N.O., Kiezun, A., Sunyaev, S., 2011. Computational and statistical approaches to analyzing variants identified by exome sequencing. *Genome biology* **12**, 227–237.
- Stone, J., Dreher, Z., 1987. Relationship Between Astrocytes, Ganglion Cells and Vasculature of the Retina. *The Journal of Comparative Neurology* **255**, 35–49.
- Strader, C.D., Fong, T.M., Tota, M.R., Underwood, D., 1994. Structure and function of G protein-coupled receptors. *Annu. Rev. Biochem* **63**, 101–32.
- Styrkarsdottir, U., Thorleifsson, G., Sulem, P., Gudbjartsson, D.F., Sigurdsson, A., Jonasdottir, A., Jonasdottir, A., Oddsson, A., Helgason, A., Magnusson, O.T., Walters, G.B., Frigge, M.L., Helgadottir, H.T., Johannsdottir, H., Bergsteinsdottir, K., Ogmundsdottir, M.H., Center, J.R., Nguyen, T. V, Eisman, J. a, Christiansen, C., Steingrimsson, E.,

- Jonasson, J.G., Tryggvadottir, L., Eyjolfsson, G.I., Theodors, A., Jonsson, T., Ingvarsson, T., Olafsson, I., Rafnar, T., Kong, A., Sigurdsson, G., Masson, G., Thorsteinsdottir, U., Stefansson, K., 2013. Nonsense mutation in the LGR4 gene is associated with several human diseases and other traits. *Nature* **497**, 517–20.
- Tagami, M., Kusuhara, S., Honda, S., 2008. Rapid regression of retinal hemorrhage and neovascularization in a case of familial exudative vitreoretinopathy treated with intravitreal bevacizumab. *Graefes Arch Clin Exp Ophthalmol* **246**, 1787–1789.
- Taillard, D., Waelti, P., Zuber, J., 2008. Few statistical tests for proportions comparison. *European Journal of Operational Research* **185**, 1336–1350.
- Tamai, K., Semenov, M., Kato, Y., Spokony, R., 2000. LDL-receptor-related proteins in Wnt signal transduction. *Nature* **407**, 530–535.
- Tamai, K., Zeng, X., Liu, C., Zhang, X., Harada, Y., Chang, Z., He, X., 2004. A Mechanism for Wnt Coreceptor Activation. *Molecular Cell* **13**, 149–156.
- Tammela, T., Zarkada, G., Nurmi, H., Jakobsson, L., Heinolainen, K., Tvorogov, D., Zheng, W., Franco, C.A., Murtomäki, A., Aranda, E., Miura, N., Ylä-herttua, S., Fruttiger, M., Mäkinen, T., Eichmann, A., Pollard, J.W., Gerhardt, H., Alitalo, K., 2011. VEGFR-3 controls tip to stalk conversion at vessel fusion sites by reinforcing Notch signalling. *Nature Cell Biology* **13**, 1202–1213.
- Thorpe, C.J., Schlesinger, A., Carter, J.C., Bowerman, B., 1997. Wnt Signaling Polarizes an Early *C. elegans* Blastomere to Distinguish Endoderm from Mesoderm. *Cell* **90**, 695–705.
- Thusberg, J., Olatubosun, A., Vihinen, M., 2011. Performance of Mutation Pathogenicity Prediction Methods on Missense Variants. *Human mutation*.
- Tomizuka, K., Horikoshi, K., Kitada, R., Sugawara, Y., Iba, Y., Kojima, A., Yoshitome, A., Yamawaki, K., Amagai, M., Inoue, A., Oshima, T., 2008. R-spondin1 plays an essential role in ovarian development through positively regulating Wnt-4 signaling. *Human molecular genetics* **17**, 1278–1291.

- Toomes, C., Bottomley, H.M., Jackson, R.M., Towns, K. V, Scott, S., Mackey, D. a, Craig, J.E., Jiang, L., Yang, Z., Trembath, R., Woodruff, G., Gregory-Evans, C.Y., Gregory-Evans, K., Parker, M.J., Black, G.C.M., Downey, L.M., Zhang, K., Inglehearn, C.F., 2004a. Mutations in LRP5 or FZD4 underlie the common familial exudative vitreoretinopathy locus on chromosome 11q. *American journal of human genetics* **74**, 721–30.
- Toomes, C., Bottomley, H.M., Scott, S., Mackey, D.A., Craig, J.E., Appukuttan, B., Stout, J.T., Flaxel, C.J., Zhang, K., Black, G.C.M., Fryer, A., Downey, L.M., Inglehearn, C.F., 2004b. Spectrum and Frequency of FZD4 Mutations in Familial Exudative Vitreoretinopathy. *Investigative Ophthalmology & Visual Science* **45**, 2083–2090.
- Toomes, C., Downey, L.M., Bottomley, H.M., Mintz-Hittner, H. a, Inglehearn, C.F., 2005. Further evidence of genetic heterogeneity in familial exudative vitreoretinopathy; exclusion of EVR1, EVR3, and EVR4 in a large autosomal dominant pedigree. *The British journal of ophthalmology* **89**, 194–7.
- Toomes, C., Downey, L.M., Bottomley, H.M., Scott, S., Woodruff, G., Trembath, R.C., Inglehearn, C.F., 2004c. Identification of a fourth locus (EVR4) for familial exudative vitreoretinopathy (FEVR). *Molecular vision* **10**, 37–42.
- Trapani, I., Puppo, A., Auricchio, A., 2014. Progress in Retinal and Eye Research Vector platforms for gene therapy of inherited retinopathies. *Progress in retinal and eye research* **43**, 108–128.
- Tur-Kaspa, I., Aljadeff, G., Rechitsky, S., Grotjan, H.E., Verlinsky, Y., 2010. PGD for all cystic fibrosis carrier couples : novel strategy for preventive medicine and cost analysis. *Reproductive Biomedicine* **21**, 186–195.
- Urbich, C., Dimmeler, S., 2004. Endothelial progenitor cells: Characterization and role in vascular biology. *Circulation Research* **95**, 343–353.
- Valenta, T., Hausmann, G., Basler, K., 2012. The many faces and functions of  $\beta$ -catenin. *The EMBO Journal* **31**, 2714–2736.
- Vanhollebeke, B., Stone, O. a, Bostaille, N., Cho, C., Zhou, Y., Maquet, E., Gauquier, A., Cabochette, P., Fukuhara, S., Mochizuki, N., Nathans, J., Stainier, D.Y., 2015. Tip cell-specific requirement for an atypical Gpr124-

- and Reck-dependent Wnt/ $\beta$ -catenin pathway during brain angiogenesis. *eLife* **4**, 1–25.
- Vassart, G., Pardo, L., Costagliola, S., 2004. A molecular dissection of the glycoprotein hormone receptors. *Trends in Biochemical Science* **29**, 119–126.
- Wang, Y., Huso, D., Cahill, H., Ryugo, D., Nathans, J., 2001. Progressive Cerebellar , Auditory , and Esophageal Dysfunction Caused by Targeted Disruption of the frizzled- 4 Gene. *The Journal of Neuroscience* **21**, 4761–4771.
- Wang, Y., Rattner, A., Zhou, Y., Williams, J., Smallwood, P.M., Nathans, J., 2012. Norrin/Frizzled4 signaling in retinal vascular development and blood brain barrier plasticity. *Cell* **151**, 1332–1344.
- Wang, Z., Jin, C., Li, H., Li, C., Hou, Q., Liu, M., Da, X., Dong, E., Tu, L., 2010. GPR48-Induced keratinocyte proliferation occurs through HB-EGF mediated EGFR transactivation. *FEBS letters* **584**, 4057–4062.
- Warren, J.T., Zou, W., Decker, C.E., Rohatgi, N., Nelson, C.A., Fremont, D.H., Teitelbaum, S.L., 2015. Correlating RANK Ligand/RANK Binding Kinetics With Osteoclast Formation and Function. *Journal of Cellular Biochemistry* **116**, 2476–2483.
- Wehrli, M., Dougan, S.T., Caldwell, K., Keefe, L.O., 2000. arrow encodes an LDL-receptor- related protein essential for Wingless signalling. *Nature* **407**, 527–530.
- Wei, Q., Yokota, C., Semenov, M. V, Doble, B., Woodgett, J., He, X., 2007. R-spondin1 Is a High Affinity Ligand for LRP6 and Induces LRP6 Phosphorylation and  $\beta$ -Catenin Signaling. *The Journal of biological chemistry* **282**, 15903–15911.
- Weleber, R.G., Pennesi, M.E., Wilson, D.J., Kaushal, S., Erker, L.R., Jensen, L., McBride, M.T., Flotte, T.R., Humphries, M., Calcedo, R., Hauswirth, W.W., Chulay, J.D., Stout, J.T., 2016. Results at 2 Years after Gene Therapy for RPE65-Deficient Leber Congenital Amaurosis and Severe Early-Childhood Onset Retinal Dystrophy. *Ophthalmology* **123**, 1606–1620.
- Weng, J., Luo, J., Cheng, X., Jin, C., Zhou, X., Qu, J., Tu, L., Ai, D., Li, D., Wang, J., Martin, J.F., Amendt, B. a, Liu, M., 2008. Deletion of G

- protein-coupled receptor 48 leads to ocular anterior segment dysgenesis (ASD) through down-regulation of Pitx2. *Proceedings of the National Academy of Sciences of the United States of America* **105**, 6081–6.
- West, H., Richardson, W.D., Fruttiger, M., 2005. Stabilization of the retinal vascular network by reciprocal feedback between blood vessels and astrocytes. *Development* **132**, 1855–1862.
- Wieschaus, E., Riggleman, R., 1987. Autonomous Requirements for the Segment Polarity Gene armadillo during Drosophila Embryogenesis. *Cell* **49**, 177–184.
- Wimmers, K., Reyer, H., Ponsuksili, S., Kanitz, E., Po, R., Murani, E., 2016. A Natural Mutation in Helix 5 of the Ligand Binding Domain of Glucocorticoid Receptor Enhances Receptor-Ligand Interaction. *PLoS one* **11**, e0164628.
- Wodarz, A., Nusse, R., 1998. Mechanisms of Wnt signaling in development. *Annu. Rev. Cell Dev. Biol.* **14**, 59–88.
- Woods, N.T., Baskin, R., Golubeva, V., Jhuraney, A., De-gregoriis, G., Vaclova, T., Goldgar, D.E., Couch, F.J., Carvalho, M.A., Iversen, E.S., Monteiro, A.N.A., 2016. Functional assays provide a robust tool for the clinical annotation of genetic variants of uncertain significance. *Genomic medicine* **16**, 1–9.
- Wright, G.J., Leslie, J.D., Ariza-mcnaughton, L., Lewis, J., 2004. Delta proteins and MAGI proteins: an interaction of Notch ligands with intracellular scaffolding molecules and its significance for zebrafish development. *Development* **131**, 5659–5669.
- Wright, M., Aikawa, M., Szeto, W., Papkoff, J., 1999. Identification of a Wnt-Responsive Signal Transduction Pathway in Primary Endothelial Cells. *Biochemical and biophysical research communications* **388**, 384–388.
- Wu, J., Liu, J., Ko, Y., Wang, C., Chu, K., Liu, T., Chao, H., Jiang, Y., Chen, S., Chung, M., 2016b. Haploinsufficiency of RCBTB1 is associated with Coats disease and familial exudative vitreoretinopathy. *Human molecular genetics* **25**, 1637–1647.
- Xia, C., Yablonka-reuveni, Z., Gong, X., 2010. LRP5 Is Required for Vascular Development in Deeper Layers of the Retina. *PLoS one* **5**, 1–7.
- Xie, Y., Zamponi, R., Charlat, O., Ramones, M., Swalley, S., Jiang, X.,

- Rivera, D., Tschantz, W., Lu, B., Quinn, L., Dimitri, C., Parker, J., Jeffery, D., Wilcox, S.K., Watrobka, M., Lemotte, P., Granda, B., Porter, J.A., Myer, V.E., Loew, A., Cong, F., 2013. Interaction with both ZNRF3 and LGR4 is required for the signalling activity of R-spondin. *Scientific reports* **14**, 1120–1126.
- Xu, K., Xu, Y., Rajashankar, K.R., Robey, D., Nikolov, D.B., 2013. Crystal structures of Lgr4 and its complex with R-spondin1. *Cell* **21**, 1683–1689.
- Xu, Q., Wang, Y., Dabdoub, A., Smallwood, P.M., Williams, J., Woods, C., Kelley, M.W., Jiang, L., Tasman, W., Zhang, K., Nathans, J., 2004. Vascular development in the retina and inner ear: control by Norrin and Frizzled-4, a high-affinity ligand-receptor pair. *Cell* **116**, 883–895.
- Yamaguchi, T.P., Dumont, D.J., Conlon, R.A., Breitman, M.L., Rossant, J., 1993. flk-1, an flt-1-related receptor tyrosine kinase is an early marker for endothelial cell precursors. *Development* **498**, 489–498.
- Yamashita, R., Takegawa, Y., Sakumoto, M., Nakahara, M., Kawazu, H., Hoshii, T., Araki, K., Yokouchi, Y., Yamamura, K., 2009. Defective Development of the Gall Bladder and Cystic Duct in Lgr4 - Hypomorphic Mice. *Developmental dynamics* **238**, 993–1000.
- Yao, H.H.C., Matzuk, M.M., Jorgez, C.J., Menke, D.B., David, C., Swain, A., Capel, B., 2004. Follistatin Operates Downstream of Wnt4 in Mammalian Ovary Organogenesis. *Developmental dynamics* **230**, 210–215.
- Ye, X., Wang, Y., Cahill, H., Yu, M., Badea, T.C., Smallwood, P.M., Peachey, N.S., Nathans, J., 2009. Norrin, frizzled-4, and Lrp5 signaling in endothelial cells controls a genetic program for retinal vascularization. *Cell* **139**, 285–298.
- Ye, X., Wang, Y., Nathans, J., 2010. The Norrin/Frizzled4 signaling pathway in retinal vascular development and disease. *Cell. Review* **16**, 417–425.
- Yi, J., Xiong, W., Gong, X., Bellister, S., Ellis, L.M., Liu, Q., 2013. Analysis of LGR4 Receptor Distribution in Human and Mouse Tissues. *PloS one* **8**, e78144.
- Yoshikawa, Y., Yamada, T., Nagara, I.T., Okabe, K., Kitagawa, Y., Ema, M., Kubota, Y., 2016. Developmental regression of hyaloid vasculature is triggered by neurons. *The Journal of Experimental Medicine* **213**, 1175–1183.

- You, S., Kim, H., Hsu, C., Halawani, M.E. El, Foster, D.N., 2000. Three Different Turkey Luteinizing Hormone Receptor (tLH-R) Isoforms I: Characterization of Alternatively Spliced tLH-R Isoforms and Their Regulated Expression in Diverse Tissues 1. *Biology of reproduction* **62**, 108–116.
- Zacharias, D.A., Violin, J.D., Newton, A.C., 2002. Partitioning of Lipid-Modified Monomeric GFPs into Membrane Microdomains of Live Cells. *Science* **296**, 913–916.
- Zhang, J., Li, Q., Zhang, S., Xu, Q., Wang, T., 2016. Lgr4 promotes prostate tumorigenesis through the Jmjd2a/AR signaling pathway. *Experimental Cell Research* **349**, 77–84.
- Zhang, K., Harada, Y., Wei, X., Shukla, D., Rajendran, A., Tawansy, K., Bedell, M., Lim, S., Shaw, P.X., He, X., Yang, Z., 2011a. An essential role of the cysteine-rich domain of FZD4 in Norrin/Wnt signaling and familial exudative vitreoretinopathy. *The Journal of biological chemistry* **286**, 10210–5.
- Zhang, K., Harada, Y., Wei, X., Shukla, D., Rajendran, A., Tawansy, K., Bedell, M., Lim, S., Shaw, P.X., He, X., Yang, Z., 2011b. An essential role of the cysteine-rich domain of FZD4 in Norrin/Wnt signaling and familial exudative vitreoretinopathy. *The Journal of biological chemistry* **286**, 10210–10215.
- Zhang, X., Gaspard, J.P., Chung, D.C., 2001. Regulation of Vascular Endothelial Growth Factor by the Wnt and K-ras Pathways in Colonic Neoplasia. *Cancer Research* **61**, 6050–6054.
- Zhou, L., Kuhnert, F., Kuo, C.J., Ben, A., 2009. Wnt/ $\beta$ -catenin signaling is required for CNS , but not non-CNS, angiogenesis. *Proceedings of the National Academy of Sciences of the United States of America* **106**, 641–646.
- Zhou, Y., Nathans, J., 2014. Gpr124 Controls CNS Angiogenesis and Blood-Brain Barrier Integrity by Promoting Ligand-Specific Canonical Wnt Signaling. *Developmental Cell* **31**, 248–256.
- Zhou, Y., Williams, J., Smallwood, P.M., Nathans, J., 2015. Sox7, Sox17, and Sox18 Cooperatively Regulate Vascular Development in the Mouse Retina. *Plos One* **10**, e0143650.

- Zhu, M., 2000. The Human Hyaloid System: Cell Death and Vascular Regression. *Exp. Eye Res* **70**, 767–776.
- Zou, Y., Ning, T., Shi, J., Chen, M., Ding, L., Huang, Y., Kauderer, S., Xu, M., Cui, B., Bi, Y., Liu, S., Hong, J., Liu, R., Ning, G., Wang, J., 2016. Association of a Gain-of-Function Variant in LGR4 with Central Obesity. *Obesity* **25**, 252–260.

## 8 Appendices

### 8.1. Human LGR4 and zebrafish Igr4 protein alignment

Range 1: 27 to 971		Graphics		▼ Next Match ▲ Previous Match	
Score	Expect	Method	Identities	Positives	Gaps
1103 bits(2853)	0.0	Compositional matrix adjust.	569/967(59%)	699/967(72%)	61/967(6%)
Query	24	AAPPLCAAPCSCDGRVDCSGKGLTAVPEGLSAFTQALDISMNNITQLPEDAFKNFPFL			83
		+ P C+ C CD D DCSG+GLT+VP GLSAFT LDISMNNIT+LP + F+N P+L			
Sbjct	27	STPATCSPLCRCEDEGGADCSGRGLTSVPTGLSAFTYYLDISMNNITELPANVFRNLPYL			86
Query	84	EELQLAGNDLSFIHPKALSGLKELKLVTLQNNQLKTVPSEAIRGLSALQSLRLDANHITS			143
		EEL+LAGNDL+FIHP+ALSGL +LKVL LQNNQLKTVPS A++ L+ALQSLRLDANHITS			
Sbjct	87	EELRLAGNDLAFIHPEALSGLHQLKVLMLQNNQLKTVPSAALKNLNALQSLRLDANHITS			146
Query	144	VPEDSFEGLVQLRHLWLDNLSLTEVPVHPLSNLPTLQALTLALNKISSIPDFAFTNLSSL			203
		VPEDSFEGL QLRHLWLDNLSLTEVP+ PL + LQALTLALN+I+ IPD AF NLSSL			
Sbjct	147	VPEDSFEGLQQLRHLWLDNLSLTEVPI SPLQHSNLQALTLALNRITHIPDNANANLSSL			206
Query	204	VVLHLHNNKIRSLSQHCFDGLDNLLETLDLNYNNLGEFPQAIKALPSLKEGFGHSNSISVI			263
		VVLHLHNN+I+ + ++CF+GLDNLLETLDLN+NNL FP+AI+ LP LKELGFGHSN+I+ I			
Sbjct	207	VVLHLHNNRIQEIGKNCFNGLDNLLETLDLNFNNLKIFPEAIQMLPKLKEGFGHSNNIASI			266
Query	264	PDGAFDGNPLLRTHIHYDNPLSFVGNFAFNHLSLSDHSLVIRGASMVQFPNLTGTVHLES			323
		P+GAF N LLRTIHL+DNPLSFVG +AF NLSDLHSL++RGASM+Q FP+LTGT++LES			
Sbjct	267	PEGAFCRNSLLRTHIHLFDNPLSFVGTTFQNLSDHSLMLRGASMMQDFPSLTGTINLES			326
Query	324	LTLTGTKISSIPNNLCQEQMLRRTLDLSYNNIRDLPFNGCHALEEISLQRNQIYQIKEG			383
		LTLTGTKI SIP +LC++ +LRT+DLSYN+I DLPSF GC L++I+LQ NQI QI G			
Sbjct	327	LTLTGTKIRSI PADLCEDELTVLRTVDLSYNDIEDLPSFQGCVRQLQDINLQHNQIKQIDRG			386
Query	384	TFQGLISLRILDLSRNLIHEIHSRAFATLGPITNLDVSNELTSPFTEGLNGLNQLKLVG			443
		TFQG+ SLR+LDLSRN I IH AF +L +TNLD+S N L S PT GL+ LNQLK L G			
Sbjct	387	TFQGMTSLRVLDLSRNQIKFIHRDAFLSLSALTNLDLSLNSLASVPTAGLSALNQLKLTG			446
Query	444	NFKLKEALAAKDFVNLRSLSVPYAYQCCAFWGCDSYANLNTEDNSLQDHSVAQEKGTADA			503
		N +L+ L +K LRS++VPYAYQCCAF DS N +D +			
Sbjct	447	NMELRNGLMSKTLPKLRSITVPYAYQCCAFVAYDSAVNPAEDD-----ER			491
Query	504	ANVTSTLENEEHSQIIHCTPSTGAFKPCYLLGSMIRLTVWFIFLVALFFNLLVILTT			563
		N E+ E +++HC+P GAFKPC+LLGSMIRLTVWFI LVAL FN LV+ T			
Sbjct	492	RNAFGGEEDMERIPVMHCSPLPGAFAKPCHELLGSMIRLTVWFI CLVALLFNCLVLAAT			551
Query	564	FASCT-SLPSSKLFIGLISVSNLFGIYTGILTFDLAVSWGRFAEFGIWWETGSGCKVAG			622
		F+ T SL S+ + L++ +NL G+Y LT LD V+WG FAE+G+WWETG+GC+V G			
Sbjct	552	FSPRTSSLSPSRFLVALLASANLLTGVYVAALTLTDTVTWGSFAEYGVWWTGAGCQVVG			611
Query	623	FLAVFSSESAIFLLMLATVERSLSAKDIMKNGKSNHL-----KQFRVAALLAFLG			672
		FLAVFSSE A+ LL LA VER L+ + +M GK+ L ++F +AALL L			
Sbjct	612	FLAVFSSEWAVLLLALAAVERCLAVRALM--GKAGALRSRGERRRRRFAIAALLLGLV			669
Query	673	ATVAGCFPLFHRGEYSASPLCLFPPTGETPSLGFVTVLVLLNSLAFLLMAVIYTKLYCNL			732
		+ A C L+H G SPLCLPF G +P LGFTV LVL+N+LA+LL AV+YT+LYC L			
Sbjct	670	SVAACLSLYH-GSAMGSPCLPFSEGSFGLGFTVALVLMNTLAYLLSAVVYTRYLYCRL			728
Query	733	EKEDLSENSQSSMIKHVAWLIFTNCFIFCPVAFFSFAPLITAISSIS---PEIMKSVTLIF			789
		+ L++ Q+ ++H+AWLIFTNCFIFCPVA FSPAPL+ S + PE+ KSVTLIF			
Sbjct	729	GRAQLADPEQAGSVRHIAWLIFTNCFIFCPVAAFSFAPLLAGTSNAVGGPEMAKSVTLIF			788
Query	790	FPLPACLNPNVLYVFNPKFKEDW-----KLLKRRVTKKSGSVSVSISQGGC			836
		FPL ACLNPNVLYV F+P F+ DW +L+ + VTK + + +S G			
Sbjct	789	FPLSACLNPNVLYVCFSPSFRYDHLHLRGRGRTGGCGRLVAKTVTKGTVAGGSPVSDDG--			846
Query	837	LEQDFYYDCGMYSHLQGN-LTVCDCCESFLTKP-----VSKHLIKSHSCPALA-			885
		+ DCGMY+ L G+ +C+ C++ L + +C+HL+KSHSCPAL			
Sbjct	847	--EGLSSDCGMYTKLHGDSRGMCEHCDAALHIRTSSSSGSSSSSACRHLVKSHSCPALMG			904
Query	886	-VASCQRPEGYWSDCGTQSAHSDYADEEDSFVSDSSDQVQACGRACFYQSRGFPLVRYAY			944
		V C EGYW D GT SA S+Y DE DSFVSDSS+QVQACGRACF QSRG PLV Y+Y			
Sbjct	905	NVPQCLSSEGYWPDGTLSAQSEYGDGDSFVSDSSEQVQACGRACFCQSRGLPLVHYYS			964
Query	945	NLPRVKD 951			
		N+PR+ D			
Sbjct	965	NIPRMTD 971			

## 8.2. MO sequences

Splice MO: 5' AGAGCTACACCAAAAAGTCATACCA 3'

Translational MO: 5' CGGACGGCCAGCAATGCCATTATTC 3'

## 8.3. Primers used in RT-PCR

LGR4 ex1 RT-Forward: 5' CTAGGGCTGCTCTGCTTCCT 3'

LGR4 ex5 RT-Reverse: 5' TCCGTCAAGCTGTTGTCATC 3'

Product size: 488 bp

NDP 2 end F: 5' CTGCATCCTTTTCTATGCTC 3'

NDP 3 start R: 5' CAGTGCCTTCAGCTTGGAAGTC 3'

Product size: 400 bp

FZD4-1-2F: 5' GGGACGTCTAAAATCCCACA 3'

FZD4-2-1R: 5' TTGGTTCCCACAGAGTGACA 3'

Product size: 745 bp

LRP5-SSCP-9F: 5' GTGCCTGAGGCCTTCTTGGTCT 3'

LRP5-SSCP-12R: 5' CATCACGAAGTCCAGGTGG 3'

Product size: 747 bp

TSPAN12-RT-2F: 5' CTCTCCGCGAAGAAGTTCC 3'

TSPAN12-RT-2R: 5' ACGCCACAAGCCAGTTCTAC 3'

Product size: 299 bp

RT-PCR p53-Forward: 5' GTA CTCCCCTGCCCTCAACA 3'

RT-PCR p53-Reverse: 5' CTGGAGTCTTCCAGTGTGA 3'

Product size: 408 bp

## 8.4. SDM primers

LGR4 c.118C>T-F: 5' TGCGACGGCGACCGTTGGGTGGAC 3'

LGR4 c.118C>T-R: 5' GTCCACCCAACGGTCGCCGTCGCA 3'

LGR4 c.933G>C-F: 5' CAAGCATGGTGCAGCACTTCCCCAATCTTACAG 3'

LGR4 c.933G>C-R: 5' CTGTAAGATTGGGGAAGTGCTGCACCATGCTTG 3'

LGR4 c.1289C>T-F:

5' AGTTTCAATGAATTAACCTTCCTTTCTATGGAAGGCCTGAATGG 3'

LGR4 c.1289C>T-R:

5' CCATTCAGGCCTTCCATAGGAAAGGAAGTTAATTCATTGAAACT 3'

LGR4 c.2164G>A-F:

5' TTAAACTCACTAGCATTTTTATTAATGACCGTTATCTACACTAAGCTATAC 3'

LGR4 c.2164G>A-R:

5' GTATAGCTTAGTGTAGATAACGGTCATTAATAAAAATGCTAGTGAGTTTAA 3'

LGR4 c.2248G>A-F:

5' CTAGCATGATTAAGCATGTCACTTGGCTAATCTTCACCAAT 3'

LGR4 c.2248G>A-R:

5' ATTGGTGAAGATTAGCCAAGTGACATGCTTAATCATGCTAG 3'

LGR4 a2854t c2855a-F:

5' TCTACCAAGAGTTAAAGACTAGCGTACGCGGCCGC 3'

LGR4 a2854t c2855a-R:

5' GCGGCCGCGTACGCTAGTCTTTAACTCTTGGTAGA 3'

TSPAN12-c542t-F: 5' GGGTAGAGGAAGCAGTCATTTTGACTTACTTTCTCTG 3'

TSPAN12-c542t-R: 5' CAGGAAAGTAAGTCAAATGACTGCTTCTCTACCC 3'

## 8.5. attB primers for Gateway technology constructs

attB-LGR4-ZK-F:

5' GGGGACAAGTTTGTACAAAAAAGCAGGCTTCGCCGCCGCATGCCGGG  
CCCGCTAGGGCTGC 3'

attB-LGR4-ZK-2R:

5'GGGGACCACTTTGTACAAGAAAGCTGGGTCTCAGTCTTTAACTCTTGGTAG 3'

attB-FZD4-F:

5' GGGGACAAGTTTGTACAAAAAAGCAGGCTTCGCCGCCGCATGCCATG  
GCCTGGCGGGGCGCAGGGC 3'

attB-FZD4-R:

5' GGGGACCACTTTGTACAAGAAAGCTGGGTCTACCACAGTCTCACTGCCTT 3'

attB-LRP5-F:

5' GGGGACAAGTTTGTACAAAAAAGCAGGCTTCGCCGCCGCATGCCATG  
GAGGCAGCGCCGCCCGGGCCGC 3'

attB-LRP5-R:

5' GGGGACCACTTTGTACAAGAAAGCTGGGTCTCGGATGAGTCCGTGCA  
GGGGG 3'

attB-TSPAN12-F:

5' GGGGACAAGTTTGTACAAAAAAGCAGGCTTCGCCGCCGCATGCCATGG  
CCAGAGAAGATTCCGTGA 3'

attB-TSPAN12-R:

5' GGGGACCACTTTGTACAAGAAAGCTGGGTCTAACTCCTCCATCTCAAAG 3'

## 8.6. Sequencing primers of expression constructs

pENTR-R: 5' GTAACATCAGAGATTTTGAGACAC 3'

pENTR-F: 5' TCGCGTTAACGCTAGCATGGATCTC 3'

FZD4-1-3F: 5' GGTTGCTCCTGCAGTTGCT 3'

FZD4-2-1R: 5' TTGGTTCCCACAGAGTGACA 3'

FZD4-Kondo-2BF: 5' CAGCCTGTGTTTCATCTCCA 3'

TSPAN12-RTF: 5' AAGATTCCGTGAAGTGTCTGC 3'

TSPAN12-RT2R: 5' ACGCCACAAGCCAGTTCTAC 3'

TSPAN12-RTR: 5' GCATGAGTAAGCCACCGATA 3'

LRP5-SSCP-2F: 5' CAAGCAGACCTACCTGAACC 3'

LRP5-SSCP-3F: 5' CGGATTGAGCGGGCAGGGAT 3'

LRP5-SSCP-3R: 5' GGATGAAGCTGAGCTTGCGGTC 3'

LRP5-SSCP-6F: 5' CGACCCGCTAGAGGGCTATGT 3'

LRP5-SSCP-6R: 5' GTCGACCGCGATGCCATCGG 3'

LRP5-SSCP-9F: 5' GTGCCTGAGGCCTTCTTGGTCT 3'

LRP5-SSCP-9R: 5' CCGTGAGCGGGATGGCCACG 3'

LRP5-SSCP-12F: 5' CTAGCGGCCGGAACCGCA 3'

LRP5-SSCP-12R: 5' CATCACGAAGTCCAGGTGG 3'

LRP5-cDNA-14F: 5' GACCTCTCTGAGCCAAGGCC 3'

LRP5-cDNA-16F: 5' CAAGCATCTCTACTGGATCG 3'

LRP5-cDNA-19F: 5' CAGTGTGTCCTCATCAAACAG 3'

LRP5-cDNA-22F: 5' CTACTCTTCAAACATTCCGG 3'

LRP5-cDNA-15R: 5' GTGAAGAGGACCTCGCGCTC 3'

LRP5-cDNA-18R: 5' GTGACGGCTTTCCCGAGTGC 3'

LRP5-cDNA-20R: 5' CTATGAAATTGAGGGGCACG 3'

LGR4-RT1-F: 5' AGTCAAATAATTATCCATTGTACACCT 3'

LGR4-RT1-R: 5' TCAAGAAAAGTTAGGATGCCAGT 3'

LGR4-RT2-F: 5' ATGCAGCAAATGTCACAAGC 3'

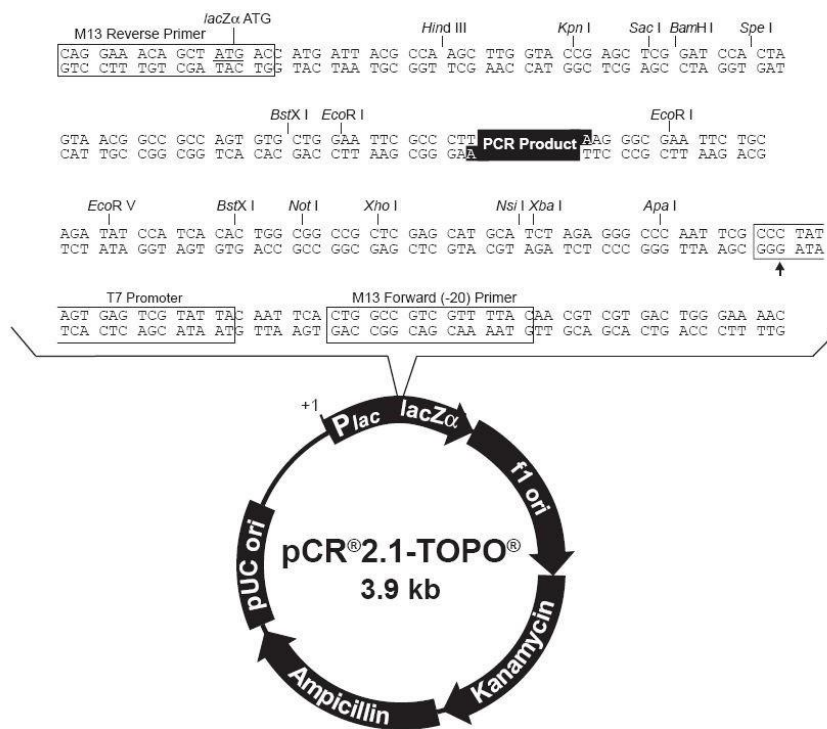
LGR4-RT2-R: 5' CAGCTACTTTGCAGCCACTG 3'

LGR4-Int1-R: 5' TTGTTGAGAGCCAGGGTCA 3'

LGR4-Int2-R: 5' ACTTGAAGGTCTCTTATATTA 3'

LGR4-Int3-F: 5' GCTGTTTTCCCCTTTTCCAT 3'  
LGR4-Int3-R: 5' CCTGTTCCAGACAACCCACCT 3'  
LGR4-Int4-F: 5' TCCCTGATGGAGCATTGAT 3'  
LGR4-Int4-R: 5' TGGTCCTGGAGGCTGTTATC 3'  
LGR4-Int5-F: 5' GTA CTACATTTGCAGGGCA 3'  
LGR4-Int7-F: 5' CAATCTACCAAGAGTTAAAGAC 3'  
LGR4-Int6-F: 5' CTACCAGAGTAGAGGATTCC 3'

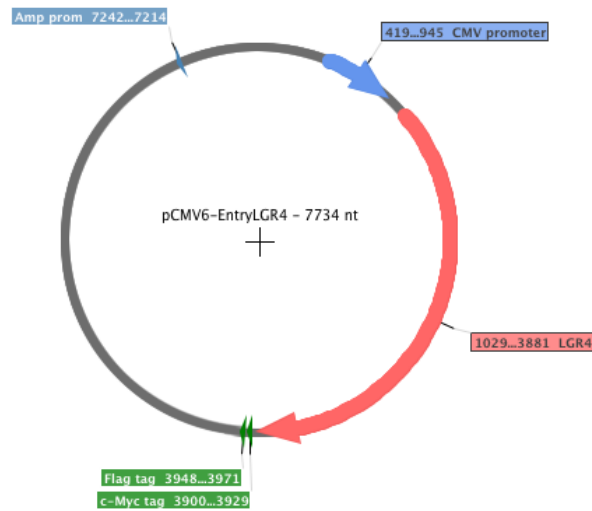
## 8.7. pCR2.1-TOPO vector



Schematic diagram of the pCR2.1-TOPO vector is shown. The sequence of the region surrounding the PCR inserted product is shown. Restriction sites are also shown together with the sequence for M13 Reverse primer, T7 promoter and the M13 Forward primer.

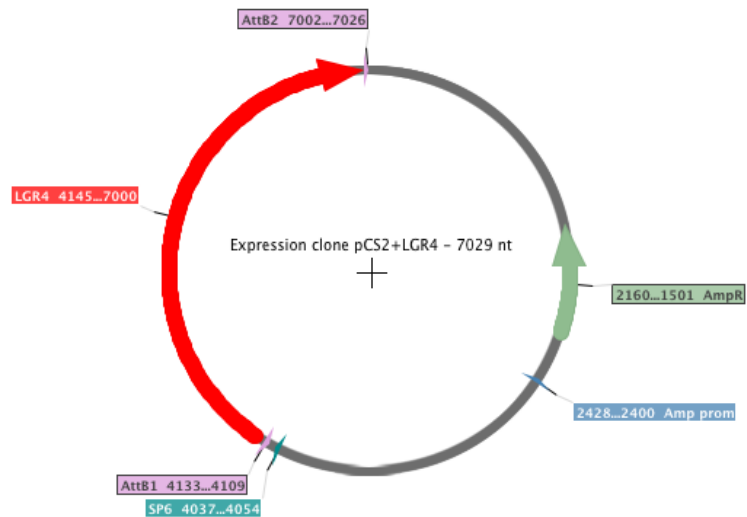
## 8.8. Expression vectors

### pCMV6 LGR4



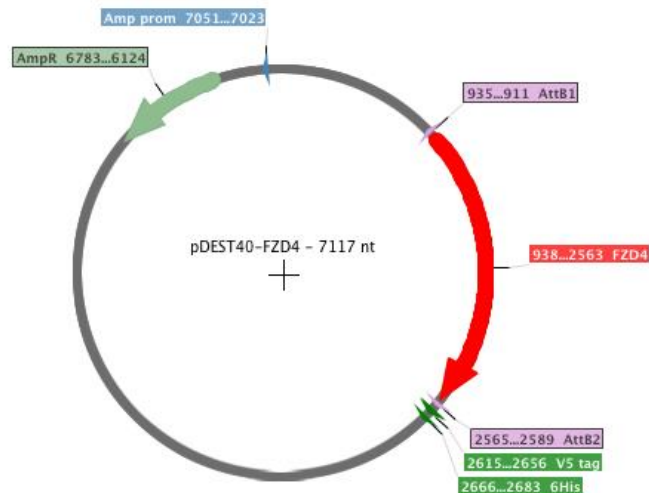
Schematic representation of pCMV6\_LGR4. In red the LGR4 ORF tagged at the C-terminal with Flag-Tag and C-Myc Tag. The CMV promoter is represented in blue before the LGR4 ORF.

### pCS2+LGR4



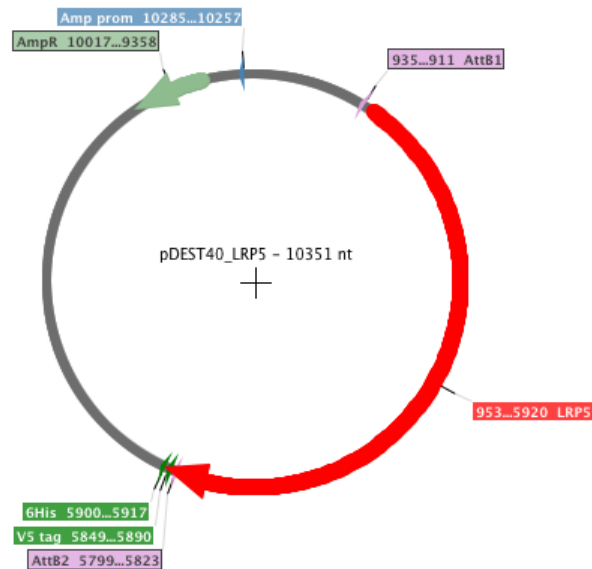
Schematic representation of pCS2+\_LGR4. In red the LGR4 ORF flanked by the attB sites. The SPS6 RNA polymerase promoter is represented. In green the Ampicillin resistance gene.

## pDEST40 FZD4



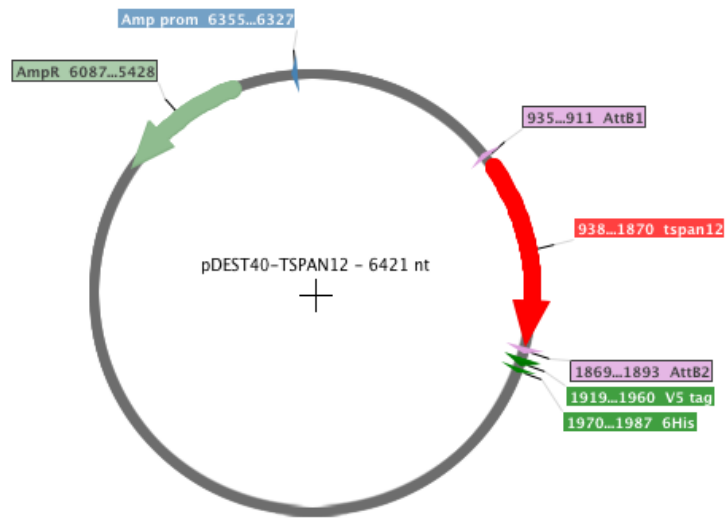
Schematic representation of pDEST40\_FZD4. In red the FZD4 ORF flanked by the attB sites and V5-tag and His-tag represented at the C-terminal of the FZD4 ORF. In green the Ampicillin resistance gene.

## pDEST40 LRP5



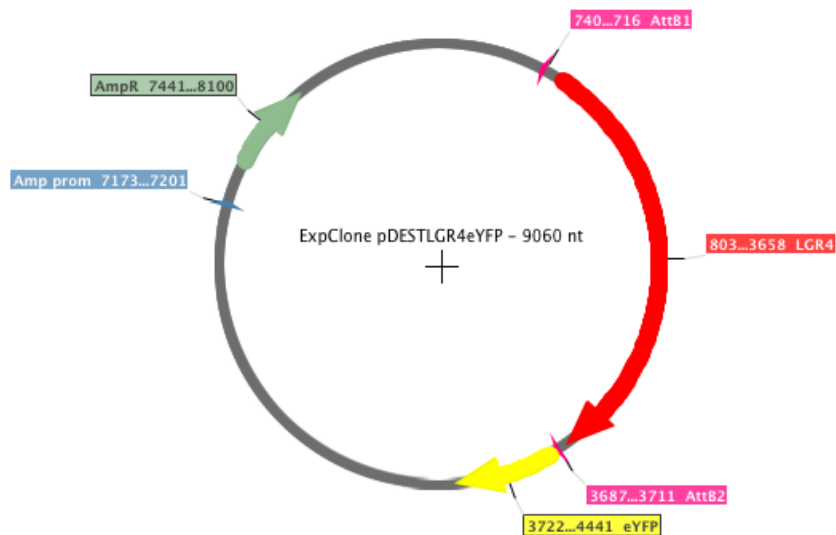
Schematic representation of pDEST40\_LRP5. In red the LRP5 ORF flanked by the attB sites and V5-tag and His-tag represented at the C-terminal of the LRP5 ORF. In green the Ampicillin resistance gene.

## pDEST40 TSPAN12



Schematic representation of pDEST40\_TSPAN12. In red the TSPAN12 ORF flanked by the attB sites and V5-tag and His-tag represented at the C-terminal of the TSPAN12 ORF. In green the Ampicillin resistance gene.

## pDEST504 LGR4



Schematic representation of pDEST504\_LGR4. In red the LGR4 ORF flanked by the attB sites and eYFP represented in yellow at the C-terminal of the LGR4 ORF. In green the Ampicillin resistance gene.

